

**Western Australia School of Mines: Minerals, Energy and Chemical
Engineering**

Microwave Assisted Catalytic Dry Reforming of Methane

Minh Hoang Nguyen

**This thesis is presented for the Degree of
Doctor of Philosophy**

of

Curtin University

September 2019

Declaration

To the best of my knowledge and belief this thesis contains no material previously published by any other person except where due acknowledgement has been made.

This thesis contains no material which has been accepted for the award of any other degree or diploma in any university.

Signature:

Date: **13/09/2019**

Acknowledgement

I would like to express my heartfelt to my principal supervisor Prof. Shaomin Liu. His knowledge in academic research always gives me huge motivations. I am greatly thankful for his insightful review and comments on my works. His valuable suggestions have turned my research in positive ways. I also would like to thank him for supporting my study here continuously. His shared experience in academic writing and publishing is great values bringing along with my future academic career.

Equally, I also owe deep gratitude to my co-supervisor Dr. Gia Hung Pham for helping me continuously with his patient supervision. His unconditional guidance, training, and persistent support are unmeasurable. His engineering knowledge, intelligence, and a huge passion for engineering and research have always inspired me. I am also thankful for his examples of how to pursue an academic life.

Once again, thank you very much, Prof. Shaomin Liu and Dr. Gia Hung Pham. Without your warm encouragement and thoughtful guidance, I had no chance to complete this thesis. It is my great honor to be one of your students and be a part of our amazing research group.

My warm thanks are given to Mr. Robert Vargoni, CEO of EcoTechnol Pty Ltd., for his engineering advice and kind supports during my PhD study.

I am grateful to the Curtin International Postgraduate Research Scholarship (CIPRS) of Curtin University, Australian Research Council Linkage project - LP150101158, and Echotechnol Co Ltd., for their scholarship and financial support making my PhD study to be possible.

I gratefully acknowledge Curtin laboratory technicians, Jason Wright, Araya Abera, Roshanak Doroushi, Andrew Chan, Ann Carol, and Jimmy, who gave me valuable help for my experimental works, training on various equipment, and software. I also owe gratitude to Prof. Martin Saunders, Prof. Peta Clode, Dr. Alexandra Suvorova, and the Centre for Microscopy, Characterization, and Analysis at the University of Western Australia for training and helping me in using FESEM, STEM, and XRD analyses.

My sincere gratitude must go to Dr. Min Ao, Dr. Ran Ran, Dr. Ting Ting Li, Nabil Alawi, Fuping Li, and Ning Han. They were not only the greatest members of our research group but also my dear friends and elder brothers. I am also thankful to Dr. Duy Thong Kieu, Dr. Van Anh Cuong Le, Dr. Bao Trung Nguyen, Dr. Khai Tran, Dr. Hoang Long Nguyen, Dr. Phu Pham, Dr. Viet Pham Nguyen, Dr. Tin Do Van, Xaomin Xu for unforgettable moments that we have been through in Perth. It is hard to imagine how my PhD life is without them.

And last, but not the least, I would like to thank my parents, my beloved wife and my little daughter, who always give me their patience and unconditionally love. I truly thank them for sticking by my side, even when I was irritable and depressed. I am very lucky to have you in my life. I love you all, dearly.

Abstract

The gradual depletion of oil resources and more stringent greenhouse gas emission controls have secured the sustainably high demand for the conversion of natural gas to valuable and easily transportable fuel forms, such as syngas (H_2 , CO). Syngas is an important intermediate feedstock for chemicals and petrochemicals production from methane via Fischer-Tropsch synthesis. It is peculiarly important to exploit stranded natural gas from inaccessible reserves at offshore ocean areas, in which, conventional pipeline infrastructure is unavailable to transport it to a sizeable market in an economical manner. Because of this, associated CH_4 generated as a by-product of the oil production is often re-injected. Offshore stranded gas is unused and wasted whilst associated methane is often flared causing global warming. Catalytic dry reforming of methane is a feasible and effective solution to transform that untapped CH_4 and CO_2 to value-added syngas. In the meantime, microwave (MW) is a time – and energy – saving heating method while light weight MW reactor system is flexible, re-allocable, quick, and straightforward on/off control, which is suitable for Floating production storage and offloading vessels (FPSOVs) operating at offshore areas. Most of the works applying MW irradiation for DRM used carbon-based materials as catalysts due to their strong MW absorption ability. Nonetheless, carbon-based catalysts have significantly low stability due to their reaction with CO_2 during DRM process. In the meanwhile, it is difficult to find a metallic catalyst, which can be activated under MW heating for reforming reactions due to its high reflection of MW. This thesis aims to develop stable metallic-based catalysts, which can be activated under MW irradiation for methane reforming processes. The fresh and spent catalysts were characterized by the X-ray diffraction (XRD), N_2 adsorption isotherm, Temperature-programmed reduction TPR- H_2 , Field emission scanning electronic microscopy (FESEM) with corresponding Energy-dispersive X-ray (EDX) detector, Scanning Transmission Electron Microscope (STEM) with EDX detector, the superconducting quantum interference device (SQUID), Thermogravimetric analysis (TGA), and the Reflection Loss (R_L) measurement. The gaseous elements of reforming reactions were analyzed by using gas chromatography - mass spectrometry (GCMS).

The first part of this study reported the screening of catalytic activity of monometallic

(cobalt, molybdenum) and bimetallic (CoMo) catalysts supported on Al₂O₃ for the DRM reaction under MW irradiation. Experimental results indicate that monometallic catalysts, either Co or Mo, with a wide range of metal molar ratios were inactive for DRM under MW irradiation with the power up to 1,000 W. In contrast, CoMo bimetallic catalyst with a Co/Mo molar ratio of two could be able to catalyze DRM reaction at a low MW power of 200 W. The formed magnetodielectric Co_{0.82}Mo_{0.18} alloy of bimetallic catalyst played a dual role as a good MW acceptor and as an internal heating source to provide extra active centers for DRM reaction under MW irradiation. Moreover, the MW power level required to activate such bimetallic catalysts for DRM is significantly dependent on the molar ratios between Co and Mo. The CoMo₂ catalyst supported on Al₂O₃ showed the best catalytic performance while other CoMo catalysts with higher Co/Mo molar ratio e.g., 2.5 resulted in the skin effects to reflect MW wave given the presence of a large amount of highly conductive metallic Co particles, and thereby, reducing its activity. The syngas ratio (H₂/CO) of 0.80 at the total volumetric hourly space velocity (VHSV) of 10 L.g⁻¹.h⁻¹ and 200 W was produced over CoMo₂ catalyst. Compared to carbon-based catalysts under similar reaction conditions, CoMo catalysts delivered highly favourable stability for DRM under MW irradiation. The good stability of CoMo catalyst is attributed to its intrinsic ability to absorb MW without the inclusion of auxiliary MW-acceptor such as carbon.

Based on the above findings, the second part of this work was to study the catalytic performance of CoMo catalyst supported on TiO₂ for DRM under MW irradiation. To improve the produced syngas ratio, the steam was also added into the reactant feed (CH₄ and CO₂). It was surprisingly found that CoMo/TiO₂ catalysts could be activated at a MW power of 100 W, much lower than the previously-studied CoMo/Al₂O₃ catalyst. It has been found that TiO₂ offered better exposure of the well-defined Co_{0.82}Mo_{0.18} particles to the incident MW wave leading to stronger MW absorption and better catalytic activity. The CoMo₁ catalyst (Co/Mo molar ratio of 1) displayed a highest catalytic activity for both DRM and steam combined dry reforming of CH₄ (SDR) converting 81 % CH₄ and 86 % CO₂ to a syngas ratio (H₂/CO) of 0.92 at a low MW power of 100 W. The H₂/CO ratio above of two could be simply obtained by adding steam with the inlet steam-to-methane (S/C) molar ratio of 0.1. A further increase in Co/Mo ratio, such as 1.5, led to the decline in catalytic activity due to the lower accessibility of reactants into active centers inside the pores of TiO₂. As

compared to the carbon-based catalysts, the CoMo/TiO₂ catalysts exhibited a strikingly stable catalytic performance for both DRM and SDR reactions over 62 h time-on-stream (TOS) under MW irradiation. The good stability of CoMo/TiO₂ was attributed to the strong interaction between CoMo and TiO₂, which reduced catalyst sintering and coke formation. Moreover, the presence of steam also gasified deposited coke.

Researchers have recently paid attention towards wide abundance, high activity, and less safety concern materials like copper-based catalysts for fuel production processes. The third part of this study attempted to take such advantages of copper-based catalysts for MW assisted SDR reaction for syngas production. In this section, the single Cu, Mo, and bimetallic CuMo catalysts were prepared and tested for MW assisted SDR reactions, respectively. Experimental results show that the single Cu or Mo catalyst supported on TiO₂ was unable to absorb MW while the formation of a dielectric layer of MoO₂ surrounding the adjacent Cu⁰ particles accounted for the high catalytic activity of the binary CuMo catalysts at a low MW power of 100 W. It was also found that 82 % of CH₄ and 61 % of CO₂ were converted to a syngas ratio of 2.1 over the CuMo1 catalyst (Cu/Mo molar ratio of 1) at the MW power of 100 W. The syngas ratios could be obtained by adjusting the steam addition. Moreover, the CuMo catalysts were stable for at least 72 hrs on the SDR test. The unprecedented results in this work provide initial insights into the activation mechanism of earth-abundant metallic catalysts for gas-solid reactions under MW heating.

Given the results from this thesis, MW assisted catalytic reforming of CH₄ exhibits as the highly practical and effective processes for syngas production. These exploited advantages are primary premises for further developments of such advanced MW heating assisted catalytic reforming processes to exploit stranded natural gas at offshore deep seawater/remote areas, where the pipeline systems are not available or uneconomical. The findings from this study also provide fundamental insights into the MW activation for metallic-based heterogeneous catalysts for gas-phase reactions.

Publications/ Presentations with Materials Produced in This Study

Published paper:

1. **Hoang M. Nguyen**, Gia Hung Pham*, Ran Ran, Robert Vagnoni, Vishnu Pareek, Shaomin Liu*, *Dry reforming of methane over Co-Mo/Al₂O₃ catalyst at low microwave power irradiation*, Catalytic Science and Technology, (2018). DOI: 10.1039/C8CY01601A.

Patent filed:

2. **Hoang M. Nguyen**, Gia Hung Pham, Shaomin Liu, *A catalyst*. Filed No. 2019903821.

Manuscripts in preparation:

3. **Hoang M. Nguyen**, Gia Hung Pham*, Robert Vagnoni, Shaomin Liu*, *M-Mo/TiO₂ bimetallic catalysts (M = Co, Cu) for microwave-assisted methane reforming*.
4. **Hoang M. Nguyen**, Jaka Sunarso*, Gia Hung Pham, Shaomin Liu*, *Catalysts for MW- assisted methane reforming: a review*.

Presentation at Conference:

5. **Hoang M. Nguyen**, Gia Hung Pham*, Robert Vagnoni, Shaomin Liu*, *Syngas production via steam combined dry reforming of methane under microwave heating*, ICCCP 2019, 25-28th February, 2019, Singapore. (**the best Oral presentation award**. Link: <http://www.icccp.org/2019.html>)

Table of Contents

Acknowledgement	i
Abstract.....	iii
Publications/ Presentations with Materials Produced in This Study	vi
List of Figures.....	xi
List of Tables	xv
List of Abbreviations and Symbols.....	xvi
Chapter 1 Introduction.....	1
1.1. Background and motivation.....	1
1.2. Objectives.....	4
1.3. Thesis organization	4
Chapter 2 Literature review.....	6
2.1. Introduction.....	6
2.2. Offshore GTL processes	8
2.2.1. Stranded gas utilization alternatives	8
2.2.2. GTL process	9
2.3. Methane reforming to syngas.....	10
2.3.1. Steam reforming of methane.....	11
2.3.2. Partial oxidation of methane	12
2.3.3. Dry reforming of methane.....	13
2.3.3.1. Thermodynamic and reaction mechanism	14
2.3.3.2. Carbon deposition	18
2.3.4. Combined reforming of methane processes.....	22
2.4. Catalyst development for reforming of methane	23
2.4.1. Active metals.....	24
2.4.1.1. Noble catalysts	25
2.4.1.2. Non-noble catalysts.....	28
2.4.2. Catalyst preparation methods.....	37
2.4.3. Supports	42

2.4.3.1.	Alumina.....	46
2.4.3.2.	TiO ₂	46
2.5.	Catalytic reforming of methane under MW heating	48
2.5.1.	MW heating.....	48
2.5.1.1.	Background of MW heating.....	48
2.5.1.2.	Microwave-Material Interactions.....	53
2.5.1.3.	Microwave-Enhanced Heterogeneous Gas-Solid Catalytic	57
2.5.1.4.	Temperature measurement in MW reactor system	62
2.5.2.	Catalysts for MW assisted reforming of methane.....	64
2.5.2.1.	Carbon-based catalysts.....	64
2.5.2.2.	Metallic-based catalysts	69
2.6.	Conclusion	70
Chapter 3	Research Methodology and Analytical Techniques.....	73
3.1.	Catalyst screening	73
3.1.1.	Catalyst preparation	73
3.1.1.1.	Chemicals and materials	74
3.1.1.2.	Catalyst preparation	74
3.1.2.	Catalyst reduction.....	75
3.2.	Catalyst characterization	75
3.2.1.	N ₂ adsorption and BET surface area measurement.....	76
3.2.2.	X – Ray diffraction analysis.....	76
3.2.3.	Field Emission Scanning Electron Microscope equipped with Energy - dispersive X-ray spectroscopy (FESEM-EDX)	76
3.2.4.	Hydrogen Temperature-programmed reduction analysis (H ₂ -TPR) 76	
3.2.5.	Thermogravimetric Analysis (TGA).....	77
3.2.6.	Scanning Transmission Electron Microscopy-EDX (STEM-EDX) 77	
3.2.7.	Magnetic properties measurement	77
3.2.8.	Reflection loss measurement.....	78
3.3.	Catalytic performance test.....	78
3.3.1.	DRM reaction.....	78
3.3.2.	SDR reaction	80

3.4.	Calculations.....	81
Chapter 4	Screening catalysts activated under MW irradiation for DRM	82
4.1.	Introduction.....	82
4.2.	Result and discussion.....	82
4.2.1.	Catalytic activity.....	82
4.2.2.	Catalyst stability.....	85
4.2.3.	Catalyst characterization.....	87
4.2.4.	The mechanism of catalytic activation for DRM under MW irradiation	101
4.3.	Summary.....	104
Chapter 5	Role of TiO₂ support in the enhancement of catalytic activity of CoMo catalyst for dry and steam combined dry reforming of methane under microwave heating.....	105
5.1.	Introduction.....	105
5.2.	Results and Discussion.....	105
5.2.1.	Characterization of fresh catalysts.....	105
5.2.2.	Catalytic activity.....	113
5.2.3.	Catalytic stability.....	116
5.2.4.	Characterisation of spent catalysts.....	117
5.3.	Summary.....	122
Chapter 6	Syngas production via steam combined CO₂ reforming of methane over CuMo/TiO₂ catalyst under MW heating.....	123
6.1.	Introduction.....	123
6.2.	Results and Discussion.....	123
6.2.1.	Catalytic activity.....	123
6.2.2.	Catalytic stability.....	127
6.2.3.	Catalyst characterization.....	128
6.3.	Summary.....	137
Chapter 7	Conclusions and Recommendations.....	139
7.1.	Conclusions.....	139

7.2. Recommendations	141
References	143
APENDIX	203

List of Figures

Figure 2-1- Global GHG emissions in 2010 [83].....	7
Figure 2-2 - Diagram of multiple stages for syngas production from SRM.	12
Figure 2-3 – Schematic diagram of main routes of CO ₂ utilization into fuels [108].	14
Figure 2-4 - Scheme of general reaction mechanism of DRM.	16
Figure 2-5 - Coke deposited on the metal catalyst particle and support.	19
Figure 2-6 - TPH profiles of Ni/MgO catalyst at different contact times and temperature. Reprinted with permission from Ref. [140]. Copyright© 1997 Elsevier.	20
Figure 2-7 - A general energy surface of non-catalytic and catalytic process.	24
Figure 2-8 - The mechanism of DRM reaction over La _{0.8} Sr _{0.2} Ni _{0.8} Fe _{0.2} O ₃ perovskite catalyst. Reprinted with permission from Ref. [253]. Copyright© 2012 Elsevier. ...	32
Figure 2-9 - Electronic properties of cobalt compared to common active metals according to the Pauling scale [279].	34
Figure 2-10 - Scheme illustrated the wet and dry impregnation method.	40
Figure 2-11 - Scheme of co – impregnation method to prepare of Co-Pd/Al ₂ O ₃ catalysts [378].	41
Figure 2-12 – Advantages of MW irradiation and its role in chemistry [467]	49
Figure 2-13 – Conductive (A), ran (B), and absorbing (C) materials under MW irradiation [473].	50
Figure 2-14 – MW heating mechanism of dipolar loss [482].	54
Figure 2-15 - MW heating mechanism of conduction loss.	54
Figure 2-16 – The magnetization (B vs. H) curve.....	55
Figure 2-17 – Two-way hybrid MW heating with susceptor [499].	57
Figure 2-18 – The formation carbonaceous species over Ni/CeO ₂ and 2Cr-Ni after 14 h. Reproduced with permission from Ref [30]. Copyright © 2016 Elsevier.	67
Figure 3-1 – Research methodology.	73
Figure 3-2 – MW reactor system for catalytic DRM.	79
Figure 3-3 - Scheme of the catalytic SDR system heated by MW.....	80
Figure 4-1 - CH ₄ conversion (a), CO ₂ conversions (b), H ₂ selectivity (c), and CO selectivity of DRM reaction for all the CoMo catalysts under MW irradiation at different MW power levels. [Reaction parameters: CH ₄ /CO ₂ =1, VHSV = 10 L.g ⁻¹ .h ⁻¹].	

Reproduced from Ref. [579] with permission from the Royal Society of Chemistry.	83
Figure 4-2 - H ₂ /CO ratio. [DRM reaction parameters: CH ₄ :CO ₂ =1, VHSV = 10 L.g.h ⁻¹]. Reproduced from Ref. [579] with permission from the Royal Society of Chemistry.	84
Figure 4-3 - Catalytic stability of CoMo ₂ catalyst at three different MW power levels. [Reaction parameters: CH ₄ :CO ₂ =1, VHSV = 10 L.g.h ⁻¹]. Reproduced from Ref. [579] with permission from the Royal Society of Chemistry.....	86
Figure 4-4 - N ₂ absorption/desorption isotherm curves of monometallic and CoMo ₂ (a); and all bimetallic catalyst samples (b). Reproduced from Ref. [579] with permission from the Royal Society of Chemistry.....	88
Figure 4-5 - TPR-H ₂ profiles of monometallic and CoMo ₂ (a); bimetallic catalysts (b). Reproduced from Ref. [579] with permission from the Royal Society of Chemistry.....	90
Figure 4-6 - XRD of fresh (a) and spent (b) catalysts. [Reaction parameters: 500 W, CH ₄ :CO ₂ =1, VHSV = 10 L.g.h ⁻¹]. Reproduced from Ref. [579] with permission from the Royal Society of Chemistry.....	92
Figure 4-7 - X-ray diffraction patterns fitted using the Rietveld refinement method for CoMo ₂ catalyst sample. $\chi^2 = 1.12$. Reproduced from Ref. [579] with permission from the Royal Society of Chemistry.....	93
Figure 4-8 - FESEM (a ₁ , b ₁), BF-STEM, (a ₂ , b ₂), and HRTEM images (a ₃ , b ₃) of fresh (a ₁ -a ₃) and spent (b ₁ -b ₃) CoMo ₂ catalysts. [Reaction parameters: 200 W, CH ₄ :CO ₂ =1, VHSV = 10 L.g.h ⁻¹]. Reproduced from Ref. [579] with permission from the Royal Society of Chemistry.....	95
Figure 4-9 – FESEM-EDX images of fresh Co/Al ₂ O ₃ (a), Mo/Al ₂ O ₃ (b), and CoMo ₂ (c) catalysts. Reproduced from Ref. [579] with permission from the Royal Society of Chemistry.....	96
Figure 4-10 - STEM-HAADF (a), line-scanning signals (b), and STEM-EDX (c) of fresh CoMo ₂ catalyst. Reproduced from Ref. [579] with permission from the Royal Society of Chemistry.....	98
Figure 4-11 - STEM-EDX qualitative spectrum of fresh CoMo ₂ catalyst. Reproduced from Ref. [579] with permission from the Royal Society of Chemistry.....	99

Figure 4-12 - FESEM images of fresh and spent CoMo ₂ bimetallic catalysts at different magnifications. The results of fresh CoMo ₂ catalyst is represented here for comparison purpose. Reproduced from Ref. [579] with permission from the Royal Society of Chemistry.....	100
Figure 4-13 - STEM-HAADF (a), line-scanning signals (b), and STEM-EDX (c) of spent CoMo ₂ catalyst. [Reaction parameters: 500 W, CH ₄ :CO ₂ =1, VHSV = 10 L.g.h ⁻¹]. Reproduced from Ref. [579] with permission from the Royal Society of Chemistry.	101
Figure 4-14 - Hysteresis loops of curves of fresh Mo/Al ₂ O ₃ ; Co/Al ₂ O ₃ and CoMo ₂ catalyst. Reproduced from Ref. [579] with permission from the Royal Society of Chemistry.	102
Figure 5-1 - N ₂ absorption/desorption isotherm curves of fresh CoMo/TiO ₂ catalysts.	106
Figure 5-2 - TPR-H ₂ profiles of TiO ₂ and CoMo/TiO ₂ catalysts.....	108
Figure 5-3 - XRD of calcined CoMo ₁ (a), fresh CoMo _{0.5} (b), CoMo ₁ (c) and CoMo _{1.5} (d) catalysts.	109
Figure 5-4 - FESEM (up-row) and BF-STEM (down-row) images of fresh CoMo _{0.5} (a ₁ , a ₂), CoMo ₁ (b ₁ , b ₂), CoMo _{1.5} (c ₁ , c ₂).	110
Figure 5-5 - STEM-EDX (a), STEM-HAADF (b) and line-scanning (c) of fresh CoMo ₁ catalyst.	111
Figure 5-6 - Reflection loss as a function of frequency of CoMo catalysts.....	112
Figure 5-7 - Catalytic activity of fresh CoMo/TiO ₂ catalyst. [Reaction conditions: CH ₄ /CO ₂ = 1, S/C = 0.1 (for SDR)]......	113
Figure 5-8 – Syngas ratio produced DRM and SDR reactions over CoMo ₁ catalyst. [Reaction conditions: CH ₄ /CO ₂ = 1, VHSV = 10 L.g ⁻¹ .h ⁻¹ S/C = 0.1 (for SDR)]....	115
Figure 5-9 - Catalytic stability of CoMo/TiO ₂ catalyst. [Reaction conditions: CH ₄ /CO ₂ = 1, VHSV = 10 L.g ⁻¹ .h ⁻¹ S/C = 0.1 (for SDR)]......	117
Figure 5-10 - XRD pattern (A) of CoMo _{0.5} (a), CoMo ₁ (b), CoMo _{1.5} (c) over DRM reaction, and CoMo _{1.5} (d) over SDR reaction; textural properties (B) of all CoMo catalysts spent over DRM and CoMo ₁ spent over SDR reaction. [Reaction conditions: 100 W, CH ₄ /CO ₂ = 1, VHSV = 10 L.g ⁻¹ .h ⁻¹ S/C = 0.1 (for SDR)]......	118
Figure 5-11 - FESEM (up-row) and BF-STEM (below-row) of catalysts spent for DRM CoMo _{0.5} (a ₁ , a ₂), CoMo ₁ (b ₁ , b ₂), CoMo _{1.5} (c ₁ , c ₂) and CoMo ₁ for SDR (d ₁ ,	

d ₂). [Reaction conditions: 100 W, CH ₄ /CO ₂ = 1, VHSV = 10 L.g ⁻¹ .h ⁻¹ S/C = 0.1 (for SDR)].	119
Figure 5-12 - STEM-EDX, STEM-HAADF and line-scanning results of DRM (a ₁ , a ₂ , a ₃) and SDR (b ₁ , b ₂ , b ₃) spent CoMo/TiO ₂ catalyst. [Reaction conditions: 100 W, CH ₄ /CO ₂ = 1, VHSV = 10 L.g ⁻¹ .h ⁻¹ S/C = 0.1 (for SDR)].	119
Figure 5-13 - Particle size distribution of fresh CoMo1, CoMo1 spent DRM and CoMo1 spent SDR. [Reaction conditions: 100 W, CH ₄ /CO ₂ = 1, VHSV = 10 L.g ⁻¹ .h ⁻¹ S/C = 0.1 (for SDR)].	120
Figure 5-14 - TGA profiles of CoMo/TiO ₂ catalysts after 62 h test for DRM and SDR reactions. [Reaction parameters: 100 W, CH ₄ :CO ₂ =1, VHSV _{DRM} = 10 L.g.h ⁻¹ , S/C _{SDR} = 0.1].	121
Figure 6-1 - The catalytic SDR performance over the CuMo catalysts. [Reaction parameters: CH ₄ :CO ₂ =1, S/C _{SDR} = 0.2].	124
Figure 6-2 - Effects of the S/C ratios on the SDR performance and syngas ratio over CuMo1 catalyst. [Reaction parameters: 100 W, CH ₄ :CO ₂ =1].	126
Figure 6-3 - Catalytic stability of the CuMo1 catalyst. [Reaction parameters: CH ₄ /CO ₂ = 1, MW power = 100 W].	128
Figure 6-4 -The minimum reflection loss (RL) of the fresh Mo/TiO ₂ , Cu/TiO ₂ , and CuMo catalysts.	129
Figure 6-5 - XRD patterns of calcined and fresh (A) and spent (B) catalysts: (a) Mo/TiO ₂ ; (b) Cu/TiO ₂ ; (c) calcined CuMo1; (d) CuMo0.5; (e) CuMo1; (f) CuMo1.5;	131
Figure 6-6 - C, C ₁ : FESEM; D, D ₁ : STEM-BF; E, E ₁ : HRTEM; and F, F ₁ : EELS mapping of fresh (top row) and spent (below row) CuMo1 catalysts. [Reaction conditions: MW power of 100 W, CH ₄ /CO ₂ ratio of 1; S/C = 0.2].	133
Figure 6-7 - EELS mapping of fresh CuMo1 (A) and spent CuMo1.5 (B) catalysts. [Reaction parameters: 100 W, CH ₄ :CO ₂ =1, S/C _{SDR} = 0.2].	134
Figure 6-8 . STEM – HAADF (A), line scanning (B), and corresponding EDX of the fresh CuMo1 catalyst.	135
Figure 6-9 - STEM – HAADF and corresponding EDX of the spent CuMo1 catalyst. [Reaction parameters: 100 W, CH ₄ :CO ₂ =1, S/C _{SDR} = 0.2].	136
Figure 6-10 – TGA profiles of CuMo/TiO ₂ catalysts after 72 h test for SDR reactions. [Reaction parameters: 100 W, CH ₄ :CO ₂ =1, S/C _{SDR} = 0.2].	137

List of Tables

Table 2-1 - Possible reactions in DRM ([109-111]).....	15
Table 2-2 - Summary of coke deposition mechanism reported.....	21
Table 2-3 - Noble metals catalysts for DRM.	26
Table 2-4 – Ni-based catalysts for DRM.....	30
Table 2-5 - The properties of catalyst supports.	45
Table 2-6 – The ϵ' , ϵ'' , and $\tan\delta$ of some materials measured at 298 K [473].....	52
Table 2-7 - Gas-solid catalytic reactions under MW radiation [508].....	59
Table 2-8 - Dielectric loss tangents of different carbon materials. [recorded at 2.45 GHz and 298 K] [35].....	65
Table 3-1 - List of the chemicals used in the study	74
Table 4-1 - BET and porosity of the fresh catalysts. Reproduced from Ref. [579] with permission from the Royal Society of Chemistry.	88
Table 4-2 - BET and porosity of the spent catalysts. [Reaction parameters: $\text{CH}_4:\text{CO}_2=1$, $\text{VHSV} = 10 \text{ L.g.h}^{-1}$]. Reproduced from Ref. [579] with permission from the Royal Society of Chemistry.	89
Table 4-3 - The Rietveld refinement results. Reproduced from Ref. [579] with permission from the Royal Society of Chemistry.	94
Table 6-1 - Textural properties of the fresh catalysts and TiO_2	130
Table 6-2 -Textural properties of the spent catalysts. [Reaction parameters: 100 W, $\text{CH}_4:\text{CO}_2=1$, $\text{S}/\text{C}_{\text{SDR}} = 0.2$].....	130

List of Abbreviations and Symbols

MW	Microwave	-
DRM	Dry reforming of methane	-
SDR	Steam combined dry reforming of methane	-
FTS	Fischer – Tropsch synthesis	-
LNG	Liquefied natural gas	-
GTL	Gas-to-liquid	-
FPSOVs	Floating production, storage and offloading vessels	-
GHG	Greenhouse gas	-
CNG	Compressed natural gas (CNG)	-
POM	Partial oxidation of methane	-
SRM	Steam reforming of methane	-
GCMS	Gas chromatography/ mass spectroscopy	-
FESEM	Field Emission Scanning Electron Microscope	-
XRD	X-ray powder diffraction	-
TOS	Time-on-stream	-
STEM	Scanning transmission electron microscopy	-
HAADF	High-angle annular dark-field	-
BF	Bright field	-
EDX	Energy-dispersive X-ray	-
TGA	Thermogravimetric analysis	-
BET	Brunauer, Emmett, and Teller	-
LHHW	Langmuir–Hinshelwood–Hougen–Watson	-
X_i	Conversion of reactant gas i	%
S_i	Selectivity of product i	%

Chapter 1 Introduction

1.1. Background and motivation

Natural gas is a powerful and friendly fuel resource compared to oil for energy and chemicals productions. Nonetheless, small or remote natural gas reserves have not been developed economically. A significant amount of contained CH_4 gas is therefore stranded whilst associated methane gas generated from oil productions processes is normally flared or re-injected. Such CH_4 amount is unused and wasted while the energy crisis is a visibly existing challenge. The natural gas reserves located in remote or deep offshore areas can be harnessed by liquefying the natural gas (LNG) for transportation using tanks. The main challenge for these processes is logistical barriers for transportation to the resident market, and thereby, associated methane gas is often re-injected or flared. These issues not only result in the loss of income but also pollute the environment due to gas leakage to air. The catalytic conversion of CH_4 to valuable products, such as syngas is a promising solution to tackle the mentioned problems. For the short term perspective, the demand for energy, the reduction of greenhouse gas emission, and liquid fuels of the Fischer-Tropsch products (alcohols, dimethyl ether) from syngas is necessary to be satisfied. Catalytic reforming of natural gas has drawn vast interests of both academic scientists and commercial companies. Among the three methane reforming methods (dry, steam, and partial oxidation), dry reforming of methane (DRM) can satisfy both GHG reduction and alternative fuels production. In fact, DRM has gained growing attention over the last few decades [1]. Moreover, it is well-known that liquid fuel production via the FTS process is heavily dependent on the syngas ratio (H_2/CO) [2-4]. The DRM process can produce an H_2/CO smaller than one which is suitable for heavy hydrocarbons [5-8]. To produce oxygen-contained chemicals via the FTS process, a syngas ratio of ≥ 2 is required [9, 10]. By virtue of an available reactant, the water employed as a co-reactant with dry methane reforming processes to produce an expected syngas ratio is a promising approach to obtain an expected syngas ratio. The combined steam and DRM (SDR) is considered as an industrially practical process to achieve the desired H_2/CO by simply adjusting the amount of water in the feed [11]. The primary obstacle of applying DRM or SDR to produce syngas is the high thermodynamic barrier due to the high thermal stability of methane and carbon dioxide, which requires high temperature (700 – 1200 °C) to be

dissociated and achieve an expected conversion [12]. Notwithstanding a wide prevalence in reforming processes, conventional heating methods consume a considerable amount of energy to break two tenacious reactants [13]. Moreover, employing these heating techniques also requires large and heavy heat exchanger tubes causing difficulties to operate the reforming of methane processes on FPSOVs vessels [14]. In the meanwhile, microwave (MW) reactor system allows reducing equipment, which is at the favor of the riser and mooring systems to produce syngas. MW reactor system is also highly flexible, straightforward to be controlled in its size, quick start/stop facility, high level of safety and automation [15]. Therefore, performing methane reforming reactions under MW heating system is a promising technology, particularly appropriate for FPSOVs to produce liquid fuels from syngas via Fischer – Tropsch synthesis (FTS). In addition, MW is known as a rapid, non-contacted, and energy-saving heating method [16]. The application of MW heating for chemical processes can reduce energy consumption effectively. The MW plasma DRM [17-20], and SDR [21, 22] reactions in the absence of catalysts have been studied by several researchers. Nonetheless, plasma processes have low energy efficiency. This is because a high MW power is required to initiate and stabilize the plasma condition [23]. The introduction of a catalyst irradiated under MW energy has been considered as an effective approach to reduce energy consumption. The primary idea of combining MW and heterogeneous catalytic is to exert volumetric controllable electromagnetic action on the catalyst–reagents system. This action alters the state of the reaction system and leads to a great change in the apparent thermodynamic of the gas-phase reactions resulting in higher conversion values at less extreme conditions [24].

Most of the published works on DRM under MW heating simply used carbon-based materials as a catalyst [25-34] since carbon-based materials are strong MW absorbers. However, the carbon-based catalysts have significantly low stability due to its consumption by its reaction with CO₂ to form CO [35]. Consequently, there is a huge room for the development of catalysts for DRM heated by MW irradiation. Metallic-based catalysts for reforming of methane under conventional heating have been widely studied. Nonetheless, only a few studies on employing metal catalysts for DRM under MW irradiation have been reported yet. This is due to the fact that metals reflect almost the incident MW wave due to its high conductivity, which causes skin effects to reflect MW energy. Zhang and co-workers [36] were pioneers to employ Pt catalyst supported

on aluminum oxide for DRM reaction under MW heating. However, noble metal catalysts are not feasible for large scale applications. Other researchers [37] perform the DRM reaction under MW heating over ruthenium-doped SrTiO₃ perovskite catalyst. In this work, an excessive amount of CO₂ was required to prevent carbon deposition via Boudouard reaction. This addition incurs a heavy down-stream burden to separate or recycle the unreacted CO₂. Moreover, the issue also leads to the complexity of the DRM process [24]. The most recent works producing syngas via MW assisted DRM over Co-Ni catalyst was reported by Varsano et al., [38]. Specifically, the authors employed cobalt as a magnetic component to promote the MW absorption of Ni-Co catalyst for DRM reaction. These studies are the rare reports on MW assisted reforming of methane reactions over metallic-based catalysts in the literature. In the meanwhile, it has been indicated that magnetodielectric materials, which possess both magnetic and dielectric properties simultaneously are strong MW absorbers [39-41]. Cobalt, known as a ferromagnetic element [42], can combine with other paramagnetic metals such as molybdenum [43], to form magnetodielectric materials [44]. In addition to this, cobalt is known as a good catalyst/promoter for reforming reactions [45-48]. The coke – deposition which leads to catalyst deactivation, is one of the main constraints of the cobalt-based catalyst applications [49]. Moreover, molybdenum is considered as an environment-friendly and cost-effective catalyst with longstanding stability for hydrogenating reactions [50]. Thus, the addition of Mo in Co catalyst supported on Al₂O₃ suppresses coke deposition during the reforming process [51]. In the literature, Co/Al₂O₃ [52, 53] and Mo/Al₂O₃ [54] catalysts exhibit catalytic activity for DRM under conventional heating. Meanwhile, Co-Mo catalyst has been intensively investigated as an efficient catalyst for several processes including hydrodesulfurization [55-58], hydrotreatment [59, 60], syngas conversion [61], and natural gas decomposition [51]. Nonetheless, a high efficient Co-Mo catalyst for DRM, particularly under MW irradiation, has not been reported. In the meanwhile, the research community has also paid huge attention to earth-abundant, affordable, less safety concern, and high activity metallic catalysts for gas-phase reactions. One of the most well-known of such catalysts is copper. Supported copper-based catalysts are widely employed in many industrial applications not just only because of their high catalytic performance but also due to their affordability. Moreover, the reduction of Cu²⁺ to Cu⁺/Cu⁰ deposes copper as a redox-active center for chemical reactions [62-65]. Such advantages render Cu-based materials as highly favorable

catalysts for gas-phase reactions in industry [66-69]. Copper-based catalysts have been illustrated their high activity for DRM [70-75] and SDR [75-77] under conventional heating. Nonetheless, none of the copper-based catalysts utilized for reforming of methane under MW irradiation have been reported. One of the possible reason is that copper is one of the opaque materials together with silver and aluminum reflecting MW wave due to its high conductivity [78]. All mentioned advantages and existing challenges have thus simulated the huge interests to develop a novel copper-based catalysts for MW assisted reforming of methane.

1.2. Objectives

To understand these questions and fill up the above-mentioned knowledge gaps are the main motivation of this research. The objectives of this work are to explore the catalytic activity and stability of metallic-based catalysts for MW assisted reforming of methane reactions for producing syngas. The detailed objectives of this thesis are:

- to design, prepare, and study the catalytic activity and stability of metallic-based catalysts for MW assisted reforming of methane.
- to investigate the effects of supports on the catalytic performance of catalysts for reforming of methane under MW heating.
- to study the effects of steam addition on the catalytic performance and the syngas ratio.
- to elaborate the activation mechanism of metallic-based catalysts under MW heating for reforming of methane reactions.
- to provide fundamental insights to catalyst design for MW assisted gas-phase reactions.

1.3. Thesis organization

This thesis consists of seven chapters as the following:

Chapter 1: introduces the background and objectives of the current work.

Chapter 2: provides a comprehensive literature review on catalytic reforming of methane processes for syngas production. The applications of MW heating for chemical processes are also discussed. Catalysts for reforming of methane reactions, particularly for DRM

and SDR processes under both conventional and MW heating are critically reviewed. This chapter aims to identify the existing research gaps and potential catalyst candidates for the current study.

Chapter 3: provides the details of research methodology, materials, experimental setup, analytical technique, and instruments.

Chapter 4: studies the catalytic activity and stability of single Co (Mo), and bimetallic CoMo catalysts supported by Al₂O₃ for DRM reaction under MW irradiation. The catalytic activation mechanism under MW irradiation is also attempted.

Chapter 5: studies the catalytic activity and stability of CoMo catalyst supported by TiO₂ for both DRM and SDR reactions under MW irradiation.

Chapter 6: studies the catalytic activity and stability of CuMo catalyst for SDR. The activation mechanism of the non-magnetic CuMo catalyst under MW irradiation is also investigated.

Chapter 7: summarizes meaningful findings of this study. This chapter is also devoted to the recommendations for future works.

Chapter 2 Literature review

2.1. Introduction

The amount of easily accessible oil is gradually reducing while the demand for the world's energy is increasing consecutively [79]. The investigations on alternative resources, for example, the associated and stranded gas reserves are considered as one of a promising approach to deal with the energy crisis. According to statistics of January 2016 [80], global offshore resources were about 135 billion tones while offshore natural gas resources were about 40 trillion cubic meters. As predicted by 2040, the amount of oil and gas - related offshore activity is poised to increase [81]. The natural gas reserves that are located in remote areas or deep offshore can be harnessed by liquefying the natural gas (LNG) for transportation using tanks. The main challenge of LNG process is transportation to the resident market. Hence, such natural gas is often stranded. In the meantime, associated CH₄ gas formed during oil productions is re-injected or flamed in the reservoir, which is wasted and uneconomical. More importantly, flaring has become more stringent due to environmental pollution from gas leakage to air. Gas – to – liquid (GTL) processes are promising approaches to exploit and employ associated and remote natural gas resources as the feedstocks for liquid fuel production. The specialized GTL process companies have turned to focus on associated gas, which has not currently been exploited economically [82]. Nonetheless, there are several issues needed to be taken into account when applying the GTL process on floating production, storage and offloading vessel systems (FPSOVs). One of the first and foremost considerations is the mechanical stability of the equipment used that needs to be stable for marine motions to deal with inclination and inertia effects. The system weight is also a very important factor to ensure its suitability for floating vessels.

In the main stream, the issues associated with greenhouse gases (GHG) emission have become a large concern of the global community. GHG is one of principal reasons to provoke an escalation in global warming, climate change, ozone depletion, and adverse effects on biodiversity as well as humans. The statistics of global GHG emission in 2010 is shown in **Figure 2-1**. There were two main carbon dioxide sources: (i) forestry and other land use; and (ii) fossil fuel and industrial processes which accounted for more than half of GHG emissions. Other GHG such as methane, nitrogen oxide (N₂O), and

fluorinated gases (F-gases) were 16, 6 and 2 %, respectively. By statistic, CH₄ and CO₂ are the two most dominant elements of the GHG distribution presented in the atmosphere.

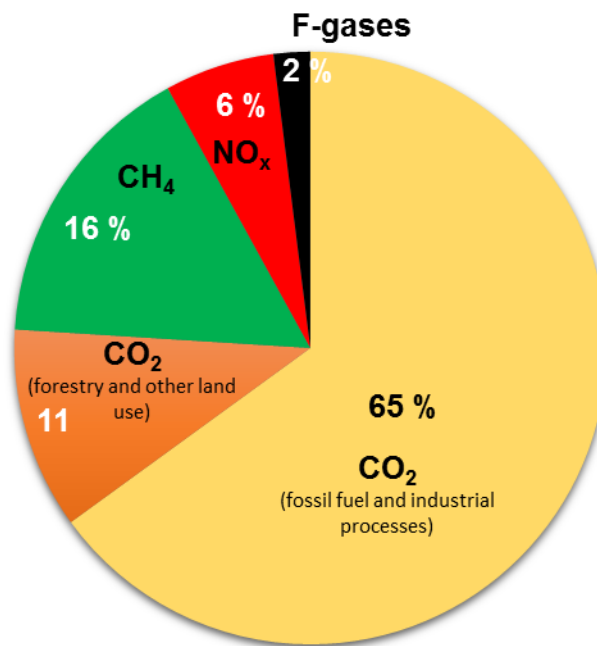


Figure 2-1- Global GHG emissions in 2010 [83].

Extensive researches have been made to turn GHG to valuable syngas (H₂ and CO), such as steam reforming of CH₄ (SRM), partial oxidation of CH₄ (POM), and CO₂ reforming of CH₄ or also called dry reforming of methane (DRM). Among these reforming processes, DRM utilizes two GHG components to produce syngas directly. Nonetheless, due to the high stability of methane and carbon dioxide molecules, a larger energy input is required to convert these molecules into hydrogen and carbon monoxide. Microwave (MW) is known as a non-contact, effective and selective heating method for chemical reactions [84]. Moreover, MW heating is a rapid heating method, which can reach a high temperature in a very short time compared to conventional heating [85]. More importantly, the MW reactor system is flexible, re-allocable with appropriate size, which is suitable for FPSOVs to produce liquid fuels via FTS. Most of the work on DRM under MW irradiation reported in the literature have used carbon-based materials as a catalyst due to its strong MW absorption ability. These kinds of catalyst, nonetheless, has limited catalytic stability. The research activities have turned to use supported metallic-based catalysts to achieve a higher reforming performance and better catalytic stability. Nonetheless, there only a few researchers reported in the literature who use the MW

activated metallic-based catalysts for DRM. In another aspect, DRM produces syngas with an H₂/CO ratio of ≤ 1 , which is preferred for hydrocarbons synthesis only and not favorable for oxygen-contained production via FTS process. Moreover, DRM always involves rapid coke deposition resulting in low catalyst stability. The introduction of steam in the feed gases has been illustrated to produce higher H₂/CO ratio and to limit coke deposition due to the oxidation of steam.

This chapter aims to review critically the development and current status of catalytic reforming processes under both conventional and MW heating for syngas production from 1970s to date. This review starts by introducing background of offshore GTL processes. Then, methane reforming processes including steam reforming of methane (SRM), partial oxidation of methane (POM), DRM, and combined reforming of methane are discussed with emphasis on DRM and SDR processes. Catalysts and supports reforming of methane reactions are reviewed comprehensively and followed by catalyst preparation methods. Background of MW heating and catalysts for MW assisted reforming of methane are presented in the latter sections followed by the evaluation of the previous and existing work. Challenges and opportunities of MW assisted methane reforming are identified to propose a suitable research methodology to fill existing knowledge gaps in this field.

2.2. Offshore GTL processes

2.2.1. Stranded gas utilization alternatives

Presently, crude oil is predominantly used as a feedstock for synthesizing of many chemicals and fuels. Nevertheless, the recent dramatic escalation in the crude oil price and the ongoing depletion of oil reserves have resulted in a renewed interest in alternative energy resources. Moreover, there are also problems related to environmental risks due to GHG emissions, which have been a major concern over the last few decades. For these matters, the development of alternative renewable energies has become more significant. While the known reserves of crude oil have appeared to be trapped, the known availability of natural gas has increased. This has led to the utilization of natural as an energy source. Notwithstanding the reserves of natural gas are plentiful; nonetheless, they are located in remote areas, for instance in Australia, they are north-west Western Australia and off Victoria's south-east coast areas, where transportation to the market is problematic.

Significant quantities of natural gas can also be flared as an unwanted by-product in oil production. On the other hand, most of the small reserves are stranded: in the case of related products, for example, gas produced with crude oil, the natural gas has to be re-injected [86]. This not only results in the loss of income but also pollutes the environment due to gas leakage to air. Moreover, the unavailability of pipeline systems, particularly for remote offshore areas, makes the issue is more difficult. Because of this, there is a sustained demand for small-to-medium-sized process to use and store natural gas on floating production, storage, and offloading vessels (FPSOVs). A number of solutions have been proposed to exploit stranded gas, such as compressed natural gas (CNG), Liquid natural gas (LNG), Methanol and Gas-to-liquid (GTL) process. In LNG, natural gas is cooled down to $-162\text{ }^{\circ}\text{C}$ to liquid form while it is compressed at a high pressure 20-30 MPa for safe non-pressurized storage or transport. LNG offers a lower volume than CNG processes. Specifically, the volumetric energy density of LNG is about 2.4 times larger than that of CNG (at 25 MPa). Consequently, LNG is more efficient in long-distant marine transport than CNG. Natural gas, on the other hand, can be effectively converted to syngas or other liquid synthetic fuels. Since the final product is a chemically synthesized liquid, it is distinguished from a liquefied natural gas (LNG), which is a physically liquefied natural gas by treatment of natural gas at low temperature or high pressure. Compare to LNG and CNG which require larger and expensive equipment, GTL technology is one promising possibility for making these remote gas reserves commercially attractive, particularly in Australia.

2.2.2. GTL process

The recent rapid depletion of oil sources has resulted in huge concerns on looking for alternative energy resources. The production of synthetic oil from natural gas stored in stranded gas fields as a new energy resource is considering as a promising approach. The GTL process refers to a chemical process of converting natural gas to syngas or hydrocarbon produced therefrom. With GTL technology, natural gas can be converted to liquid fuels, which can be liquefied and allows straightforward transportation. The interest in GTL technology is not only due to plentiful reserves but also because of strict restrictions on allowable emissions of dangerous gases such as SO_x and NO_x . Consequently, fuels produced from natural gas offer great environmental advantages over transportation fuels derived from crude oil. This is because they are essentially free of

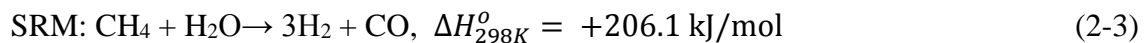
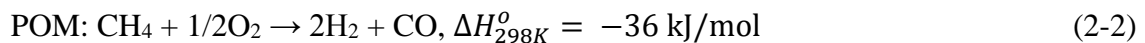
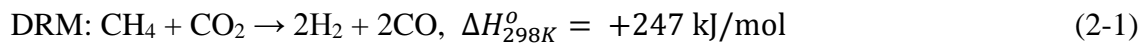
metals, aromatics, and sulfur. More importantly, the GTL process has been applied in medium-to-large sized on-land gas fields, which is suitable for using on FPSOs. Natural gas in many offshore areas is plentiful [87]. Nonetheless, it is hard to access to exploit and transport to the market due to the logistical obstacles leading to high production costs. Most large offshore gas discoveries are plugged, leading to the re-injection or flaring gas associated with oil production. Another highly interesting option is to convert the gas into a liquid products via the GTL technology on FPSOs. Being obtained in liquid, stranded gas can be easy to handle and transport. Further, the synthetic oil products produced by the GTL process passes through a desulfurization process, and thus, the resulting product is a sulfur- free clean fuel and is advantageous over petroleum or other automobile fuels. With GTL, the fuels product can be stored, grasped, and retailed by well-established methods for today's diesel engines. Moreover, the GTL is particularly advantageous when the crude oil price is significantly higher than the gas price. The GTL products can also be shipped by blending with the produced crude oils. A typical GTL process, is a process whereby liquid fuel or chemical products are produced by the FTS process using syngas (CO and H₂), which can be manufactured by reforming processes. Basically, the GTL process can be followed by three steps: (i) in this first stage, syngas gas is manufactured from reforming processes such as DRM, SRM, or POM; (ii) a second stage is to converts the syngas into liquid hydrocarbons over the FTS; (iii) in the final stage, products with desired properties are tailored by cracking and isomerization. This yields high-quality liquids such as alcohols, diesel, lubricant oil, which are refined into a specific state of liquid fuels. The next following sections are going to review single steps of the GTL process.

2.3. Methane reforming to syngas

The production of syngas via reforming processes is the initially important step of the GTL process. According to the report of International Energy Agency (IEA) [1], natural gas reserves requested for the world's energy is estimated to raise by thirty to forty percent in the next 25 years. Despite a huge availability of natural gas, most of them are stranded in remote areas. The exploitation and transportation of these reserves to the market incurs a heavy burden due to a huge distance. Hence, converting methane to other useful chemicals, which can be transportable conveniently, is a promising solution to approach this issue. Ever since the formation of syngas from methane and steam discovered by

Sabatier and Senderens in 1902 [88], many different routes on reforming of methane have been developed. As an obvious consequence, there have been given several reviews on this topic [89]. Moreover, methane is also a GHG element together with CO₂ causing global warming. Therefore, the transformation of methane to syngas is considered as a promising solution to contribute to a carbon-neutral energy chain in the future. For the short term perspective, the demand for energy and liquid fuels such as the FTS products (or methanol) from methane is very is necessary to be satisfied [90].

Syngas (H₂ and CO) which can be produced by reforming of methane can be used for producing liquid fuel is a valuable feedstock of the FTS process. Basically, there are three main reforming processes of methane with the corresponding reactions expressed as following:



Each reforming process allows the possibility to achieve various objectives. For instance, SRM can produce a high syngas ratio while POM reduces the required input energy consumption. In the meantime, DRM displays its environmental benefit, utilizing GHG to produce syngas. The next sections will evaluate both the advantage and drawback of each process.

2.3.1. Steam reforming of methane

In 1868, Tessie du Motay and Marechal, were the firsts to report the transformation of hydrocarbons into hydrogen in the presence of steam [91]. Nonetheless, the detailed study on catalytic SRM was first published in 1924 by Neumann and Jacob [91]. Many patents were issued around 1930 and the first industrial steam reformer was also installed in this year at Baton Rouge by Standard Oil of New Jersey [92]. This reforming process is known as a preponderant industrial process for syngas production. The SMR process is a mature technology operating at or close to the theoretical limits of the reforming process. The SRM can produce nearly all the idea H₂/CO ratio of three (**E.q. (2-3)**). It has been reported that SRM accounts for about 95 % of hydrogen production in the United States in 2012 [93]. A fact that the SRM process can be used with many different feedstocks

including methane, ethane or higher hydrocarbon, methanol, and ethanol. Much research has been performed to employ and character heterogeneous catalysts using these feedstocks. A great deal of attention is focused on utilizing methane as a feedstock due to favorable byproduct formation as compared to other counterparts [93]. Syngas production through steam reforming is can be performed over multiple stages; a typical SDR process as can be seen in the process train shown in **Figure 2-2**.

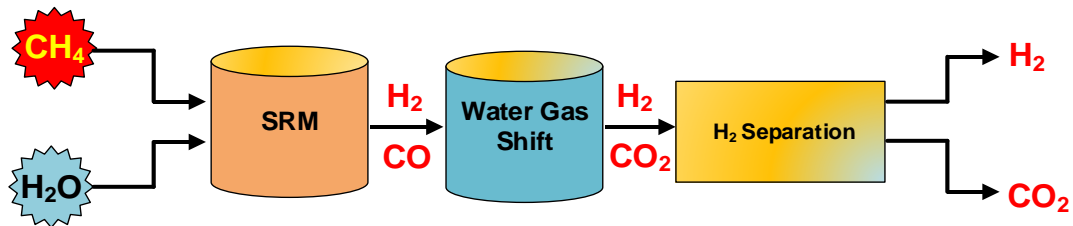


Figure 2-2 - Diagram of multiple stages for syngas production from SRM.

The SRM process is usually operated in harsh reaction conditions, for example, the temperature is in range of 800 – 1000 °C with pressure range of 14–20 bar over heterogeneous catalysts, such as nickel [94]. The products include H₂, CO, CO₂, and H₂O [95]. Hydrogen can be produced via the SRM effectively. This is due to the co-product, CO, reacts with the reactant H₂O through the forward water-gas shift (WGS) reaction ($\text{CO} + \text{H}_2\text{O} \leftrightarrow \text{CO}_2 + \text{H}_2$) to produce additional hydrogen and the obtained syngas ratio is thus always above 2. Furthermore, oxygen is not available in the reforming reactor which can help to improve operating safety. In addition to this, carbon deposition is considerably limited by its gasification reaction with steam on the catalyst surface. The availability of water reactant also makes SDR to be more attractive. Nonetheless, the WGS reaction, which forms unexpected CO₂, is inevitable during SRM. Hence, a separation unit in the downstream section (**Figure 2-2**) is necessary to separate CO₂. Moreover, the SRM process requires an excess superheat steam into the feed to reduce side products formed by WGS reactions. The high-temperature inter-surface tubular heat exchanger is inefficient and expensive for its material and manufacture, which is in overall, lead to heavy capital investment. Therefore, pursuing a more efficient way to reform methane for syngas production is a continuing objective.

2.3.2. Partial oxidation of methane

An alternative process for syngas production is partial oxidation of methane (POM). This

is exothermic and normally performed over a metallic catalyst system [96]. In this process, CH_4 reacts with oxygen, or even with air to form H_2 and CO upon a heterogeneous catalyst. Ideally, the syngas ratio of 2 can be produced (**Eq. (2-2)**). Thermodynamic analysis of POM process indicated its superiority towards SRM [97, 98]:

- Partial oxidation reaction is exothermic whilst SRM is a highly endothermic reaction. Hence, the POM reaction would be more economical than SRM in terms of heating energy. Due to the mild exothermicity of the POM reaction, it can be performed autothermally.
- The syngas ratio produced in stoichiometric partial oxidation is approximately of two, which is ideal for the subsequent FTS process to synthesize methanol.
- The syngas produced from POM reaction can be extremely low in carbon dioxide content, which reduces the burden for the downstream separation unit.
- Partial oxidation reaction excludes the expensive superheated steam systems.

Despite the advantages of high energy efficiency, none of the commercial POM plants are available. The reason for this is a number of engineering problems related to POM reaction such as mass and heat transfer issues, safety concerns with the presence of oxygen in the reaction at extreme reaction conditions [99, 100]. Moreover, a pure oxygen source is also needed to obtain the high quality of produced syngas, and this resulted in a need for heavy capital investment [101].

2.3.3. Dry reforming of methane

DRM is a fuel-switching process utilizing GHG elements (CH_4 and CO_2) to produce valuable syngas. The DRM reaction was first studied over nickel and cobalt catalysts by Fisher and Tropsch in 1928 [102]. Ever since that, the research on DRM has been drawn constantly growing attention. Recently, the interest in the DRM process for syngas production has noticeably escalated owing to environmental concerns and commercial application needs. **Figure 2-3** shows the most common chemical conversion routes of CO_2 into hydrocarbons and liquid fuels. Methanol production from the hydrogenation of CO_2 is intensively studied in literature [103], [104], [105], [106], [107]. This process can be used as a direct route to methanol. Compared with the hydrogenation process or other CO_2 conversion routes, such as reversed water gas shift (RWGS), Boudouard reaction, DRM provides wider applications for liquid fuels production [108].

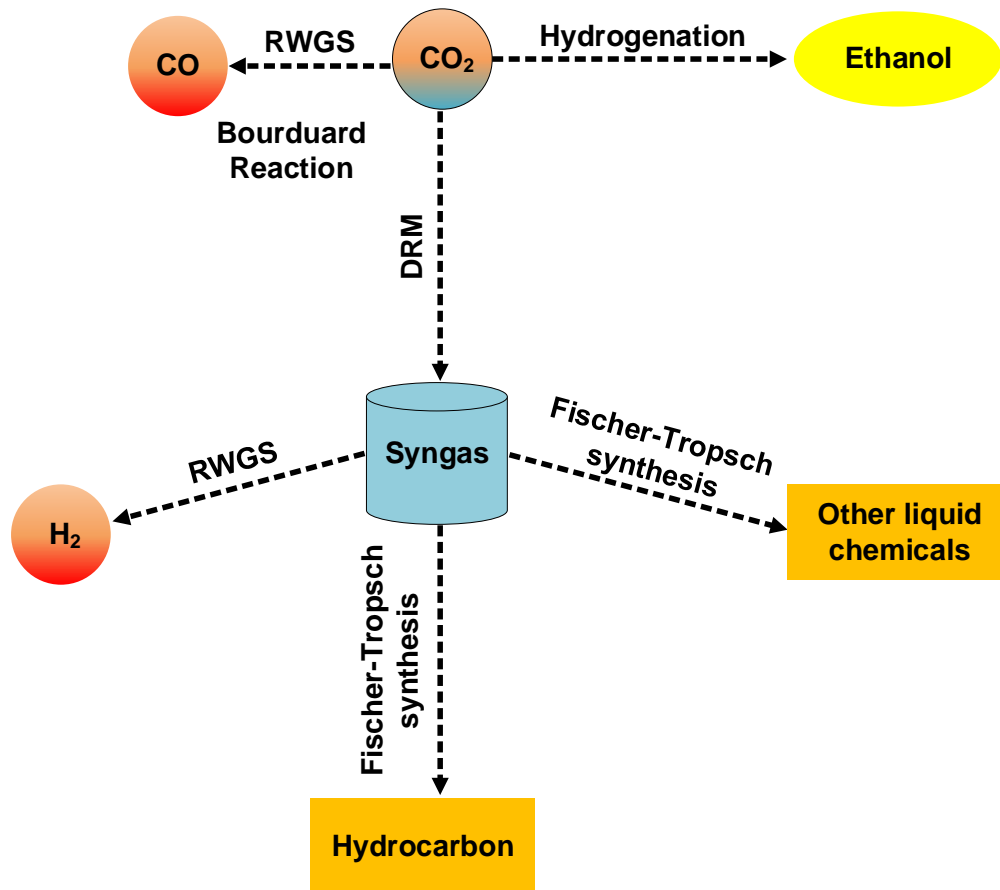


Figure 2-3 – Schematic diagram of main routes of CO₂ utilization into fuels [108].

The scope of this section is to critically review the present state of works on the DRM process. The thermodynamics of DRM is first evaluated, followed by the discussion on the mechanisms of DRM reaction and coke deposition.

2.3.3.1. Thermodynamic and reaction mechanism

As per **Eq. (2-1)**, the thermodynamics of DRM reactions are not favorable at low temperatures. The thermodynamic barrier is a huge obstacle and unfavorable for DRM reaction, which is based on the input heat to convert the two stable molecules (CH₄ and CO₂). The thermodynamic characteristic of the DRM reaction is necessary to be considered in order to apprehend the constraints, and therefore, provide optimum operating conditions for the DRM reaction.

DRM reaction is a straight reaction of CO₂ and CH₄ as represented by **Eq. (2-1)**. Nonetheless, many other side reactions should also be taken into account. **Table 2-1** shows reactions possibly involved in DRM.

Table 2-1 - Possible reactions in DRM ([109-111]).

Reactions	ΔH_{298K}^0 , kJ/mol	Eq.
$\text{CO}_2 + \text{H}_2 \leftrightarrow \text{H}_2\text{O} + \text{CO}$	41	2-4
$\text{CH}_4 \leftrightarrow \text{C} + 2\text{H}_2$	74.9	2-5
$\text{CO}_2 + \text{C} \leftrightarrow 2\text{CO}$	172.4	2-6
$\text{CO}_2 + 2\text{CH}_4 \leftrightarrow \text{C}_2\text{H}_6 + \text{CO} + \text{H}_2\text{O}$	106	2-7
$\text{CO}_2 + 2\text{H}_2 \leftrightarrow \text{C} + 2\text{H}_2\text{O}$	-90	2-8
$2\text{CO}_2 + 2\text{CH}_4 \leftrightarrow \text{C}_2\text{H}_4 + 2\text{CO} + 2\text{H}_2\text{O}$	284	2-9
$\text{C}_2\text{H}_6 \leftrightarrow \text{C}_2\text{H}_4 + \text{H}_2$	136	2-10
$\text{CO} + 2\text{H}_2 \leftrightarrow \text{CH}_3\text{OH}$	-90.6	2-11
$\text{CO}_2 + 2\text{H}_2 \leftrightarrow \text{CH}_3\text{OH} + \text{H}_2\text{O}$	-49.1	2-12
$2\text{CH}_3\text{OH} \leftrightarrow \text{CH}_3\text{OCH}_3 + \text{H}_2\text{O}$	-37	2-13
$\text{CH}_3\text{OCH}_3 + \text{CO}_2 \leftrightarrow 3\text{CO} + 3\text{H}_2$	258.4	2-14
$\text{CH}_3\text{OCH}_3 + \text{H}_2\text{O} \leftrightarrow 2\text{CO} + 4\text{H}_2$	204.8	2-15
$\text{CH}_3\text{OCH}_3 + 3\text{H}_2\text{O} \leftrightarrow 2\text{CO}_2 + 6\text{H}_2$	136	2-16
$\text{CO}_2 + 4\text{H}_2 \leftrightarrow \text{CH}_4 + 2\text{H}_2\text{O}$	-165	2-17
$\text{CO} + 3\text{H}_2 \leftrightarrow \text{CH}_4 + \text{H}_2\text{O}$	-206.2	2-18

As can be seen that all reactions presented in **Table 2-1** are governed by the reaction temperature. It was found that coke formation reactions such as **Eq. 2-5 & 2-8** are highly preferred at high temperature while the reaction to form complex molecules such as dimethyl ether (**Eq.2-13**) are less favored at high temperatures [112]. Therefore, the **Eq. (2-11), 2-12, and 2-13** are less prone to occur at temperatures in which the DRM reaction usually takes place (in the range of 650– 1000°C). Likewise, the reactions to form ethane

Eq. 2-7 or ethylene **Eq. 2-10** and **2-9** are not inclined to occur despite the fact that these hydrocarbons are the side products of the DRM reaction [14]. The **Eq. 2-14** and **2-15** reactions impossibly occur at high temperature of DRM due to their strong exothermic nature. Nevertheless, at high temperature (exceeding 1093K [110]), the reverse water-gas shift (RWGS) reaction (**Eq. 2-4**), methane decomposition (**Eq. 2-5**), and Boudouard reaction (**Eq. 2-6**) are vigorously promoted and mostly control the amount of carbon formation and the produced syngas ratio (H_2/CO).

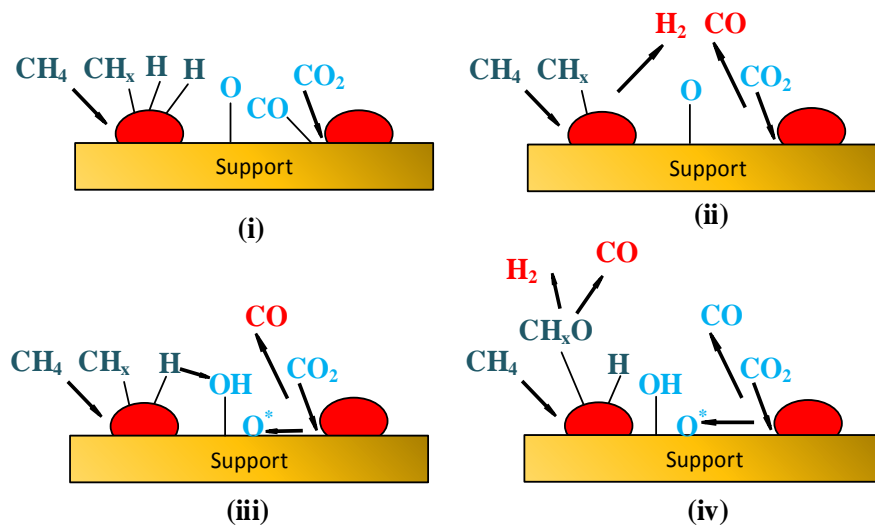


Figure 2-4 - Scheme of general reaction mechanism of DRM.

As such, reactions involved in DRM are complex and have synergistic effects on each other. The mechanism of DRM reaction is thus needed to be interpreted to optimize the expected syngas ratio and limit side products. Researchers have intensively studied the mechanism of the DRM reaction [113-117]. They found that the reaction mechanism of DRM is varied by the catalysts and operating conditions, such as temperature, feed flowrate, reactor, and pressure. In general, the DRM reaction mechanism can be illustrated by **Figure 2-4** and summarized by the following steps [25]:

- (i). Dissociation of methane: This step is determined as the rate determining step. The dissociation energy of C-H_x or CH_x-H_x bonds is also controlled by the surface properties. Each partially dissociated CH_x species adsorbs on the catalyst surface (Figure 2-4).
- (ii). Dissociation of CO₂: The adsorption and dissociation of CO₂ can be occurred by the two different ways: (i) C-only coordination, in which, oxygen and carbon radicals adsorb on the catalyst surface simultaneously. By this way, one exposed

oxygen atom is left; (ii) O-only coordination, in which, both oxygen atoms bond with the catalyst surface. The latter manner is rapid and CO_2 prefers to adsorb on the metal-support interface.

- (iii). Formation of O-H group: Surface hydroxyl groups formed from the reaction between CO_x and H radicals. These groups interact with adsorbed CH_x species to form CH_xO intermediates. After that, these intermediates are decomposed to form CO and H_2 , subsequently. In this approach, the decomposition of CH_4 and CH_xO is slow kinetic steps. The metal-support interface was supposed as an active site for CH_xO formation [118].
- (iv). Oxidation and desorption of intermediates: Oxygen atoms on the metal catalyst surface reacts with a surface group such as CH_x group, CH_xO or $\text{CO}_{\text{surface}}$. Carbon monoxide can be formed by the dissociation of CH_xO and $\text{CO}_{\text{surface}}$ or the reduction of adsorbed CO_2 by carbon on the metal via Boudouard reaction.

The reaction pathways of catalytic methane reforming reaction under MW irradiation are similar to those under conventional heating, but they are exceptionally promoted by MW energy. There are two factors accelerating the reforming reaction pathways under MW heating: (i) thermal and (ii) non-thermal effects. Thermal effects of MW heating represented by hot-spot formation and selective heating have been widely accepted as the primary reasons for the enhancement of reactant conversion and product selectivity of gas-phase reactions [119-123], of course, including methane reforming reactions. Specifically, the temperature of the catalyst surface was accelerated rapidly under MW heating. In such ways, micro-plasma or local hot spots having highest temperature due to their greater MW absorption are formed on the catalyst surface, in which, adsorbed CH_4 and adsorbed co-reactants (O_2 , CO_2 , or H_2O) are dissociated vigorously to form syngas. Meanwhile, selective heating resulted in the differences of temperature between the catalyst surface with support or with the average catalyst bed and reactants gas. Due to the gas-phase reforming reaction occurring mainly on the catalysts surface, such this selective heating advantage of MW has been reported to promote reaction rate, higher selectivity for catalytic reforming of methane reactions by promoting the dissociation of adsorbed CH_4 , CH_x , or co-reactants (CO_x , CH_xO) to form syngas and gasifying deposited coke (C^*) [124]. When these thermal effects are taken into account, it can be concluded that the escalation in the reforming reaction rates by MW energy is due to the temperature, and such these rate accelerations is largely dependent on the MW absorption ability of

17

the given catalyst. On the perspective of the later factor, non-thermal effects, which are generated by physical interaction between gaseous molecules and MW, is an ongoing-controversial topic. Though several studies, both theoretically and experimentally, conclusively illustrated that non-thermal MW effects are dubious and non-existent. More convincingly, advanced IR camera (as discussed above) displays the formation of hot spots on the catalyst's surface with a higher temperature than the average temperature of the catalytic bed. Notwithstanding this, several authors [125-129] have claimed the role of non-thermal effects on the enhancement for product selectivity of MW assisted catalytic gas-phase reactions. Several authors [130-132] have stated that MW absorption routine initiates from the coupling of radiation to dipole moments of a given matter, and thereby, there is no reason why MW energy is unable to couple to a gaseous molecules to populate quantum vibrations, which is defined as rotational excited states to promote its dissociation. In such ways, Arrhenius activation energies of gaseous are decreased. These and other fundamental issues related to the non-thermal effects of MW have been discussed lucidly and thoughtfully by Stuerger and Gaillard [133, 134] the reader can look there for more detailed discussions. Another possible witness for the presence of non-thermal effects is from the experimental results of MW assisted reforming of CH₄ [36, 135, 136], which all displayed the exceptionally higher activity of a given catalyst at a similar temperature than that achieved by conventional heating. Therefore, in this perspective, the fundamental mechanism of catalytic reforming of methane under MW heating can be inferred as follows: (i) CH₄ and co-reactants are possibly excited by MW electromagnetic field resulted in their slight vibrations; (ii) these absorbed excited molecules are dissociated, which follows the above mentioned steps of reforming of methane reaction observed under thermal heating, on the catalyst activated by MW energy due to catalyst's ability to absorb MW. The former represents the non-thermal effects whilst the later stands for the thermal effects of MW with hot spot formation and selective heating characteristics, which both accounted for the higher conversions of reactants and the better syngas selectivity attaining by MW heating

2.3.3.2. Carbon deposition

The formation of coke on the catalyst surface is inevitable during DRM reaction. Coke deposition following either the **Eq.2-5** or the reversed Boudouard reaction ($2\text{CO} \leftrightarrow \text{CO}_2 + \text{C}$) is unable to occur in DRM reaction due to their high exothermic characteristic,

which is favorable at low temperature. The methane cracking reaction, shown in the **Eq.2-5**, is highly preferred at high temperature and this reaction is found to be the main source of coke deposition. Without a doubt, coke deposition adversely impacts on catalytic performance of DRM since it blocks catalyst's pores, encapsulates active centers, and collapses the catalyst support [74]. More seriously, coke escalates pressure drop and loss of activity by blocking the reactor, which can ultimately lead to reactor failure [137] (**Figure 2-5**). It is therefore desirable to apprise the reasons, mechanism, and conditions of the formation of coke to limit carbon deposition and promote DRM efficiency.

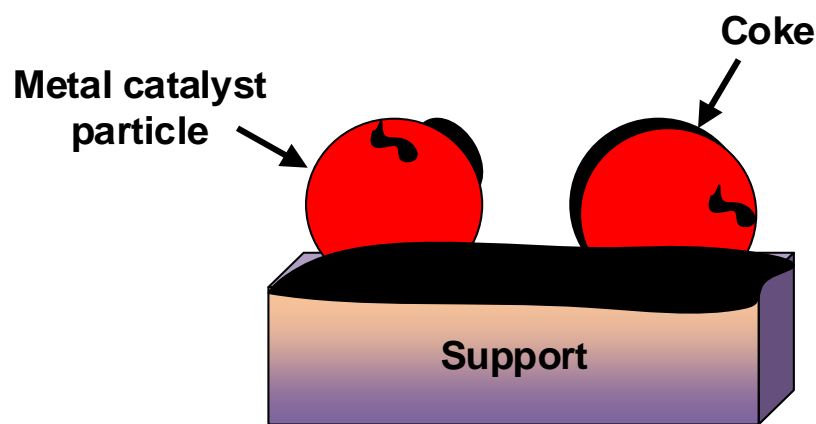


Figure 2-5 - Coke deposited on the metal catalyst particle and support.

There are different types of carbon can be generated during the DRM reaction [138]. Typically, there are three types of carbon which are α -C (carbide surface), β -C (amorphous carbon), and γ -C (graphite) [139]. Among these, α -C was proved to assist the formation of CO whilst other types (β -C and γ -C) lead to catalyst deactivation due to its less activity [140]. To apprise this conclusion, the spent Ni/MgO catalyst characterized by the temperature programmed hydrogenation (TPH) and the result shown in **Figure 2-6** [140].

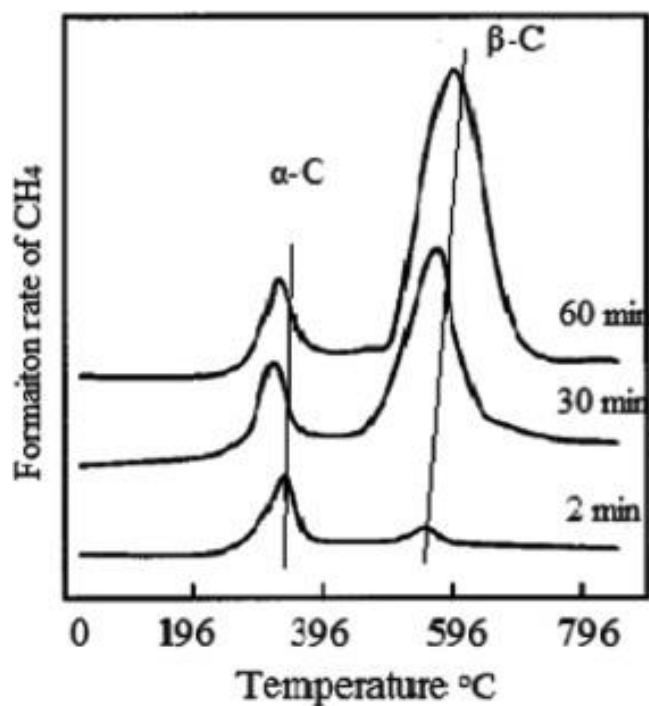


Figure 2-6 - TPH profiles of Ni/MgO catalyst at different contact times and temperature. Reprinted with permission from Ref. [140]. Copyright© 1997 Elsevier.

There are two peaks visibly observed from the TPH graph. The first peak, which is in the range of 300 to 310 °C, was denoted to α -C. β -C was detected at higher temperature regions (580 - 600 °C), which affirms the lower reactivity of β -C towards hydrogen compared to that of α -C. **Table 2-2** summarizes the mechanisms of coke formation during DRM reaction reported in the literature. Basically, the first step of coke formation is the adsorption of methane on the catalyst surface or the interface between the catalyst and the support. The C- H bonding is subsequently dissociated to generate adsorbed carbonaceous species. These formed coke then either stays inside catalyst's pores or desorb to the outer. The growing high strength carbon inside the catalyst particles can push out fragments of the active centers of catalysts as it grows. The catalyst pores can be broken once coke growth reached pore diameter.

Table 2-2 - Summary of coke deposition mechanism reported.

Author	Findings	Ref.
Baker et al.,	The diffusion of carbon over nickel catalysts is the rate determining step.	[141]
Gronchi et al.,	The driving force for carbon diffusion is the dissociation of CH ₄ at high temperature.	[142]
Baker et al.,	Carbon growth is equally governed by the diffusion of carbon through the metal particles and the activation energy of methane decomposition.	[143]
Baghalha et al.,	Coke formation follows four main steps: (i) separation of a catalyst particles; (ii) adsorbed hydrocarbons are decomposed into carbon; (ii) diffusing deposited coke to the catalyst particles; and (iv) coke growth.	[144]
Alstrup et al.,	Coke growth is controlled by the concentration gradient crossing catalyst particles.	[145]
Rostrup-Nielsen et al.,	Coke was dissolute and precipitated driven by temperature. The diffusion mechanism of carbon formation over nickel – based catalysts is the concentration gradient.	[146]

The carbon formation is proportional with the feed reactant ratio. Due to methane cracking as the main reaction to form coke, the excessive presence of CO₂ in the feed such as the CO₂/CH₄ ratio of above 1, deposited coke can be partly gasified by the unreacted CO₂ via the Boudouard reaction, shown in **E.q 7**. Pakhare et al., [147] indicated that the amount of coke deposited at high CO₂/CH₄ ratio is less than that of lower reactant gas ratio. In a good agreement, Guo and co-workers [148] confirmed that the increase in CH₄ in the feed reactant is beneficial to the methane decomposition, and thus, promotes carbon deposition. Nonetheless, the unreacted amount of CO₂ can lead to a heavy burden for a downstream separation to separate CO₂ from syngas product. In addition to the feed reactant ratio, coke deposition is also governed by the reaction temperature since the CH₄ cracking or the Boudouard reaction is the functions of reaction temperature [149]. At above 557 °C, the decomposition of CH₄ takes place preferably whilst the Boudouard reaction occurs at below 700 °C. Therefore, the temperature range of 557 – 700 °C is

widely accepted as preferred conditions for a maximum coke deposition [150-154]. The operating temperatures also effects the types of carbon formed during the DRM reaction. The temperature required for each type of carbon formation is in the order $\alpha\text{-C} < \beta\text{-C} < \gamma\text{-C}$ [111]. The increase in reaction temperature enhances reactants conversions; however, it also promotes carbon deposition. Moreover, it is proved that the presence of steam in the feed gas can reduce coke deposition significantly owing to the coke gasification of steam [155]. Consequently, combining DRM with steam reforming of methane is considered as a promising solution to approach related-coke deposition issues and achieves an expected syngas ratio [156]. Noticeably, MW heating offers another eminent advantage in coke removal due to a well-known strong MW absorption capacity of carbon-based materials [157-160]. A large number of reported works on employing MW irradiation to re-generate catalyst' active centers from coke deposition [161-165] have reflected the great benefits of MW heating for reforming of CH_4 . The research in this field has thus been enormously attractive for both scientists and industries.

2.3.4. Combined reforming of methane processes

From the review above, DRM obtained considerable attention due to its advances in shale gas recovery and turning GHGs to valuable syngas products. Notwithstanding, the syngas ratio (H_2/CO) produced by the DRM process is always lower than unity [82] while the synthesis of oxygenated liquid fuels such as alcohols or dimethyl ether via F-T synthesis is favored at $\text{H}_2/\text{CO} > 1$ [5-8]. The feasible solution is to combine DRM with other reforming processes, such as partial oxidation or steam. Due to highly flammable and extreme purity requirement of oxygen raising operating safety concerns, the combination of partial oxidation of methane with DRM is not highly recommended [166, 167]. On the other hand, by virtue of an available reactant, employing water as a co-reactant with CO_2 to reform methane has drawn much of attention from the research community [168, 169]. The merger between steam and DRM (SDR process) is also indicated as an industrially practice process to achieve the desired H_2/CO by simply adjusting the amount of water in the feed [11]. By only adding a small amount of water into the feed, SDR process lowers operating costs [170, 171] and simplifies process operation than other reforming combinations [166, 172]. Coke deposition caused by methane cracking is considerably reduced by its vigorous oxidation in a highly oxygen-rich system of SDR [173]. Nonetheless, both DRM and SDR reactions are strongly endothermic, and thus, craves a

large input energy for their operations [174]. Most of the current catalytic SDR processes [175-178] are operated under conventional heating, which not only consumes considerable energy but also requires heavy heat exchanger tubes making the reformer system to be complex [14]. Recently, Li et al., [34, 179] is the pioneer group to study the SDR under MW heating over carbon-based catalysts. These works illustrated that expected syngas ratio could be obtained by adjusting the input steam flowrate. Moreover, energy efficiency was found to be 49.2 % at 800 °C with the energy consumption of 4.14 kW.h per m³ syngas produced based on a model of scale-up MW device. Notwithstanding the approved advantages, the short stability of carbon-based catalysts under MW irradiation is a huge challenge. These mentioned matters excite intensive researches to develop better catalysts and optimize process conditions to achieve a better reforming performance.

2.4. Catalyst development for reforming of methane

Perhaps, Kokarev et al., [180] are pioneers reporting catalytic development for reforming of methane processes. Ever since this work, research on DRM have increased explosively [14]. This visible trend is due to the growing interests in producing alternative fuels and reducing GHGs. The DRM has challenged chemical engineering processes for decades due to its high endothermic characteristic requiring high temperature operations. Therefore, energy consumption is a real existing obstacle to operate DRM process. In fact, none of commercial DRM process for syngas production is available in industry. Performing the DRM reaction over a highly active catalyst can reduce reaction temperature and improve reforming efficiency significantly [181]. The catalytic activity for the DRM reaction is mainly governed by active metals, support properties, and the metal-support interaction [111]. Metallic catalysts for DRM are diverse, including many different types such as noble (e.g., Pt, Ru, Rh), non-noble (e.g., Ni-based, Co-based, Cu-based), and perovskite-type catalysts (e.g., LaNi_{1-x}Ru_xO₃, LaNi_{1-x}Mg_xO₃). The metal catalysts are usually supported on a metal oxides, such as Al₂O₃, TiO₂, CeO₂, MgO, and ZrO₂, which provide better stability and hinder coke deposition [182, 183]. These oxides are characterized by surface Lewis base sites. Nevertheless, each parameter has complex effects on the overall performance, and therefore, the catalyst design for the DRM process has considered a tradeoff between activity and stability [70]. The aim of this section is to review the development of catalysts for DRM and SDR under conventional heating. On

the basic of this review, the reason for choosing active centers, supports, and preparation method of catalysts for this project is elaborated.

2.4.1. Active metals

The appropriate selection of active metals for the DRM is a first important step to achieve better catalytic activity and stability. At first for most chemical reactions, the construction of organic molecules requires understanding of the formation and ruination of carbon-carbon (C-C) bonds. It is well known that the C-C bond is difficult to be dissociated owing to its high strength [184, 185]. The non-catalytic processes rearrange organic molecular fragments, therefore, necessitate to vanquish high activation barriers. The power of active catalysts allows one to assemble fragments on the catalyst surface or inside the catalyst's pores as a stepwise process. Specifically, each step has a considerably smaller activation barrier than non-catalytic counterpart (**Figure 2-7**). The competitive bond between metal-carbon (M-C) affords the necessary background for catalysts to transfer reactants to products. It is indicated that the bond dissociated energy of M-C bonds is $38.0 - 66.5 \text{ kcal. mol}^{-1}$, which is much lower than that of C-C bond of $87.4 \text{ kcal. mol}^{-1}$. The rearrangement of organic groups on a catalyst surface results in the breakage of M-C bonds.

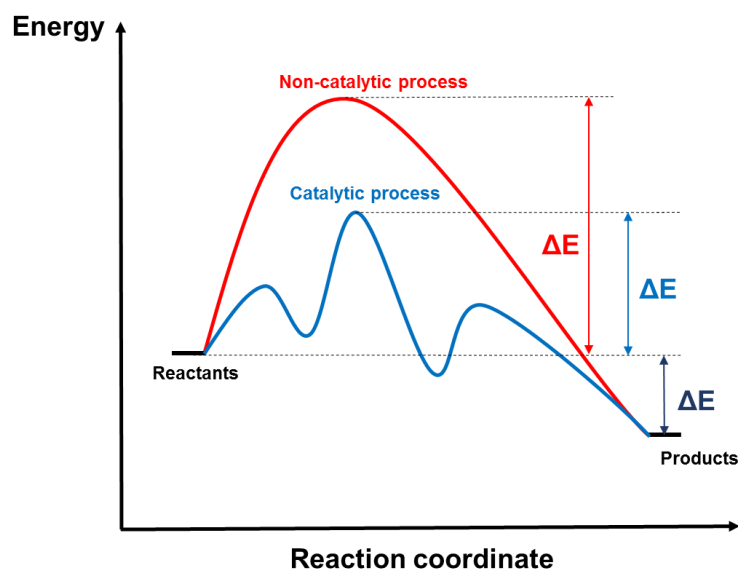


Figure 2-7 - A general energy surface of non-catalytic and catalytic process.

It has been observed that the activation of both CH₄ and CO₂ molecules on the surface of the active metal and of the support depends upon electronic and geometric factors [110, 186]. Therefore, the dissociative adsorption of both molecules is structure sensitive. In other words, the reforming of CH₄ efficiency is strongly dependent on the selection of the active metals, supports, and promoters (if any). These parameters will be critically reviewed in the following sections to propound for the proper catalyst design, particularly, for methane reforming under MW irradiation.

2.4.1.1. Noble catalysts

Without a doubt, the widely-common noble metals, such as rhodium (Rh), ruthenium (Rh), iridium (Ir), palladium (Pd), and platinum (Pt) are highly active towards DRM and are highly-coke resistance than other transition metals [187-189]. The list of noble catalysts employed for DRM reactions is shown in **Table 2-3**.

Table 2-3 - Noble metals catalysts for DRM.

Metal	Support	W (%)	P	RC		Reactor	Conversion (%)		Ref.
				T (°C)	T (h)		CH ₄	CO ₂	
Pt	ZrO ₂	1	IMP	700	4	FBR	79.0	86.0	[190]
Rh	CeO ₂	0.5	IMP	800	50	FBR	50.7	63.2	[191]
	ZrO ₂						65.9	74.2	
Pt	Al ₂ O ₃	1	IMP	800	97	FBR	46.0	48.0	[192]
	ZrO ₂						83.0	94.0	
Ru	Al ₂ O ₃	3	IMP	750	20	FBR	46.0	48.0	[193]
	CeO ₂	3					52.0	60.0	
Pt-Ni	MgO-SiO ₂	0.01-5	IMP	700		FBR	80.7	-	[194]
Rh-Ni	Ce _{0.75} Zr _{0.25} O	14-0.7	IMP	750	17	FBR	6.9	11.8	[195]
Ru	Al ₂ O ₃	5	IMP	750	-	FBR	91.0	90.0	[196]
	CeO ₂	5					90.0	96.0	
Ru-Ce	Al ₂ O ₃	3-5	IMP		-	FBR	97.0	97.0	
Rh-Ni	MCM-41	0.19	DHT	600	14	FBR	31.0	41.0	[197]
Rh	SiO ₂	0.5	IMP	800	50	MR	71.9	77.2	[191]
Pd	CeO ₂	0.06	IMP	800	12	FBR	92.5	97.3	[198]
Pd-Ni	Al ₂ O ₃	0.1	IW	700	2	FBR	83.2	92.3	[199]
Ir	Ce _{0.9} Gd _{0.1} O _{2-x}	0.2	WI	800	22	MR	99.0	99.0	[200]

W: metal weight; P: Preparation method; T: temperature; t: time; IMP: Impregnation; IW: Impregnation wetness; WI: Wet Impregnation; DHT: direct hydrothermal synthesis; FBR: Fixed bed reactor; MR: Micro-reactor.

The superiority of the noble metals is due to their high coke-resistant ability compared to non-noble counterparts [201]. Almost noble metals display no coke deposition, except for Pd-based catalyst, which has coke formation with the deposited rate of 4.9 mg coke.g⁻¹.cat⁻¹.h⁻¹ [111]. Nonetheless, this rate is found to be much smaller than nickel - or cobalt-based catalysts, which, in turns, are approximately 24 and 49.4 mg coke.g⁻¹.cat⁻¹.h⁻¹

respectively [202]. Other researchers [203], [196], [204], [190] also confirmed the exceptional resistance to carbon deposition of noble catalysts. Such values evidently reflect the advantages of noble metal catalysts for the DRM. By comparing among common noble catalysts, Rh supported catalysts display the best catalytic efficiency and stability. This is followed by Ru, Ir, Pd, and Pt [111]. Moreover, it was found that Ru and Rh exhibit higher catalytic activity than Pd and Pt at a same particle size and dispersion [205-207]. The lower catalytic performance of supported Pd and Pt catalysts are due to their lower thermal stability causing their worst sintering at high temperatures. Such observation were also affirmed by Tsyganok et al. [202] and Matsui et al. [208].

Furthermore, noble metals are also employed as a promoter to improve catalytic performance for non-noble catalysts such as nickel or cobalt. Nickel catalysts promoted by Rh [209], [210], [211]; Pt [212], [213], [214]; Pd [215], [216] or Ru [217], [197] possessed higher activity and better stability than non-promoted Ni catalysts. For instance, Pt promoted for Ni catalyst supported on ZrO₂ prolonged a longer period of time on the DRM stream test in comparison with single Ni catalyst supported on ZrO₂ [214]. In another study, the presence of Rh enhanced catalytic activity of nickel catalyst significantly due to the role of Rh preserving nickel particles in metallic form by hydrogen spill-over [218]. The similar observation was also confirmed via the XANES analysis results of Rh-Ni catalyst for DRM [219]. Arandiyan et al. [220] elaborated the catalytic performance of different perovskite catalysts promoted with different noble metals for DRM reaction. In this study, La_{0.4}M_{0.6}Al_{0.2}Ni_{0.8}O₃ with M is doped with noble metals of Ir, Pd, Pt, Rh, and Ru, respectively. This work found that the improvement for La_{0.4}M_{0.6}Al_{0.2}Ni_{0.8}O₃ catalyst is in the order of Rh > Ru > Ir > Pt > Pd. Hou and co-workers [205] also made a similar observation. Specifically, the authors also found that Rh and Ru catalysts have higher stability than Pd catalyst, which is mostly deactivated at 850 °C on the DRM stream test. El Hanssan and co-workers [221] also found that the conversion of the reactants were higher with the presence of Rh compared to those of monometallic Co₁₂/SBA-15 and Co₁₂/SiO₂ catalysts over about nine hours of the DRM stream test. In addition to the catalytic activity, the study also found that a significant amount of cobalt particles migrated to the outer of the pores of Co₁₂/SBA-15 catalyst, which resulted in the sintering of these particles forming the bigger size of 30 nm compared to that of the reduced Co⁰ species in the pores with 11.6 nm, approximately. In contrast, the presence of Ru in Co₁₂ catalyst supported on SBA-15 diminishes the

movement of active metals to the pores' outer, and therefore, minimizes the sintering and improves the catalytic activity. These results further reinforce the conclusion on the important roles of noble metals in offering superior anti-sintering and providing a highly stable catalyst. The presence of noble elements in non-noble catalysts improves reducibility, surface oxygen concentration, and surface area [205], which enhance non-noble catalytic activity, limit coke formation [222], and reduce catalyst sintering [221].

Notwithstanding a large amount of coke deposited on Ni-based and Co –based catalysts over the DRM reaction, the higher initial reactant conversions are observed from these non-noble catalysts compared to the noble metals, except for Rh [223, 224]. Such observations reflect the high catalytic activity of transition non-noble metal catalysts. Nonetheless, under different specific support and reaction conditions, noble metals show better catalytic activity than those of nickel and cobalt. From **Table 2-3**, it is well established that the monometallic noble metal catalysts or catalysts doped noble metals display high catalytic activity and high coke-resistance for DRM reaction. Despite these advantages, the expensive cost and less availability of these noble catalysts limit their large scale applications. Therefore, low-cost catalysts are at a high interest for the commercialization of DRM for syngas production.

2.4.1.2. Non-noble catalysts

Non-noble metals have been commonly employed as catalysts in many chemical reactions such as photocatalytic [225], [226], electrocatalytic [227], [228] and gas-solid reactions [229], [230] owing to their affordability, availability, and high catalytic activity. The expansion of this non-noble catalysts began in 1964 when Jasinski [231] reported a novel cobalt catalyst for oxygen reduction in an alkaline environment. The non-noble catalysts for DRM reaction first reported in 1988 was nickel [232]. The subsequent evolution in this field was made 90's, when it was discovered that the heat treatment for nickel-based catalyst producing a comparable activity for DRM towards noble catalyst such as Pt, Ru, and Ir [223], [233]. Despite its highly catalytic activity, none-noble catalysts have low stability [201, 234, 235]. In the literature, the main reason of the deactivation of non-noble catalysts over DRM is coke deposition [235, 236]. This section is dedicated to review the prevalent non-noble catalysts employed for reforming of methane process by highlighting the major advances and existing downsides of this class

of catalysts. Following this, a short discussion on the selection of catalysts for DRM in this study is also attempted.

2.4.1.2a. Nickel - based catalysts

By comparing with the noble catalysts, nickel – based catalysts are more practical from industrial standpoints because of their high catalytic activity, affordability, and wide availability [237]. Ever since the hydrogenation reactions of unsaturated compounds at atmospheric pressure over a nickel catalyst was first discovered in 1897 by Sabatier and Senderens, who were then awarded the Nobel Prize in 1912 [238], the history of heterogeneous nickel catalysts has initiated. The revolution for the prevalence of nickel catalysts officially came in 1927 when Murray Raney [239] patented a highly reactive form of nickel catalyst, which was prepared by the treatment of nickel-aluminum alloy with sodium hydroxide solution. The primary properties of nickel catalyst are represented via elementary steps, which can promote different transformations of reactant molecules [240]. **Table 2-4** presents the applications of nickel –based catalysts for DRM reactions. Many different preparation methods including impregnation, co-precipitation or hydrothermal methods can be used to prepare nickel-based catalysts. Monometallic nickel catalysts with different supports displayed its greatly catalytic activity, averagely, above 70 % conversions of CO₂ and CH₄ (**Table 2-4**). The nickel-based bimetallic catalysts or perovskite catalysts, similarly, also provide the high reactant conversions.

Table 2-4 – Ni-based catalysts for DRM.

Metal	Support	W	P	RC		Reactor	Conversion		Ref.
				T	t		CH ₄	CO ₂	
Ni	Al ₂ O ₃	0.2	WI	700	24	FBR	78.2	78.5	[241]
	ZrO ₂	0.2	-	800	50	FBR	84.1	81.4	[242]
	CeO ₂	0.02	CS	650	12	FBR	65.2	-	[243]
	MgO	0.2	CP	900	-	FBR	98.1	95.6	[244]
	MCM-41	0.12	CH	750	30	FBR	82.4	86.5	[245]
	SBA-16	0.05	IWP	700	100	TR	73.4	78.2	[246]
	TiO ₂	0.01-5	IMP	700	16	FBR	79.1	80.2	[247]
	La ₂ O ₃	0.002-0.01	CS	700	110	FBR	82.1	84.5	[114]
	SiO ₂	0.05	IMP	700	50	FBR	78.5	71.6	[248]
	Li-SiO ₂						15.4	10.8	
Ni-Mo	SBA-15	5-25	IWIMP	800	120	FBR	84.0	96.0	[249]
Ni-Ce	SiO ₂	10-5	IWIMP	800	30	FBR	81.4	87.5	[250]
Ni-Rh	MCM-41	0.19	DHT	600	14	FBR	31.0	41.0	[197]
Ni-Zr		0.12	IMP	750	30	FBR	90.5	-	[251]
Ni-Fe	-	0.1	DP	650	10	FBR	31.2	32.4	[252]
La _{0.8} Sr _{0.2} Ni _{0.8} M _{0.2} O	-	4.9	SG	800	24	MR	75	60	[253]
(M=Bi, Co, Cr, Cu, Fe)									
Pd-Ni	Al ₂ O ₃	0.1	IW	700	2	FBR	83.2	92.3	[199]
Ni-Co		0.18	IMP	700	6	FBR	62	71	[254]

PBR: bubbling-bed reactor; CS: Combustion synthesis; CP: co-precipitation; CH: conventional hydrothermal; TR: Tubular reactor;

IMP: Impregnation; DP: discontinuous precipitation.

Researchers [229, 255] indicated that the low dissociative energy of absorbed hydrocarbon on nickel surface (Ni-C bond energy is about 38.0-51.1 kcal.mol⁻¹) within the group of metals accounted for its exceptional catalytic activity for hydrogenation reactions. Due to the strong endothermic characteristic of the DRM reaction, nickel-based catalysts cope with severe problems associated with coke deposition, which is promoted under high reaction temperatures. In this respect, the stability of the nickel-based catalysts becomes an important parameter to compare with other metal catalysts. Bartholomew and co-workers [256] indicated five distinguished types of carbon deposited on nickel-based catalysts:

- (i) C_α: It is dispersed coke formed from adsorbed atomic carbon.
- (ii) C_β: It is an amorphous carbon type. Typically, it includes polymeric films and filaments.
- (iii) C_ν: It is coke whiskers/fibers/filaments.
- (iv) C_γ: It is carbide bulk.
- (v) C_c: It is crystalline carbon in form of graphitic platelets or films.

It has been illustrated that C_c and C_ν, which have a diameter in a vicinity of Ni metal crystal preferred to be formed on the Ni catalyst surface during DRM reaction at 700-850 °C. Meanwhile, ordered graphite layers on the Ni surface formed from graphitic platelets/films.

Many efforts have been mounted to develop stable Ni-based catalysts for DRM. Wei et al., [242] improved the stability of nickel catalyst up to 600 h on a DRM stream test at 1030 K by employing an ultra-fine Zr(OH)₄ support, which had a particle diameter of 6 nm. The authors found that by increasing concentration of defected oxygen and basic sites for the support surface derived from the ultra-fine Zr(OH)₄, the deposited coke was effectively gasified by these oxidizing species. In another work, Roh et al., [257] promoted nickel supported on ZrO₂ with cerium. The results exhibited a stable stability of Ni-Ce/ZrO₂ catalyst due to the synergistic effects of the Ce modifier, which offered a high capacity to store and produce mobile oxygen for carbon gasification. In the meanwhile, Zhang and co-workers [258] found that Ni/SBA-15 catalyst was highly stable for the DRM reaction. This type of catalyst could be able to deal with carbon deposition and preserve catalytic activity over 600 h owing to the good dispersion of nickel particles onto the porous SBA-15 support surface. Moreover, researchers [259], [260], [261],

[262], [263], and [264], indicated that nickel-based bimetallic catalysts provide better catalytic stability for DRM reactions compared to monometallic nickel counterparts. The production of new properties from the combination of two individual metals is also believed to enhance catalytic activity further. Theofanidis and co-workers [265] found that the Fe-Ni alloy provided a better catalytic activity than monometallic Ni catalyst due to the partial segregation from the alloy forming FeO_x, which can reduce the accumulated carbon by its interaction with FeO_x lattice oxygen on the catalyst surface. This also further promotes CO formation. The addition of La into Ni/SiO₂ catalyst promoted catalytic activity significantly by offering the good dispersion of nickel active centers [266]. In addition to nickel-based metallic catalysts, nickel – based catalysts with perovskite structure are also indicated to possess high stability for DRM due to the high resistance to active metal sintering of perovskite structure [267]. Sutthiumporn et al., [253] explained the mechanism of the DRM reaction over La_{0.8}Sr_{0.2}Ni_{0.8}Fe_{0.2}O₃ perovskite catalyst. This study found that the presence of iron and the well-dispersed Ni particles prevented its agglomeration during the DRM reaction. Further, the adsorption of deposited coke on the catalyst surface to form La₂O₂CO₃ improved catalytic stability, as shown in Eq. 2-19.



Moreover, surface carbon species reacted with the carbonate species formed over the La_{0.8}Sr_{0.2}Ni_{0.8}Fe_{0.2}O₃ perovskite on Ni sites (**Figure 2-8**) and gasify more carbon species to carbon monoxide [268, 269].

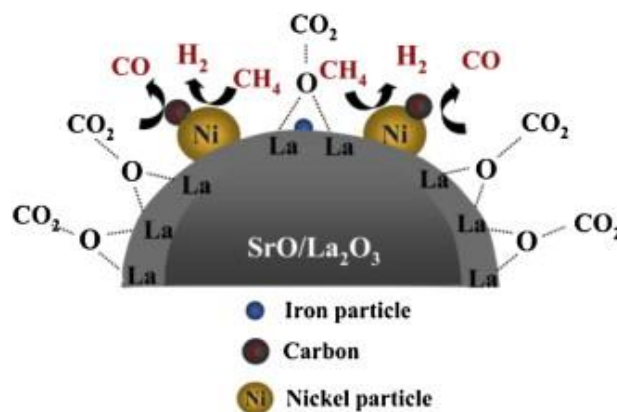


Figure 2-8 - The mechanism of DRM reaction over La_{0.8}Sr_{0.2}Ni_{0.8}Fe_{0.2}O₃ perovskite catalyst. Reprinted with permission from Ref. [253]. Copyright© 2012 Elsevier.

Undoubtedly, nickel-based catalysts display significantly high catalytic activities for reforming of methane but there also still exists the severe problems with coke deposition, which leads to catalyst deactivation [270, 271]. Though many intensive works to improve the catalytic stability of this type of catalyst have been reported; nonetheless, nickel-based catalyst still exhibit a short stability under reforming of methane reaction (**Table 2-4**). The matter of proper selection of active metals is thus still being continuous to achieve better catalytic performance and stability for syngas productions via DRM process.

2.4.1.2b. Cobalt-based catalysts

Offered a comparable catalytic activity to nickel-based catalyst, cobalt-based catalysts have been intensively employed for reforming of CH₄ processes [261]. Karash and Fields [272] discovered the cobalt-catalyzed the coupling of Grignard reagents in 1941. Subsequent to this pioneering finding, seventy years of scientific research has turned cobalt into one of the most potential active heterogeneous catalysts in many important applications. As per literatures [273], [274], [275], and [276], the strong C–H bonding energy (439 kJ mol⁻¹) accounted for the high endothermic characteristic that requires a high temperature to achieve a practical methane conversions. It is illustrated that cobalt complexes are advantageous in activating the C-H chemistry of methane molecule because it belongs to the precious 4d and 5d transition metal group with d8 and d10 electron configuration, which are highly sensitive to activate C-H bonds [277]. Nonetheless, the electronic properties of the 3d transition metal cobalt are significantly different from those of 4d or 5d homologues among others in terms of electronegativity (**Figure 2-9**) and spin-orbit couplings. The lower electronegativity of cobalt by comparing to other metals in the homologs group 9 elements assists the translation of the electrons into more nucleophilic organometallic cobalt intermediates, which promotes syngas selectivity significantly [278].

26 Fe 1.83	27 Co 1.88	28 Ni 1.91
44 Ru 2.20	45 Rh 2.28	46 Pd 2.20
76 Os 2.20	77 Ir 2.20	78 Pt 2.28

Figure 2-9 - Electronic properties of cobalt compared to common active metals according to the Pauling scale [279].

Intensive research on catalytic DRM over cobalt-based catalysts has been conducted due to their high activity for DRM reaction [280]. It was proved by researchers [281], [282], [283], [280], and [284], cobalt-based catalysts possess a comparable catalytic activity with nickel-based catalyst and several noble metal catalysts, such as Pt and Ru. Moreover, other researchers, such as [285], [286], [287], and [288] confirmed that cobalt-based displayed a better catalytic activity for hydrogen generation reactions than nickel-based catalysts at low reaction temperature. In addition to this, cobalt catalysts supported on silica and alumina supports have a better durability with the changes in reaction temperature compared to nickel-based counterparts [278]. More importantly, cobalt – based catalysts have better coke resistance than nickel-based catalysts [289-291]. These results further recommend cobalt is a promising non-noble catalyst for DRM and SDR. Nonetheless, the field of heterogeneous catalytic for reforming of methane processes has recently shifted its attention to apply bimetallic catalyst systems due to its superior properties than monometallic catalysts [292]. The structure of bimetallic catalyst is a combination of the advantageous characteristics of two single elements. The incorporation between metals can lead to the formation of an alloy, cluster-in-cluster or core-shell catalyst particles, which can provide a superior activity and better stability [70, 293]. In fact, there has been significant research activity in bimetallic catalytic recently. By combining cobalt with other metals, catalyst’s surface properties are altered resulting

in to achieve better catalytic performance [294]. This phenomenon that is also termed the synergistic effects between two metallic species [295]. Bimetallic combination of cobalt and noble metals, such as Pt and Ru was found to have a high catalytic activity and coke-resistance, due to a proper tuning of the O* binding strength via the Co-M interactions [296], [297], [298], [299]. Guzzi et al., [295] found that the performance of mono-cobalt and bimetallic cobalt doped with noble catalysts for hydrocarbon reforming processes was in the order of Pt-Co > Pd-Co > Ru-Co > Re-Co > Co. Nonetheless, using noble metals are not favorable from the economic point of view due to their expensive cost. The combination between non-noble metals, is therefore, more preferable. In this respect, nickel is of at a great interest. The Ni-Co bimetallic catalyst has been commonly used for DRM process [261], [300], [301], [302] because of its high activity, availability, and affordability. More importantly, there are many significant improvements of nickel for supported cobalt catalysts for DRM reported in the literature. Specifically, Xu et al. [282] found that bimetallic Ni/Co catalysts supported on commercial γ -Al₂O₃ doped with La₂O₃ with a Ni/Co ratio of 7/3 converted 90 % reactant gas and last for 250 h on stream. The exceptional performance compared to monometallic cobalt catalyst was attributed to the synergistic effects of Ni-Co bimetallic. In a good agreement, Takanabe et al., [29] and Zhang et al., [70] reported that Ni-Co bimetallic catalyst supported on TiO₂ and MgO, respectively, showed both higher catalytic activity and better coke resistance than each monometallic counterparts [303]. Nonetheless, it was indicated that Co-Ni bimetallic catalysts have much lower coke resistance and thermal stability than Co-Mo catalyst [111, 304, 305]. Moreover, the single molybdenum catalyst supported on Al₂O₃ showed a comparable activity with Pt/Al₂O₃ catalyst for reforming of hydrocarbons [306]. Chen et al., [307] found that the introduction of Mo positively altered methanation reaction over in Co supported on SiO₂. In fact, Co-Mo bimetallic catalyst has been widely used for hydrodesulfurization reactions [308], [309], [310], [311], [312], [313]. Nonetheless, there are not many reports in the literature on the catalytic activity of Co-Mo catalysts for reforming of methane though it has displayed its superior activity and stability for hydrogen-involved reactions. The work employing supported Co-Mo catalyst was published by Khavarian and co-workers [314], [315], which showed 98.6 % of CH₄ and 99.1 % CO₂ stably converted over Co-Mo/MgO-SWCNTs catalyst over 100 h on the stream test. Due to a high temperature DRM operation, a developed catalyst is required to be highly catalytic activity and strongly thermal stability, in which, supported Co-Mo

catalysts can be satisfied. More importantly, cobalt, known as a ferromagnetic element [42], can combine with other paramagnetic metals such as molybdenum [43], to form magnetodielectric materials for MW absorbing applications [44]. This finding lighted up the ideas to use Co-Mo catalyst for DRM under MW irradiation, which can reduce the energy consumption for the DRM process.

2.4.1.2c. Copper-based catalysts

Copper-based catalysts have played an important role in industrial settings, such as synthesis alcohols from syngas [316], [317], steam reforming of methanol [318], oxidation of carbon monoxide and hydrocarbons [319], water gas-shift reaction[320], and selective hydrogenations [321], and dehydrogenation of alcohols [322]. Copper - based catalysts can compete with other metallic - based catalysts by its affordability, high activity, and less safety concerns, which are essential for industrial applications. Though the physicochemical properties of metallic catalysts employed in chemical reactions have been extensively studied for many decades, the nature of the active site of copper is yet ambiguous. It has been first pointed out that the performance of copper-based catalyst is controlled by the status of copper. Because of this, many copper-based catalysts used commercially are in the form of copper oxides like CuO/ZnO or CuO/Cr₂O₃ formulations, which can be reduced to highly dispersed Cu⁰ enhancing catalytic activity. In fact, it is indicated that the reduction of Cu²⁺ to Cu⁺/Cu⁰ deutes copper as a redox active center for chemical reactions [62-65]. Some researchers found that the performance of methanol synthesis reaction is directly proportional to the surface area of metallic Cu and methanol is formed on a metallic Cu surface [323], [324] while others [325] [326] indicated the good copper dispersion with an appropriate ratio of Cu⁰/Cu⁺ producing a high catalytic activity for hydrogenation reactions. Moreover, researchers [327], [328], [329], [330] also found that copper dispersion significantly influence to its catalytic activity. These works indicated that the better copper dispersion on the support resulting in higher catalytic activity for SRM.

The rich redox nature, high abundance, and low toxicity has rendered Cu-based catalysts to be more favorable for gas-phase reactions [62-65]. One of the most well-known is the ternary system Cu-ZnO-Al₂O₃ employed in methanol synthesis from gas mixtures (H₂/CO₂/CO) [327, 331-334]. For syngas production, copper has been employed in the binary system with other metals, such as nickel for DRM [70-75] and SDR [75-77] under

conventional heating. Somewhat surprisingly, none of copper-based catalysts has been applied for methane reforming under MW irradiation. One of the possible reasons is that copper is one of the opaque materials together with silver and aluminum reflecting MW wave due to its highly conductivity [78]. Nonetheless, it was indicated that conductive metal catalysts can absorb MW energy by adding a dielectric layer surrounding conductive elements [335]. Researchers [336] employed polyaniline as dielectric layer to decorate graphene to reduce its high conductivity and improved the MW absorption capacitance significantly. Moreover, despite their high activity and selectivity, the long-term stability is still an existing shortcoming of the conventional copper – based catalysts. This is a possible reason for the absence of applications of copper-based catalysts for chemical reactions under MW heating. Nonetheless, it was found that the addition of promoters to copper catalyst systems can improve the catalytic stability for gas-solid reactions significantly [337-339]. All mentioned advantages and existing challenges simulated the huge interests to develop a novel copper-based catalyst for syngas production under MW heating.

2.4.2. Catalyst preparation methods

The first factor influencing the catalyst efficiency is the preparation techniques and thermal treatments including calcination temperature and reduction process. Heterogeneous catalysts for reforming of methane processes are commonly prepared using precipitation/co-precipitation, sol-gel, electrostatic adsorption, and impregnation/co-impregnation methods including wet and dry impregnation [340]. The aim of this section is to review these catalyst's preparation methods to select an appropriate preparation method for catalysts in this study.

Several researchers employed precipitation/co-precipitation to prepare supported catalysts for DRM [341-345]. Precipitation can be performed by altering the conditions such as temperature, pH, or evaporation. Specifically, precipitation is the control of a precursor solution following the mechanism of nucleation and growth. In this method, a precursory crystallite nucleation is formed and followed by its subsequent growth to form catalyst particles. In co-precipitation method, active metal salts and support are mixed and dissolved together. In such conditions, the combined precursor solutions of the active metals and support is achieved in a single nucleation and growth step. By doing this, a metal loading up to 70 w.t % or higher can be prepared whilst catalyst particles can also

be preserved at small size [346]. As such, co-precipitation/precipitation is the most convenient method to prepare catalysts with a large metal mass fraction to volume ratio. Nonetheless, this advantage also leads to the insoluble combined material due to a very high level of supersaturation leading to the formation of big particles [347]. Therefore, this preparation technique for high metal loadings is needed to ensure that all precursor nucleates at a high rate simultaneously. Moreover, washing steps is also necessary for co-precipitation to eliminate residual nitrates, sodium or potassium from precursor solutions [348]. These residues can cause sintering and agglomeration for the catalyst particles at later thermal treatment steps, and ultimately, it leads to surface area lost [349]. Moreover, during co-precipitation, the local instability, which can lead to additional nucleation events, has to be carefully taken into account by controlling temperature gradients and mixing effectively.

Intensive research has been focused to catalytic preparation via metallic salt precursor. Whereby, the deposition of the metal precursor is well controlled. By this way, the catalysts can be synthesized in a reproducible manner. Electrostatic adsorption is one such rational synthesis technique, which has been proven to be reproducible [350]. Moreover, this technique is able to produce high dispersed catalysts with smaller metal particles than those prepared by impregnation methods [351, 352]. Depositing metal particles by electrostatic adsorption includes electrostatic (non-specific) interactions between the metal precursors and the support. Some metal–support systems exhibit chemical (specific) interactions with the support in addition to electrostatic ones. For instance, cobalt catalyst supported on Al_2O_3 displayed its high catalytic activity and stability due to the well-dispersed of cobalt catalyst particles [52]. Nonetheless, electrostatic adsorption technique cannot be applied for larger or industrial scale because complexed equipment are required and it is also difficult to be controlled [351].

The sol-gel method is an alternatively reproducible method for heterogeneous catalyst preparation with high dispersion and small particle size [353-355]. Basically, the sol-gel process includes the transformation of a liquid “sol” (mostly colloidal particles) into a solid “gel” phase. In this method, the “sol” is prepared from inorganic metal or metal compounds precursor solutions. Sol-gel method can prepare a wide range of catalyst forms, such as thin film, microporous, spherical shape, or ultra-fine powders [356]. This benefits is derived from the flexible rheology allowing easy shaping and embedding

[357]. Moreover, sol-gel method is low of processing and high versatility [356]. One of the featured characteristics of catalysts prepared by sol-gel technique is high purity and well controlled physical properties including pore size distribution and pore volume [358]. Low synthesis temperature, homogenous dispersion, and a good control of stoichiometry can be achieved with sol-gel method [359]. The catalysts prepared by the sol-gel method is strongly influenced by factors including gelation condition, drying condition, and solvent [360]. Sajjadi et al., [361] found that Ni-Co/Al₂O₃-ZrO₂ catalyst particles with nanoscale was well controlled by the sol – gel method resulted in high H₂ (96.9 %) and CO (97.1 %) yield . Meanwhile, Hao and co-workers [362] indicated that aerogel Co/Al₂O₃ catalyst provide a much higher methane conversion than that catalyst in the conventional fluidized bed operation. Nonetheless, the sol-gel technique deals with the high cost of precursors due to the solvent used. Moreover, it is difficult to control the wet gel when drying due to the strong shrinkage causing the surface fracture [363], and therefore, sol-gel method cannot be applied on large scale [364].

Compared to the above-mentioned technique, impregnation/co-impregnation method is a most common catalyst preparation technique because of its simplicity and low waste streams [365]. Impregnation/co-impregnation is particularly effective for preparing bimetallic catalyst by virtue of producing a better dispersion and interactions between active metals compared to other catalyst' preparation method [366]. The noticeable advantage of impregnation/co-impregnation method compared to sol-gel is employing water as a solvent for inorganic salts due to the high solubility of the precursor. Nonetheless, the precursor concentrations below super-saturation are required to prevent premature deposition of active metals in bulk solution [367]. Impregnation/co-impregnation includes wet and dry techniques. In wet impregnation/co-impregnation, the pore space of the support is pre-filled by solvent to impregnate precursor solution while dry impregnation/co-impregnation is not required this step [368]. The mechanism of wet impregnation is simpler than that of dry impregnation (**Figure 2-10**) [369]. In wet impregnation, the distribution of the precursor solution onto the support is assumed to be governed by (i) diffusion of precursor solution inside the pores and (ii) adsorption of precursor solution onto the support. These diffusion and adsorption steps are dependent on the adsorption ability of the surface and the adsorption equilibrium constant.

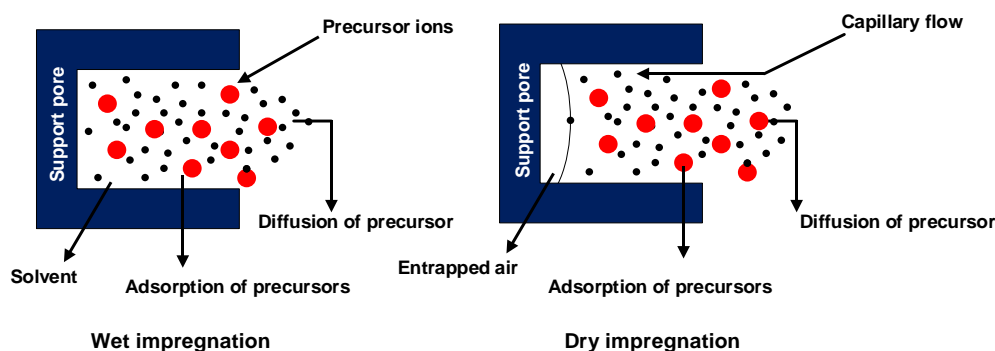


Figure 2-10 - Scheme illustrated the wet and dry impregnation method.

Moreover, the distribution of the precursor ions within the pellets is also dependent on the equilibrium between the diffusion and adsorption phenomenon. In dry impregnation, apart from these diffusion and adsorption processes, entrapped air, which is the pressure, drives the capillary flow of the precursor solution inside the empty pores (**Figure 2-10**). The pore volume of the support is sufficiently filled by a solution of metal salt. Therefore, in the dry impregnation method, only low weight loadings can be achieved due to the excessive concentration of the metal salt, which is beyond the solubility of solvent or water amount [370]. The huge advantage of dry impregnation method is that no filtration is necessary, and therefore, no metal is wasted. Compared to wet impregnation, the dry method produces a low dispersion of catalyst particles and weak metal-support interactions due to the deposition of the metal precursor occurring through precipitation during drying, which is difficult to be controlled [371]. In contrast, wet impregnation exhibits great advantage with respect to its simplicity to control layers of active metal onto the support surface and inside the support pores. This could be attributed to the changes in the solution from a capillary action process to a diffusion process, which is much slower [371]. Impregnation/co-impregnation method is routinely implemented to synthesize catalysts on an industrial scale. Catalysts used in DRM processes are commonly prepared by impregnation/co-impregnation technique [262, 372-377]. Satsuma et al., [378] indicated that Co-Pd catalysts supported on Al_2O_3 prepared by co-impregnation (**Figure 2-11**) showed the better metal-support interface resulted in higher activity at lower temperatures than those prepared by sequential impregnation. In a good agreement with above study, Huang and co-workers [379] confirmed that the co-impregnation method offers the flexibility to adjust bimetallic Ni/Mo ratio, which results in a better metal-support interaction, and therefore, longer catalytic stability.

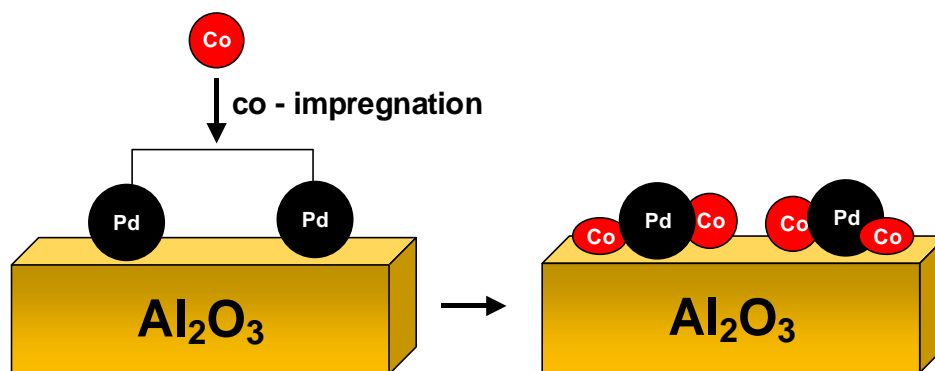


Figure 2-11 - Scheme of co – impregnation method to prepare of Co-Pd/Al₂O₃ catalysts [378].

Nonetheless, impregnation/co-impregnation method is followed by subsequent elimination of the solvent. The impregnated sample is pre-heated in an oven inflow of gas, such as nitrogen, oxygen, or air depending on the requirement. The temperature is generally preserved slightly higher than the boiling point of the solvent, for example, 110-120 °C for water. The aim of this step ensures to eliminate solvent slow enough from the support pores. The concentration of precursor increased up to saturation gradually, and finally, is crystallized to form catalyst particles by the subsequent calcining process. The calcining parameters, such as heating rate and temperature influence to physical catalyst properties [380], and hence, the effects to the overall catalytic performance significantly. Wang and coworkers [381] found that Co₃O₄ initiated to be formed and remained on the support surface within the first 500 °C. This phase was then transformed to two different phases Co₂AlO₄ and CoAl₂O₄ once the calcining temperature reached 1,000 °C [382]. The exposed surface area of cobalt supported on Al₂O₃ at 1,000 °C was considerably smaller than that at 500 °C because the formation of inactive spinel, which has low reducibility and covers active cobalt species [53, 383, 384]. In another study, Hou et al., [385] studied the influences of different calcining temperatures of 400, 600, 800, 1,000, and 1,200 °C on the catalytic activity of Co/Al₂O₃ catalysts. This work also found that the low reducibility of CoAl₂O₄ spinel, which was formed at high calcining temperature, reduce the catalytic performance of Co/Al₂O₃ catalyst. In fact, it is widely accepted that surface area, and reduction degree decrease of cobalt –based catalysts increase when increasing the calcining temperature [230, 386, 387]. By these observations, the calcining temperatures above 800 °C are not recommended for supported cobalt-based catalysts.

2.4.3. Supports

Support plays an important role in the field of heterogeneous catalytic. The support acts as a mesoporous substrate, on which, metal particles disperse and be held to prevent its sintering [388]. Indeed, bulk metal catalyst particles are prone to sintering under reaction conditions rapidly [389]. Therefore, heterogeneous catalyst particles are necessary to be stabilized in a certain way against sintering. This can be simply achieved by dispersing these small particles on a support, which are thermally stable and chemically inert. By dispersing metal particles upon the porous structure, a large active metal area is produced relative to the weight of the actual metal weight employed. The surface to volume ratio of the active component is especially beneficial in the case of precious metals. In an aspect of the engineering view, the support can help to distribute reaction heat and retards the sintering of metal crystallites, and thus, preserving the active surface for a longer catalyst life. Moreover, the supports also provide other benefits including maximizing the surface area of the active sites and conceding the catalyst to be tossed into the form of gruff bodies, which are suitable for use in the reactor [390]. In many cases of the catalytic reactions, the good combination between active metal and support can considerably enhance the catalytic functionalities [391]. These visible advantages have led to the prevalence of supported metal catalysts over non-supported metal catalysts for chemical processing [392]. Although the support material only serves as a medium for keeping the catalytically active species supported, these species interact to some degree with the support. The catalytic performance is heavily dependent on a complex metal-support interaction, which is governed by the morphology and dispersion of active metal particles. Consequently, the selection of support for reforming of methane catalysts needed to be taken into account throughout.

For both catalytic DRM and SDR processes, an appropriate selection of the support not only assists to promote catalytic activity but also to suppress carbon deposition for the active metal catalyst [393, 394]. Moreover, it was illustrated that the coke deposition on the catalyst surface is affected by the basicity of the support significantly [283]. Specifically, coke deposition can be diminished by increasing Lewis basicity for support [112, 395]. In DRM reaction, the adsorption and dissociation of an acidic carbon dioxide on the catalyst surface promoted by strong basic support reduces carbon formation and results in high catalytic stability [396]. In addition to this, the high thermal stability of the

support, which is represented by the Hu'ttig and Tamman temperature values, can help to reduce catalyst sintering [397]. By heating up to the Hu'ttig temperature, atoms at the defects of metal catalyst will initiate to be mobile before exhibiting the visible mobility from the whole bulk when reaching the Tamman temperature. The mobility of atoms would lead to the formation of larger aggregates, and thus, reduces the catalyst's active surface [398]. The properties of common supports for cobalt-based catalysts are summarized in **Table 2-5**. The SiO₂ supports was indicated as high stable support for cobalt-based catalysts [399, 400]. Compared to γ - aluminum dioxide, silicon dioxide can be reduced by lower temperature and produces a good active metal dispersion [401, 402]. Nonetheless, silica has a much lower improvement for catalytic activity compared to α -Al₂O₃ due to its acidic nature, which is not preferred for activating the acidic gas like CO₂ [110, 403, 404]. Alkaline-based oxides such as BaO, CaO, and SrO also employed as the supports for metal catalysts in the DRM process. Liu and co-workers [405] found that nickel supported on CaO–ZrO₂ converted 86 % methane due to the high basic nature of produced by Ca²⁺ supported on ZrO₂. The presence of CaO produces the acidic–basic character to repress water generation generated by the RWGS reaction, and therefore, promotes methane conversion. The alkaline-based supports, nonetheless, are relatively less to promote catalytic activity of metal catalyst owing to their low surfaces after reduction [149]. Notwithstanding possessing a NaCl type structure, such as BaO, CaO and SrO has no lattice parameters closing to Co-species leading to a very weak metal-support interaction, and thus, reduce catalytic stability. In contrast, MgO support enhances the catalytic activity for cobalt-based catalyst significantly [280]. It was illustrated that MgO has lattice parameters close to CoO, which makes MgO to be miscible and can form a solid solution with cobalt, and consequently, reduces catalyst sintering. Furthermore, small cobalt clusters were formed on the MgO support surface on account of shared oxygens in the solid solution between Mg and Co [406]. These clusters have high thermal stability, and therefore, are less to be sintered than the usual cobalt particles [407]. In addition to MgO, ZrO₂, and CeO₂ are also considered as good catalyst supporters since they provide a strong metal-support interaction [408]. Researchers [409, 410] have reported that CeO₂ could improve the dispersion of catalyst particles and reduce the sintering. These studies also found that the strong metal–support interaction with a high oxygen storage capacity of redox Ce⁴⁺/Ce³⁺ contributed to the high catalytic activity for reforming of methane. By adding ZrO₂, CeO₂ structure was modified and could

provide better thermal stability and excellent oxygen mobility compared to CeO₂ alone [411]. Likewise, ZrO₂ is also reported by researchers [305, 412-415] as another common support for cobalt-based catalysts for DRM reactions.

Table 2-5 - The properties of catalyst supports.

Type	Support	Melting point (°C)	Hu'ttig Temperature (°C)	Tamman Temperature (°C)	Surface area at 673 K (m ² .g ⁻¹)	Surface acidity ^a	Surface basicity ^b
Basic	MgO	3,073	921.9	1536.5	197.0	0.054	1
	CaO	2,853	855.9	1426.5	29.0	0.0029	17.8
	Ca ₂ SiO ₄	2,407	722.1	1203.5	-	-	-
	BaO	2,196	658.8	1098	-	-	-
	Ca ₂ SiO ₃	2,173	651.9	1086.5	-	-	-
Amphoteric	ThO ₂	2,323	696.9	1161.5	7.5	0.037	12.9
	ZrO ₂	2,988	896.4	1494	63.3	3.81	0.540
	CeO ₂	2,873	861.9	1436.5	-	-	-
	Cr ₂ O ₃	2,708	812.4	1354	-	-	-
	La ₂ O ₃	2,588	776.4	1294	13.0	0	-
	α-Al ₂ O ₃	2,318	633.9	1056.5	120.0	1.87	0.088
	TiO ₂	2,113	633.9	1056.5	120.0	1.87	0.088
Neutral	MgAl ₂ O ₄	2,404	721.2	1202	-	-	-
	MgCr ₂ O ₄	2,300	690	1150	-	-	-
	ZnCr ₂ O ₄	2,173	651.9	1086.5	-	-	-
	α-Al ₂ O ₃	2,100	630	1050	-	-	-
	CaSiO ₃	1,813	543.9	906.5	-	-	-
Acidic	γ-Al ₂ O ₃	2,318	659.4	1159	124.4	1	0.021
	SiO ₂	1,973	591.9	986.5	117.5	0	-
	SiO ₂ -	1,818	545.4	909	-	-	-
	Al ₂ O ₃						

^a Acidity referred to γ-Al₂O₃ at 473 K

^b Basicity referred to MgO 473 K .

2.4.3.1. Alumina

Compared to other oxides, alumina is the most widely-used supports for heterogeneous catalytic [416, 417]. The γ - Al_2O_3 is obtained from the thermal dehydration of aluminum hydroxides and oxy-hydroxides ($\text{Al}_2\text{O}_3 \rightarrow \gamma\text{-Al}_2\text{O}_3 \rightarrow \delta\text{-Al}_2\text{O}_3 \rightarrow \theta\text{-Al}_2\text{O}_3 \rightarrow \alpha\text{-Al}_2\text{O}_3$) [418]. The transformation sequence between alumina forms is heavily dependent on the calcination temperature [419]. Though existing in various structures, only three phases of alumina are of interest, α - Al_2O_3 , γ - Al_2O_3 , and δ - Al_2O_3 . γ - Al_2O_3 is reported to be formed within the temperature range from 350 and 1000 °C. This form of alumina oxide can be stable at temperatures as high as 1200 °C, and therefore, commonly employed as the support in heterogeneous catalytic [420-422]. Alumina offers high surface areas (50 – 300 $\text{m}^2 \cdot \text{g}^{-1}$), mesopores of between 5 and 18 nm, the pore volume of about 0.6 $\text{m}^3 \cdot \text{g}^{-1}$ [423] as well as high thermal stability (**Table 2-5**). Cobalt-based catalysts supported on alumina are widely used as an important catalyst for various areas such as hydrogenation, hydrotreating, and combustion processes. It has been reported that metal-support interaction between cobalt and alumina determines its catalytic reactivity [424]. This metal-support interaction is dependent upon the concentration of metal species, the nature of the support, preparation method, and calcining temperature [52]. The surface-active phases can be significantly altered depending on the preparation methods. Compared to MgO supported for nickel, Al_2O_3 showed its higher enhancement for the catalytic activity at similar reaction conditions [425]. In contrast, Rh supported on MgO and γ - Al_2O_3 exhibited similar CH_4 and CO_2 conversions [191]. Nonetheless, the comparison between γ - Al_2O_3 and Al_2O_3 supported for Rh catalysts [78] displayed that Rh/ γ - Al_2O_3 had higher catalytic activity compared to Rh/ Al_2O_3 at high reaction temperature [191, 426]. Bychkov and co-workers [427] reported that Ni/ γ - Al_2O_3 displayed a higher catalytic activity and better coke-resistance than Ni/ α - Al_2O_3 and Ni/ θ - Al_2O_3 . In a good agreement, Zeng et al., [428] also indicated that Co-based catalyst supported on γ - Al_2O_3 could be stable over 320 h on the DRM stream test at 800 °C.

2.4.3.2. TiO_2

Titanium dioxide has been illustrated as the excellent support of catalyst for DRM because of availability, affordability, good redox properties, surface acidity, and reducibility [429]. Moreover, researchers reported that TiO_2 can break large ensembles

of metal species, and therefore, suppress the carbon deposition [430]. Seo et al. [431] compared the catalytic activity of Ni/TiO₂ and bare Ni catalysts for the DRM reaction. It was shown that Ni/TiO₂ catalyst was far more active and stable than bare Ni catalyst, with higher CH₄ (45 %) and CO₂ (68 %) conversion. The XPS results of this study also proved that the better coking resistance of Ni catalyst supported on TiO₂ also promoted the catalytic stability. Among supports, as shown in **Table 2-5**, TiO₂ and ZrO₂ exhibit a better interaction with metals [430]. Compared to alumina, TiO₂ is one of the most studied functional supports because of its outstanding enhance the catalytic activity as well as good structural stability, nontoxicity, low-cost, and environmentally friendly nature [111, 432]. By supported for Mo-based catalysts for hydrogen-involved reactions, TiO₂ has proved its better enhancement for catalytic stability and coke resistance than aluminum oxide [340, 433]. This is due to a better metal – TiO₂ interaction, which fractures large aggregation between metallic particles providing more active sites for the reforming of methane reactions at the boundary between metal and support, and hence, obstructs coke deposition [434]. More importantly, TiO₂ was found to be highly stable in water and steam environment [435] which make its dominance in steam reforming processes. Nagaoka et al., [436] reported that the activities of cobalt supported on TiO₂ for DRM were not as high as that supported on alumina, nonetheless, it has better coke resistance. In the meanwhile, TiO₂ has also been widely used as the supports for copper-based catalysts [437, 438]. TiO₂ containing greater anatase can produce strong metal-support interaction with copper species, and therefore, promote catalytic activity [439]. Compared to cobalt catalysts supported on Al₂O₃ or SiO₂, Co/TiO₂ are more active for CO hydrogenation [440]. However, the formation of Co-titanates is inevitable from Co/TiO₂ catalysts is during a catalytic process. Brik and co-workers [441] found that CoTiO₃ and Co₂TiO₄ were formed by the reactions between Co₃O₄ and TiO₂ under regeneration conditions. Similarly, Voß et al., [442] also observed the formation of high-temperature compounds, CoTiO₃ and Co₂TiO₄. These two CoTiO₃ and Co₂TiO₄ phases are highly stable and do not have catalytic activity for hydrogenation reactions [443]. To prevent the formation of these inert phases, researchers have suggested the addition of secondary metallic to the Co/TiO₂ catalyst [444-448]. Though, TiO₂ supported Co-Mo bimetallic has been widely used as a catalyst for hydrodesulfurization reactions [58, 433, 448, 449], none of this catalyst employed for DRM under MW heating has been reported. One of the reported reaction not to use TiO₂ reforming of methane processes is the low specific

surface area of TiO₂ [58, 111, 448] leading to form bigger catalyst particles [450]. Nonetheless, this impediment for catalyst heated by MW wave would be beneficial. It is the fact that the amount of MW energy absorbed is dependent on how well exposed of absorber component to the incident wave [451-453]. In this possible case, TiO₂ is expected to expose active centre/MW absorber components to the incident MW wave promoting MW absorption ability, and hence, enhance the catalytic performance. This knowledge gap stimulates the study's interests to investigate TiO₂ to support for Co-Mo bimetallic catalyst for DRM and DRM reactions under MW irradiation.

2.5. Catalytic reforming of methane under MW heating

2.5.1. MW heating

2.5.1.1. Background of MW heating

A huge interest in applying MW technology for chemical reaction and chemistry processes has been observed in recent years. This “new way” of heating to provide energy for chemical reactions has thus been extensively investigated [454]. MW is estimated to be the common heating technique for organic synthesis [454, 455]. The significant enhancements of reactant conversion, product selectivity, and a huge reduction of reaction time for chemical reactions have been reported [2–6]. MW are electromagnetic waves with the length of 1 mm to 1 m corresponding to the frequencies of 30 GHz to 300 MHz [456]. The most common frequency for MW heating is 2.45 GHz utilized as home MW ovens [457]. As for particularly industrial processes, MW can be operated up to 915 MHz [458]. Initially, MW were widely used for radar detection during the Second World War [459]. Subsequently, MW irradiation as a heating source was well developed and established in society, for example, domestic MW ovens and industrial heating systems [460]. Though first reports indicating the potential of the MW heating technique for polymer applications (1967) [461] and chemical synthesis (1981) [462], [463] had been reported, the two important reports [464], [463] published in 1986 applying MW dielectric heating to chemical systems attracted great interest. Ever since then, the development of MW heated for chemistry processes has witnessed an explosive growth (**Figure 2-12**). Not surprisingly, the number of research publications and researchers involved in this field have dramatically increased. For instance, approximately 50 papers had been published in 1993; Up to 2000, the total number of published papers studied on

using MW in chemical processes is around 2000 [465]. Nonetheless, it was escalated more than 5-fold in 2004. To date, the MW research is extended to almost areas including chemistry synthesis, heterogeneous catalytic, analytical chemistry, materials, polymers, drug discovery, biochemistry, and syngas production [466]. This strong development of MW applications is reflected in the increasing number of papers, reports and reviews published recently.

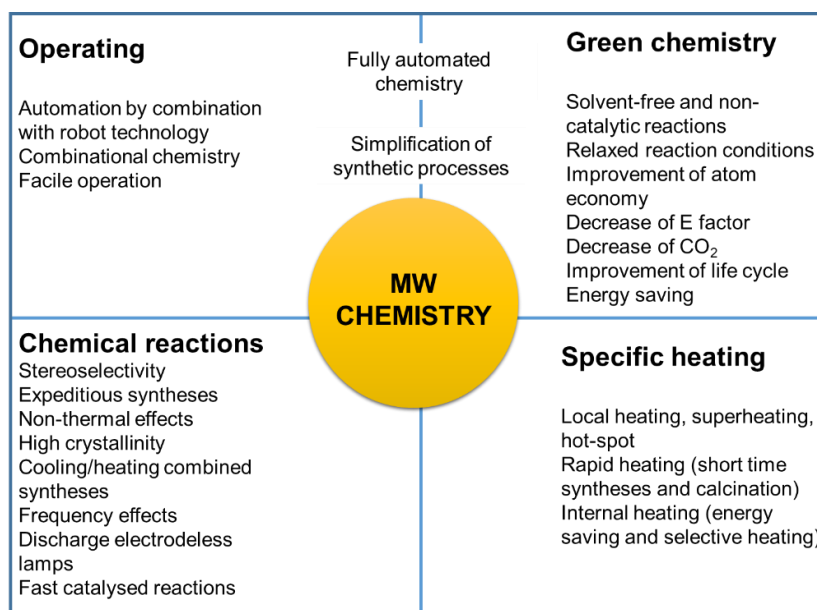


Figure 2-12 – Advantages of MW irradiation and its role in chemistry [467] .

The employment of MW irradiation in chemistry, which can also be called MW chemistry – can be classified into four different areas as shown in **Figure 2-13**. In terms of operation, chemicals can be heated by domestic ovens directly or under an automated robot controller for chemical synthesis into four different categories [468]. MW is also a beneficial technique for green chemistry by virtue of its reduction of reaction time without the presence of solvent or catalyst [469]. Moreover, the kinetics of chemical reactions are vigorously enhanced by MW heating [469]. MW also offers a specific heating characterized by superheating and hot-spot formation (**Figure 2-12**).

To understand the enhancement of MW irradiation for chemical and chemistry processes, the viewpoint of electric and magnetic fields must be taken into account. This viewpoint is particularly significant due to the fact that the heating mechanism of MW is totally different from that of conventional heating methods. Though thousands of publications in MW heated chemical reactions, very little study has focus on the characteristics or

mechanism of MW irradiation. Given by the invisibility, the increase in temperature of a heated substance is considered as a standard method to confirm the effects of MW energy [470]. Nonetheless, the current techniques cannot provide an accurate value of temperatures of catalyst irradiated under MW wave due to its complexity [471]. Basically, when a material is exposed to MW irradiation (**Figure 2-13**), three different cases would be involved [472]: (i) Reflect MW from its surface (highly conductive bulk materials, such as, metals); (ii), allow MW pass through (insulators such as ceramics, quartz); and (iii) absorb incident MW wave leading to heating (dielectric lossy materials such as carbon). In order to apply MW, at least one component of the system must has ability to absorb MW.

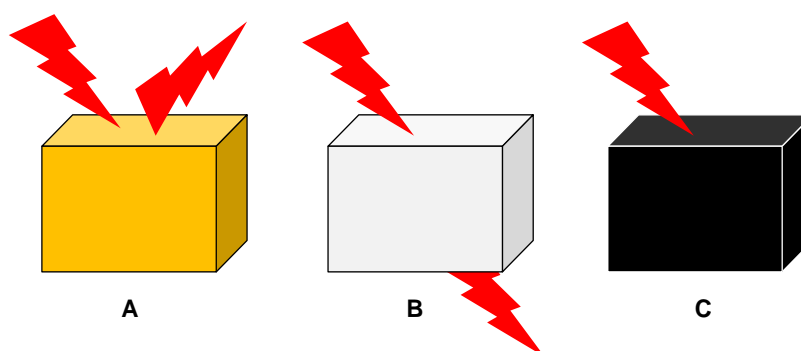


Figure 2-13 – Conductive (A), ran (B), and absorbing (C) materials under MW irradiation [472].

In fact, many organic compounds, metal powders and several solvents are MW absorbers. There are two parameters describing the MW propagation and the capacity to absorb MW of a material, which are complex permittivity, ε^* and complex permeability μ^* .

$$\varepsilon^* = \varepsilon' - f\varepsilon'' = \varepsilon_o(\varepsilon_r' - f\varepsilon_r'') \quad 2-20$$

$$\mu^* = \mu' - j\mu'' \quad 2-21$$

Where, ε' is the dielectric constant representing for the ability of a material to store electrical energy; ε'' is the loss factor standing for dissipated electrical energy of a material; μ' is the complex permeability standing for stored magnetic energy of a material; μ'' is the magnetic energy loss, which can be transformed to thermal energy. Magnetic losses are high and important parameter, particularly for magnetic metal oxides such as cobalt, nickel, and iron. Nonetheless, non-magnetic metals, such as copper, can ignore this parameter.

The loss tangent ($\tan \delta$) and magnetic loss tangent ($\tan \delta_\mu$) are defined as follows:

$$\tan \delta = \frac{\varepsilon''}{\varepsilon'} \quad 2-22$$

$$\tan \delta_\mu = \frac{\mu''}{\mu'} \quad 2-23$$

As can be seen from **Eq. (2-22)**, the good MW absorbing material producing an effective heating should has as high as possible ε'' while ε' should be kept in a moderate range to ensure a deep enough penetration inside a material [473]. Moreover, the ratio between ε' and ε'' is defined by $\tan \delta$ value, which represents for the ability of MW coupling [474]. **Table 2-6** shows exemplary values of ε , ε'' , and ($\tan \delta$) of several common materials.

Table 2-6 – The ϵ' , ϵ'' , and $\tan\delta$ of some materials measured at 298 K [472].

Material	ϵ'	ϵ''	$\tan\delta$
Vaccum	1.00	0	0
Air	1.0006	0	0
Water	80.4	9.89	0.123 (2.45 GHz)
Methanol	32.6	21.48	0.659
Ethanol	24.3	22.86	0.941
Glass	4.82	0.026	0.0054
Styrofoam	1.03	0.0001	0.0001
PTFE	2.08	0.0008	0.0004
TiO ₂	50	0.25	0.005
ZrO ₂	20	2	0.1
ZnO	3	3	1
MgO	9	0.0045	0.0005
Al ₂ O ₃	9	0.0063	0.007

Hence, the efficiency of MW heating is proportional with dielectric and magnetic properties of the material and the frequency of the electromagnetic field. Moreover, MW absorption is also dependent on the material dimension since MW wave can penetrate inside the material at only a certain depth, which is defined as the penetration depth, D_p (m) [475]. The penetration depth is a depth in which the MW energy is reduced to approximately 37 % of the initial value [476]. The D_p value is dependent to the MW wavelength, the dielectric, and magnetic properties of the materials. The D_p can be described as follows [477]:

$$D_p = \frac{\lambda \sqrt{\epsilon'}}{2\pi \epsilon''} \quad 2-24$$

Two assumptions were proposed to interpret the enhancement of MW on the reactant conversion and product selectivity of chemical reactions. The first hypothesis assumed that the presence of pure thermal effects caused by MW irradiation, for example, a different temperature regime, is the principal reason to promote chemical reactions [478]. Meanwhile, the second theory highlights the role of non-thermal effects, such as molecular interactions with the MW field, which lead to the shifting of reaction equilibrium and enhance conversions. The presence of non-thermal effects was often claimed in MW – assisted chemical processes, particularly for compared studies between conventional and MW heating. Stuerger and Gillard [133] confirmed the presence of non-thermal MW effects, which altered chemical reactions. Nonetheless, non-thermal effects of the magnetic field have not been elucidated conclusively, and hence, it is still a controversial matter [125, 454, 479, 480].

2.5.1.2. Microwave-Material Interactions

Many mechanisms and theories have been proposed to explain the MW heating when a material bringing to contact with MW wave. Basically, the materials interact with MW wave can be classified into two main groups: (i) non-magnetic materials including Cu, Al, Si, water, polymers, and ceramics; and (ii) magnetic materials, such as iron, nickel, and cobalt [481]. For non-magnetic materials, two loss mechanisms which are dipolar losses and conduction losses are used to explain for its heating [482]. The dipolar loss is effectively explained for dielectric materials. By this mechanism, dipoles are generated when exposed to external a MW electric field [456]. **Figure 2-14** describes the mechanism of MW heating of water contained in the MW transparent container (quartz beaker). Whereby, molecular dipoles, such as positive polarity hydrogen and negative polarity oxygen are agitated by the oscillating MW wave. These molecular are reoriented in order to be phased with the incident oscillating electric field [483]. Nonetheless, molecular interaction forces, frictional, and inertial elastic resist these frequent changes in orientations of molecules. This leads to the increase in the molecular kinetic energy, and thus, results in volumetric heating [484, 485]. Moreover, the escalation of the dipoles kinetic energy causes the increase of its temperature within a very short time [486].

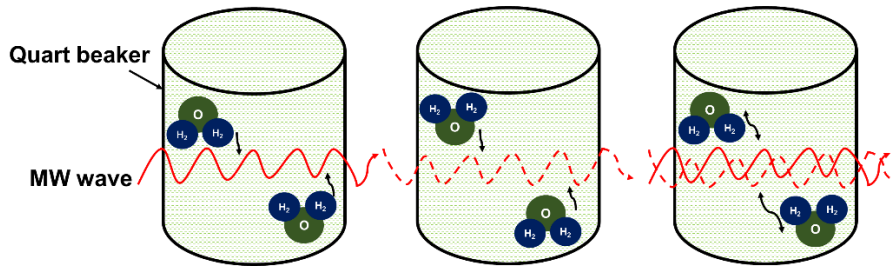


Figure 2-14 – MW heating mechanism of dipolar loss [481].

Conduction loss mechanism is also used to explain for the MW heating of non-magnetic metallic-based materials such as Cu, Al or Si. The electric field is attenuated rapidly inside the materials owing to material' high conductivity. This phenomenon can also be reflected by the opposite direction between induced magnetic field (H_i) and external magnetic field inside the material. In most case, the induced magnetic field produces a force to move conducting electrons in the reverse direction with velocity (**Figure 2-15**), v [487]. This movement creates a kinetic energy that is imparted on electrons. Nonetheless, it is controlled by the inertial, elastic, frictional and molecular interaction forces [488]. By circling this phenomenon rapidly, the oscillating electric generates volumetric heating inside the material as shown in **Figure 2-15**.

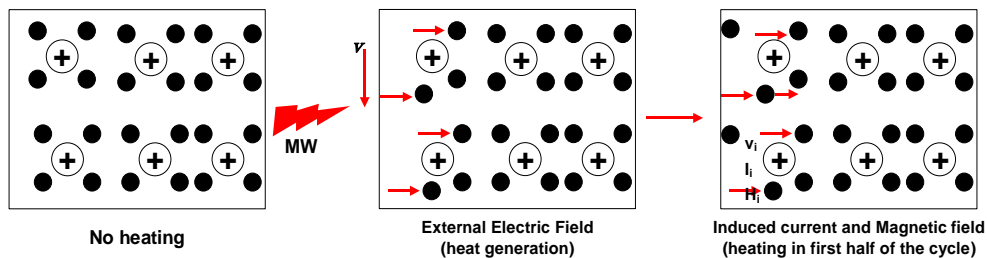


Figure 2-15 - MW heating mechanism of conduction loss.

Furthermore, the MW heating mechanisms of such magnetic materials are controlled by both the electric field and magnetic field [489]. The magnetic field creates the electron spin, domain wall, and orients electron domains [490]. Apart from conduction losses, the loss mechanisms in magnetic materials also include other mechanisms, such as hysteresis, eddy current, domain wall resonance, and electron spin resonance [39, 491]. Eddy current loss is generated by the eddy current created by the alternating magnetic field [492]. The eddy current density can be expressed as the **E.q. 2-25**[40].

$$J = \sigma.E$$

Where, σ is the electric conductivity; E is the electric field generated by the alternating H field.

Hence, the eddy current loss is dependent on the conductivity of the material. The eddy current loss can also be used to explain for MW heating of conductors or semiconductor materials [493]. In the meantime, hysteresis loss is generated by the reversal magnetization when a material is placed under an alternating magnetic force [494]. Hysteresis losses are well presented in magnetic materials. Basically, the magnetic dipoles is agitated due to the changes in the magnetic poles for every half cycle when a magnetic material subjected to an alternating magnetic field [495]. This rapid oscillation lead to a considerable friction and generates the heat inside the material. Therefore, the mechanism of MW heating over the oscillation of magnetic domain is defined as hysteresis loss. **Figure 2-16** presents a typical magnetization (B vs. H) curve. Accordingly, a hysteresis loop is generated when a magnetic material irradiated under an alternating magnetic field. The area within this hysteresis loop is the energy obtained by plotting the B versus H hysteresis curve.

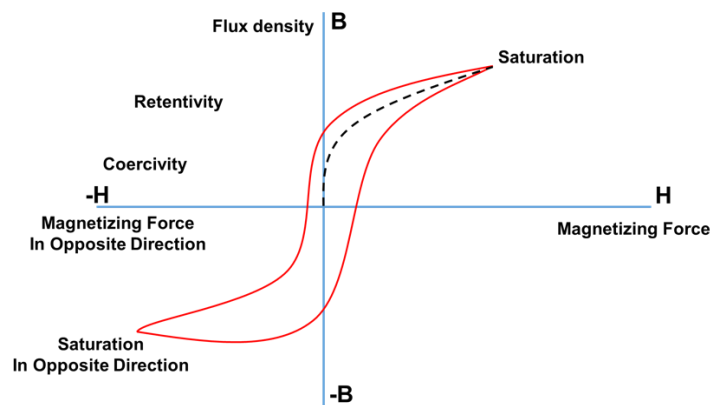


Figure 2-16 – The magnetization (B vs. H) curve.

In addition to these two losses, magnetic resonance losses also contribute MW heating of several metal oxides such as ferrites. Domain wall resonance and electron spin resonance are the sources to generate magnetic resonance losses, which is distinguished with hysteresis and eddy current losses [492, 496]. By considering this mechanism, the realistic part is the magnetic permeability while the theoretical part is the magnetic loss.

To achieve an optimum MW absorption, magnetic materials should be placed at the position with a maxima of the incident magnetic field. High magnetic materials, such as cobalt can be employed as lossy impurities or additives to induce magnetic losses within solids for materials with small dielectric losses leading to the MW absorption for these materials [497]. Conclusively, hysteresis loss occurs inside ferrous magnetic materials while the eddy current loss takes place in conductor and semiconductor materials under MW heating. In the meantime, magnetic resonance loss generates heat inside the magnetic materials when they are irradiated under a change in magnetic field. In particularly specific situations, both of the magnetic loss, eddy current loss, and hysteresis loss, works together to contribute to the MW heating of a material.

Notwithstanding many visible advantages of MW heating overwhelmed the conventional heating, the materials working under MW irradiation require the tactful dealing with some of the issues. The fact that MW heating increases the temperature of materials continuously owing to the continuous rise of the MW absorption. The uncontrolled heating devastates the materials and leads to irreproducible process. To tackle this problem, the dielectric properties of the material is needed to be enhanced by doping or incorporating other MW absorber to produce an indirect heating [498]. The material also undergoes a two-way heating in the presence of the susceptors, as shown in **Figure 2-17**. Susceptors are highly lossy materials, for examples, SiC or carbon, which are characterized by a rapid MW absorption ability resulting in their fast heating. By heating by MW, heat is transferred from susceptors to the sample via the conventional heat transfer [499]. Due to this phenomenon, the temperature of the sample is elevated and they become increasingly lossy to enable the interaction with the MW once the expected temperature is achieved [499]. The rest of the heating takes place via the direct interaction of the sample with the MW wave. The susceptor assisted MW heating is also called “hybrid heating”.

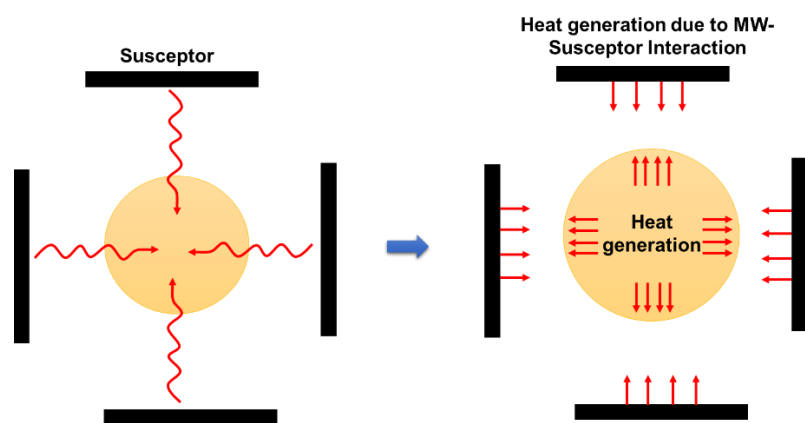


Figure 2-17 – Two-way hybrid MW heating with susceptor [500].

The material surface is heated up by the susceptors while the MW energy heats the material from its center. By this way, the material is provided a more uniform heating compared to the direct MW heating, in which, the center of the material remains a higher temperature than the surface. Heat loss from the material surface can be reduced by the existence of the susceptors assists, and therefore, the thermal homogeneity can be preserved during heating process. This hybrid MW heating technique makes the MW heating to be less dependent on the material dielectric properties, consequently, enhances the reproducibility of the heating process [499]. Nonetheless, susceptors are far more suitable for MW food processing and not appropriate for chemical engineering processes because of the continuous reaction leading to the complexity of using susceptors [467]. Moreover, chemical composition of the original material is altered by the doping method, and thus, doping with a susceptors is not a feasible approach. Alternatively, the employment of metallic oxides such as Al_2O_3 , TiO_2 or CeO_2 , which have no or very low ability to absorb MW wave owing to their high dielectric characteristic [476], is considered as an effective way to overcome uncontrolled heating of catalyst particles under MW heating. The supports are used as insulators to help maintain the temperature since the metal catalyst particles heat up rapidly by MW wave leading to sintering [501]. The heat is disintegrated by transferring from metallic particles to the inert supports and reactant feed flow by conventional heat transfer.

2.5.1.3. Microwave-Enhanced Heterogeneous Gas-Solid Catalytic

The employment of MW irradiation to perform chemical reactions involving heterogeneous transition-metal catalysts has been studied and becoming increasingly

since the 1980s in the scientific community. A brief summary is presented in **Table 2-7**. The selective heating characteristics of MW irradiation with so-called “specific microwave effects” provide better performance reaction rates and selectivity of chemical reaction over heterogeneous catalytic. Wan et al., [502-504] and Ioffe, Pollington and Wan [505] are one of the first pioneers, who utilized MW energy for chemical reactions. This research group mixed the MW absorber in reaction mixtures because most organic compounds and solvents are not strong MW absorbers. By mixing up with a MW absorber, MW wave can further catalyze for reactions in which MW-transparent components are dominant. The concept of “MW catalytic” is thus introduced. Wan and co-workers [506] recommended to employ ferromagnetic and paramagnetic metals as MW catalysts due to their excellent MW absorption ability. This research group converted methane to acetylene over activated carbon under MW heating. They found that randomly oriented active carbon particles led to the existence of local hot-spot plasma in the catalyst bed, which accounted for a higher acetylene selectivity compared to the conventional heating. Zhang et al. [121] reduced SO₂ with methane to form CO₂ and sulfur over MoS₂ catalysts supported on Al₂O₃. A higher conversion of sulfur dioxide and methane was claimed when MW irradiation was employed. Compared to conventional heating, the obtained conversion under MW irradiation was as high as the one at temperatures around 200 K lower. Moreover, the transformation from γ -alumina to α -alumina, which only occurs at temperatures above 1273 K, was observed. This result echoed that the average temperature measured of the catalytic bed (1000 K) is far lower than the local temperature under MW irradiation, which can be considered as a visible evidence of hot-spot formation inside the catalytic bed.

Table 2-7 - Gas-solid catalytic reactions under MW radiation [507].

Reactions	Compared with conventional heating	Reasons	Reference
CH ₄ decomposition	Higher selectivity	Non-uniform temperature distribution	[505]
	None	n/a	[508-510]
	Higher conversion, high selectivity	Plasma formation, arcing	[511]
CH ₄ oxidation	Higher conversion, higher selectivity reduction of reaction temperature	Hot-spot formation	[512, 513]
	None	n/a	[514, 515]
	Reduction of reaction temperature	Hot-spot formation	[516, 517]
	None	n/a	[516, 518]
	None	n/a	[519]
CH ₄ oligomerization	No comparison with conventional process	n/a	[520, 521]
CH ₄ reforming	Higher conversion, higher selectivity	Hot-spot formation	[36]
CH ₄ synthesis	none	n/a	[502, 504]
HCN synthesis	Higher selectivity	Selective catalyst heating	[522]
H ₂ S decomposition	Higher selectivity	Hot-spot formation	[523]
NO _x , SO ₂ reduction	Higher conversion, enhanced reaction rate	No explanation	[509, 524-526]
SO ₂ reduction	Higher conversion, phase transition of catalyst	Hot-spot formation	[121]

	Higher rate	Imprecise temperature measurement	[527]
CO oxidation	No effects	n/a	[528, 529]
	Little improved	n/a	[119, 530]
Propane oxidation	Higher conversion, reduction of reaction temperature	Hot-spot formation	[531]
Ethane/propane/n-butane dehydrogenation	None	n/a	[532]
Ethane dehydrogenation	Higher conversion	Phase transition of catalyst	[533]
o-Xylene/toluene oxidation	Higher conversion, higher selectivity	Hot-spot formation, more homogeneous dispersion of metallic particle	[534]
2-methylpentane isomerization	Higher conversion, higher selectivity	Changed dispersion of metallic particles	[535, 536]
Methanol steam reforming	Higher production rate and selectivity	n/a	[537]
	Reduction of the reaction temperature	Homogeneous energy dissipation	[538]
2-propanol dehydration	Reduction of the reaction temperature	No explanation	[539]

Zhang et al. [540] observed the double higher conversion of H₂S under MW irradiation compared to electric furnace heating. Moreover, this work claimed that the existence of hot-spot was a possible reason for the observed results. Another gas-solid reaction enhanced by MW irradiation is the reduction of sulfur dioxide and NO_x. The first study in this area was reported by Tse [509] in 1990. Specifically, the Ni-based catalyst was heated by the pulsed MW reactor. A considerable decline in the SO₂ concentration and the O₂ selectivity were observed. Cha and co-workers [524] conducted a similar reaction in a char-bed reactor and also observed a significant enhancement of MW heating for SO₂ and NO_x conversion compared to conventional heating. Another work reducing NO_x over carbon-based adsorbents under MW enhanced adsorption was reported by Kong et al., [526]. These researchers found that NO_x could be easily reduced under MW irradiation. Chang et al., [525] and Wang et al., [525] reduce NO_x with methane over ZSM-5 zeolite-based catalysts. They both found that MW irradiation significantly boosted the reduction of NO though some of these catalysts could not show any conversion of NO and CH₄ under conventional heating even at high temperature. Reported by Roussy and co-workers [516, 518], C₂₊ selectivity from oxidative coupling of methane was much higher under MW heating than that under electric furnace heating, particularly at low conversions from 0 – 40 %. Moreover, this work also found that C₂₊ selectivity was highly stable (maintained at 60 % approximately) under the reaction temperature range from 550 to 750 °C heated by MW irradiation. Meanwhile, it was gradually increasing in the case of conventional heating and achieving 60 % at 700 °C. Zhang et al. [519] studied the oxidation of methane and found that the formation of arcing and plasma formation promoted the conversion of methane and the selectivity of hydrogen under the absence of oxygen. Other researchers [520, 521] utilized MW energy as a heating source for methane oligomerization reaction over activated carbon, iron and nickel catalysts. It was found that C₂ product distribution was governed by the applied MW power and frequency. Nonetheless, it was reported that there was insignificant difference in performance of the CO oxidation reaction under the MW and conventional heating [528, 529]. Other researchers performed a comparative study between the conventional and the MW heating system for the isomerization reaction of 2-methylpentane over Pt catalyst

supported on Al₂O₃ and indicated the better enhancement of MW irradiation [535, 536]. Likewise, Liu et al., [534] oxidized o-xylene over V₂O₅/SiO catalyst under MW irradiation and found that higher reactant conversions and product yields were achieved by MW irradiation compared to conventional heating. The reasons for the exceptional enhancement of MW energy was the superheating of V₂O₅ molecules made by MW wave. This conclusion was further examined by Zhang et al. [537], who studied methanol steam reforming over modified Cu/ZnO/Al₂O₃ catalyst under MW heating. It was found that the MW-irradiated catalyst process produced higher hydrogen and CO production rate than the catalytic process under conventional heating. Moreover, methanol steam reforming reaction was also studied by Perry and co-workers [538]. This research group found that the reforming reaction could be conducted at a temperature lower 20 K than conventional equivalence while the kinetic was similarly preserved for both processes. Bond et al., [539] converted 2-propanol over carbon-based (charcoal and graphite) catalysts under MW irradiation. It was found that graphite exhibited a better activity than the charcoal. Moreover, this study also firmed the existence of non-uniform temperature distribution inside the catalytic bed as well as the formation of local hot-spots under MW irradiation, which is consistent with other researchers [514, 515].

2.5.1.4. Temperature measurement in MW reactor system

The measurement of the catalyst temperature in the presence of MW wave is a touch challenge. Unlike reactions under thermal heating, thermocouples cannot be placed into the catalyst bed directly due to the interactions between magnetic field and metallic probe, which may lead to parking [471, 541]. It has been suggested that shielding or grounding the thermocouples can partly solve this problem [542]. An example for such attempts reported by Li and co-workers [34, 179], who placed a thermocouple in a 1-mm-thick quartz tube and grounded that thermocouple by a filter capacitor to reduce the interactions between the thermocouple with MW wave. Nonetheless, other researchers have implied that the problems cannot be completely avoided because of MW transparent properties of quartz [530]. Some authors [119, 520, 521, 543], on the other hand, attempted to place the thermocouple inside the catalytic bed rapidly after switching off the

MW irradiator. Nonetheless, recent experiments have indicated that this technique is infeasible owing to its complexity to stop the reaction periodically and the recorded values were also inaccurate [544]. Durka et al., [545] employed two external fiber optic probes by placing in the axis and close to the MW reactor wall to measure the temperature of small amount of catalyst under a single mode MW cavity. The authors observed a significant temperature gradient, in which, the temperature at the core of MW reactor was considerably larger than that at zone near the wall. Meanwhile, Ramírez and co-worker [546, 547] employed a thermography combined with an optical fiber to measure gas–solid temperature under MW heating with a relatively low range from 100 to 250 °C. Such low temperature range can also be examined by using a simpler temperature measurement method, for example, using common optical fibers [548]. Above 300 °C, the measurement of catalyst bed temperature is a huge technical challenge towards optical fibers due to its limitation (< 300 °C) [471, 549]. The most popular and common measurement technique to examine the reaction temperature in MW reactors is using infrared (IR) thermometry, which is able to record the surface temperature of catalyst [550, 551]. The IR measurement can consist internal IR sensor or external camera. Gangurde et al., [552] used the later IR measurement to examine the temperature of PtC catalyst bed during CO₂ reforming of CH₄ reaction under MW heating. Experimental results highlighted the huge advantage of this IR technique that allows real-time temperature records up to 1000 °C. Nonetheless, the authors also claimed that the thermal camera does not ensure the precise temperature values because the multi-parameter emissivity is dependent on many complex factors. Kappe and co-workers [553] primarily admitted that the accurate measurement of temperature of the reaction mixture under MW heating is a complex affair though the thoughtful calibrations was made. The authors' later efforts have found that an external calibration can reduce the deviation of temperature values. Specifically, the reaction temperature was suggested to be determined by employing a calibrated external infrared sensor, which had been integrated into the microwave cavity. This setup was supposed to be used over a temperature range of – 40 to 2,200 °C. The external sensors are normally made by lead to deal with electromagnetic wave, and therefore, this method is affordable and often acceptable for measuring temperature under MW

heating. Nonetheless, cares must be taken into account when relying on the temperature values from the recorded data of external measurement. This is due to the fact that the IR sensor needs to be re-calibrated each time to achieve a repeatable results [542]. Moreover, the built-in sensors is often drifting during the reaction, particularly for in long-term tests [554]. Though efforts and progresses have been made, the technique for recording the reaction temperature of catalyst inside MW reactor accurately is still pending. At this time, one has to realize that, none available technology can measure temperature locally, such as on the micrometer scale, even in homogeneous liquid systems [555, 556]. Temporarily, the combination between noncontact infrared thermal cameras with thoughtful calibrations together with MW power values can be employed as process parameters to study MW assisted chemical reactions.

2.5.2. Catalysts for MW assisted reforming of methane

2.5.2.1. Carbon-based catalysts

Not surprisingly, there is an overwhelming increase in the applications of MW energy in the area of syngas production. It is a fact that there exists difficulties to select an active catalysts, which have high activity and long durability under MW irradiation. What is clear from the above discussion and the recent reports is that a catalyst, can be active for MW assisted reforming of CH₄, needs to consist at least one component having ability to absorb MW energy. This requirement helps to classify the development of catalysts for MW assisted chemical reactions with that for processes under conventional heating. Carbon-based materials are one of such strong MW absorbers [557]. The MW absorption ability of different types of carbon-based materials is shown in **Table 2-8**. All values are compared to distilled water ($\tan \delta$ is of 0.118 at 2.45 GHz and 298 K). It can be seen that most of the carbon-base materials possess higher loss tangent than distilled water, except for coal. Therefore, carbon – based materials are capable to convert radiation energy to thermal energy heating up the catalysts for chemical reactions. There are two types of chemical reactions preferred by MW heated carbon-based catalysts: (i) high endothermic reactions, such as reforming of methane; and (ii) reactions involving organic chemical compounds possessing low dielectric loss. Because of

these, MW heating have been commonly employed to accelerate reaction-rate spectacularly for organic compounds from the last decades [457, 558-560].

Table 2-8 - Dielectric loss tangents of different carbon materials. [recorded at 2.45 GHz and 298 K] [35].

Carbon material	$\tan\delta = \frac{\epsilon''}{\epsilon'}$	Ref.
Coal	0.02-0.08	[561, 562]
Carbon foam	0.05–0.20	[563]
Charcoal	0.11-0.29	[564, 565]
Carbon black	0.35–0.83	[565-567]
Activated carbon	0.57–0.80	[568, 569]
Activated carbon ^a	0.22–2.95	[570]
Carbon nanotube	0.25–1.14	[571, 572]
CSi nanofibers	0.58–1.00	[573]

^a Activated carbon values were recorded at 398 K.

Perhaps, Domínguez and co-workers [574] are the pioneers in applying MW heating for syngas production with the findings of catalytic activity of carbon-based materials, coffee hulls. Shortly later, Domínguez et al., [31] performed the DRM in the presence of MW heating over potassium char obtained from biomass pyrolysis. Experimental results of this work showed that MW produced hot spots (micro- plasmas) inside the catalyst bed, which accounted for the better reactant conversions than those from conventional heating. A year later, Fidalgo et al., [25] conducted a comparative study on DRM reaction over activated carbon under MW and conventional heating. Higher conversions of both CH₄ and CO₂ were achieved over the process under MW heating. This study also investigated DRM under a wide range of testing conditions. In the range of the optimum temperature range (700 – 800 °C), the reforming reaction was supposed to be taken place as a

combination of CH₄ decomposition and CO₂ gasification. Fidalgo and co-workers [32] also investigated the role of porosity and pore size of different carbon catalysts, such as metallurgical coke, re-activated carbon, and activated carbons for DRM under MW heating. It was found that the DRM reaction occurred mainly in micro-pores of these carbon-based catalysts. The larger micro-pore volume, the better CO₂ reactivity was. Moreover, this study, [32], also found that oxidized activated carbon is not an appropriate catalyst for DRM compared to other carbonaceous materials owing to oxygen surface groups of oxidized activated carbon reduce the catalytic activity significantly. Recently, Hamzehlouia et al., [26] developed carbon supported on SiO₂ by chemical vapor deposition method as a MW receptor for DRM. The conversion of CH₄ and H₂ selectivity were close to unity whilst the respective CO₂ and CO were surrounding 80 % at 800 °C. Moreover, a significant thermal gradient between the catalyst surface and gas phase was visibly observed. Therefore, Hamzehlouia and co-workers concluded that MW heating promoted the reaction kinetics on the catalyst surface. To further improve catalytic activity for reforming of methane reaction, carbon-based materials were recommended to be used as a MW absorber to mix with higher active metallic catalysts, such as Ni. Fidalgo et al., [135] mixed commercial activated carbon and a metallurgical coke with nickel supported on Al₂O₃ catalyst for DRM under MW heating. The results displayed the exceptional activity of commercial activated carbon in a mixture with Ni/Al₂O₃ for the conversion of reactants under MW heating compared to metallurgical coke- Ni/Al₂O₃ catalyst [135]. This work also pointed out the higher conversions achieved by MW heating compared to those obtained by conventional heating at the similar testing conditions. Likewise, Bermudez and co-workers [33] confirmed the higher CH₄ and CO₂ conversions gained by the DRM under MW heating over a mixture of activated carbon-steel-making slag/Al₂O₃ catalyst. Odedairo et al., [30] cleverly grew in-situ carbon-based materials (graphene and carbon nanotubes) on the Ni/CeO₂ catalyst doped by Cr/Fe/Ta to increase MW absorption for DRM. The DRM reaction was performed over a MW power a range of 350 – 600 W with the total VHSV of 10.2 L.g⁻¹.h⁻¹. By this way, Odedairo and co-workers observed the formation of multi-walls carbon nanotube/ graphitic nanofiber composite over Ni/CeO₂ catalyst **Figure 2-18-I**. This carbon composite covered by nanoparticles

at 23- 33 nm in diameter, approximately (**Figure 2-18-I a & b**). Meanwhile, Ni particles and CeO₂ support were partly coated with carbon shells. **Figure 2-18-I c, d & e** confirmed the crystallinity of carbon shell.

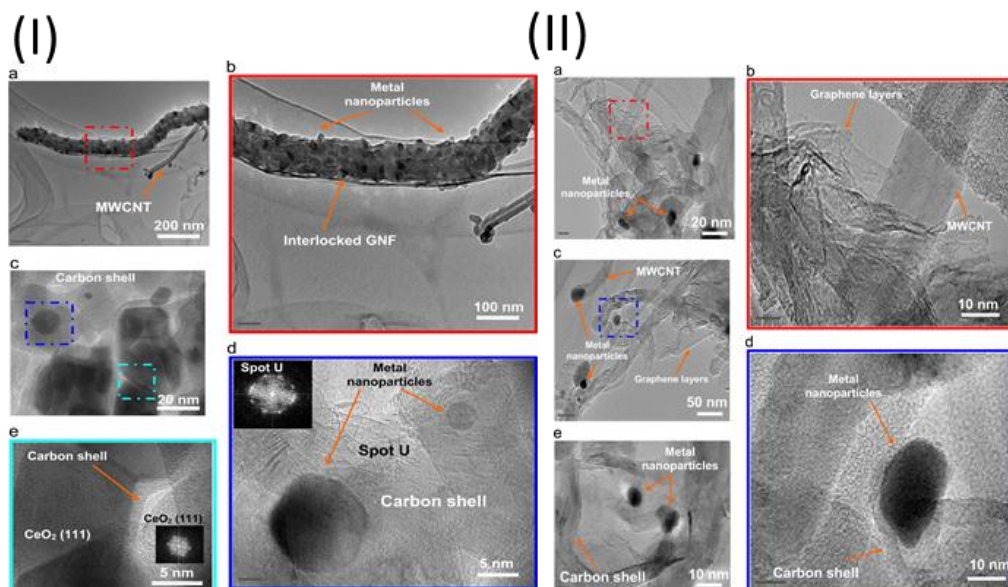


Figure 2-18 – The formation carbonaceous species over Ni/CeO₂ and 2Cr-Ni after 14 h. Reproduced with permission from Ref [30]. Copyright © 2016 Elsevier.

By adding promoters, such as Cr, the formation and distribution of carbon species were becoming complicated. Accordingly, the Cr-Ni particle was dispersed on the continuous and wrinkled graphene layer, as shown in **Figure 2-18-II a & b**. Some Cr-Ni particles coated on the tips of carbon shells **Figure 2-18-II c, d & e**. The formation of these types of carbon promoted the MW absorption ability, and therefore, enhanced catalytic activity for the DRM reaction. In the most recent works, Gangurde et al., [552] employed 10 % platinum supported on activated carbon for the DRM reaction under MW heating. The maximum conversion of both CH₄ and CO₂ could be achieved within the first 1.5 hours on the DRM stream test.

In addition to DRM reaction, carbon-based materials are also employed as catalysts for the SDR reaction. Li and co-workers [179] are the first pioneers in this field by studying both DRM and SDR reactions under MW heating over biochar produced from biomass. The influence of biochar on reactant conversions were examined by altering feeds ingredients, reaction temperature, and heating

method (MW and conventional heating). It was found that combined reforming produces higher CH₄ conversion and syngas ratio than dry reforming owing to the extra supplementary of H₂ from the steam. Noticeably, biomass-derived char delivered a better catalytic activity for combined reforming than that for dry reforming reaction. This observed results were blamed for the optimization role of steam for the competition between coke deposition and carbon consumption, which, in turns, controlled the overall reforming efficiency. Li et al., [34] also found that specific energy consumption was 4.14 kW.h/m³ syngas, which is appropriate for a scale-up MW –assisted SDR reaction. This study indicated that the contained metals in biochar, such as alkaline metal and alkaline earth metals, were crucial to improve the conversions of reactants. By mixing biochar with nickel, Li and co-workers [28] found that the conversions of CH₄ and CO₂ were higher than that obtained the MW assisted SDR reaction over biochar alone. Nonetheless, the reforming performance is significantly dependent on the source of carbon. Specifically, carbon-based catalysts obtained by agriculture residues pyrolysis, such as cotton stalk biochar, wheat biochar, and corn straw biochar exhibited different catalytic activity for DRM under MW heating [27]. Given the similar active metal, such as nickel, cotton stalk biochar had highest catalytic activity whilst corn straw biochar was lowest performance. In the most recent work [29], this group mixed biomass derived char with Fe₂O₃. It was showed that 95 % methane and almost 100 % CO₂ conversion were achieved with the addition of 10 % . wt of Fe₂O₃. In the meanwhile, Kustov et al., [575] exploited the strong MW absorption of deposited to recover deactivated Ni/Al₂O₃ during a continuous DRM reaction by using MW irradiation. This idea prolonged Ni/Al₂O₃ catalyst for further extended 12 hours on the stream test compared to that under conventional heating. Notwithstanding a lot of advantages of carbon-based catalysts for reforming of methane under MW heating, such as plentiful sources, availability, affordability, and strong MW absorption, carbon consumption via the Boudouard reaction (CO₂ + C ↔ 2CO), which reduces catalytic stability significantly, is inevitable for reforming of methane processes [35]. Particularly, Hunt et al., [576] indicated that MW energy promotes the Boudouard reaction vigorously owing to the strong MW absorption of carbon. Specifically, the incident MW radiation created transient electron–hole pairs on carbon surface,

which acted as radical anions and cations reducing CO₂ molecules to generate CO. Such rapid carbon consumption during the reforming reactions leads to the unavailability of commercially catalytic reforming of methane processes over carbon-based catalysts under MW heating in industry.

2.5.2.2. Metallic-based catalysts

Most of the heterogeneous catalytic reactions take place at the active surface of the catalysts. Therefore, the combination of metallic-based catalyst with MW generates locally high temperature on the catalyst surface is expected to accelerate the reforming reactions in less extreme ways. For metallic-based catalysts highly absorbing MW energy, they can also be considered as internal heat source [467]. By using itself as an internal heating source, it can provide more active centers for reforming of methane reactions by heating other elements, which is unable to absorb MW energy directly, via conventional heat transfer. Despite proven benefits of MW irradiation in heterogeneous catalytic reactions, the employment of metallic-based catalysts for reforming of CH₄ in the presence of MW has been limited over the past few decades. The reason for this is the high MW reflection of most bulk metals due to their high electric conductivity causing skin effects. Moreover, the presence of metals under MW irradiation vulnerably forms arcing phenomena producing hazardous conditions, particularly in the existence of flammable gases like CH₄ and H₂. Moreover, metals are prone to sintering under MW irradiation, especially at high MW power. By supporting metallic-based particles on a MW-inert supports, such as, Al₂O₃, TiO₂ can tackle sintering problems. Nonetheless, the development of an active metallic-based catalysts under MW heating for reforming of methane reactions is an arduous task. Zhang and co-workers [36] are the first group studying DRM over platinum catalyst supported on alumina under MW irradiation. The comparative experiments with DRM over Pt/Al₂O₃ catalyst under conventional heating was also performed. Zhang and co-workers found that both of the conversions of reactants and the selectivity of syngas were greatly higher in the presence of MW irradiation. The reason for such results were blamed for the formation of local hot spots promoting the catalytic performance of Pt/Al₂O₃. Gangurde et al., [37] conducted CO₂ reforming of methane over developed Ru -doped SrTiO₃ perovskite catalysts,

which was able to absorb MW energy intrinsically. Stable maximum methane and carbon dioxide conversions of ~ 99.5 and ~ 94 %, respectively, with $H_2/CO \sim 0.9$ were obtained with 7 wt.% of Ru-doped $SrTiO_3$ catalyst under MW heating with the recorded maximum temperature in the vicinity of 940 °C. The reason for the activation of Ru- $SrTiO_3$ catalysts under MW irradiation was its high loss dielectric factor. Nonetheless, an excessive amount of CO_2 was needed to be present in the feed gas to limit carbon formation. This, without doubt, increases the down-stream burden to separate or recycle the unreacted CO_2 leading to the complexity for the DRM process [24]. In the most recent works, Varsano et al., [38] produced syngas via DRM under MW heating over Ni-Co catalyst. The study reported that $Ni_{60}Co_{40}$ was able to absorb MW energy and catalyze the DRM reaction by virtue of the magnetic induction of cobalt species. Varsano et al., also found that the conversions of reactants and syngas yield reached values in line with those produced by conventional furnace heating with a high heating rate of 200 °C.min⁻¹. Such these results further affirmed the advantages of the combination of metallic-based catalysts with MW energy for chemical processes, particularly for reforming of methane reactions. These reports are all studies on MW assisted reforming of CH_4 over metallic-based catalysts. The further development in this research field is thus highly demanded, not only for exploiting advantages of MW heating but also for offering an effective reforming process to produce fuel syngas.

2.6. Conclusion

Given the gradual exhaustion of oil resources and the constantly growing emissions of GHGs, exploiting stranded and associated CH_4 to provide renewable fuels, such as syngas, has drawn a huge interest of research community and industry. Small-to-medium size GTL plants on FPSOVs is particularly appropriate for stranded gas reserves located at remote areas, in which, gas - pipeline option is completely uneconomical. MW reactor system for reforming of CH_4 offers higher performance, flexibility, re-allocation, and lightweight, to be used suitably on small-to-medium size GTL processes. Moreover, reports on applications of MW assisted reforming processes are mostly consistent that the presence MW irradiation can alter the state of the reaction system as well as apparent thermodynamic natures, and thereby, accelerating reforming reactions in

less extreme manners. From the literature, DRM is considered as a superior process in transforming two greenhouse gases (CO_2 and CH_4) into valuable fuel syngas. In the meantime, SDR is considered as an industrial process to produce syngas with expected ratio suitable for Fischer – Tropsch synthesis.

In this chapter, an extensive account of catalytic reforming of methane processes reported in the literature from 1970 up to 2019 is provided. Catalysts for the DRM and SDR reactions under conventional heating is various in types, activity, and stability. From the reviewed literature, satisfactory catalytic activity and stability are dictated in large part by active metals and supports. Transitional metals, such as nickel and cobalt are highly recommended for DRM owing to their high activity and low cost. Nonetheless, their catalytic stability is visibly lower than expensive noble counterparts, like Pt and Ru. Moreover, earth-abundant metals, such as copper have recently been employed as catalysts for gas-phase reactions owing to their affordability and flexible redox properties. Compared to other metal oxides, alumina and TiO_2 support offer superior properties to catalysts for reforming of methane processes, such as availability, high thermal stability, good interaction with metals. In the meanwhile, catalysts for MW assisted methane reforming is classified with those for reforming under conventional heating by a top priority requirement of containing at least one element absorbing MW energy. By virtue of a strong MW absorption ability, carbon-based materials, such as charcoal, biochar, activated carbon, and agriculture pyrolysis residues, are dominantly employed as catalysts for MW assisted reforming of methane. Mixing carbon-based material with other active metals, such as nickel and iron can further improve catalytic activity for both DRM and SDR under MW irradiation. The unfavorable problem of carbon-based catalysts, nonetheless, is the significantly low stability due to carbon loss via the reactions with CO_2 . Compared with carbon-based catalysts, metallic-based catalysts display higher activity and stability. Despite some progress, the modest number of works that employed metallic-base catalysts, such as $\text{Pt}/\text{Al}_2\text{O}_3$, Ru-doped SrTiO_3 perovskite, and Co-Ni for DRM under MW irradiation have been reported. The principal challenge for applying metallic –based materials in this field is their high MW reflection. Though indicated that by introducing magnetic components onto dielectric supports can promote MW absorption of metallic-based catalyst, the MW absorption

mechanism is still on-going debate leading to the lack of intensive research and commercial works on methane reforming processes.

Such challenges have simulated huge motivations of this study to develop a highly active and stable catalysts system for methane reforming under MW irradiation. The first and foremost purpose is to transform greenhouse gas into valuable syngas. The study also aims to provide insights into the activation of heterogeneous catalysts for gas-solid phase reactions under advantageous MW heating method.

Chapter 3 Research Methodology and Analytical Techniques

The methodology of this work is summarized in **Figure 3-1**. Basically, it can be classified into three main steps: (i) catalyst screening; (ii) catalytic activity and stability; (iii) Optimize reforming of methane processes. The first step aimed to find the catalysts, which can be activated under MW heating for reforming of methane reactions. In the second step, the catalytic activity and stability of active catalysts were intensively studied. The last step was dedicated to optimize the reforming of methane processes by studying the effects of operating parameters on the performance of reforming of methane processes.

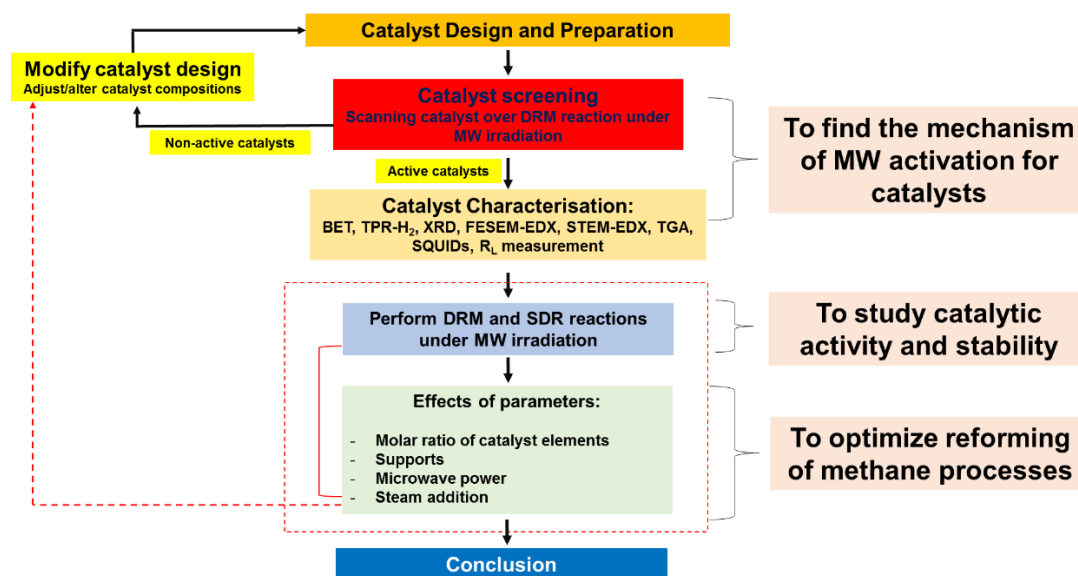


Figure 3-1 – Research methodology.

3.1. Catalyst screening

3.1.1. Catalyst preparation

3.1.1.1. Chemicals and materials

The chemicals employed in this study are listed in **Table 3-1**. Quartz tube reactors were purchased from Monash Scientific Glass Blowing Services, Australia.

Table 3-1 - List of the chemicals used in the study.

Name	Formula	Grade, %	Supplier
Cobalt (II) Nitrate	$\text{Co}(\text{NO}_3)_2 \cdot 6\text{H}_2\text{O}$	99	Chem. Supply
Ammonium Molybdate Tetrahydrate	$(\text{NH}_4)_6\text{Mo}_7\text{O}_{24} \cdot 4\text{H}_2\text{O}$	99	Chem. Supply
Copper (II) Nitrate	$\text{Cu}(\text{NO}_3)_2 \cdot 6\text{H}_2\text{O}$	99	Chem. Supply
Quartz wool	-	99.3	Thermo Fisher Scientific
Aluminium Oxide	Al_2O_3	99	Sasol Germany GmbH
Ethanol	$\text{C}_2\text{H}_6\text{O}$	98.9	Chem. Supply
Titanium dioxide	TiO_2	99	Chem. Supply

3.1.1.2. Catalyst preparation

Given superior advantages analysed from the above **Chapter 2, Section 2.4.**, the wet co-impregnation method was selected to prepare catalysts in this work. Different catalysts were prepared as following:

- For screening catalysts, monometallic catalysts of Co, Mo catalysts with the molar fractions of each metallic component from 0.1 to 0.6 were prepared respectively. Meanwhile, different Co/Mo molar ratios of 0.5 (CoMo0.5), 1.0 (CoMo1), 1.5 (CoMo1.5), 2.0 (CoMo2), and 2.5 (CoMo2.5) supported on Al_2O_3 were subsequently prepared for Co – Mo bimetallic catalysts.
- For the second part of the study, Co-Mo catalysts with corresponding molar Co/Mo ratios 0.5 (CoMo0.5), 1.0 (CoMo1), and 1.5 (CoMo1.5) supported on TiO_2 were impregnated respectively.

- Finally, single Cu, Mo catalysts with the respective molar fractions of 0.1, 0.2, 0.3, 0.4, and 0.5 supported on TiO₂ whilst the binary CuMo/TiO₂ catalysts with Cu/Mo molar ratio of 0.5, 1.0, and 1.5 were also prepared for SDR reaction.

For monometallic catalyst preparation: nitrate salts of cobalt (or copper) were weighted respectively and well dissolved into deionized water. In the meanwhile, for bimetallic catalyst preparation, nitrate salts of cobalt (copper) were weighted respectively and well dissolved into deionized water containing ammonium molybdate tetrahydrate. The solution was stirred for 4 hours. Supports, alumina spheres or TiO₂, were subsequently dried at 105 °C in the oven overnight to eliminate the humidity. They were respectively added into their corresponding solutions and stirring for 2 hours at room temperature. The precursor mixtures were slowly heated up to 60 °C with the heating rate of 1 °C/min and kept at this temperature for 12 hours in the furnace. The sample was then ramped to 250 °C for 4 hours before ramping to 600 °C and kept at this temperature for 6 hours with the heating rate of 1 °C/min.

3.1.2. Catalyst reduction

Prior to reforming of methane reactions, all calcined catalysts were subsequently reduced in the tube furnace with the mixture of 10 % H₂/N₂. N₂ was first introduced through the tube furnace at 600 °C for 1 h to remove moisture and impurities of the catalysts. A gas mixture of 10 % H₂/N₂ with a total flowrate of 10 mL.min⁻¹ was injected through the furnace for 6 hours at 600 °C to reduce the catalyst samples. After finishing the reduction, N₂ gas with the flowrate of 10 mL.min⁻¹ was introduced into the tube furnace to cool down the reduced catalysts. All reduced catalysts were denoted as the fresh catalysts.

3.2. Catalyst characterization

In order to elaborate the MW activation of catalysts and explain for the catalytic activity and stability, comprehensive characterization techniques were employed.

3.2.1. N₂ adsorption and BET surface area measurement

Catalyst surface area is a fundamental property of most heterogeneous catalysts. The specific surface area influences catalytic activity significantly. In this work, the specific surface area measurements of the catalysts were carried out on a Micro Tristar II apparatus at liquid nitrogen temperature using the Brunauer– Emmett– Teller (BET) method. The samples were degassed by evacuation at 250 °C for 12 h before N₂ adsorption measurements. The N₂ adsorption measurement isotherm was also performed at 77 K with liquid nitrogen.

3.2.2. X – Ray diffraction analysis

X-ray crystallography is a common and rapid technique primarily employed for identifying crystalline phase and interpreting unit cell dimensions. In this work, the powder X-Ray diffraction (XRD) analysis of the catalysts was performed by using the Empyrean X-ray Cu K α radiation ($\lambda=0.15418\text{ nm}$) operating at 40 kV from the scan range 10° - 90° with a scanning step size of 0.01° and time of 2 s. Moreover, the Rietveld refinement analysis was also performed by using the FullProf Suite program.

3.2.3. Field Emission Scanning Electron Microscope equipped with Energy - dispersive X-ray spectroscopy (FESEM-EDX)

The Field emission scanning electron microscope (FESEM) is a type of microscope producing high-quality images of catalysts with a focused beam of electrons. In this study, the morphology and elemental distribution of catalysts were analyzed by using FESEM, Zeiss NEON 40 EsB CrossBeam equipped with the Energy - dispersive X-ray spectroscopy (EDX) at 20 keV acceleration voltage.

3.2.4. Hydrogen Temperature-programmed reduction analysis (H₂-TPR)

Hydrogen temperature-programmed reduction (H₂-TPR) is a technique to study the reducibility characteristics of a solid catalyst. All prepared catalysts in this work were performed H₂-TPR analyse by using a ChemBET 3000 equipment. For each analysis, 0.1 g of catalyst powder was subsequently loaded into a quartz cell. The sample was outgassed at 250 °C for 4 h with flowing nitrogen through the

cell to eliminate the contaminants from the catalyst samples. The gas mixture of 5 % H₂/N₂ with a total flow of 20 ml/min was induced through the quartz cell. The reduction temperature was increased from room temperature to 950 °C.

3.2.5. Thermogravimetric Analysis (TGA)

Thermogravimetric analysis (TGA) is an analysis method, in which, the mass of a sample is measured against the temperature and/or time. This measurement used in this study to quantify the amount of deposited coke on the spent catalyst. The TGA analysis for all catalysts in this work was performed by using a Mettler Toledo TGA/DSC instrument. For CoMo/Al₂O₃ and CoMo/TiO₂ catalysts, TGA analysis was performed from 25 to 1000 °C at a heating rate of 5 °C /min whilst the coke amount of CuMo/TiO₂ catalysts was characterized from 25 to 800 °C under an air flow of 60 mL/min.

3.2.6. Scanning Transmission Electron Microscopy-EDX (STEM-EDX)

The scanning transmission electron microscope (STEM) is an invaluable tool for characterizing solid catalyst at atomic level. In this study, the STEM-EDX analysis is performed by the FEI Titan G2 80-200 TEM/STEM microscope equipped with an EDX detector. The STEM analyses with Bright field (BF), Dark field, and High angle annular dark field (HAADF) detectors was performed. All of the catalyst samples is deposited by immersing onto a copper support grid.

3.2.7. Magnetic properties measurement

The magnetic properties of catalysts were measured by using the superconducting quantum interference device (SQUID), Quantum Design MPMS-7 with a maximal applied field of 20 kOe. A SQUID is a highly sensitive magnetometer, which can be used to characterize subtle magnetic materials based on its superconducting loops containing Josephson junctions. The catalyst powder was pressed into a small quartz tube of diameter around 3 mm to fit with the SQUID sample holder.

3.2.8. Reflection loss measurement

The reflection loss (RL) measurements of the prepared catalyst samples over the low frequency range of 1– 10 GHz were performed by using an Agilent 8510C vector network analyzer. The aim of this measurement is to verify the MW absorption ability of catalysts. Specifically, the toroidal-shaped samples (1.5×3.5 mm of in - and outer diameter) were tightly put inside the place between the outer of the conductor and the inner of the coaxial airline. Calibration test was performed before running the analysis. The RL measurement results were obtained by assuming a normal or nearly perpendicular incident of the MW field onto the sample surface, which had been backed by a conductor. The sample can be assumed to have a constant thickness. The RL was calculated based on the computed Weir's reflection/transmission formulation.

3.3. Catalytic performance test

3.3.1. DRM reaction

In this study, the commercial MW reactor system (**Figure 3-2**) for DRM (Alter, SM 1150T, Canada) was employed to test the catalytic performance. The output power of the MW generator can be set flexibly between 0 and 3,000 W at a fixed frequency of 2.45 GHz. Two directional couplers were inserted into the microwave guide system to monitor the forwarded/reflected MW power. As discussed at the section 2.5.1.4 in the **Chapter 2**, the accurate measurement for the temperature of catalyst particle/catalyst bed in MW irradiation systems is a highly complex task. The IR Thermometer (IR-730, - 32 °C – 1,250 °C, Amprobe) was, therefore, used as a temperature indicator for catalyst screening whilst MW power was used as a process parameter to investigate its effects on catalytic activity and to repeat the experiments.

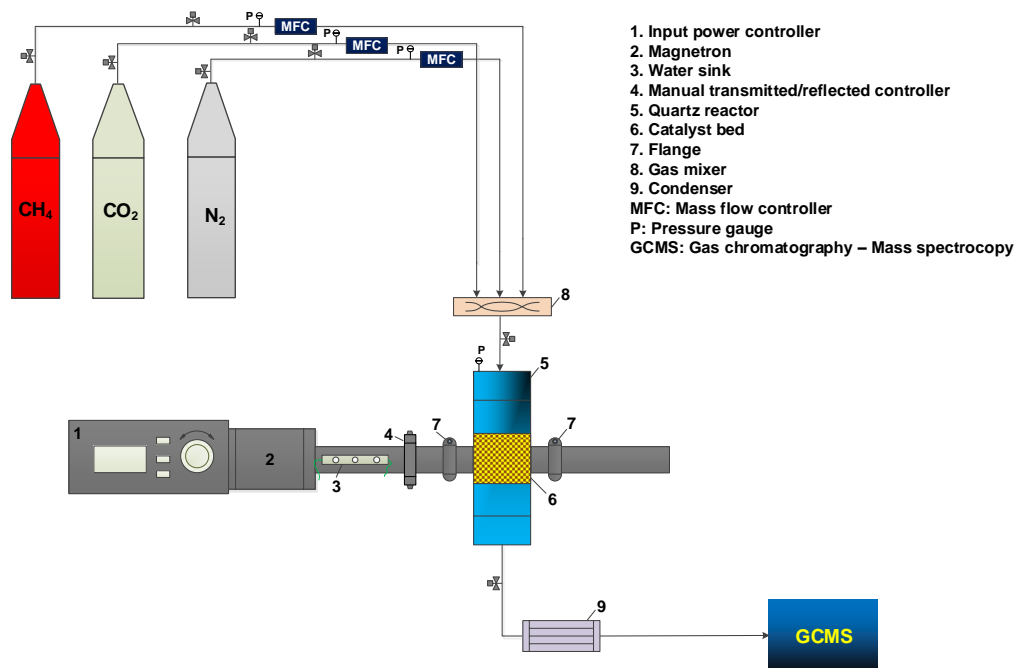


Figure 3-2 – MW reactor system for catalytic DRM.

The catalyst bed dimension inside the quartz tube reactor is $120 \times 25 \times 1.68 \text{ mm}$. The total feed flowrate fixed for all tests was controlled at $10 \text{ L.g}^{-1}.\text{h}^{-1}$ VHSV with $\text{CO}_2/\text{CH}_4 = 1.0$. In the downstream section, the product stream passes through a condenser to separate condensable products (if any). The effluent gas was analyzed by the Gas chromatography (Agilent 7890A) equipped with two columns: (i) HP-5 connected to a MS detector for analyzing C_{2+} compounds; and (ii) TDX 01 connected to a TCD detector for H_2 , CO , CO_2 , N_2 and CH_4 quantitative analysis. The analysis was commenced after DRM reaction was stable and each analysis was repeated three times. In order to improve the quantitative analysis results, N_2 with a constant flowrate (0.01 L.min^{-1}) was added to the feed and used as an internal standard. For all catalytic activity tests, 4 g of respective catalysts were loaded and packed with quartz wool. For catalyst screening of Co, Mo, and Co-Mo catalysts supported on Al_2O_3 , the MW power was increased gradually from 50 to 1000 W with 50 W intervals to determine the MW power value, at which, the catalysts initiates to catalyse DRM reaction. Once determined the active catalysts, the effects of MW power and of metallic molar ratios upon the catalytic performance were intensively studied. The MW power used for testing catalytic activity of CoMo/TiO_2 and CuMo/TiO_2 catalysts was from 50 to 400 W.

3.3.2. SDR reaction

Similarly, the catalytic activity and stability test for the SDR reaction was performed by using the same MW system described above. Nonetheless, a steam generator system was employed and connected to the MW reactor to supply steam for the SDR reaction. The reactor setup is shown in **Figure 3-2**. The heat insulation system was employed to prevent the re-condensation of steam in the pipeline between the mixer and the reactor.

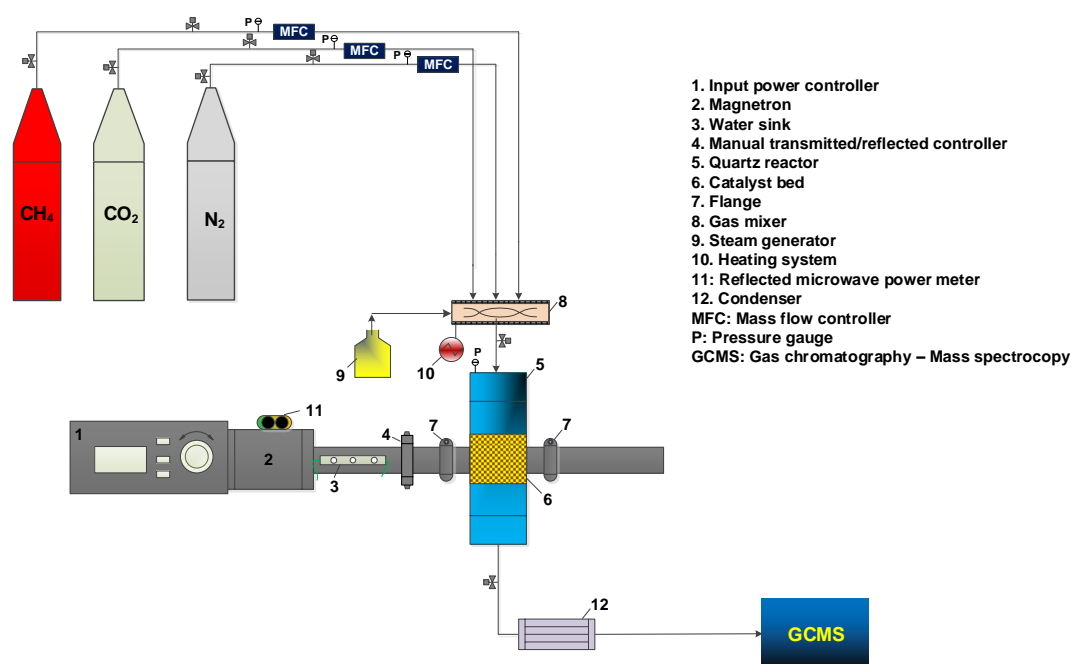


Figure 3-3 - Scheme of the catalytic SDR system heated by MW.

The similar total feed flowrates with DRM test was also fixed for all SDR tests (VHSV of $10 \text{ L.g}^{-1}.\text{h}^{-1}$ with $\text{CO}_2/\text{CH}_4 = 1.0$). To study the difference between SDR and DRM catalytic performance of CoMo/TiO_2 catalyst, the steam-to-methane (S/C) molar ratio was fixed at 0.1. Meanwhile, the S/C ratios of 0, 0.05, 0.1, 0.15, 0.2, 0.25, and 0.3 were used to study the ratio effects on the SDR performance over CuMo/TiO_2 catalysts.

3.4. Calculations

The conversion of the reactants is determined by the following equation:

$$X_i = \frac{\text{mole}_{\text{converted}}^i}{\text{mole}_{\text{in}}^i} \cdot 100\% \quad (3-1)$$

Where, X_i is the conversion of gas, i , %; $\text{mole}_{\text{converted}}^i$ is the converted mole of gas i (mole); $\text{mole}_{\text{in}}^i$ is the inlet mole of gas i (mole).

The selectivity of H₂ and CO from DRM reaction and SDR can be calculated as:

$$S_{\text{H}_2}^{\text{DRM}} = \frac{\text{mole}_{\text{H}_2}}{2 \cdot \text{mole}_{\text{CH}_4}^{\text{converted}}} \cdot 100\% \quad (3-2)$$

$$S_{\text{H}_2}^{\text{SDR}} = \frac{2 \cdot \text{mole}_{\text{H}_2}}{4 \cdot \text{mole}_{\text{CH}_4}^{\text{in}} + 2 \cdot \text{mole}_{\text{H}_2\text{O}}^{\text{in}}} \cdot 100\% \quad (3-3)$$

$$S_{\text{CO}} = \frac{\text{mole}_{\text{CO}}}{\text{mole}_{\text{CH}_4}^{\text{converted}} + \text{mole}_{\text{CO}_2}^{\text{converted}}} \cdot 100\% \quad (3-4)$$

Where, $S_{\text{H}_2}^{\text{DRM}}$ and $S_{\text{H}_2}^{\text{SDR}}$ are the selectivity of hydrogen from DRM and SDR reaction (%), respectively; mole_{H_2} and mole_{CO} are mole of hydrogen and carbon monoxide formed (mole), respectively; $\text{mole}_{\text{CH}_4}^{\text{converted}}$ and $\text{mole}_{\text{CO}_2}^{\text{converted}}$ are the mole of methane and carbon dioxide converted (mole), respectively; $\text{mole}_{\text{H}_2\text{O}}^{\text{in}}$ and $\text{mole}_{\text{CH}_4}^{\text{in}}$ are the input mole of steam and methane (mole), respectively.

Meanwhile, syngas ratio can be defined as:

$$\text{H}_2/\text{CO} = \frac{\text{mole}_{\text{H}_2}}{\text{mole}_{\text{CO}}} \quad (3-5)$$

Where, mole_{H_2} and mole_{CO} are mole of hydrogen and carbon monoxide formed (mole).

Chapter 4

Screening catalysts activated under MW irradiation for DRM

4.1. Introduction

As reviewed in Section 2.4. , **Chapter 2**, cobalt and molybdenum are strong magnetic and paramagnetic materials, respectively. These two metals also exhibit a high catalytic activity for reforming reactions. Moreover, the presence of molybdenum in metal catalyst structure support to improve the catalytic stability. This chapter is thus devote to screen cobalt, molybdenum monometallic and cobalt-molybdenum bimetallic catalysts with different metal loading and ratios supported on Al_2O_3 for DRM reaction under MW heating. All of the catalysts were throughout examined by characterization techniques mentioned in **Chapter 3**, section 3.2. This is a significant step in this study to determine the active catalysts under MW heating for DRM reaction.

4.2. Result and discussion

4.2.1. Catalytic activity

The activity data of all fresh catalyst samples were collected under steady-state conditions with results shown in **Figure 4-1**. Noteworthy that the monometallic catalyst either $\text{Co}/\text{Al}_2\text{O}_3$ or $\text{Mo}/\text{Al}_2\text{O}_3$ was inactive for DRM under MW heating. Thus, no reactant conversions or syngas selectivity was detected at all tested MW power levels from 50 to 1, 000 W. By contrast, bimetallic catalysts of $\text{Co-Mo}/\text{Al}_2\text{O}_3$ started to convert approximately 35 % CH_4 and 47 % CO_2 at molar ratio of 0.5 Co: 1.0 Mo ($\text{CoMo}_{0.5}$) and MW power of 500 W. There is another observation that the required minimum MW power level to activate bimetallic catalysts declines with the increase of Co loading up to Co:Mo of 2.0. The bimetallic catalysts of CoMo_2 and $\text{CoMo}_{2.5}$ could be activated at a far lower MW power (200 W) than those with CoMo_1 (400 W) and $\text{CoMo}_{1.5}$ (300 W), respectively. Furthermore, the higher Co/Mo molar ratio value resulted in larger reactant conversion and syngas selectivity. However, both of CH_4 or CO_2 conversions and H_2 or CO selectivity increased with the increment of Co/Mo

loading up to 2.0. A further addition of cobalt such as Co/Mo ratio of 2.5 will result in a reversible effect, possibly due to the fact that the excessive amount of cobalt promotes the formation of inactive phases to suppress surface active sites to prevent the incident MW wave adsorption, and thus, lowering the activity. Such influence will be discussed shortly.

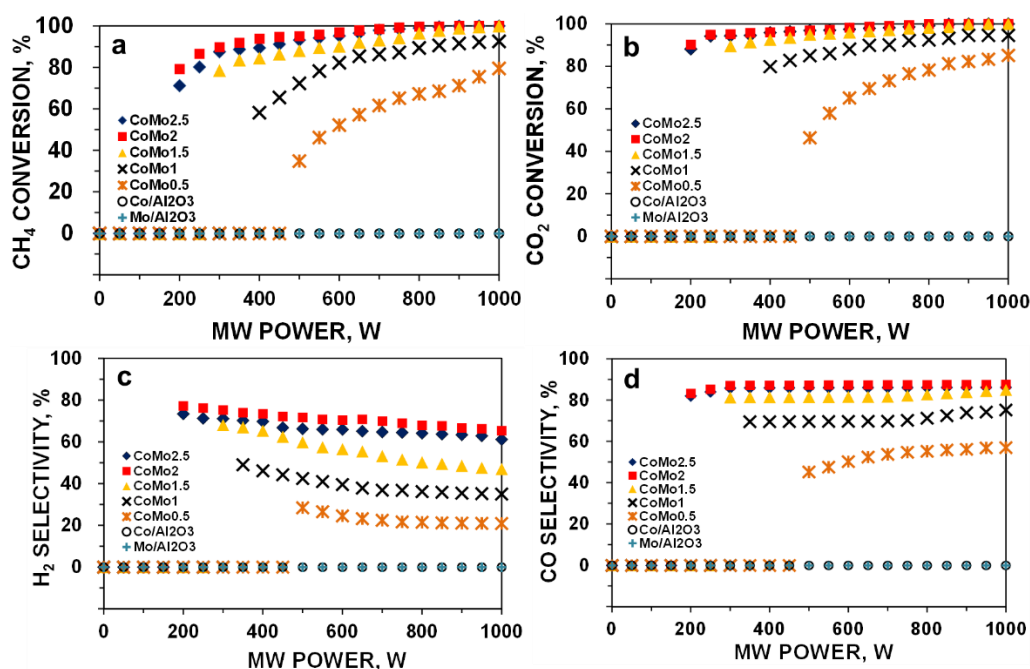


Figure 4-1 - CH₄ conversion (a), CO₂ conversions (b), H₂ selectivity (c), and CO selectivity of DRM reaction for all the CoMo catalysts under MW irradiation at different MW power levels. [Reaction parameters: CH₄/CO₂=1, VHSV = 10 L.g⁻¹.h⁻¹]. Reproduced from Ref. [577] with permission from the Royal Society of Chemistry.

Notably, the conversion of CO₂ was higher than that of CH₄ and the selectivity of CO was also higher than that of H₂ in all cases tested. Moreover, both CH₄ and CO₂ conversion raises with the escalation in MW power (**Figure 4-1a & b**). By contrast, there are two opposite trends of H₂ and CO selectivity variation towards the MW power levels employed (**Figure 4-1c & d**). Whereby, the selectivity of H₂ gradually declined while that of CO sharply increased when rising MW power which also leads to the decrease in syngas ratio of H₂/CO (**Figure 4-2**).

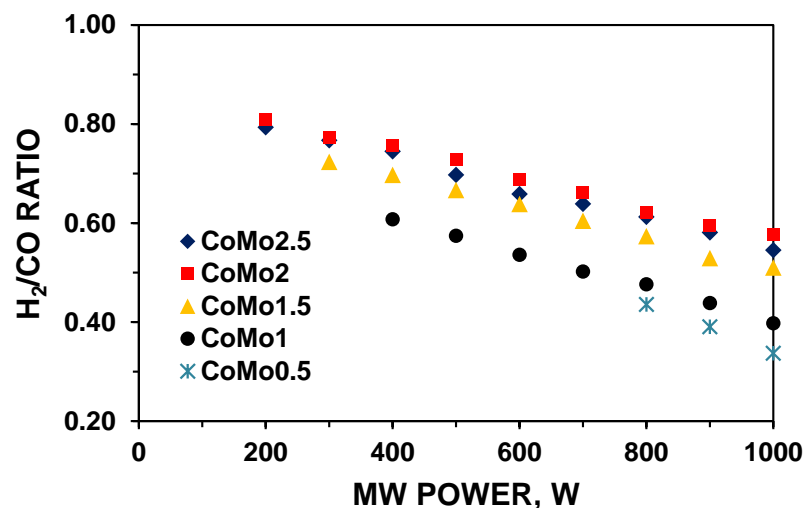


Figure 4-2 - H₂/CO ratio. [DRM reaction parameters: CH₄:CO₂=1, VHSV = 10 L.g.h⁻¹]. Reproduced from Ref. [577] with permission from the Royal Society of Chemistry.

This observation reveals that in addition to the major DRM reaction (**Eq.4-1**), other reactions such as carbon deposition (**Eq.4-2**), the Boudouard reactions (**Eq.4-3**) and reversed water gas shift (RWGS) (**Eq.4-4**) would simultaneously occur.



The numerous papers in the literature have been reported about the observation of water as a by-product of DRM reaction [251, 578]. In this work, a tiny amount of water production was observed verifying the occurrence of the RWGS reaction (**Eq.4-4**). The side reactions such as (**Eq.4-3**) and (**Eq.4-4**) are highly endothermic [579] and thus H₂/CO ratio declined when increasing MW power. Furthermore, it is noted that carbon is a strong MW absorber [35], consequently, the Boudouard reaction (**Eq.4-3**) would be further facilitated for carbon removal, suppressing the carbon residue (deposition) under MW irradiation. A similar observation was made by other researchers [576]. The incident MW radiation creates transient electron-hole pairs on carbon surface, which act as radical anions and cations

reducing CO₂ molecules to generate CO. Therefore, the usage of MW irradiation exhibits additional advantages which is not only promote the Boudouard reaction to produce more CO, but also reduce the carbon deposition. However, this advantage of using MW irradiation for DRM can only be reflected for the heterogeneous catalyst system with inherent capability to absorb MW without the need of including other MW absorbers such as carbon. Other researchers explored the catalytic performance with carbon (a good MW acceptor) or mixed carbon with more active catalyst such as Ni/Al₂O₃ [28, 135]. However, the decrease in catalytic activity was rapidly observed in less than 1 or 2 hours. The reason for such poor stability is due to the occurrence of Boudouard reaction (**Eq.4-3**) leading to the carbon loss during DRM process [20]. Pt known as a noble metal with high catalytic activity was also mixed with active carbon for DRM under MW heating [552]. As reported, the amount of carbon catalyst was decreased over approximately 270 minutes at 34 mL.min⁻¹, CH₄/CO₂=1 and MW power of 150 W. Compared to the reported carbon-based catalysts [28], the CoMo₂ catalyst showed a good catalytic activity converting around 80 % CH₄ and 91 % CO₂ to the syngas ratio (H₂/CO) of 0.80 at the higher total VHSV of 10 L.g⁻¹.h⁻¹ and a low MW power of 200 W.

4.2.2. Catalyst stability

In addition to the higher catalytic activity, the bimetallic catalyst also exhibited the better stability. The long-time test of CoMo₂ for DRM over 16 TOS under MW irradiation with three typical MW power levels (200, 500 and 1000 W) was conducted and the result is shown in **Figure 4-3**. The catalytic performance of tested bimetallic catalyst is almost constant over 16 TOS at MW power of 200 W. At a higher MW power of 500 W, a minor decline in catalytic activity was observed. However, at MW power of 1000 W, the decline in catalytic performance was more apparent compared to the operation under lower MW.

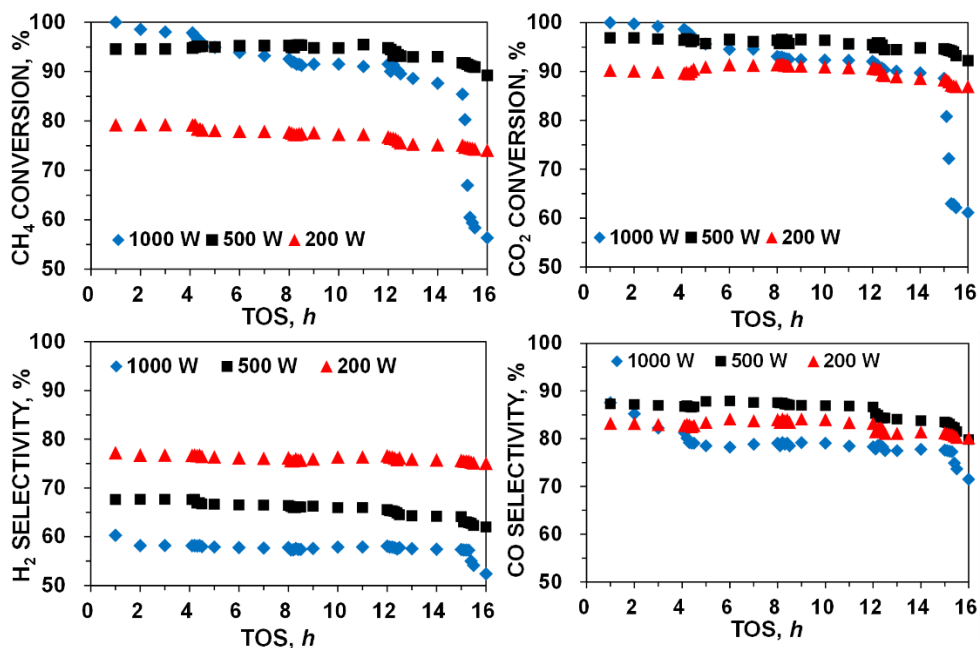


Figure 4-3 - Catalytic stability of CoMo₂ catalyst at three different MW power levels. [Reaction parameters: CH₄:CO₂=1, VHSV = 10 L.g.h⁻¹]. Reproduced from Ref. [577] with permission from the Royal Society of Chemistry.

The CoMo₂ catalyst delivers a high stable catalytic activity owing to its intrinsic ability to absorb MW energy without the need of mixing with carbon in the catalyst bed, which would lead to a shorter catalyst lifetime because of carbon loss during DRM reaction. Pt catalyst supported by γ - Al₂O₃ can also be activated under MW heating for DRM at the total VHSV of 7.2 L.g⁻¹.h⁻¹ [36]. Nevertheless, such a noble metallic-based catalyst is infeasible for larger scale applications [580] due to the high catalyst cost. Other catalyst with carbonaceous material developed by Zhu and coworkers was investigated for the syngas production via DRM heated by MW (350 – 600 W) over Ni/CeO₂ catalyst doped with Cr/Fe/Ta at the total VHSV of 10.2 L.g⁻¹.h⁻¹ [30]. The in-situ grown carbonaceous materials like graphene or carbon nanotubes were cleverly to increase the MW absorption and reaction efficiency. However, the long term stability of the catalytic performance is still a problem due to carbon loss. Very recently, Gangurde and co-workers synthesized ruthenium-doped SrTiO₃ perovskite catalysts which can also absorb MW energy for DRM [37]. Nonetheless, an excessive amount of CO₂ was needed to be present in the feed gas to limit carbon formation. This without

doubt increases the down-stream burden to separate or recycle the unreacted CO₂ leading to the complexity for DRM process [24].

4.2.3. Catalyst characterization

4.2.3.1. BET

A series of physical analyses was performed to appraise the relationship between catalyst structure and catalytic activity for DRM under MW irradiation. To elaborate the difference between mono-metallic and bimetallic catalysts, Figure 4-4a present the N₂ absorption/desorption isotherm curves of monometallic and CoMo₂ catalyst samples. As observed, the physisorption isotherms curves of both of the monometallic and the bimetallic catalyst ascribe to type IV (Figure 4-4a & b), which is a favourable feature for mesoporous materials with the high catalytic activity for gas phase reactions [581]. The isotherm adsorption at low relative pressure ratio ($P/P_0 \leq 0.3$) of all reduced catalyst samples had lower nitrogen adsorption (lines close to X axis) than that of high relative pressure ratio, indicating a weak interaction between the nitrogen and catalysts. In contrast, at higher relative pressure, molecular clustering was followed by pore filling. Moreover, the cobalt loading presents the significant effects on the structure of catalysts. The hysteresis loops shifted from H₂ type (CoMo_{0.5}, CoMo₁) to H₄ type (CoMo_{1.5}, CoMo₂, CoMo_{2.5}) (Figure 4-4). According to the IUPAC recommendations, this result suggested an transformation from a structure with narrow necks and wide bodies (ink-bottle pores) (H₂) [582] to that of with aggregated of plate-like particles leading to slit-shaped pores and narrow slit-like pore, respectively [583]. The areas of the hysteresis loops becomes smaller and the isotherms of the reduced Co-Mo/Al₂O₃ catalysts is shifted downward, which therefore suggest the decline in the BET surface areas.

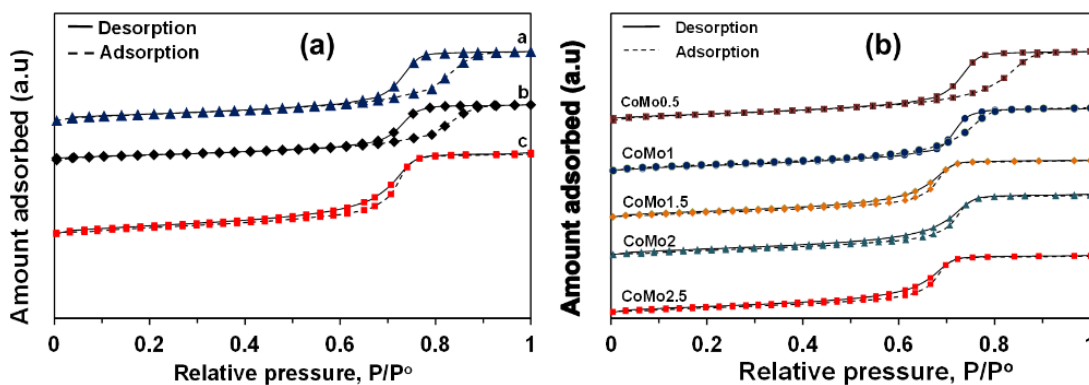


Figure 4-4 - N₂ adsorption/desorption isotherm curves of monometallic and CoMo₂ (a); and all bimetallic catalyst samples (b). Reproduced from Ref. [577] with permission from the Royal Society of Chemistry.

The decrease in pore size and BET surface area was observed by increasing molar ratio Co/Mo from 0.5 to 2.5 (**Table 4-1**). This is due to the decrease of the alumina content per weight unit as the porous support contributing the major high surface area.

Table 4-1 - BET and porosity of the fresh catalysts. Reproduced from Ref. [577] with permission from the Royal Society of Chemistry.

Sample	BET (m^2/g) ^a	Pore volume (cm^3/g) ^b	Pore size (nm) ^c
Al ₂ O ₃ *	163	0.8	17
Mo/Al ₂ O ₃	98	0.6	12
Co/Al ₂ O ₃	94	0.7	14
CoMo0.5	79	0.4	10
CoMo1	65	0.4	9
CoMo1.5	60	0.3	7
CoMo2	58	0.2	7
CoMo2.5	49	0.2	5

Noteworthy that the BET surface area as well as pore size of bimetallic catalysts was insignificantly altered at low irradiated MW power levels such as 200 W (**Table 4-2**), which mirrors the high stability under such operating conditions.

Table 4-2 - BET and porosity of the spent catalysts. [Reaction parameters: CH₄:CO₂=1, VHSV = 10 L.g.h⁻¹]. Reproduced from Ref. [577] with permission from the Royal Society of Chemistry.

Sample	BET (m ² /g) ^a			Pore volume (cm ³ /g) ^b			Pore size (nm) ^c		
	200 W	500 W	1000 W	200 W	500 W	1000 W	200 W	500 W	1000 W
Mo/Al ₂ O ₃	98	98	98	0.6	0.6	0.6	12	12	12
Co/Al ₂ O ₃	94	94	94	0.7	0.7	0.7	14	14	14
CoMo0.5	73	64	52	0.5	0.5	0.4	10	10	7
CoMo1	61	58	51	0.4	0.3	0.3	9	9	6
CoMo1.5	57	52	50	0.3	0.3	0.2	8	7	4
CoMo2	54	51	46	0.3	0.3	0.2	7	6	3
CoMo2.5	46	44	34	0.2	0.1	0.1	5	4	1

These results help to explain the conservancy of catalytic activity over 16 TOS of the bimetallic catalyst at low MW powers (**Figure 4-1**). However, a considerable deterioration in textural properties of bimetallic catalysts was observed at higher MW power i.e., 1000 W, possibly due to the high temperature sintering of metallic-based particles to form bigger particles under high MW energy heating decreasing catalyst surface area. The porosity of monometallic catalysts, conversely, is unaffected by MW energy since these catalysts was inactive.

4.2.3.2. H₂-Temperature program reduction (TPR-H₂)

Figure 4-5 presents the TPR-H₂ profiles of monometallic and bimetallic catalysts. In this TPR-H₂ analysis, each peak corresponds to a different oxide and the amplitude of each peak is proportional to the reaction rate. The amount of H₂ uptake during the reduction was measured by a thermal conductivity detector (TCD), which was calibrated by the quantitative reduction of copper oxide to the metallic copper. At a first glance, the TPR-H₂ analysis indicates the visible differences in the reducibility between the calcined mono - and bimetallic catalysts. The calcined Co/Al₂O₃ catalyst exhibits two hydrogen consumption peaks located at 454.1 and 630.7 °C, which are assigned to the reduction of Co⁺³ to Co²⁺ and Co²⁺ to Co⁰, respectively [584]. There are also two distinct hydrogen consumption peaks respectively at 753.4 and 897.1 °C observed from the calcined Mo/ Al₂O₃. The initial peak is attributed to the reduction of Mo⁺⁶ to Mo⁺⁴ while

the later is associated with the reduction of Mo^{+4} to Mo^0 or the reduction of tetrahedral Mo species [585]. Introduction of cobalt into the monometallic molybdenum supported by Al_2O_3 with molar ratio Co/Mo of 0.5 led to the improvement of catalyst reducibility. The H_2 consumption peak of cobalt species reduction shifted from 454 to 405 °C while that of Mo^{+6} was reduced from 897 to 774 °C. Moreover, by increasing Co/Mo ratio from 0.5 to 2.5, the reduction temperature of bimetallic catalyst samples also shifted to lower values (**Figure 4-5**). CoMo_2 exhibited the H_2 consumption peak for the reduction of cobalt and molybdenum species are 397.2 and 757.6 °C, respectively. Thus, in a mixture form, the synergetic effects between two metallic atoms (Co and Mo) weaken the interaction of each metallic component with Al_2O_3 support, which leads to the improvement of the reducibility for bimetallic catalyst samples.

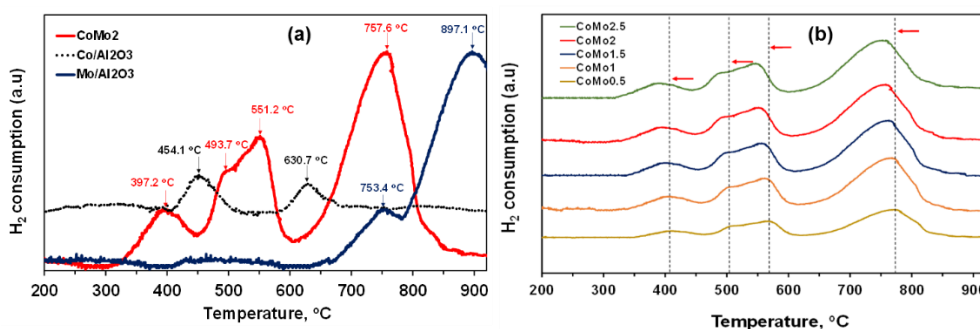


Figure 4-5 - TPR- H_2 profiles of monometallic and CoMo_2 (a); bimetallic catalysts (b). Reproduced from Ref. [577] with permission from the Royal Society of Chemistry.

Noteworthy that distinguishable hydrogen consumption peaks located at 551.2 °C and a small shoulder at 493.7 °C are observed from CoMo_2 catalyst (**Figure 4-5**). Conceivably, these observed peaks are associated to the reduction of bimetallic oxides such as CoMoO_4 to a bimetallic alloy, which will be further confirmed by XRD and FESEM-EDX and STEM-EDX. The similar observation was made by other researchers, who observed the reduction of CoMoO_4 to Co_2Mo_3 alloy at 575 °C of Co-Mo supported on SiO_2 catalyst [586].

4.2.3.3. XRD

To further verify the effects of catalyst structure on the catalytic activity, the XRD analysis of fresh and spent catalysts was performed. The results are shown in

Figure 4-6. There is a fairly low crystallinity of the reduced Co/Al₂O₃ and Mo/Al₂O₃ catalysts since the broad peaks at 45.9°, 60.6°, 67° (PDF 96 – 101 – 0462) ascribed to Al₂O₃ (**Figure 4-6a**). The TPR-H₂ profile of the calcined Co/Al₂O₃ catalyst indicates two different reducing peaks of cobalt oxides while the XRD shows the absence of Co-based diffraction peaks, all of which suggest a very well dispersion of Co-based particles in the support structure which will be further confirmed by FESEM-EDX and STEM-EDX analysis. The MoO₂ phase was detected from the reduced Mo/Al₂O₃ sample at 26.1° (PDF 96 – 153– 9091). This is in a good agreement with the reduction of molybdenum oxides at high temperature (> 750 °C) indicated by the previous TPR-H₂. Noticeably that the intensity of all diffraction peaks increased with the co-presence of cobalt and molybdenum supported on Al₂O₃ (**Figure 4-6a**). Particularly, the improvement in the degree of crystallization is observed when the increase of Co/Mo ratio from 0.5 to 2.5 (**Figure 4-6a**). The XRD patterns evoke that cobalt significantly interacts with molybdenum species and therefore improved the degree of crystallization. The XRD diffraction peak of MoO₂ respectively at 26.1°, 37.1°, 53.2°, 53.6°, 53.7° (PDF 96 – 153– 9091). The previous TPR-H₂ profile of CoMo₂ indicates the reduction-related peak of Co⁺³ species at 397.2 °C; however, the diffraction peak at 36.8° ascribed to Co₃O₄ phase (PDF 96-153-8532) was visibly detected from this bimetallic catalyst (**Figure 4-6a**). This observation displays a complex dispersion of metallic components into the support structure. It is worth noting that the diffraction peaks at 40.1°, 42.9°, 45.4° (PDF 96 – 152– 5121) ascribed to Co_{0.82}Mo_{0.18} bimetallic alloy are detected from bimetallic catalysts. Gaytan and co-workers also observed crystal pattern of Co_{0.82}Mo_{0.18} alloy when fabricating Co-based alloy by electron beam melting method [587]. The presence of this bimetallic alloy affirmed the previous TPR-H₂ profile on the prediction about the reduction of bimetallic oxide such as CoMoO₄ to Co_{0.82}Mo_{0.18} alloy within the range of temperature from 490 to 555 °C. The presence of Co_{0.82}Mo_{0.18} is very unique for bimetallic catalyst and may be the reason for Co-Mo/Al₂O₃ bimetallic catalysts to be active for DRM under MW irradiation.

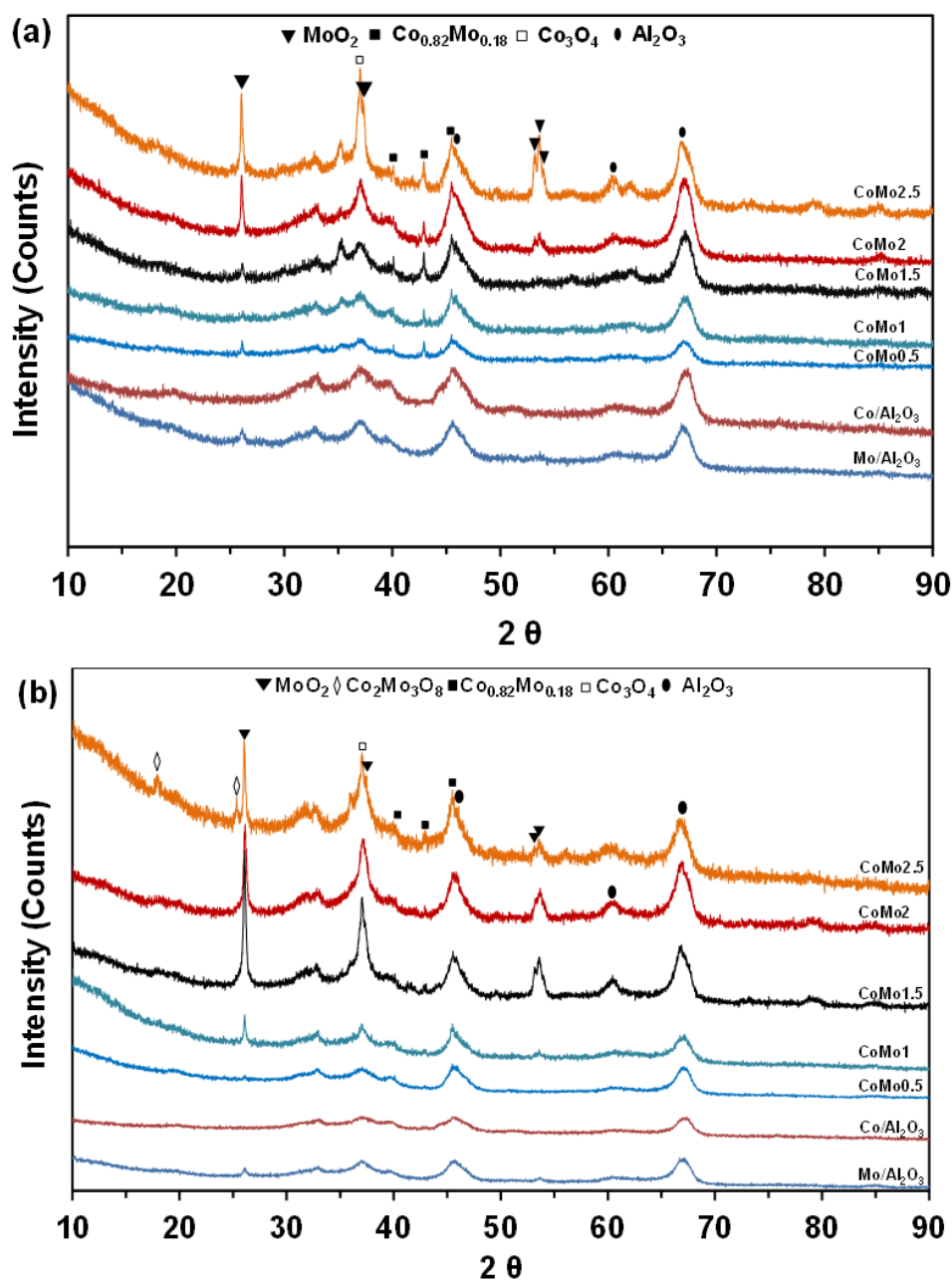


Figure 4-6 - XRD of fresh (a) and spent (b) catalysts. [Reaction parameters: 500 W, $\text{CH}_4:\text{CO}_2=1$, $\text{VHSV} = 10 \text{ L.g.h}^{-1}$]. Reproduced from Ref. [577] with permission from the Royal Society of Chemistry.

Furthermore, the Rietveld refinement analysis result of CoMo2 catalyst (**Figure 4-7**) and the cell parameters of $\text{Co}_{0.82}\text{Mo}_{0.18}$ alloy (**Table S4**) indicate that this alloy structure is assigned to a space group symmetry of $P 63/m m c$ with a hexagonal crystallography ($a = 2.5582 \text{ \AA}$ and $c = 4.2231 \text{ \AA}$, $\alpha = \beta = 90^\circ$).

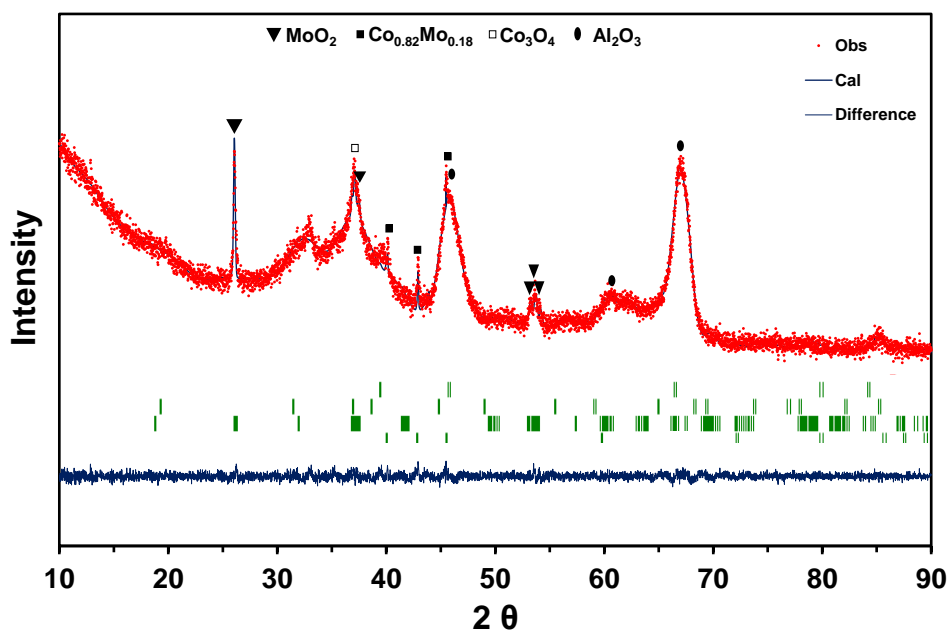


Figure 4-7 - X-ray diffraction patterns fitted using the Rietveld refinement method for CoMo2 catalyst sample. $\chi^2 = 1.12$. Reproduced from Ref. [577] with permission from the Royal Society of Chemistry.

In the present study, whole-pattern Rietveld refinement was performed on the XRD patterns to quantify the amounts of the different phases. The individual phase contribution used for Rietveld analysis are MoO₂ and Al₂O₃, Co₃O₄ Co_{0.82}Mo_{0.18}. There is also a well matching between the XRD patterns of the CoMo2 catalyst and the calculated model, as confirmed by the graphical fitting and by the values of the agreement factor ($\chi^2 = 1.42$). Moreover, the weight percentage of phases in a XRD tested sample (approx. 0.1 g) calculated from the refinement analysis was in a close agreement with the nominal loading which is 30 wt. % metallic component and 70 wt. % Al₂O₃.

Table 4-3 - The Rietveld refinement results. Reproduced from Ref. [577] with permission from the Royal Society of Chemistry.

Phase	Phase information			
	Quant. (%)	a (Å)	b (Å)	c (Å)
MoO ₂	10.25	5.5343	4.8420	5.6080
Al ₂ O ₃	68.60	3.9410	-	-
Co ₃ O ₄	14.25	8.0972	-	-
Co _{0.82} Mo _{0.18}	6.90	2.5582	-	4.2231

After 16 h TOS of DRM reaction under MW irradiation, the crystalline structure of monometallic catalysts are unaltered (**Figure 4-6b**) since Co/Al₂O₃ or Mo/Al₂O₃ does not inspire the DRM under MW heating. For the spent Co-Mo/Al₂O₃ catalyst, the patterns of MoO₂, Co_{0.82}Mo_{0.18} and Co₃O₄ are still detected. This result evokes the stability of crystalline structure of bimetallic catalysts under redox environment of DRM reaction as well as MW irradiation leading to the enduring catalytic stability. Noticeably that Co₂Mo₃O₈ phase is visibly identified at 17.8°, 25.2° (PDF 96-152-4069) from the spent CoMo2.5 catalyst (**Figure 4-6b**). The appearance of Co₂Mo₃O₈ phase elicits either the reaction between finely dispersed metallic Co⁰ and MoO_x or the oxidation of Co_{0.82}Mo_{0.18} in the oxygen-rich reforming environment.

4.2.3.4. Morphological characterization

Succinctly, this morphology of CoMo2 was characterised. **Figure 4-8** shows the FESEM (a₁-b₁), STEM (a₂-b₂), and HRTEM (a₃-b₃) of the fresh and spent CoMo2 catalysts. It can be seen that FESEM image of fresh CoMo2 catalyst exhibits randomly-oriented particles with relatively uniform size distribution (**Figure 4-8a**).

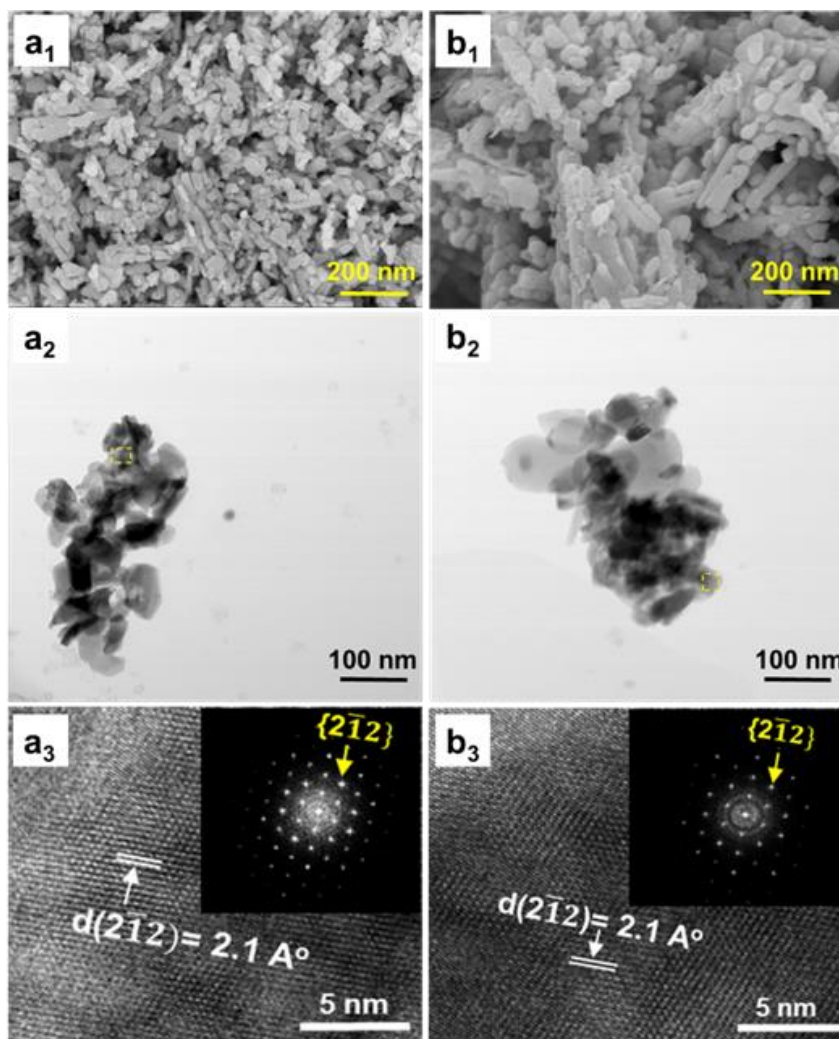


Figure 4-8 - FESEM (a_1 , b_1), BF-STEM, (a_2 , b_2), and HRTEM images (a_3 , b_3) of fresh (a_1 - a_3) and spent (b_1 - b_3) CoMo₂ catalysts. [Reaction parameters: 200 W, CH₄:CO₂=1, VHSV = 10 L.g.h⁻¹]. Reproduced from Ref. [577] with permission from the Royal Society of Chemistry.

Conversely, the MoO₂ particles are clearly observed from the FESEM-EDX images of Mo/Al₂O₃ catalyst (**Figure 4-9**). It also can be seen that the BF-STEM image of fresh CoMo₂ catalyst (**Figure 4-8a₂**) exhibiting elongated and prismatic aggregated particles is confirmed in the nanometric scale.

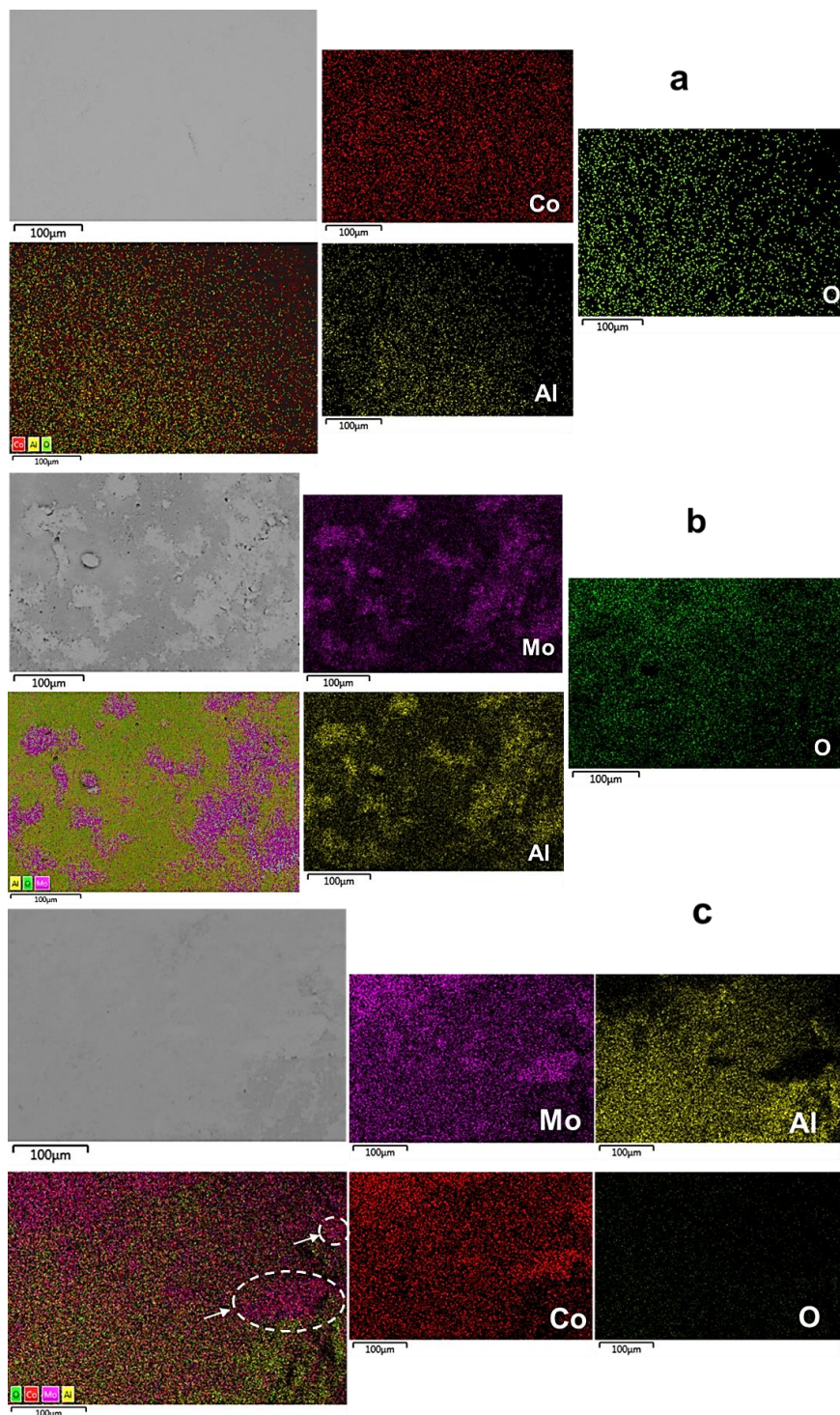


Figure 4-9 – FESEM-EDX images of fresh $\text{Co}/\text{Al}_2\text{O}_3$ (a), $\text{Mo}/\text{Al}_2\text{O}_3$ (b), and CoMo_2 (c) catalysts. Reproduced from Ref. [577] with permission from the Royal Society of Chemistry.

The HRTEM together with the corresponding Fast Fourier Transform (FFT) analysis for a selected –area (dash yellow square) indicates that the bimetallic catalyst system is extensively crystalline proven by the well-arranged dots (inserted images in **Figure 4-8a3**). The HRTEM analysis result also implies the interplanar distance ($d_{spacing}$) of 2.1 Å of lattice plane (2 $\bar{1}$ 2) along the [110] zone axis. Unfortunately, the hexagonal atomic structure of Co_{0.82}Mo_{0.18} bimetallic alloy could not be probed since it was well superimposed with other metallic species in the support leading to thick areas, which is not appropriate for fringe lattice analysis. Alternatively, the STEM-EDX analysis (**Figure 4-10**) can confirm the presence of this alloy. In a good agreement with the abovementioned FESEM –EDX results of fresh CoMo₂ catalyst, the STEM-HAADF image (**Figure 4-10a1**), which is exhibited brightest locations containing high atomic number of Co and Mo, together with the STEM-EDX results further (**Figure 4-9c**) consolidate the presence of the bimetallic alloy onto the support surface. Moreover, as shown from the line-scanning analysis (**Figure 4-10b**), the Co and Mo signals are visibly detected. The line-scanning analysis is well in accordance with the nanoscale mapping results (**Figure 4-10c**). This manifests that the Co and Mo components are overlaid on each other, eliciting the presence of Co_{0.82}Mo_{0.18} bimetallic alloy.

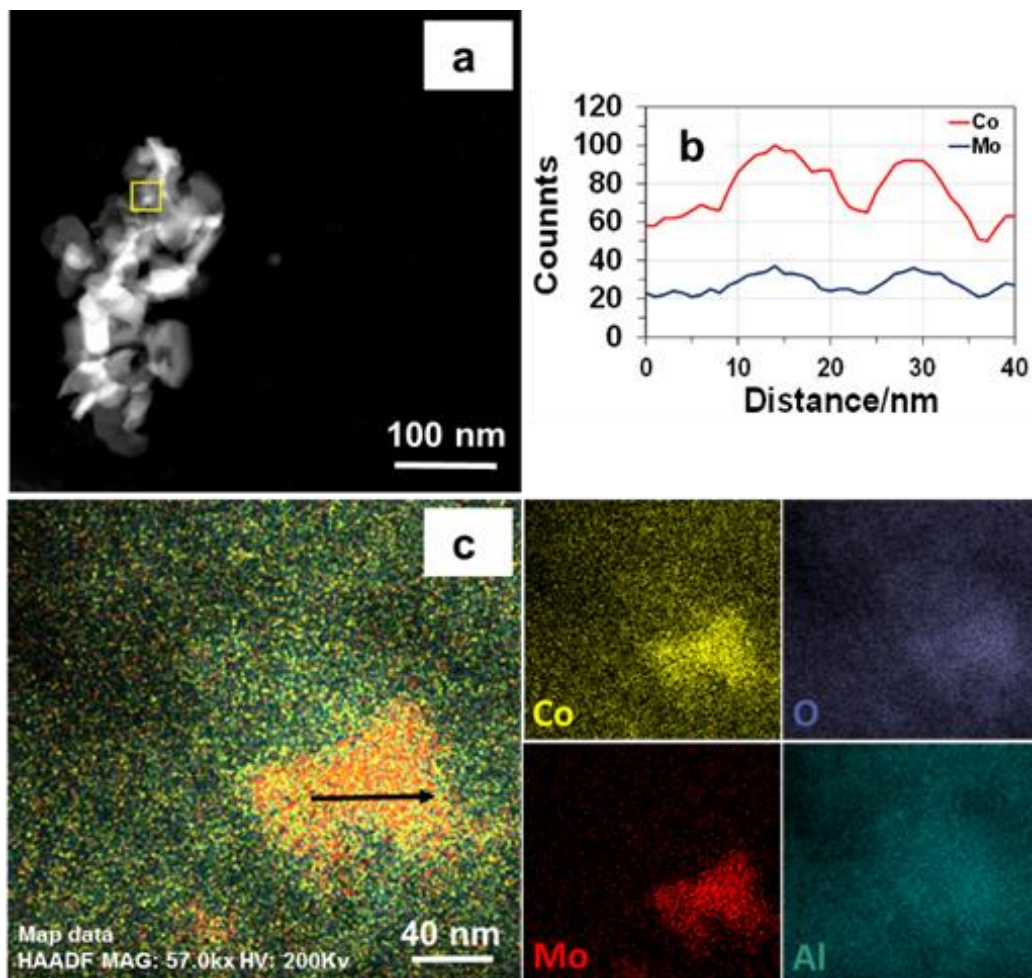


Figure 4-10 - STEM-HAADF (a), line-scanning signals (b), and STEM-EDX (c) of fresh CoMo₂ catalyst. Reproduced from Ref. [577] with permission from the Royal Society of Chemistry.

In the meantime, the STEM-EDX qualitative spectrum of fresh CoMo₂ catalyst (**Figure 4-11**) confirms all constitutive elements i.e., Co, Mo, O and Al. The unlabelled peaks are belong to the Cu-grid.

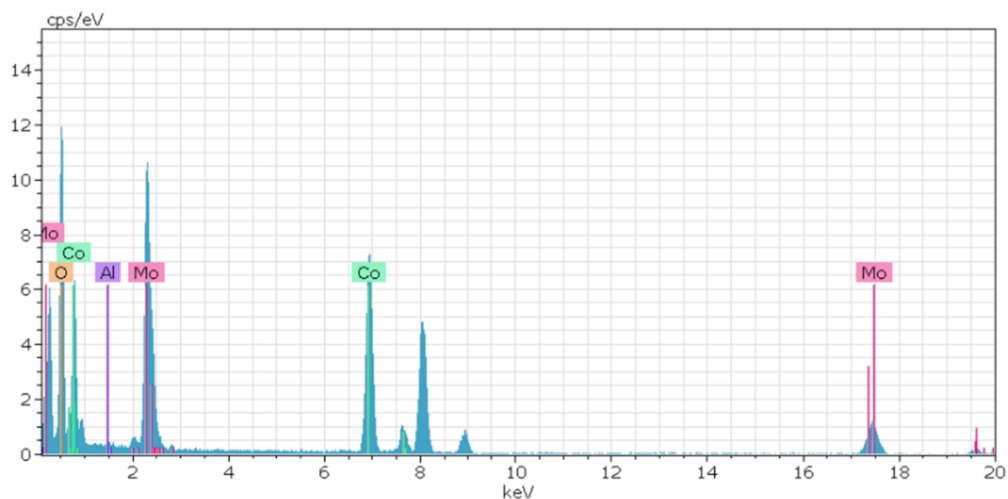


Figure 4-11 - STEM-EDX qualitative spectrum of fresh CoMo₂ catalyst. Reproduced from Ref. [577] with permission from the Royal Society of Chemistry.

For the spent CoMo₂ catalyst, an insignificant sintering of particles was observed from the catalyst surface (**Figure 4-8b₂**) echoing the physical stability of the bimetallic catalyst. Likewise, all STEM analysis results of the spent CoMo₂ catalyst (**Figure 4-8b₂ & b₃**, **Figure 4-13**) confirm the stability of the crystal structure of bimetallic catalyst maintained after 16 h on stream test under MW irradiation at a MW power of 200 W. All these observed results, thus, valid the stability of bimetallic catalyst structure under MW irradiation. However, the previous long time tests indicate the reduction of catalytic activity at high MW power levels such as 500 and 1000 W. Hence, the FESEM analysis at different magnifications for the spent CoMo₂ catalyst samples tested under MW power levels (200, 500 and 1000 W) was performed and the results (**Figure 4-12**) exhibit the visible sloughing and distortion on the CoMo₂ surface after 16 h on stream of DRM reaction under MW irradiation at 500 W. These deteriorations are particularly serious at higher MW power level of 1000 W. On the other hand, at a low MW power of 200 W in which the CoMo₂ catalyst can convert a relatively high reactant gas conversions (80 % CH₄ and 93 % CO₂), there is not visibly distinguishable differences in the morphology between the fresh and spent catalyst samples. Thus, the outer physical deterioration would be a principal reason leading to the above-observed decrease in catalytic activity at high MW power levels as shown in **Figure 4-12**.

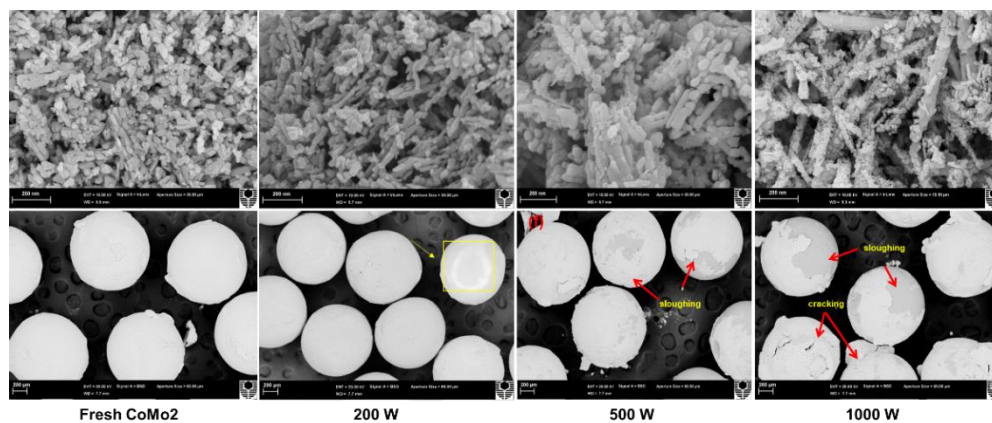


Figure 4-12 - FESEM images of fresh and spent CoMo₂ bimetallic catalysts at different magnifications. The results of fresh CoMo₂ catalyst is represented here for comparison purpose. Reproduced from Ref. [577] with permission from the Royal Society of Chemistry.

Noteworthy that no sign of coke deposition could be observed from the spent CoMo₂ catalyst (**Figure 4-13**). It is possible that the carbonaceous-free observation from spent bimetallic catalyst is due to the mentioned Boudouard reaction promoted by MW irradiation to form more carbon monoxide. The STEM-EDX qualitative spectrum also indicates the absence of carbon-related peaks from the spent CoMo₂ catalyst (**Figure 4-13**). Positively, the catalytic DRM reaction driven by MW irradiation can assist to depress the deposited coke and deliver higher catalytic activity.

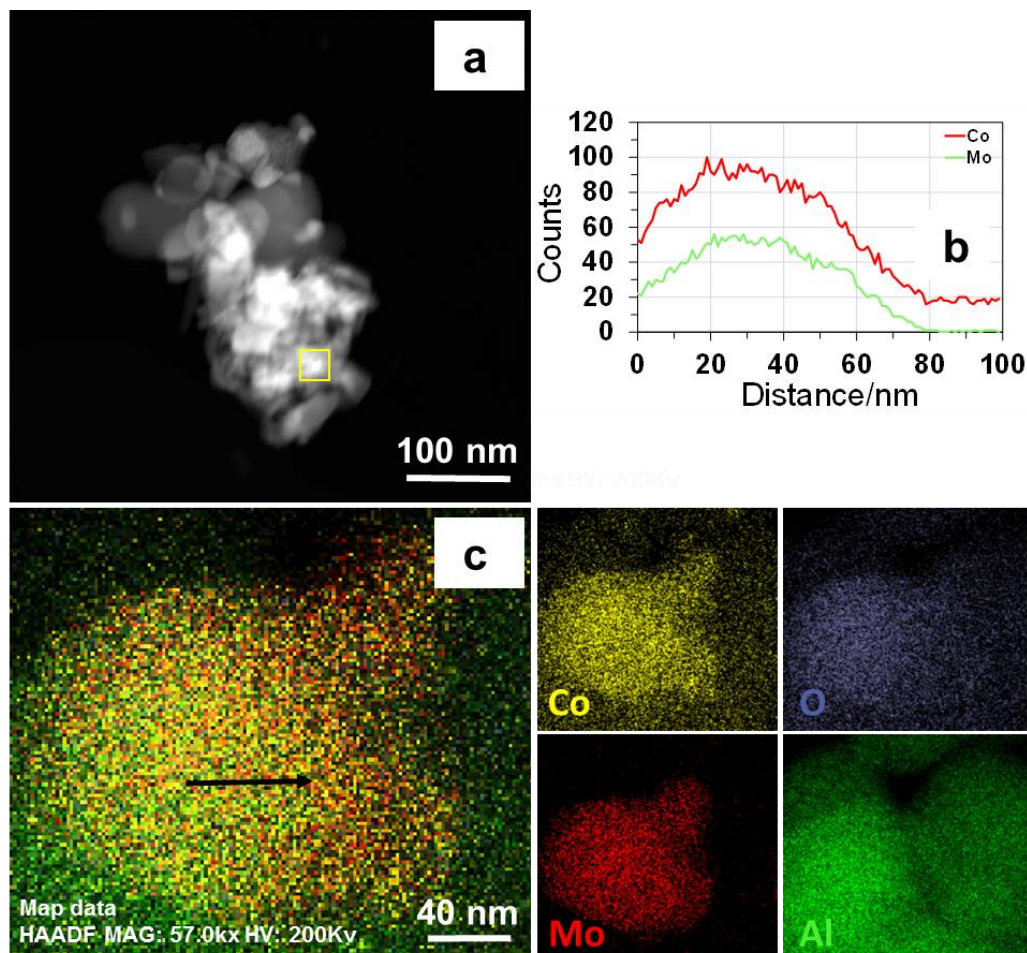


Figure 4-13 - STEM-HAADF (a), line-scanning signals (b), and STEM-EDX (c) of spent CoMo₂ catalyst. [Reaction parameters: 500 W, CH₄:CO₂=1, VHSV = 10 L.g.h⁻¹]. Reproduced from Ref. [577] with permission from the Royal Society of Chemistry.

4.2.4. The mechanism of catalytic activation for DRM under MW irradiation

Despite some research works have reported on catalytic DRM process under MW heating, the activation mechanism of metallic-based catalyst by MW irradiation has not been fully understand. This is due to the fact that almost reported works either utilizes carbon as a catalyst or mix metallic-based catalyst with a good MW absorber i.e., carbon for DRM reaction under MW heating. This study explored that Co-Mo/Al₂O₃ catalyst can absorb MW directly and exhibit a high catalytic activity for DRM while their monometallic counterparts are inactive. The XRD results indicated the presence of Co_{0.82}Mo_{0.18} alloy in bimetallic catalysts, which

are distinguishable from monometallic catalyst samples. Therefore, from this observation we can understand that $\text{Co}_{0.82}\text{Mo}_{0.18}$ alloy is the MW acceptor component, which absorbs MW energy leading to heating the catalyst and catalysing DRM reaction. Indeed, it is generally recognized that magnetodielectric materials which possess ferromagnetic and dielectric properties simultaneously, are the best MW absorbers [588-591]. Cobalt, known as a ferromagnetic element [42], can combine with other paramagnetic metals such as molybdenum [43], to form magnetodielectric materials for MW absorbing applications [44]. In this study, the magnetic properties as a function of the magnetic field of the prepared catalysts were measured by using the superconducting quantum interference device (SQUID). The results are shown in **Figure 4-14**.

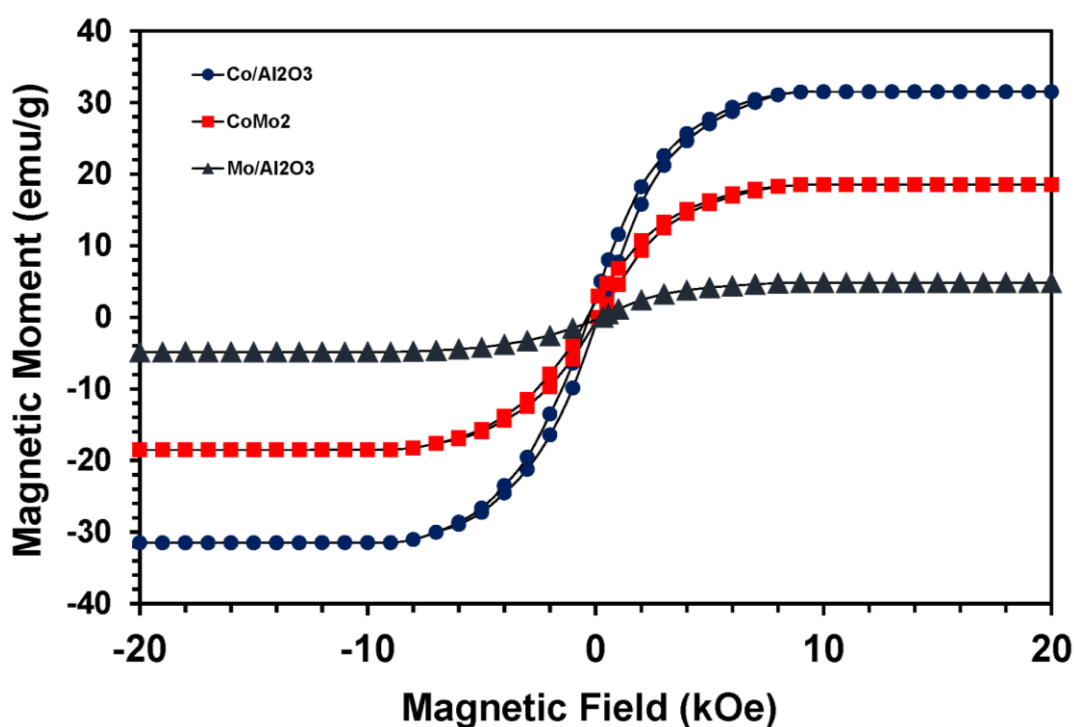


Figure 4-14 - Hysteresis loops of curves of fresh $\text{Mo}/\text{Al}_2\text{O}_3$; $\text{Co}/\text{Al}_2\text{O}_3$ and CoMo_2 catalyst. Reproduced from Ref. [577] with permission from the Royal Society of Chemistry.

It can be seen that the saturated magnetization is in the order of $\text{Co}/\text{Al}_2\text{O}_3 > \text{CoMo}_2 > \text{Mo}/\text{Al}_2\text{O}_3$. Moreover, $\text{Co}/\text{Al}_2\text{O}_3$ catalyst exhibited a small M–H (Magnetic moments - Magnetic field) loop (Figure 4-14), which is a representative feature for these soft ferromagnetic materials. However, in this work, $\text{Co}/\text{Al}_2\text{O}_3$

catalyst could not absorb MW energy presumably because of its high electrical conductivity, which causes the large reflection of incident MW wave [481]. The Mo/ Al₂O₃ catalyst exhibited a low magnetic property (**Figure 4-14**) limiting the ability to couple with incident MW wave [467]. Hence, Mo/ Al₂O₃ could not also absorb MW energy. In the mixture of Co and Mo, conversely, the resultant Co-Mo/ Al₂O₃ catalyst possesses a higher saturated magnetization compared to Mo/ Al₂O₃ (**Figure 4-14**). Though possessing the lower saturated magnetization than Co/ Al₂O₃, CoMo₂ still exhibits the characteristic as a soft ferromagnetic material (small M–H loop), which is able to couple with the incident MW wave [591, 592]. Therefore, Co-Mo/Al₂O₃ bimetallic catalysts with the presence of Co_{0.82}Mo_{0.18} possessing magnetodielectric properties promotes the MW energy acceptance, which leads to its heating up to catalyse DRM reaction. Under this situation, Co_{0.82}Mo_{0.18} alloy itself has dual function in which it can serve as a MW absorbing component and an active center for DRM reaction. This mechanism is in a good agreement with other researchers [467], [593] who also indicated that best MW absorber containing one of the phases is responsible for coupling with electromagnetic wave while the other plays as an insulator to localize MW energy conversion.

Given by the literature, both Co/Al₂O₃ and Mo/Al₂O₃ exhibits its catalytic activity for DRM under conventional heating. In these works, cobalt-based [52] and Mo-based particles [54] act as active centers for DRM reaction. Meanwhile, it is hypothesized that MW heating can generate internal heat source for heterogeneous catalyst which has an inherent MW absorbing capability [24]. In this situation, the heated Co_{0.82}Mo_{0.18} alloy can be considered as an internal heat source to simultaneously warm up adjacent metallic i.e., well dispersed Co⁰, or metallic oxides i.e., Co₃O₄ and MoO₂ due to its well dispersion with other components in the support, as shown in FESEM-EDX and STEM-EDX results. The formation of these extra active centers results in the rocketed escalation of reactant conversions when reaching an initially active MW power level before exhibiting a gradually-slow increasing rate with the subsequent increment of MW power levels (**Figure 4-1a & b**). By introduced more auxiliary active centers under MW heating, the catalytic activity and stability of Co-Mo supported Al₂O₃ catalyst was well preserved over 16 h TOS of DRM at a low MW powers (**Figure 4-3**) regardless

the observed reduction in porosity was indicated by the previous BET analyses. Nonetheless, an excessive cobalt molar loading, for instance Co/Mo ratio of 2.5, possibly either leads to an increase in electrical conductivity (generated by extra reduced cobalt particles) or promotes the formation of above-discussed inactive phases such as $\text{Co}_2\text{Mo}_3\text{O}_8$ (**Figure 4-6b**) smothering active centres from incident MW wave. These two consequences engender the reduction in the MW absorbing capability, and therefore, diminishing catalytic activity.

4.3. Summary

In this chapter, the catalytic activity of a series of Co- and Mo-based catalyst supported by Al_2O_3 for DRM under MW irradiation at the ambient pressure was explored. Compared to the reported previous work focusing on carbon-containing catalysts, the Co-Mo/ Al_2O_3 catalyst with Co/Mo molar ratio of 2 delivered higher activity and stability for DRM converting CH_4 (80 %) and CO_2 (93 %) to the syngas with the H_2/CO ratio of 0.80 under a lower MW irradiation power of 200 W. Our results highlight the high activity of bimetallic catalyst attributed to the MW absorption ability of the $\text{Co}_{0.82}\text{Mo}_{0.18}$ alloy combining the ferromagnetic and dielectric properties. The developed bimetallic catalyst with its intrinsic ability to absorb MW energy without the involvement of extra MW acceptor such as carbon-based materials leading to the better catalytic stability. There is no significant sign for catalyst decay during the 16 hours stability test at low MW power levels (< 500 W). This work represents the first important step in designing an active catalyst for DRM under MW irradiation.

Chapter 5 Role of TiO₂ support in the enhancement of catalytic activity of CoMo catalyst for dry and steam combined dry reforming of methane under microwave heating

5.1. Introduction

As compared to aluminum oxide, titanium dioxide (TiO₂) is one of the most studied functional supports because of its outstanding enhancement in the catalytic activity as well as good structural stability, nontoxicity, low-cost and environmentally benign nature [23, 24]. By employing as the support for Mo-based catalysts for hydrogen-involving reactions, TiO₂ has proved its better improvement for catalytic stability and coke resistance than aluminum oxide [340, 433]. This is due to a better metal – TiO₂ interaction, which fractures large aggregation between metallic particles to provide more active sites for the reforming at the boundary between metal and support, and thus, obstruct carbon deposition [434, 436, 594]. More importantly, TiO₂ is found to be highly stable in water and steam environment [435, 595, 596], which make its suitability in reforming of methane processes involved steam. Therefore, this chapter aims to present the roles of TiO₂ in the enhancement of catalytic activity and stability of CoMo catalysts for both DRM and SDR reaction under MW heating. The synergistic effects between the metallic catalyst and support to promote MW absorption and to preserve persistent catalytic performance are also elaborated.

5.2. Results and Discussion

5.2.1. Characterization of fresh catalysts

5.2.1.1. N₂ adsorption–desorption isotherms and BET

Figure 5-1 shows the N₂ adsorption–desorption isotherms of the fresh CoMo catalysts recorded at 77 K. The physisorption isotherms of fresh CoMo catalysts are ascribed to type II with reference to the IUPAC classification, a typical feature of mesoporous materials [597]. In the meanwhile, the hysteresis loop of the fresh

CoMo/TiO₂ catalysts is denoted to Type H₃ representing the non-rigid aggregations of plate-like particles or assemblages of slit-shaped pores according to the IUPAC classification [598].

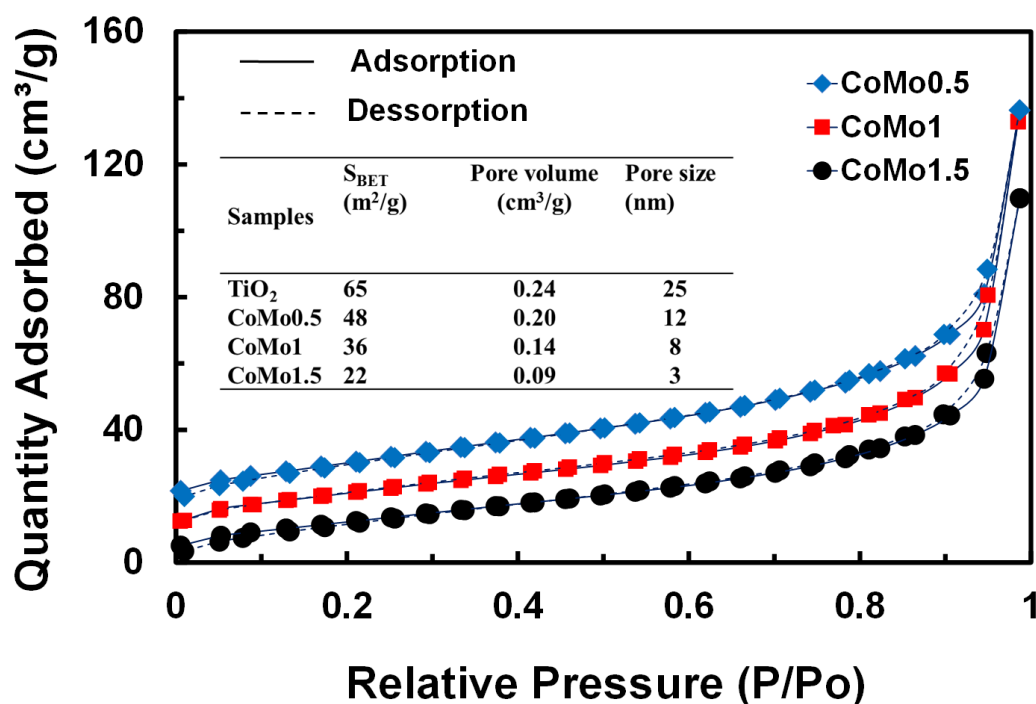


Figure 5-1 - N₂ adsorption/desorption isotherm curves of fresh CoMo/TiO₂ catalysts.

The inserted table in **Figure 5-1** shows the porosity and specific surface area of CoMo catalyst interpreted by using Brunauer–Emmett–Teller (BET) method. It indicates that the surface area (S_{BET}) of TiO₂ support (65 cm².g⁻¹) was smaller than that of the previous Al₂O₃ (163 cm².g⁻¹). The introduction of CoMo into catalyst structure reduced the S_{BET} due to the decrease of the TiO₂ content per weight unit. With the Co/Mo ratio of 0.5, S_{BET} was of 48 cm².g⁻¹ while CoMo1.5 had a much lower surface area, namely 22 cm².g⁻¹. Likewise, both of pore volume and pore size of CoMo catalyst declined with raising the Co/Mo molar ratios (inserted Table, **Figure 5-1**). Whereby, pore size volume of TiO₂ diminished from 0.24 to 0.09 cm³.g⁻¹ while its pore diameter declined from 25 to 8 nm with the Co/Mo ratio of 1.5. Compared to the previous CoMo/Al₂O₃ catalyst [577], the measured

porosity of the CoMo/TiO₂ catalysts in this work is lower, which predicted possible effects on their catalytic activity for reforming reactions.

5.2.1.2. H₂-TPR

Figure 5-2 displays the H₂-TPR profiles of fresh CoMo/TiO₂ catalysts and TiO₂ support. The H₂ consumption peak of individual TiO₂ was poorly identified at 884 °C mirroring the low reducibility [599]. Meanwhile, the H₂-TPR profiles of the CoMo/TiO₂ samples were almost similar to the previous CoMo/Al₂O₃ catalysts [577], but experienced a higher reduction temperature at about 10 °C. The shift to higher temperature reduction region of the CoMo/TiO₂ catalysts elicits the stronger metal-support interaction [600]. Moreover, it is postulated that the larger catalyst particle size leads to the higher reduction enthalpy, and thereby, increases the reduction temperature [601-603]. Thus, it is estimated that large CoMo catalyst particles were possibly formed in the catalyst system. The H₂ consumption peak at 415 °C can be ascribed to the reduction of Co-based species while the peak at 784 °C is associated with the reduction of Mo⁺⁴ [604]. The distinguishable hydrogen consumption peak located at 580 °C is possibly ascribed to the reduction of CoMoO₄ to Co_{0.82}Mo_{0.18} bimetallic alloy while a small shoulder at 517 °C is possibly related to the reduction of Mo⁺⁶ i.e., MoO₃ to Mo⁺⁴ i.e., MoO₂. The peaks initiated at above 950 °C could be possibly attributed to the reduction of complexes formed by the interactions between TiO_x species and metallic particles.

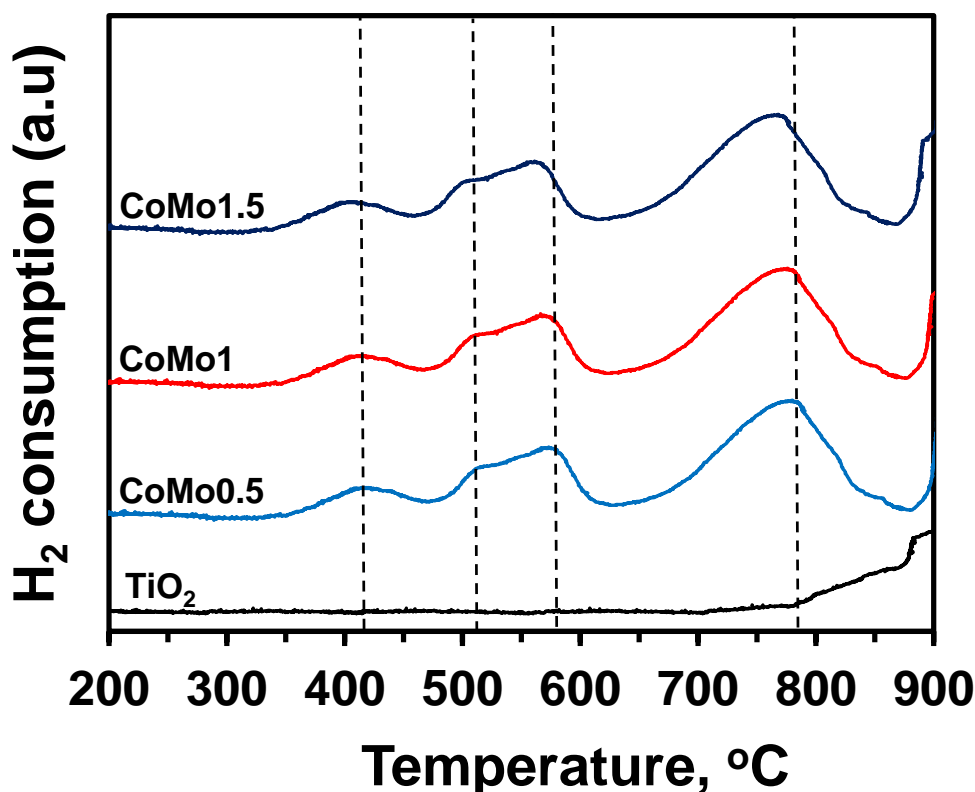


Figure 5-2 - TPR-H₂ profiles of TiO₂ and CoMo/TiO₂ catalysts.

5.2.1.3. XRD

Figure 5-3 presents the XRD patterns of the fresh CoMo catalysts and the calcined CoMo1 sample. It can be seen that CoMoO₄ were detected from the calcined sample at 23.2°, 26.5°, 32.1°, and 33.7°, respectively (PDF 96 – 153– 0868). Meanwhile, the MoO₃ phase was represented by the peak at 14.5° (PDF 96 – 153– 0706). Noteworthy that no diffraction peaks related to Co-based species were detected from all catalyst samples regardless of the previous observation from TPR-H₂ profiles of the possible reduction of cobalt-based particles at 402 °C. The absence of Co-based diffraction peaks elicits the good dispersion of these particles in catalyst structure. For fresh bimetallic catalysts, the well-defined Co_{0.82}Mo_{0.18} bimetallic alloy was detected via the diffraction peaks at 40.1°, 42.9°, and 45.4° (PDF 96 – 152– 5121). Moreover, the MoO₂ phase was also detected at 26.1° (PDF 96 – 153– 9091), which is explained by the reduction of Mo⁺⁴ at high temperature (> 750 °C) indicated by the previous TPR-H₂ profile. Compared to the CoMo/Al₂O₃ catalyst, Co_{0.82}Mo_{0.18} particles were detected with sharper and smaller full-width half-maximum peaks echoing better crystalline with the larger

size. The larger $\text{Co}_{0.82}\text{Mo}_{0.18}$ absorber component would result in better exposure to the incident MW wave promoting MW absorption capacity, and therefore, providing a better catalytic activity for reforming reactions. The formation of such large size particles also explains for the H_2 -TPR profiles of CoMo/TiO_2 , which shifted to higher temperature regions by comparing to the H_2 -TPR peaks of $\text{CoMo}/\text{Al}_2\text{O}_3$.

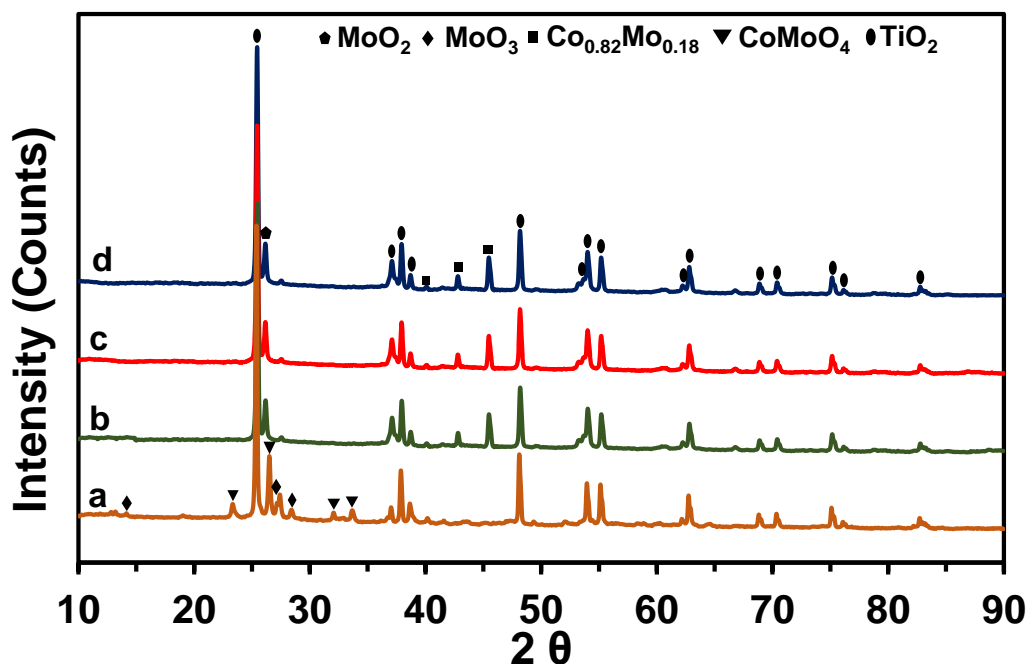


Figure 5-3 - XRD of calcined $\text{CoMo}1$ (a), fresh $\text{CoMo}0.5$ (b), $\text{CoMo}1$ (c) and $\text{CoMo}1.5$ (d) catalysts.

5.2.1.4. FESEM

The morphology of the fresh CoMo/TiO_2 catalysts characterised by FESEM of catalysts displays well-defined particles with a relatively uniform size distribution from 50 to 100 nm (**Figure 5-4a**). In a good agreement, the STEM-BF images (**Figure 5-4b**), also exhibit the nanometric particles. Compared to the previous CoMo catalyst supported on Al_2O_3 , the CoMo/TiO_2 catalysts have larger particles, and thus, resulting in the lower S_{BET} , as shown in **Figure 5-1**.

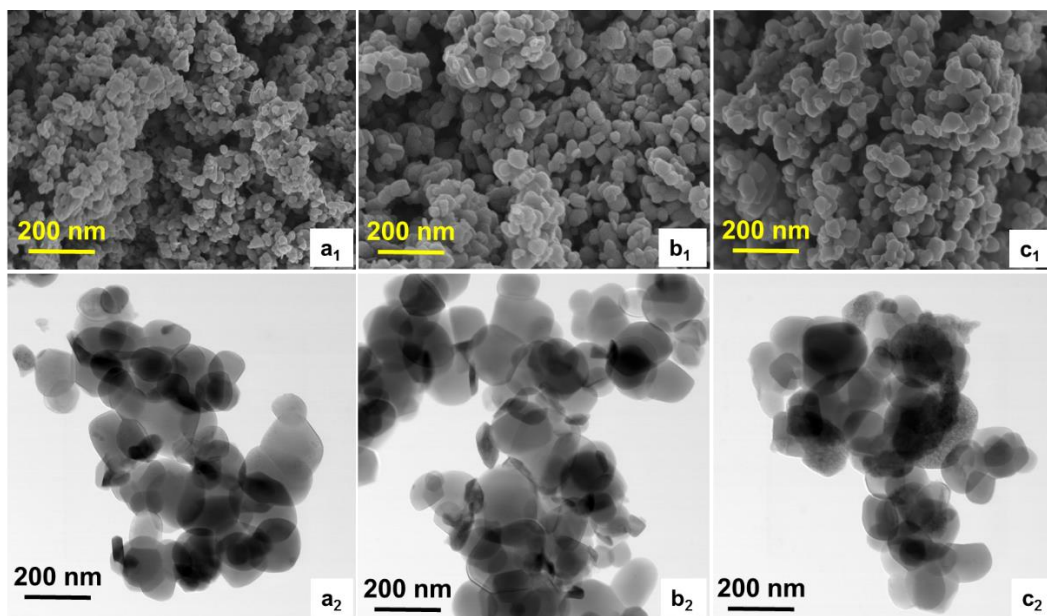


Figure 5-4 - FESEM (up-row) and BF-STEM (down-row) images of fresh CoMo0.5 (a₁, a₂), CoMo1 (b₁, b₂), CoMo1.5 (c₁, c₂).

The STEM-HAADF and STEM-EDX analysis (**Figure 5-5a**) further confirms the well-defined $\text{Co}_{0.82}\text{Mo}_{0.18}$ bimetallic alloy with a particle size around 50 to 100 nm. The line-scanning analysis (inserted image of **Figure 5-5a**) of the $\text{Co}_{0.82}\text{Mo}_{0.18}$ particle detected good signals associated with the presence of Co and Mo atoms. Such these observations confirm the bulging distribution of $\text{Co}_{0.82}\text{Mo}_{0.18}$ alloy on the TiO_2 surface.

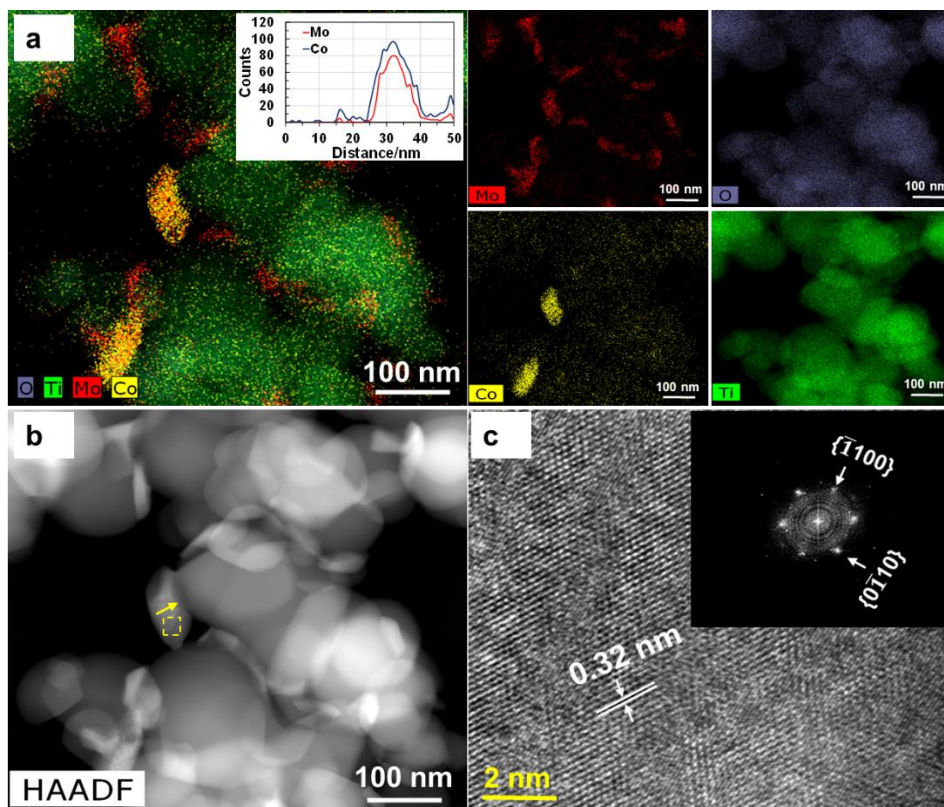


Figure 5-5 - STEM-EDX (a), STEM-HAADF (b) and line-scanning (c) of fresh CoMo1 catalyst.

Moreover, the $\text{Co}_{0.82}\text{Mo}_{0.18}$ atomic structure (dash yellow square area in **Figure 5-5b**) characterised by HRTEM together with the corresponding Fast Fourier Transform (FFT) analysis is shown in **Figure 5-5c**. It can be seen that the hexagonal atomic arrangement of $\text{Co}_{0.82}\text{Mo}_{0.18}$ structure illustrated by the previous Retrieve refinement analysis [577] can be able to be verified by well-arranged hexagonal dots (inserted, **Figure 5-5c**). The HRTEM analysis result also implies the interplanar distance ($d_{spacing}$) of 0.32 nm of lattice plane $(1\bar{1}00)$ and $(01\bar{1}0)$ along with the $[0001]$ zone axis. As observed from **Figure 5-5a**, Mo-based particles were sporadically dispersed on the TiO_2 support whilst Co-based particles were highly populated. This observation can be explained from the absence of Co-based diffraction peaks from the XRD patterns above. The protuberant distribution of MW absorber component ($\text{Co}_{0.82}\text{Mo}_{0.18}$) on the TiO_2 surface can increase its ability to contact with the incident MW wave. By this way, the MW absorption ability of the CoMo/ TiO_2 catalysts was enhanced to promote reforming performance.

5.2.1.5. Reflection Loss (R_L) measurement

To verify the MW absorption ability of the CoMo/TiO₂ catalysts, the R_L measurement was performed and the results are shown in **Figure 5-6**. For R_L measurement, the dips in the R_L curve versus frequency plot indicates low reflectivity or good MW absorption. Specifically, the deeper dips represent for the less MW reflection and better MW absorption [605, 606]. In this work, the R_L of the CoMo1 catalyst was around -11.6 dB (**Figure 5-6**). This value is relatively smaller than the reported carbon-based materials ($R_L \geq -30$ Db [607]) because of the strong MW absorption nature of carbon. Nonetheless, it is good enough to secure the strong MW absorption of CoMo catalysts and to deliver the high activity for reforming reactions. Moreover, the R_L values of CoMo0.5, CoMo1, and CoMo1.5 samples were insignificantly different at a given frequency. This observation, therefore, reveals the high activity of CoMo catalyst with different molar ratios at a similar MW power.

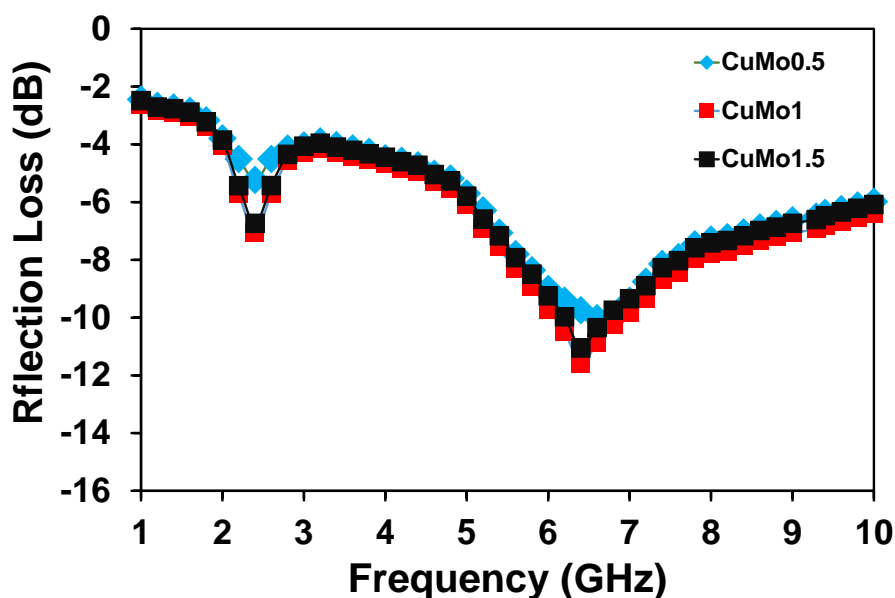


Figure 5-6 - Reflection loss as a function of frequency of CoMo catalysts.

5.2.2. Catalytic activity

The catalytic activity data of fresh CoMo/TiO₂ catalysts for both DRM and SDR at various conditions were collected under steady-state conditions with the results shown in **Figure 5-7**.

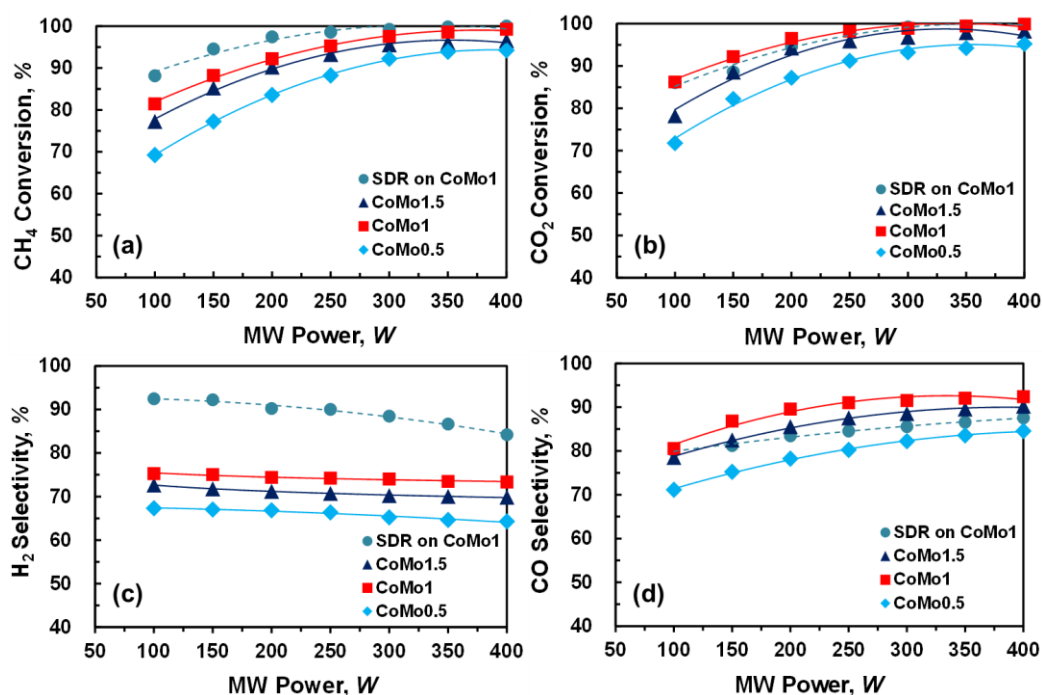


Figure 5-7 - Catalytic activity of fresh CoMo/TiO₂ catalyst. [Reaction conditions: CH₄/CO₂ = 1, S/C = 0.1 (for SDR)].

It can be seen that the MW power required to activate CoMo/TiO₂ catalyst was not dependent on the Co/Mo molar ratios, in which, all the prepared catalysts could be activated by a low MW power of 100 W. This result can be explained by the insignificant variations in the R_L values of CoMo/TiO₂ catalyst above, as shown in **Figure 5-6**. Noticeably, the CoMo/TiO₂ could be able to be activated by a low MW power of 100 W, which is smaller than that required to activate CoMo/Al₂O₃ catalyst. Specifically, at an equivalent Co/Mo molar ratio of 0.5, the CoMo/Al₂O₃ required 500 W to convert 34 % CH₄ and 46 % CO₂ while that supported on TiO₂ converted 69 % CH₄ and 72 % CO₂ at 100 W (**Figure 5-7 a & b**). Researchers have found that TiO₂ supported metal catalysts affords a lower activity for hydrogen-involved reactions [58, 111, 448] and reforming of methane

under conventional heating [191, 608] by comparing to other supports, such as Al_2O_3 or CeO_2 . The reported reason for these observations was due to the preferable formation of large catalyst particles formed on TiO_2 promoting coke deposition. Nonetheless, large catalyst particles protruding from the support surface is possibly beneficial for catalytic reactions under MW heating. It is widely accepted that the amount of MW energy absorbed is dependent on the exposure of absorber components to the incident wave [451-453]. This is particularly true for the case of metallic catalysts supported on inert supporters (e.g., Al_2O_3 , TiO_2 or CeO_2), which are unable or very low ability to absorb MW wave owing to the highly dielectric characteristic [476]. In such catalysts for reaction under MW heating, supports are mainly employed as insulators to restrict catalyst sintering [501]. In this project, well-defined $\text{Co}_{0.82}\text{Mo}_{0.18}$ absorber particles were discernibly detected from both XRD (**Figure 5-3**) and STEM-EDX (**Figure 5-5**). The protruded catalyst particles offer a better opportunity to contact with the incident MW wave, and thereby, lead to the stronger MW absorption of CoMo/TiO_2 catalyst at low MW power (100 W). Moreover, it has been indicated that TiO_2 can further support metals to have good matching with electromagnetic wave due to its suitable bandgap energy (3.2 eV) [609, 610]. Nonetheless, an excessive cobalt addition (e.g., $\text{CoMo}_{1.5}$) led to a reduction in the catalytic activity, which could only convert 77 % CH_4 and 78 % CO_2 (**Figure 5-7a & b**). Such observations are possibly due to the low surface area of $\text{CoMo}_{1.5}$ catalyst, which limits the access of reactants to extra active centres inside the pores of TiO_2 [611]. Therefore, the CoMo supported on TiO_2 catalyst with tunable size and surface area can be tailored as a novel catalyst with strong MW absorption capacity and provide a high catalytic activity for reforming of CH_4 .

It is also observed from **Figure 5-7a & b**, both of CH_4 and CO_2 conversions in all tests escalated with the increase of MW power. Given the strong endothermic characteristics of both reforming reactions [174], these reactions therefore, will be promoted with the increase of MW power. In a good agreement with the previous study [612], H_2 selectivity was found to decrease while CO selectivity was escalated with rising in MW power levels (**Figure 5-7a & b**). Moreover, the CO selectivity were slightly higher than H_2 selectivity. All these observations echo the simultaneous occurrence of side reactions, such as the Boudouard reactions

($\text{CO}_2 + \text{C} \leftrightarrow 2\text{CO}$, $\Delta H_{298\text{K}}^{\circ} = +172 \text{ kJ/mol}$) and the exothermic WGS reaction ($\text{CO} + \text{H}_2\text{O} \leftrightarrow \text{H}_2 + \text{CO}_2$) with $\Delta H_{298\text{K}}^{\circ} = -41.2 \text{ kJ/mol}$) [613]. These side reactions tend to shift to form more CO when increasing MW power levels [614]. Noticeably, CH_4 conversion and H_2 selectivity were considerably boosted with the presence of steam. Specifically, CH_4 conversion increased from 80 (**Figure 5-7a**) to 88 % (**Figure 5-7b**) whilst H_2 selectivity rose from 82 to 92 %. Nonetheless, the presence of steam has insignificant influences on CO_2 conversion. This result is due to the stronger reactions of steam compared to stable CO_2 [615]. More importantly, the syngas H_2/CO ratio produced by DRM reaction in this study is close to unity (0.91) (**Figure 5-6**), which is slightly higher than that obtained over previous $\text{CoMo}/\text{Al}_2\text{O}_3$ catalyst. Noticeably, the presence of steam boosted the syngas ratio. Specifically, the H_2/CO above 2 could be produced by adding the S/C ratio of 0.1 at a MW power of 100 W (**Figure 5-8**).

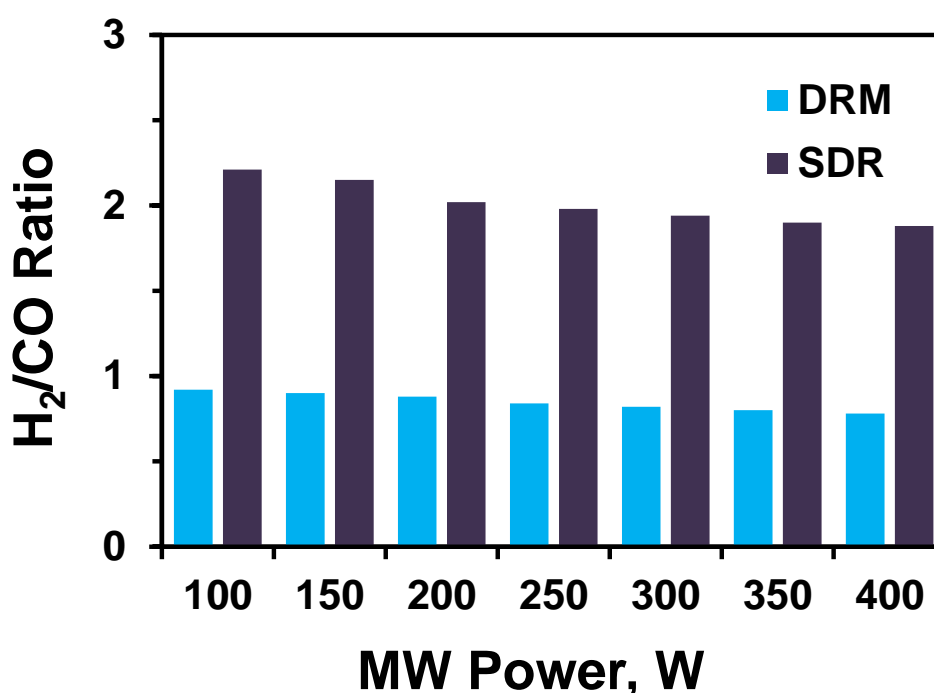


Figure 5-8 – Syngas ratio produced DRM and SDR reactions over CoMo catalyst. [Reaction conditions: $\text{CH}_4/\text{CO}_2 = 1$, $\text{VHSV} = 10 \text{ L.g}^{-1}.\text{h}^{-1}$ S/C = 0.1 (for SDR)].

Compared to the conventional methods to produce expected syngas ratios, such as increasing temperature or CH_4 concentration in the feed [616], SDR process is more straightforward, feasible, and flexible to adjust the H_2/CO ratio.

5.2.3. Catalytic stability

The catalytic stability tests of the CoMo catalysts for DRM and SDR reactions were performed over 62 h TOS under MW irradiation at the MW power of 100 W; and the results are shown in **Figure 5-9**. For DRM reaction, the prepared CoMo catalysts showed similar catalytic behaviour with comparable reactant gas conversions and syngas product selectivity. All catalysts showed an initially high catalytic activity with around 67 - 72 % for CH₄ and 71- 80 % for CO₂. The negligible drops approximately 2.5 % from the catalytic performance was observed for all tested samples within the first ten hours TOS. Then, the catalytic activity became stable at around 65 - 75 % for CH₄ and 66 - 78 % for CO₂. Likewise, H₂ and CO selectivity also preserved its good stability over CoMo catalysts (**Figure 5-9c & d**). With the presence of steam, both reactant conversions and syngas selectivity also exhibited good stability with only a 3 % drop in average within 50 h on the stream test. The minor declines with approximately 8 % for reactant conversions and 6 % for syngas selectivity were observed after 50 h TOS. Compared to the carbon-based catalysts for methane reforming under MW heating [25, 31, 32, 34, 179], which have been reported to be stable within the first 120 minutes, the Co-Mo/TiO₂ catalyst in this work displays its exceptional steadiness for both DRM and SDR. This is possibly due to the strong interaction between TiO₂ and CoMo catalysts. The good interaction between metal and support is sourced from the shift of the reduction temperature of CoMo/TiO₂ catalysts to higher temperature region compared to CoMo/Al₂O₃ (as shown in **Figure 5-2**).

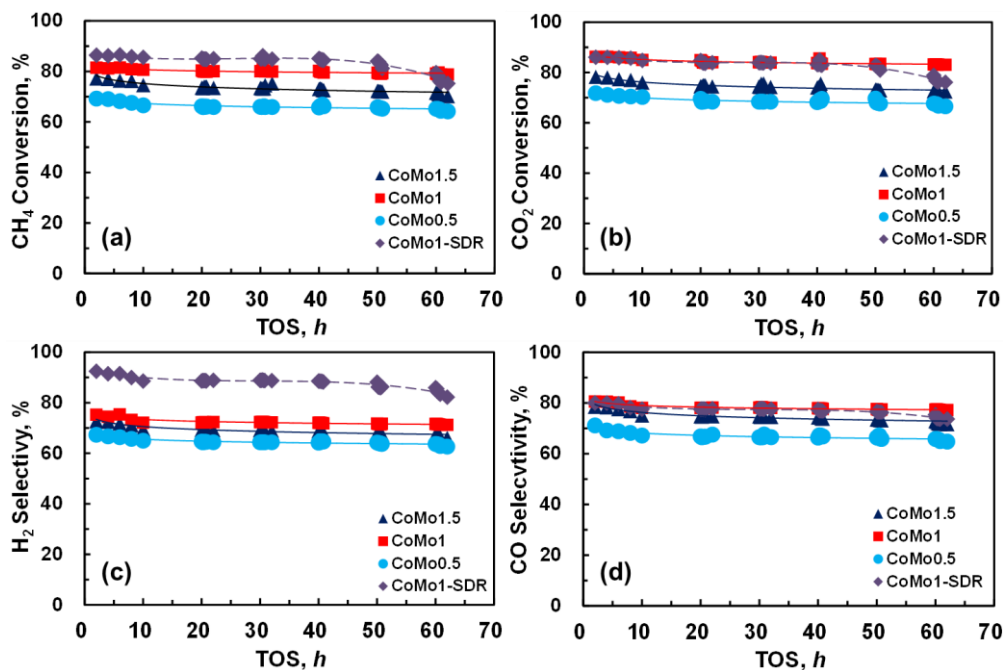


Figure 5-9 - Catalytic stability of CoMo/TiO₂ catalyst. [Reaction conditions: CH₄/CO₂ = 1, VHSV = 10 L.g⁻¹.h⁻¹ S/C = 0.1 (for SDR)].

5.2.4. Characterisation of spent catalysts

To further elaborate the high stability of the CoMo/TiO₂ catalyst for DRM and SDR under MW irradiation, the characterisations for spent catalyst samples were performed.

5.2.4.1. XRD and BET

The crystalline structure of the spent CoMo/TiO₂ catalysts was examined by XRD; and the results are shown in **Figure 5-10A**. It can be seen that the CoMo0.5, CoMo1, and CoMo1.5 catalysts (**Figure 5-10A-a, b, &c**) well preserved its structure over DRM reaction with all catalysts elements detected from their respectively refresh samples, as shown in **Figure 5-3**. This result explains for the good catalytic stability of CoMo/TiO₂ catalyst for DRM reaction observed above, as shown in **Figure 5-9**. Notwithstanding this, the Co₂Mo₃O₈ phase with the corresponding diffraction peaks at 17.87°, 32.6° (PDF 96-152-0511) (**Figure 5-10A-d**) was detected from the CoMo1 catalyst spent for SDR reaction. The presence of Co₂Mo₃O₈ phase may mask part of the active centre/absorber component [612], and thus, led to the observed decline in catalyst performance of

CoMo1 catalyst for SDR reaction. Likewise, the textural properties of the prepared catalysts were insignificantly altered after spending for DRM and SDR reaction tests over 62 h at a MW power of 100 W) (**Figure 5-10B**). Specifically, the BET surface area of CoMo1 spent over DRM was diminished from 36.4 to 30.3 $\text{cm}^2.\text{g}^{-1}$ while that of spent over SDR reaction was maintained at 34.8 $\text{cm}^2.\text{g}^{-1}$.

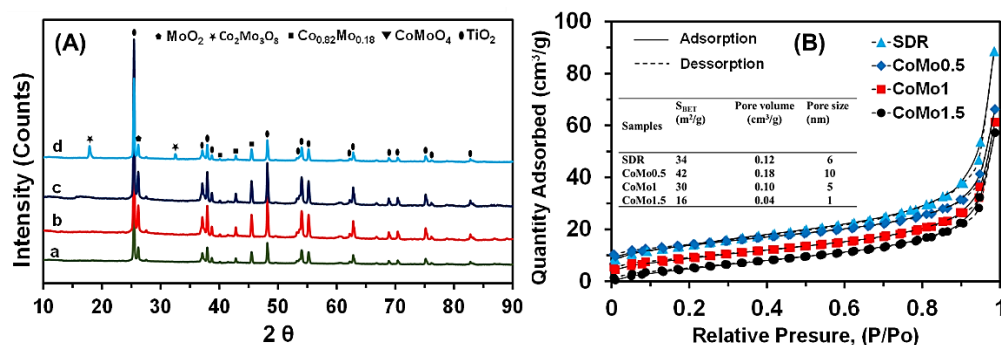


Figure 5-10 - XRD pattern (A) of CoMo0.5 (a), CoMo1(b), CoMo1.5 (c) over DRM reaction, and CoMo1.5 (d) over SDR reaction; textural properties (B) of all CoMo catalysts spent over DRM and CoMo1 spent over SDR reaction. [Reaction conditions: 100 W, $\text{CH}_4/\text{CO}_2 = 1$, $\text{VHSV} = 10 \text{ L}.\text{g}^{-1}.\text{h}^{-1}$ $\text{S}/\text{C} = 0.1$ (for SDR)].

5.2.4.2. FESEM

The morphology of spent catalysts (**Figure 5-11**) further endorses the high stability of CoMo/TiO₂ catalysts for reforming reactions. Both of FESEM (**Figure 5-11a1-c1**) and STEM-BF (**Figure 5-11a2-c2**) images of catalysts spent over DRM reaction exhibited marginal sintering of the CoMo catalyst particles, which accounts for the previously negligible reduction in its BET surface area. Meanwhile, the CoMo1 spent over SDR (**Figure 5-11d1 & d1**) exhibited a coarse-grained surface with shredded particles, which engenders a slightly larger surface area than that of spent over DRM reaction.

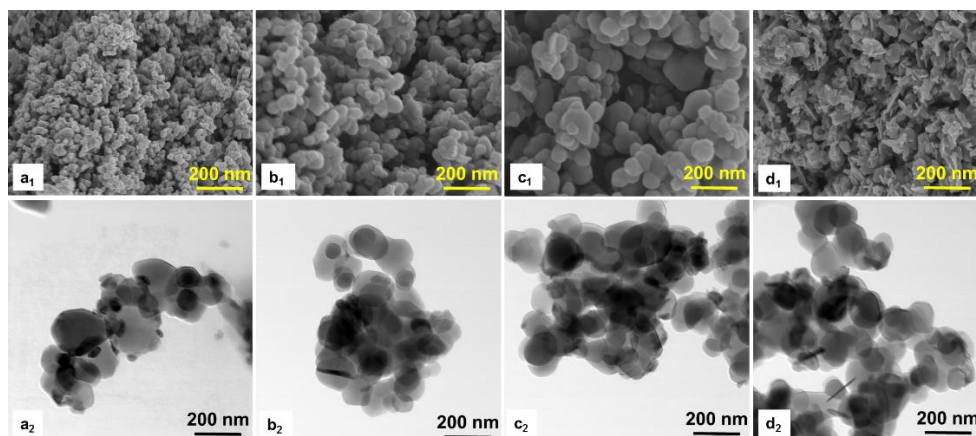


Figure 5-11 - FESEM (up-row) and BF-STEM (below-row) of catalysts spent for DRM CoMo0.5 (a₁, a₂), CoMo1 (b₁, b₂), CoMo1.5 (c₁, c₂) and CoMo1 for SDR (d₁, d₂). [Reaction conditions: 100 W, CH₄/CO₂ = 1, VHSV = 10 L.g⁻¹.h⁻¹ S/C = 0.1 (for SDR)].

As exhibited by the STEM-EDX analysis results (**Figure 5-12**), the shredded particles of SDR spent CoMo1 catalyst consist higher atomic number of Co and Mo, which signs the presence of bimetallic alloy.

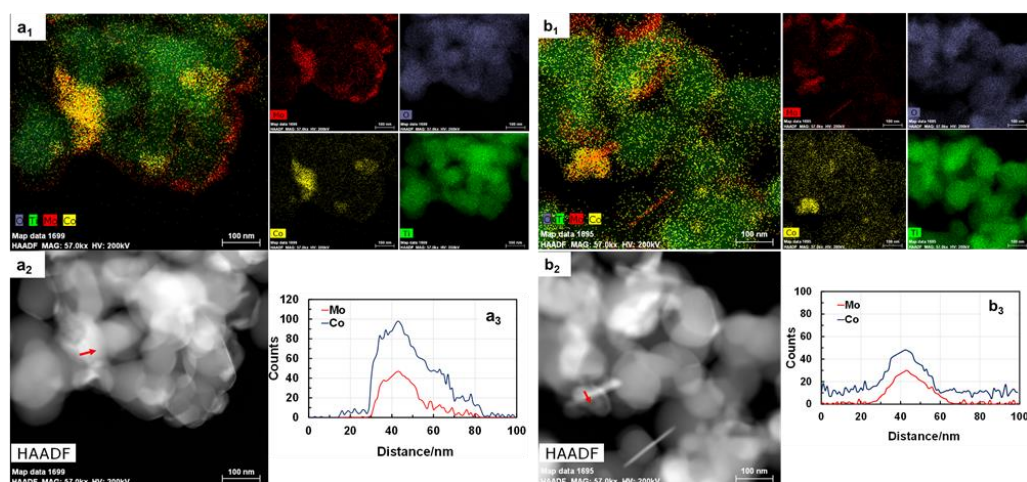


Figure 5-12 - STEM-EDX, STEM-HAADF and line-scanning results of DRM (a₁, a₂, a₃) and SDR (b₁, b₂, b₃) spent CoMo/TiO₂ catalyst. [Reaction conditions: 100 W, CH₄/CO₂ = 1, VHSV = 10 L.g⁻¹.h⁻¹ S/C = 0.1 (for SDR)].

Moreover, the particle size distributions interpreted from STEM analysis by *ImageJ*© software of the fresh CoMo1 shows dominance of particle size in a range of 160 – 200 nm (**Figure 5-13**). Nevertheless, after 62 h of TOS for DRM and SDR, the percentage of particles of more than 200 nm was prevailing, which verified minor sintering of the CoMo catalysts.

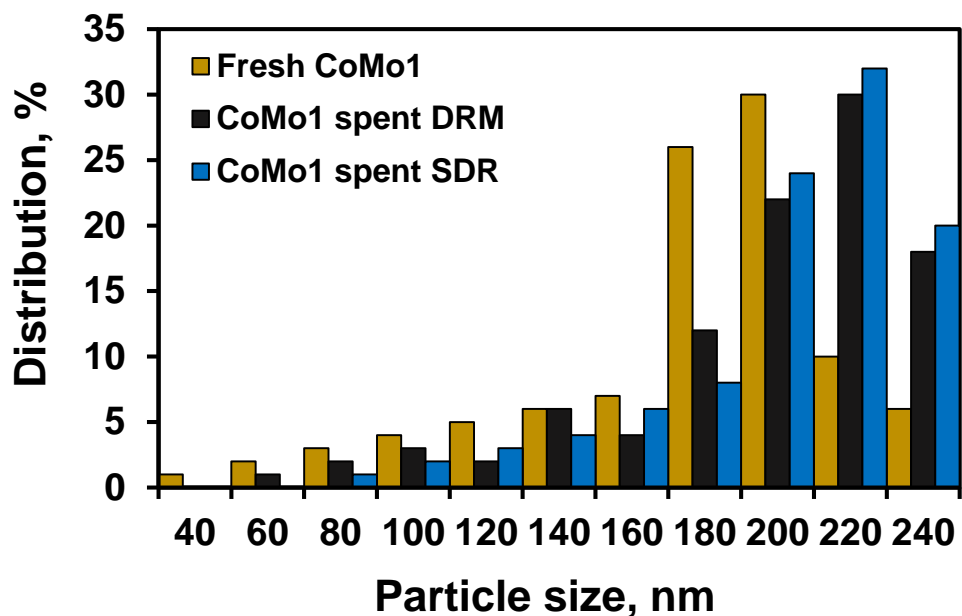


Figure 5-13 - Particle size distribution of fresh CoMo1, CoMo1 spent DRM and CoMo1 spent SDR. [Reaction conditions: 100 W, $\text{CH}_4/\text{CO}_2 = 1$, $\text{VHSV} = 10 \text{ L.g}^{-1}.\text{h}^{-1}$ $\text{S/C} = 0.1$ (for SDR)].

Noteworthy that no sign of deposited coke could be observed from spent catalysts by the XRD (**Figure 5-10a**), STEM-BF (**Figure 5-11a2-d2**), and STEM-EDX (**Figure 5-12**).

5.2.4.3. TGA

To evaluate the coking behaviour of the CoMo/TiO₂ catalysts, thermogravimetric analysis (TGA) of the spent samples were performed; the results are shown in **Figure 5-14**. There is a slight weight loss in a region below 300 °C observed from all spent catalysts. The CoMo1 catalyst spent over DRM reaction exhibited 2.3 % weight loss whilst that spent over SDR was in a slightly higher loss with 3.5 %. These losses are attributed to the evaporation of physisorbed water molecules. Particularly, catalysts employed for SDR reaction absorb more water due to the

presence of steam, and thereby, resulted in an insignificant larger loss. There were the negligible losses after 800 °C, which are 1.8 and 1.0 % for CoMo1 catalyst spent over DRM and SDR, respectively (inserted Table, **Figure 5-14**). Though we could not observe coke from the STEM-BF, STEM-HAADF, and STEM – EDX analyses, these observed weight losses are associated to the oxidation of deposited coke, which was a small amount and dispersed deeply inside CoMo/TiO₂ catalysts' structure. Such a small amount of coke was possibly dispersed in the pores of TiO₂ and reduced catalytic activity of CoMo catalysts within the initial 10 hours on the stream test, as shown in **Figure 5-9**. In the meanwhile, coke deposited on the catalyst surface was rapidly removed by gasification reactions with both CO₂ and steam (in case of SDR reaction) [575], and by this ways, stabilizing the catalytic performance during the rest of 52 h (**Figure 5-9**).

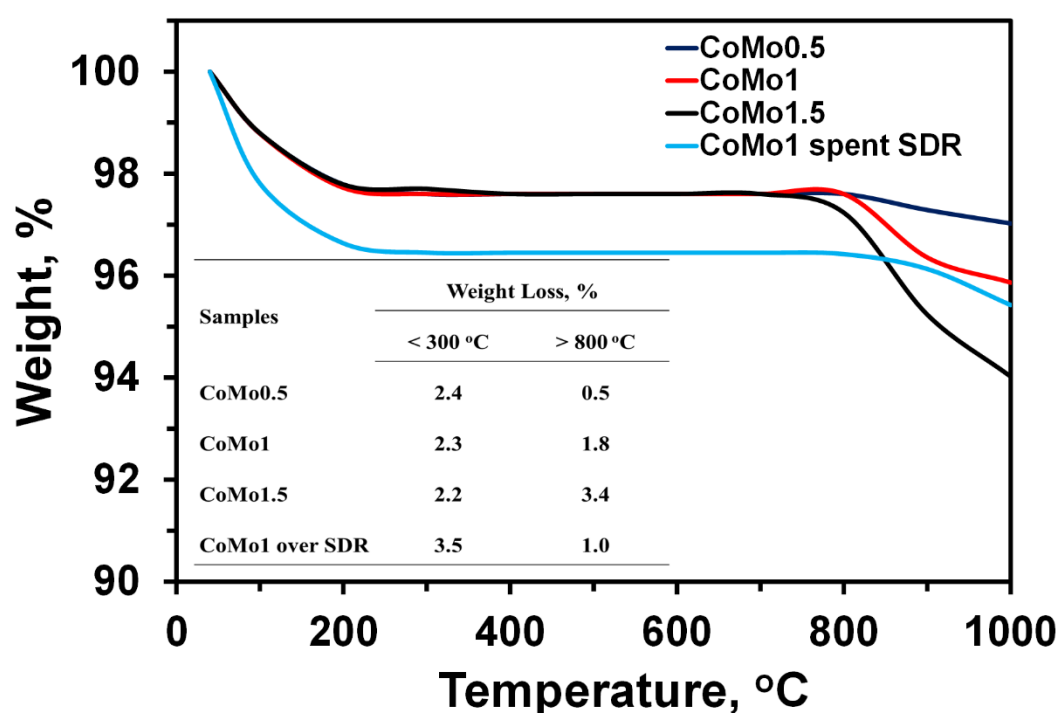


Figure 5-14 - TGA profiles of CoMo/TiO₂ catalysts after 62 h test for DRM and SDR reactions. [Reaction parameters: 100 W, CH₄:CO₂=1, VHSV_{DRM} = 10 L.g.h⁻¹, S/C_{SDR} = 0.1].

Moreover, the Co/Mo molar ratio higher than 1.0 (e.g., CoMo1.5) resulted in higher deposited coke (**Figure 5-14**), which explains for a visible decline in its catalytic activity initiated after 62 hours, as shown in **Figure 5-9**.

5.3. Summary

In this part of research, the catalytic activity and stability of CoMo with different Co/Mo molar ratios supported by TiO₂ for DRM and SDR under MW irradiation at the ambient pressure were systematically investigated. The prepared catalysts exhibited high catalytic efficiency at a low MW power of 100 W to produce the syngas with H₂/CO ratio (0.91) close to the unity. The H₂/CO ratio above of two could be obtained by adding steam in the feed with the inlet steam/carbon ratio of 0.1. The CoMo1 (Co/Mo molar ratio of 1) catalyst displayed as the best catalyst in this work to convert approximately 80 % CH₄ and 60 % CO₂ at a MW power of 100 W. An excessive addition of cobalt (e.g., CoMo1.5) reduced the catalyst surface area significantly, and thereby, diminished catalytic activity. It was found that TiO₂ offers a good exposure of the Co_{0.82}Mo_{0.18} absorber to the incident MW wave resulting in a better MW absorption and catalytic performance. Moreover, the CoMo/TiO₂ catalysts were stable for at least 62 h on the reforming stream tests. The enhancement of MW energy and the presence of steam for coke gasification jointly contributed the good catalytic stability.

Chapter 6 Syngas production via steam combined CO₂ reforming of methane over CuMo/TiO₂ catalyst under MW heating

6.1. Introduction

In the previous chapter, it was demonstrated that TiO₂ can enhance the catalytic activity owing to its role in promoting the exposure of MW absorbers/active centers of catalyst to the incident MW wave. In the meantime, research activities on catalytic chemical processes have recently paid much attention to highly abundant and low-cost catalysts with a low or minimal safety concern, such as copper. It has been indicated that the flexible transformation from Cu²⁺ to Cu⁺/Cu⁰ confers copper as a good redox-active center for chemical reactions [62-65]. The rich redox nature, high abundance, and low toxicity render Cu-based catalysts to be highly favorable for gas-phase reactions in industry [66-69]. Copper-based catalysts have been illustrated their high activity for DRM [70-75] and SDR [75-77] under conventional heating. Notwithstanding, none of the copper-based catalysts has been applied for methane reforming under MW irradiation. One of the possible reason is that copper is one of the opaque materials together with silver and aluminum, which can reflect MW wave due to its high conductivity [78]. In this chapter, the performance of copper-based catalysts for SDR under MW heating has been demonstrated. This chapter also provides some unique insights into the MW activation for abundant copper-based catalyst supported over TiO₂ catalysts for syngas production via SDR under MW heating.

6.2. Results and Discussion

6.2.1. Catalytic activity

The CH₄ and CO₂ conversions could not be observed during the SDR operation with the MW power from 100 to 400 W over the single Cu and Mo catalysts with the respective metallic molar fraction up to 0.5, as shown in (**Figure 6-1A & B**). The inactivity of Mo/TiO₂ catalyst is consistent with the previous findings, **Chapter 4, Section 4.2.1**. In the meanwhile, the high electric conductivity of the

reduced copper particles limits the penetration of electromagnetic wave [481, 501, 617], and therefore, the Cu/TiO₂ catalyst reflects the incident MW wave. In contrast, the conversion of the reactants, was observed from 100 W over the binary CuMo catalysts. These results are also in good acclimatization with the endothermic nature of the SDR process. Specifically, the increase in MW power resulted in the escalation in the reactant conversions (**Figure 6-1A&B**). In contrast, the selectivity of H₂ and CO exhibited its opposite behaviour with the escalation in MW power. At a fixed S/C ratio of 0.2, the selectivity of H₂ declined unnoticeably whilst that of CO was enhanced by 10 % (from 56 to 66 %) when increasing MW power from 100 – 400 W (**Figure 6-1C&D**). Such observations have been blamed for the occurrence of the water gas shift reaction ($\text{CO} + \text{H}_2\text{O} \leftrightarrow \text{H}_2 + \text{CO}_2, \Delta H_{298\text{K}}^0 = -41.2 \text{ kJ/mol}$) and the Boudouard reaction ($\text{CO}_2 + \text{C} \leftrightarrow 2\text{CO}, \Delta H_{298\text{K}}^0 = +172 \text{ kJ/mol}$), which tend to form more CO at high MW power [576, 577].

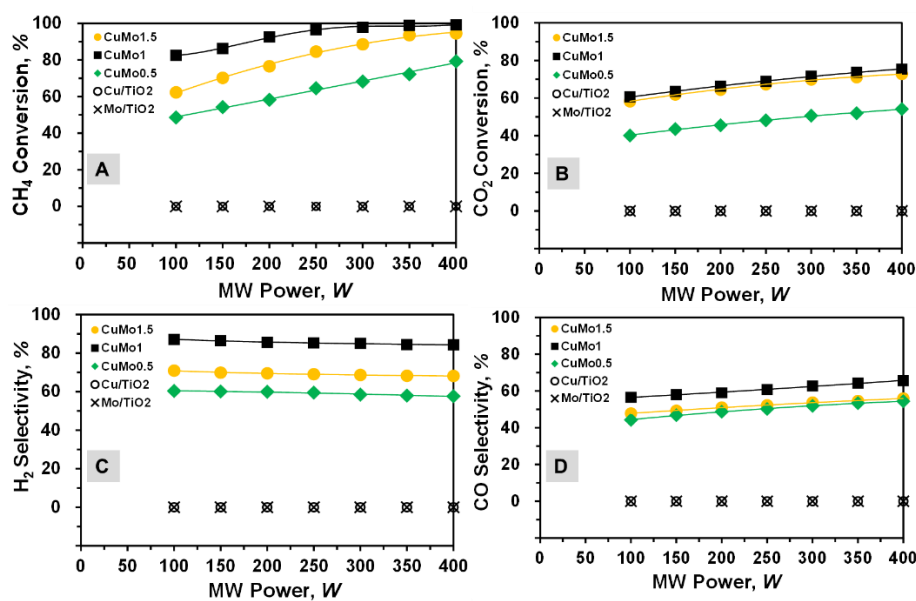
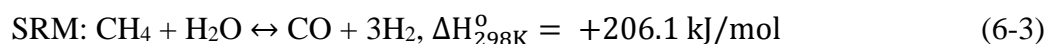


Figure 6-1 - The catalytic SDR performance over the CuMo catalysts. [Reaction parameters: CH₄:CO₂=1, S/C_{SDR} = 0.2].

Furthermore, the CuMo1 catalyst (Cu/Mo molar ratio of 1) displayed the best catalytic performance in this work. By performing the SDR reaction with the S/C ratio of 0.2 over the CuMo1 catalyst, CH₄ conversion ranged from 82 % to a maximum value close to 100 % whilst the CO₂ equivalent conversion increased

from 61 % to 75 % when raising MW power from 100 to 400 W, respectively. The larger enhancement for CH₄ conversion compared to CO₂ conversion is stemmed from the simultaneous occurrence of three methane-involved conversions, as below [174-176]:



These reactions are favourable at high MW power due to their endothermic nature. In addition to this, the influences of the feed S/C ratios to the SDR performance were also studied at a fixed MW power of 100 W over the CuMo1 catalyst samples; and the results are shown in **Figure 6-2**. The conversion of CH₄ was boosted from 62 % to 83 % when increasing the S/C ratio from 0 to 0.2 whilst the equivalent CO₂ conversion was slightly reduced from 67 % to 60 % (**Figure 6-2**). The larger presence of steam promoted the conversion of CH₄ via the steam reforming reaction. Nonetheless, the further addition of steam above the S/C 0.2 resulted in the decline of CH₄ conversion. It has been claimed that the excessive amount of steam concentration reduces the partial pressure of other reactants like methane for a give reaction pressure [618, 619]. Sharing the features of a first-order SDR reaction [620, 621], the methane disappearance rate is, therefore, limited by steam concentration changes. It was also indicated that the presence of steam in high concentration would block the absorption of CH₄ on the catalyst surface [622], and thereby, diminished methane conversion. In the meanwhile, the increase of the S/C ratio profoundly promoted the selectivity of hydrogen up to 88 % whilst the selectivity of CO was decline negligibly. Carbon dioxide conversion, on the other hands, was diminished with the presence of steam due to the competition between these two molecules to react with CH₄ [623].

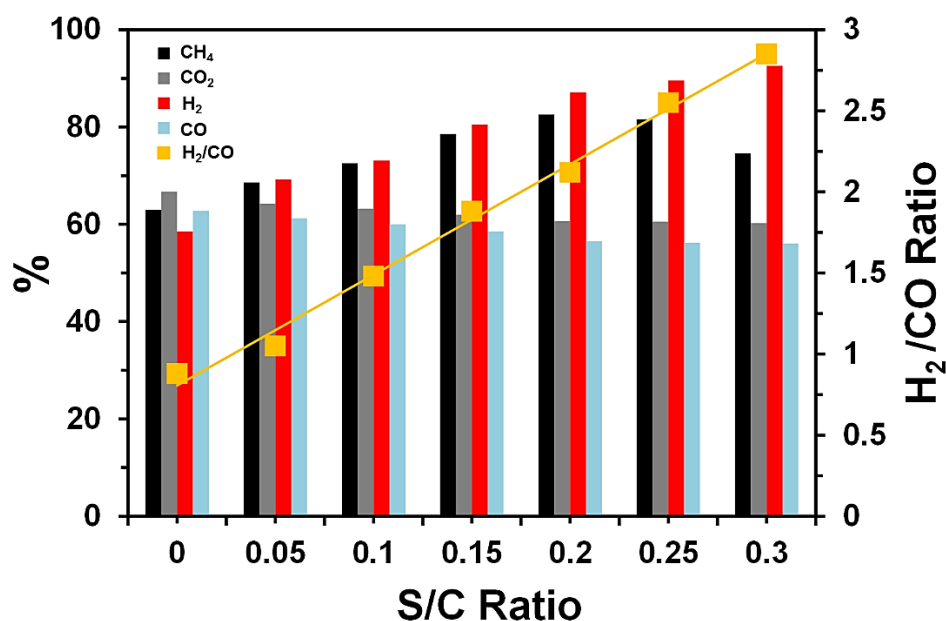


Figure 6-2 - Effects of the S/C ratios on the SDR performance and syngas ratio over CuMo1 catalyst. [Reaction parameters: 100 W, CH₄:CO₂=1].

The influences of the S/C ratios in the feed on the SDR performance and syngas ratio were displayed in **Figure 6-2**. As can be seen that the increase in the S/C ratio in the feed resulted in the improvement of the syngas ratio. As expected, the syngas ratio reached 2.15 at the feed S/C ratio of 0.2 (**Figure 6-2**). Though the increase in the feed S/C ratio above 0.2, such as 0.25 or 0.3, reduced CH₄ conversion, syngas ratio preserved its continuous growth. This is due to the water-gas shift reaction ($\text{H}_2\text{O} + \text{CO} \leftrightarrow \text{H}_2 + \text{CO}_2$, $\Delta H_{298\text{K}}^{\circ} = -41.1 \text{ kJ/mol}$) and the carbon gasification ($\text{H}_2\text{O} + \text{C} \leftrightarrow \text{H}_2 + \text{CO}$, $\Delta H_{298\text{K}}^{\circ} = +131 \text{ kJ/mol}$), which could produce more hydrogen and simultaneously reduce coke deposition [624]. Particularly, Ferrari and co-workers [625] found that the steam gasification reaction is vigorously enhanced under MW irradiation due to the strong MW absorption ability of carbon. Notwithstanding this, the excessive addition of steam marginally affected the conversion of CO₂ or the selectivity of CO. Comparatively, the conversion of the reactants and the syngas selectivity in this work surpass the estimated thermodynamic equilibrium values reported in the literature for the SDR reaction under conventional heating [170, 626, 627]. In addition to this, both the conversion of reactants and the selectivity of syngas rocketed over 60 % as soon as the CuMo1 catalyst was activated by a MW power

of 100 W (**Figure 6-1**), though it was inactive with the lower MW power (i.e., 50 W). Such exceptional performance of the SDR process in this study is associated with the distinctive properties of the selective MW heating over highly active CuMo catalyst. The selective heating properties of MW wave significantly restrict the evolution of the secondary gas-phase reactions generating side products to preserve high reactant conversions and high syngas selectivity [26, 628, 629]. The application of MW irradiation into chemical processes is, therefore, gaining commercial interests because of its low energy consumption and high performance. By comparing to the CoMo/Al₂O₃ catalysts activated at a MW power of 200 W, the CuMo/TiO₂ catalysts were active at lower MW power (100 W); nonetheless, they have a slightly lower catalytic activity than the previously-studied CoMo/TiO₂ catalysts. This is possibly due to higher activity for reforming reactions of cobalt-based catalysts compared to copper-based catalysts [111, 278].

6.2.2. Catalytic stability

The long-term test of the CuMo1 catalyst for SDR reaction at different S/C ratios under MW power of 100 W was performed; and the results are shown in **Figure 6-3**. In general, the CuMo1 sample preserved its catalytic activity over 72 hrs TOS with the negligible drop in the range of 1 - 2.3 % equivalently to the S/C from 0 to 0.2. The further increments in the feed S/C ratio, such as 0.25 or 0.3, reduced the catalytic durability significantly (**Figure 6-3**). Peculiarly, both of the conversion of the reactants and the selectivity of syngas were sharply diminished after 40 hrs on the stream test (**Figure 6-3A&B**). The selectivity of H₂ and CO, therefore, declined accordingly (**Figure 6-3C&D**). The reason for these observations is possibly due to the vigorous oxidation active centres/MW absorber components to form inactive oxides. These inactive oxides are either inert or low MW absorption, and thereby, reduced the catalytic stability. However, the catalytic stability of CuMo catalyst was much higher than that of the carbon-based catalysts for SDR reaction under MW heating, as reviewed above.

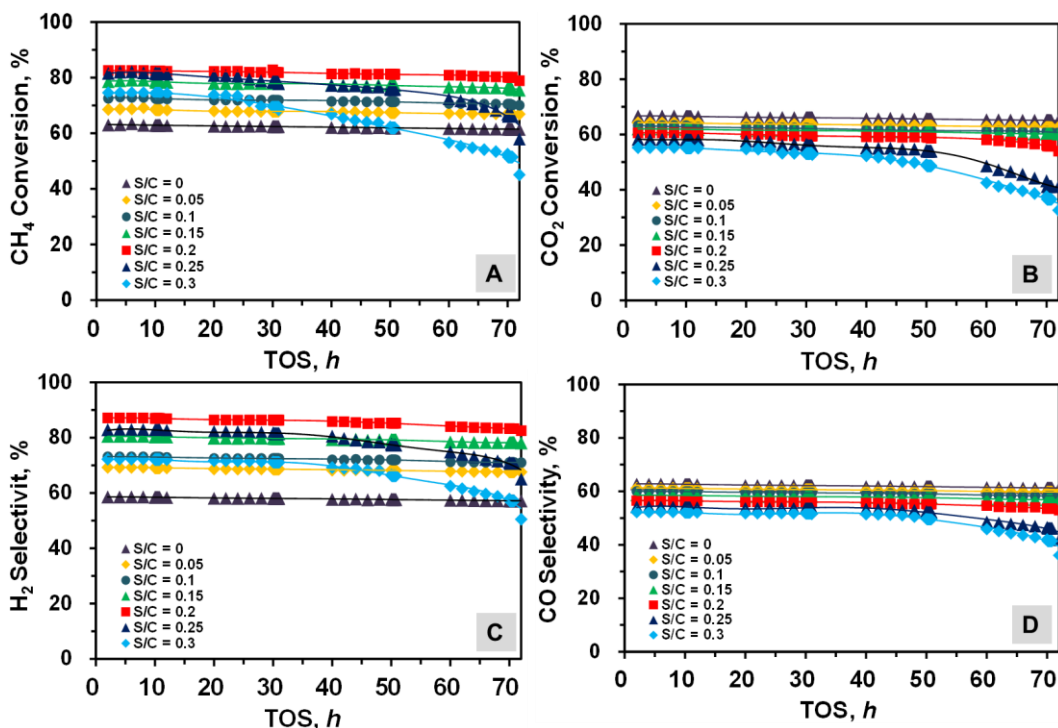


Figure 6-3 - Catalytic stability of the CuMo1 catalyst. [Reaction parameters: CH₄/CO₂ = 1, MW power = 100 W].

6.2.3. Catalyst characterization

6.2.3.1. R_L measurement

The minimum reflection loss (R_L) measurement at the low frequency was performed to verify the MW absorption ability of all prepared catalysts and the results are shown in **Figure 6-4**. As can be seen that there are only two shallow dips for the Mo/TiO₂ and Cu/TiO₂ catalysts. These both catalysts did not absorb MW, and hence, were not able to convert the reactants, CH₄, CO₂, and steam to syngas, as shown in **Figure 6-1**. In contrast, the binary CuMo1 catalysts present the two matching losses at two different frequencies, 2.4 and 6.8 GHz. The CuMo0.5 R_L was -3.3 and -6.2 dB while the CuMo1 possessed a highest R_L of -5.6 and -9.3 dB at 2.4 and 6.4 GHz, respectively. This property accounts for the highest catalytic performance of the CuMo1 catalyst, as shown in **Figure 6-4**. The further addition of copper reduced the R_L values. For example, R_L of the CuMo1.5 was -5.4 and -8.5 dB at these corresponding frequencies. In short, this work clearly shows the important correlation between MW absorption capacity, metallic ratio of the sample, and the catalytic performance.

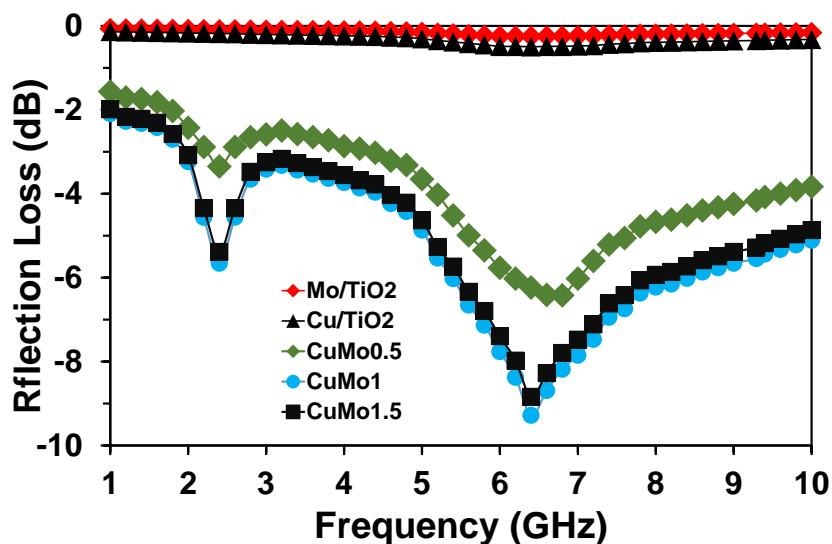


Figure 6-4 -The minimum reflection loss (RL) of the fresh Mo/TiO₂, Cu/TiO₂, and CuMo catalysts.

6.2.3.2. BET surface area

The BET surface area of monometallic (Cu, Mo) and binary CuMo catalysts was characterized by using the Micro Tristar II apparatus; and the results are shown in **Table 6-1**. It is in a good agreement with the previous studies, the introduction of a larger content of CuMo into catalyst system resulted in the decrease in BET surface area. By comparing to the previous CoMo/Al₂O₃ catalysts, the CuMo/TiO₂ samples had a lower specific surface area, which further echoes the presence of large size particles in the catalyst samples.

Table 6-1- Textural properties of the fresh catalysts and TiO₂.

Sample	BET surface area (m ² .g ⁻¹)	Pore size (nm)	Pore volume (cm ³ .g ⁻¹)
TiO ₂	65	25	0.28
Cu/TiO ₂	56	18	0.24
Mo/TiO ₂	50	17	0.23
CuMo0.5	46	15	0.18
CuMo1	40	13	0.12
CuMo1.5	32	8	0.08

Moreover, the specific surface area of fresh and spent monometallic catalysts (Cu and Mo) were constant due to their inactivity under MW heating for SDR. In the meantime, the BET surface area of the spent binary catalysts (**Table 6-2**) displayed unnoticeable changes compared to the fresh CuMo samples, which accounts for the good stability of the CuMo catalysts discussed above. Specifically, the BET surface of the CuMo1 catalyst was preserved at 39 m².g⁻¹ after 72 h on the steam test.

Table 6-2-Textural properties of the spent catalysts. [Reaction parameters: 100 W, CH₄:CO₂=1, S/C_{SDR} = 0.2].

Sample	BET surface area (m ² .g ⁻¹)	Pore size (nm)	Pore volume (cm ³ .g ⁻¹)
Cu/TiO ₂	56	19	0.24
Mo/TiO ₂	51	17	0.23
CuMo0.5	42	13	0.14
CuMo1	39	11	0.10
CuMo1.5	30	7	0.06

6.2.3.3. XRD

The above activity result confirms that monometallic catalyst of either Cu or Mo was inactive whilst its respective CuMo catalysts were highly active under MW heating for the SDR reaction. To explain for such observation, the crystalline

structure of all prepared catalysts was also examined; and the XRD results are shown in **Figure 6-5**.

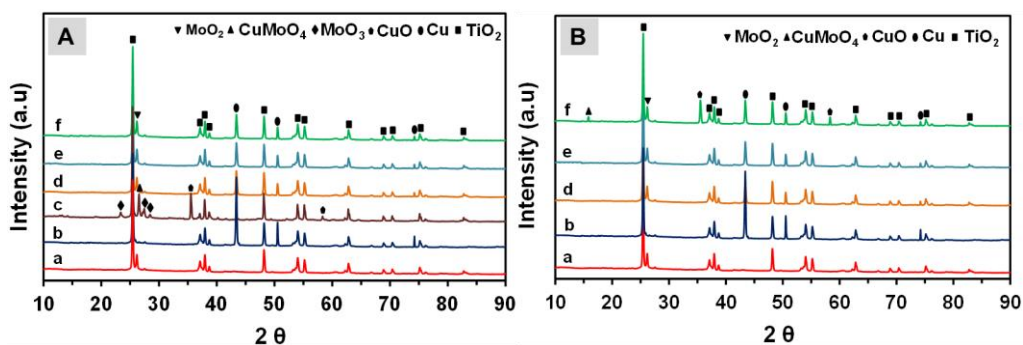


Figure 6-5 - XRD patterns of calcined and fresh (A) and spent (B) catalysts: (a) Mo/TiO₂; (b) Cu/TiO₂; (c) calcined CuMo1; (d) CuMo0.5; (e) CuMo1; (f) CuMo1.5;

It can be observed from the figure that the MoO₂ diffraction peaks (**Figure 6-5A-a**) are detected (i.e., at 26.1°) (PDF 96-153-9091) from the Mo/TiO₂ sample due to its incomplete reduction confirmed previously. Meanwhile, the well-defined Cu⁰ particles were detected with the sharp diffraction peaks of 43.4°, 50.5°, and 74.2° (PDF 96-153-0836) from the fresh Cu/TiO₂ catalyst samples (**Figure 6-5A-b**), which indicates a complete reduction of Cu⁺ to Cu⁰. For the calcined CuMo catalyst, MoO₃, MoO₂, CuMoO₄, and CuO phases were identified (**Figure 6-5A-c**). After being reduced in hydrogen at 450 °C, only MoO₂ and Cu⁰ were detected from the fresh CuMo catalysts (**Figure 6-5A-d, e, & f**) revealing a complete reduction of copper oxides. It is worth noting that the diffraction peaks of Cu⁰ were sharp with a small full-width half-maximum (FWHM) divulging its high crystalline with large particle size [630]. As per the reports in the literature [631-633], TiO₂ can preserve the catalyst particle size on account of the substituted TiO_x islands acting as nucleation and growth sites for metal nanoclusters. By this way, TiO₂ promotes the growth of catalyst particles constantly during co-impregnation process. Moreover, it has been indicated from the previous **Chapter 6** that large size particles can expose well to the incident MW wave and promote MW absorption ability resulting in a better catalytic activity. Therefore, the formation of well-defined CuMo particles offered better exposure to MW wave and promoted catalytic activity at a low MW power of 100 W, as shown in **Figure**

6-1. Whilst single catalysts either of Cu or Mo was inactive for the SDR reaction under MW heating, it is possible to conclude that the Cu^0 particles in the binary CuMo catalyst, in a certain manner, serve as MW absorbers to absorb MW energy to heat up the system for the SDR reaction. This conclusion is somewhat contrary to the reports in the literature [634-636], which indicate the presence of Cu^0 particles in the catalyst structure escalating electrical conductivity and skin effects to reflect the incident MW wave from its surface. Because of this reason, the induction of magnetic materials (ferrites and cobalt) into highly conductive metallic catalysts is compulsory for application under MW heating due to the strong MW absorption of magnetic metals via magnetic losses mechanism [38]. As per the XRD analysis results of **Figure 6-5A-a**, it can be deduced that the formation of MoO_2 particles, which acts as a dielectric layer encompassing Cu^0 particles increasing dielectric properties for the catalysts, and ultimately, reduce the skin effects and promote MW absorption. Moreover, the presence of such dielectric layers surrounding adjacent conductive Cu^0 particles prevents the connectivity percolation between the particles, and hence, increases MW absorption via both of the dielectric and conduction loss mechanism [335]. This conclusion is sourced from the observation of other researchers [336, 637]. The authors employed the polyaniline as a dielectric layer to decorate graphene to reduce graphene' high conductivity to increase MW energy absorption. Indeed, MoO_2 has a higher dielectric constant than copper [638-640].

In the meanwhile, the XRD patterns of spent catalyst samples (**Figure 6-5B-d & e**) confirmed the high catalytic stability with the preservation of all phases, such as Cu^0 and MoO_2 detected from their respective fresh samples. Noticeably, the spent CuMo1.5 catalyst exhibited the presence of CuO phase via the peaks at 35.5° , 58.4° (PDF- 96-153-1268) and CuMoO_4 phase via the peak at 15.7° (PDF- 96-153-0546). The formation of CuO and CuMoO_4 phases in the CuMo1.5 would partly cover the MW absorber components from the incident wave resulting in a weak MW absorption and low catalytic activity. Another possible reason for the lower catalytic activity of the CuMo1.5 catalyst compared to the CoMo1 sample is that the excessive addition of copper raises skin effects, and thereby, reduced MW absorption. In the meanwhile, the catalyst with the Cu/Mo molar ratio of 0.5

(CuMo0.5) might not provide enough MW absorber component (Cu^0) to promote the SDR as efficiently as the CuMo1 sample.

6.2.3.4. Morphology

The morphology of the CuMo1 catalyst was examined by FESEM, STEM-BF, and EELS mapping analysis; and the results are presented in **Figure 6-6**. The FESEM (**Figure 6-6C**) image indicates the distribution of relatively homogeneous catalyst particles on the support, which is consistent with the BF-STEM results (**Figure 6-6D**). Furthermore, the typical HRTEM image (**Figure 6-6E**) of the fresh CuMo1 catalyst displays the interfaces in the catalyst structure visibly. The respective lattice fringes for the Cu^0 facet (111) with d_{111} of 0.208 nm was well-matched with the FFT pattern. This is consistent with the XRD peak at 43.4° of Cu^0 , which is representative for the facet (111) [641]. Due to the absence of copper oxides from the XRD of the fresh CuMo catalyst (**Figure 6-5A-a**), this interface would be between either Cu^0 or MoO_2 or both and TiO_2 support. It has been indicated that the heterojunctions between Cu^0 with support or with other catalyst component contribute the promotion of catalytic activity for reforming reactions [642].

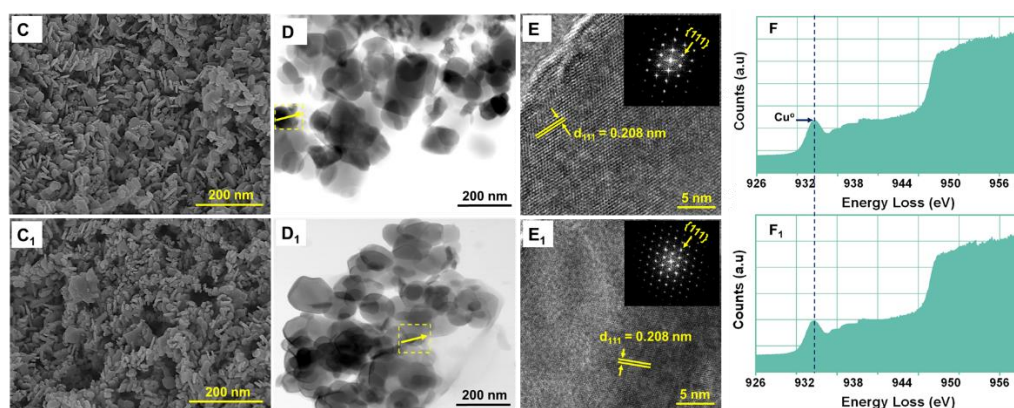


Figure 6-6 - C, C₁: FESEM; D, D₁: STEM-BF; E, E₁: HRTEM; and F, F₁: EELS mapping of fresh (top row) and spent (below row) CuMo1 catalysts. [Reaction conditions: MW power of 100 W, CH_4/CO_2 ratio of 1; S/C = 0.2].

Noticeably, the typical FESEM and BF-STEM images of the CuMo₁ catalyst did not display visible sintering. The HRTEM of the spent CuMo1 catalyst (**Figure 6-6E₁**) also confirms the lattice fringes d_{111} of 0.208 nm of copper with its

corresponding well-matched FFT pattern (inserted images of **Figure 6-6E₁**). In addition to this, the EELS electronic peaks of Cu⁰ in the spent catalyst samples (**Figure 6-6F₁**) were unaltered in comparison with that of the fresh CuMo₁ catalysts (**Figure 6-6F**). Specifically, the presence of Cu⁰ represented by the electronic peak at 935 eV [643] could be observed from the spent CuMo₁ sample (**Figure 6-5F₁**). These observations affirm the good stability of the CuMo₁ catalyst over 72 hrs on the SDR stream test, as shown in **Figure 6-3**. The good mechanical catalytic stability of CuMo₁ catalysts is possibly attributed by the low MW power applied (100 W) and the addition of Mo in Cu/TiO₂ improving the catalytic stability. Indeed, some researchers have indicated that employing Mo as a promoter can prolong copper catalyst life significantly [644, 645]. On the other hand, the EELS mapping of the spent CuMo_{1.5} samples indicated the presence of CuO (**Figure 6-7**) via the electronic peaks at 933 and 948 eV [646, 647]. The EELS spectrum of the fresh CuMo₁ catalyst was re-presented here for comparison purposes. The existence of such CuO phase would partly hide MW absorber component of catalysts, and thereby, reduce catalytic activity. This result is in a good agreement with the above XRD pattern of CuMo_{1.5} sample explaining for its lower activity than the CuMo₁ catalysts.

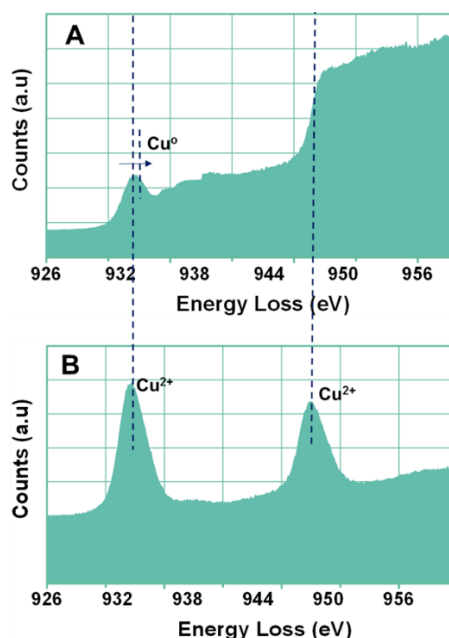


Figure 6-7 - EELS mapping of fresh CuMo₁ (A) and spent CuMo_{1.5} (B) catalysts. [Reaction parameters: 100 W, CH₄:CO₂=1, S/C_{SDR} = 0.2].

Moreover, the HAADF - STEM (**Figure 6-8A**) of the fresh CuMo1 catalyst confirmed the high atomic number from the above BF-STEM image (**Figure 6-6D**). Meanwhile, the EDX mapping (**Figure 6-8C**) depicted the good distribution of Cu and Mo elements on the TiO₂ base.

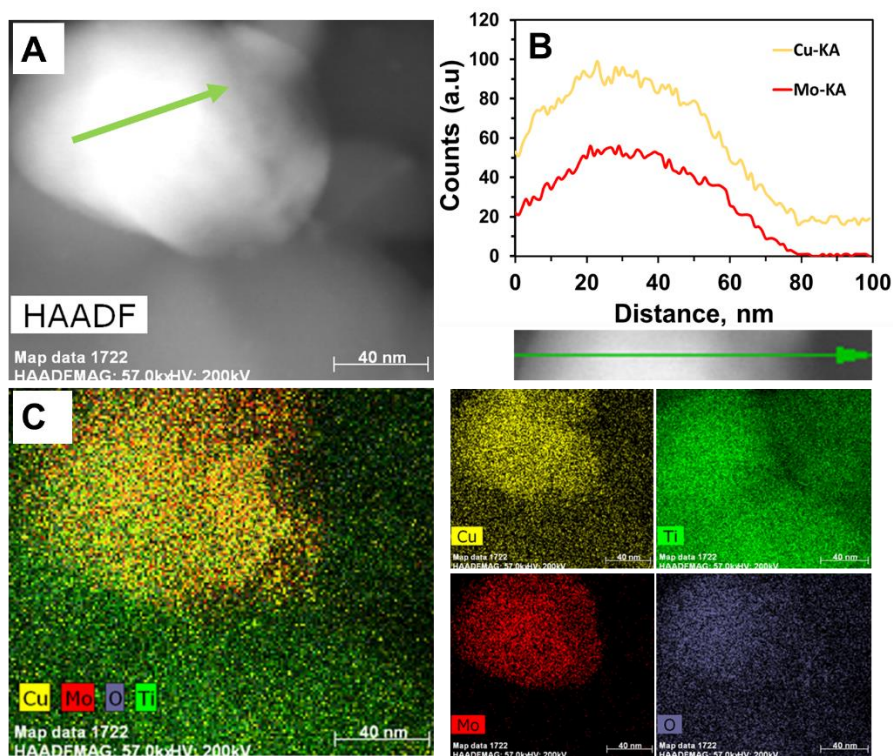


Figure 6-8. STEM – HAADF (A), line scanning (B), and corresponding EDX of the fresh CuMo1 catalyst.

Noticeably, copper species were visibly observed whilst molybdenum counterparts were detected with a slightly lower intensity though the same molar ratio was employed (Cu/Mo of 1). Nonetheless, the coincidence between local maxima of Cu and several Mo local maxima can still be determined unambiguously. To further verify this element distribution, the line scanning analysis was performed as shown in **Figure 6-8B**. It can be seen that the electronic signals corresponding to Cu and Mo atoms were well detected. By recording a larger line scanning peak, Cu⁰ particles were suggested to be formed at the outer whilst MoO₂ was both partly distributed underneath and surrounding Cu⁰ particles confirmed by its weaker line-scanning signals. These observations support the above conclusion on the presence of molybdenum oxides surrounding copper

particles, which possibly increases dielectric properties, reduces surface reflection by reducing the conductivity, and promotes MW absorption capacity.

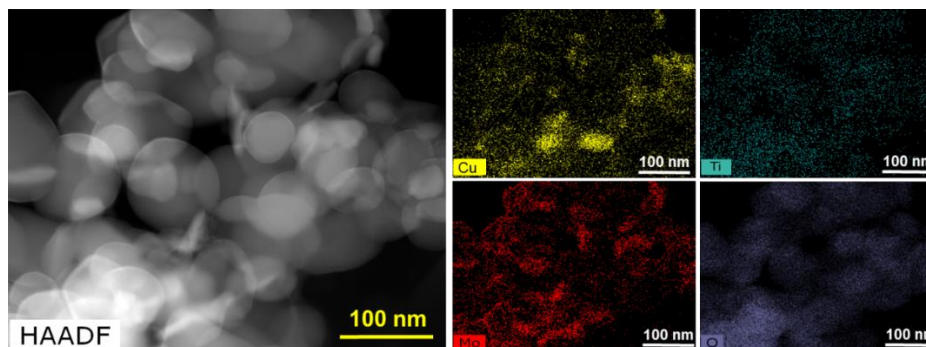


Figure 6-9 - STEM – HAADF and corresponding EDX of the spent CuMo1 catalyst. [Reaction parameters: 100 W, CH₄:CO₂=1, S/C_{SDR} = 0.2].

The STEM – HAADF and corresponding EDX of the spent CuMo1 catalyst (**Figure 6-9**) further confirmed its good stability. Specifically, metallic elements, such of Cu and Mo were persevered their homogeneous distributions. Moreover, none of deposited coke could be observed by HAADF-STEM-EDX analysis.

6.2.3.5. TGA

The TGA analysis of the spent CuMo catalysts was performed to verify coke deposition; and the results are shown in **Figure 6-10**. It can be seen that there was only a slight weight loss in a region of below 300 °C observed from all spent CuMo catalysts. This loss was possibly attributed to the evaporation of physisorbed water molecules. None of weight loss was observed on the subsequent temperature region from 300 to 800 800 °C. The results confirmed the absence of coke deposition on the catalyst structure.

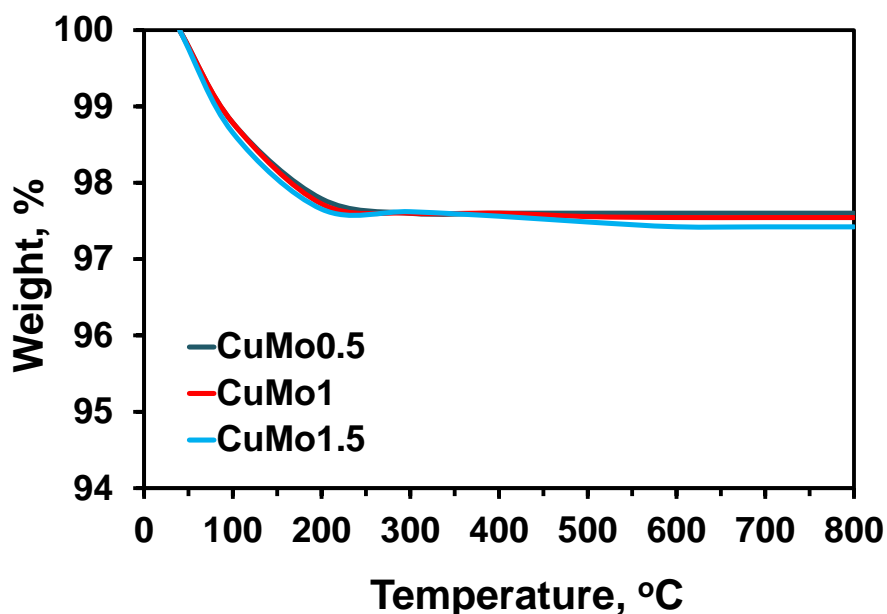


Figure 6-10 – TGA profiles of CuMo/TiO₂ catalysts after 72 h test for SDR reactions. [Reaction parameters: 100 W, CH₄:CO₂=1, S/C_{SDR} = 0.2].

Coke deposition is inevitable in the methane reforming process due to the methane cracking. Notwithstanding this, MW energy promotes coke gasification with reactants (steam and CO₂) on account of the strong MW absorption of carbonaceous species. Herein, it is once again consolidated the superior advantages of MW energy in the improvement for the coke resistance of reforming catalysts.

6.3. Summary

The activity and stability of Cu, Mo, and binary CuMo catalysts supported on TiO₂ for the SDR reaction under MW heating were tested. The formation of dielectric MoO₂ layers surrounding the active centres (Cu⁰ particles) was found as a reason for the activation of the binary CuMo catalysts under a low MW heating power (100 W). In contrast, the Cu/TiO₂ and Mo/TiO₂ were unable to absorb MW due to their high conductivity and low magnetic properties. At the S/C of 0.2, 82 % of methane and 61 % of carbon dioxide were converted to a syngas ratio of 2.1 over the CuMo1 (Cu/Mo molar ratio of 1) and MW power of 100 W. The high reactant conversions in this work further emphasize the exceptional performance of the MW heating on the productivity of gas-solid catalytic reactions. The CuMo catalyst also displayed its high durability over 72 hrs during the SDR stream test.

Copper-based catalyst has proved its promising potential to be employed as a commercial catalyst for reforming natural gas under the MW reactor.

Chapter 7 Conclusions and Recommendations

7.1. Conclusions

The works performed in this thesis deal with catalytic conversion of two dominant greenhouse gas elements, CH₄ and CO₂, to syngas under one advanced heating method of microwave (MW). The main focus of this work is to develop highly active and stable catalysts, which can be activated under MW irradiation for methane reforming to produce more useful chemicals - syngas. The first part of this thesis reported the activation of CoMo catalysts supported on Al₂O₃ for MW assisted DRM. In the second part, the role of TiO₂ in the enhancement of CoMo catalysts for both DRM and SDR was studied. In the final section, the MW activation of Cu-Mo/TiO₂ catalyst for SDR reaction was elaborated and the effects of steam addition on the reforming performance were also investigated. Simultaneously, the fundamental understanding of the activation of metallic-based catalysts under MW heating for gas-phase reactions like methane reforming has also been achieved. The following conclusions from this study can be made:

- Single metallic catalysts, such as Co, Mo, and Cu supported on Al₂O₃ or TiO₂ are inactive for methane reforming reactions under MW heating due to their inability to absorb MW energy. The inability of these monometallic catalysts under MW irradiation is due to either their high electrical conductivity (Co, Mo) or low magnetic properties (Mo), which, in turns, limit the MW absorption.
- The formed magnetodielectric alloy like Co_{0.82}Mo_{0.18} in the bimetallic CoMo/Al₂O₃ and CoMo/TiO₂ catalysts is playing a dual role. Such alloy is working not only as a MW absorber but also as an internal heating source transferring the heat to the neighbouring metallic components (such as Co-based and Mo-based oxides) leading to form extra active centres for methane reforming reactions.
- TiO₂ offers the better exposure of Co_{0.82}Mo_{0.18} MW absorbers to the incident MW wave promoting MW absorption, and thereby, delivering higher catalytic activity than Al₂O₃. Moreover, TiO₂ also provides the strong metal-support interactions resulting in good catalytic stability.

- Earth-abundant metals like copper in a binary system with molybdenum could absorb MW to catalyze the SDR reaction for syngas production on account of the formation of dielectric MoO₂ layer. Such dielectric layers are surrounding the highly conductive Cu⁰ particles to reduce skin effects, and consequently, promoting MW absorption. On account of its activation at low MW power and the good interaction between CuMo and TiO₂, the CuMo/TiO₂ catalyst could be stable for at least 72 hrs on the SDR stream test.
- The MW power needed to activate catalysts was sensitive to the molar ratios between Co (Cu) and Mo. This MW power was lowered when increasing the Co/Mo ratio up to 2.0 for CoMo/Al₂O₃ and to 1.0 for CoMo and CuMo supported on TiO₂. However, the further increase in Co (Cu)/Mo ratio was unable to reduce the activated MW power for catalyst activation since the presence of the excessive amount of highly conductive Co⁰ (Cu⁰) particles increases the MW reflection.
- The reactant conversions and product selectivity are dependent on the Co (Cu)/Mo molar ratio. The CoMo catalyst supported on Al₂O₃ with the Co/Mo molar ratio of 2 displays the best catalytic activity and stability for DRM whilst the CoMo/TiO₂ and CuMo/TiO₂ require a lower Co (Cu)/Mo molar ratio to provide the highest conversion and selectivity for reforming reactions. The higher molar ratios than these optimum values would result in the lower activity and stability of respective catalysts. This is due to the formation of non-absorber oxides, such as Co₂Mo₃O₈ (CoMo/Al₂O₃, CoMo/TiO₂) or CuMoO₄ (CuMo/TiO₂), which covered partly MW absorbing elements reducing MW absorption, and therefore, diminishing catalytic activity.
- Carbon formation was significantly limited under MW irradiation due to the strong MW absorption of carbon promoting its consumption via the gasification reaction with carbon dioxide (Bourdouard reaction) and steam.
- Due to endothermic characteristics of reforming reactions, the conversion of reactants rose when escalating MW power equivalent to improving reaction temperature. On average, about 80 % CH₄ and 75 % CO₂ were

converted via methane reforming over the prepared catalysts at relatively low MW powers. Moreover, syngas ratio could be adjusted by altering the steam addition in the feed mixture. The syngas ratio of above two could be achieved with the steam-to-methane (S/C) ratio of 0.1 (over CoMo/TiO₂ catalysts) or 0.2 (over CuMo/TiO₂ catalysts).

- The methane reforming processes over supported CoMo and CuMo catalysts under MW heating have proved its flexibility and high performance to exploit natural gas reserves for fuel production efficiently.

7.2. Recommendations

On promising outcomes of this PhD study, the following future research is recommended to further advance the development in this area:

- As per **Chapter 5** and **Chapter 6**, the catalysts with large size particles provided better catalytic activity due to the stronger MW absorption compared to catalysts with well-dispersed particles. The future work should study the effects of catalyst particle size on the performance of MW assisted methane reforming processes.
- The study has explored the combination of magnetic metals like cobalt with paramagnetic elements like molybdenum supported on dielectric supports. The next work should be extended to study other combination between magnetic metals, such as iron, nickel with cobalt, copper, and zinc supported on MgO, ZrO₂, and CeO₂.
- The exceptional enhancement of MW heating for methane reforming has been well recognized. However, a well-proven mechanism has not been reached to correlate the kinetics of methane reactions under MW heating. The reason for the spectacular escalation in the reactant conversion as soon as the catalyst was activated is stills unclear. Thus, the fundamental knowledge on the reaction mechanism and kinetics of the catalytic reforming of methane under MW heating should be further studied to optimize reaction performance.
- As per findings from **Chapter 5** and **Chapter 6**, coke deposition is restricted under MW due to its strong MW absorption. The future work should attempt to design a cycle step to enhance catalytic stability further.

Also based on the findings of this thesis, the syngas production via the reactions between steam, carbon, and carbon dioxide under MW heating should be clarified.

References

1. Ao, M., et al., *Structure and activity of strontium substituted LaCoO₃ perovskite catalysts for syngas conversion*. Journal of Molecular Catalytic A: Chemical, 2016. **416**(Supplement C): p. 96-104.
2. Yang, J., et al., *Fischer–Tropsch synthesis: A review of the effect of CO conversion on methane selectivity*. Applied Catalytic A: General, 2014. **470**: p. 250-260.
3. Bukur, D.B., B. Todic, and N. Elbashir, *Role of water-gas-shift reaction in Fischer–Tropsch synthesis on iron catalysts: A review*. Catalytic Today, 2016. **275**: p. 66-75.
4. Guettel, R. and T. Turek, *Comparison of different reactor types for low temperature Fischer–Tropsch synthesis: a simulation study*. Chemical Engineering Science, 2009. **64**(5): p. 955-964.
5. Dadgar, F., et al., *Direct dimethyl ether synthesis from synthesis gas: The influence of methanol dehydration on methanol synthesis reaction*. Catalytic Today, 2016. **270**: p. 76-84.
6. Ao, M., et al., *Selectivity enhancement for higher alcohol product in Fischer-Tropsch synthesis over nickel-substituted La_{0.9}Sr_{0.1}CoO₃ perovskite catalysts*. Fuel, 2017. **206**: p. 390-400.
7. Ribeiro, A.T.S., et al., *Influence of sucrose addition and acid treatment of silica-supported Co-Ru catalysts for Fischer-Tropsch synthesis*. Fuel, 2018. **231**: p. 157-164.
8. Pendyala, V.R.R., et al., *Fischer-Tropsch synthesis: Effect of carbonyl sulfide poison over a Pt promoted Co/alumina catalyst*. Catalytic Today, 2018. **299**: p. 14-19.
9. Pei, Y.-P., et al., *High alcohols synthesis via Fischer–Tropsch reaction at cobalt metal/carbide interface*. ACS Catalytic, 2015. **5**(6): p. 3620-3624.
10. Ao, M., et al., *Active centers of catalysts for higher alcohol synthesis from syngas: a review*. Acs Catalytic, 2018. **8**(8): p. 7025-7050.
11. Jabbour, K., et al., *Factors affecting the long-term stability of mesoporous nickel-based catalysts in combined steam and dry reforming of methane*. Catalytic Science & Technology, 2016. **6**(12): p. 4616-4631.

12. L fberg, A., et al., *Ni/CeO₂ based catalysts as oxygen vectors for the chemical looping dry reforming of methane for syngas production*. Applied Catalytic B: Environmental, 2017. **212**: p. 159-174.
13. Usman, M., W.M.A. Wan Daud, and H.F. Abbas, *Dry reforming of methane: Influence of process parameters—A review*. Renewable and Sustainable Energy Reviews, 2015. **45**(Supplement C): p. 710-744.
14. Lavoie, J.-M., *Review on dry reforming of methane, a potentially more environmentally-friendly approach to the increasing natural gas exploitation*. Frontiers in Chemistry, 2014. **2**: p. 81.
15. Varisli, D., C. Korkusuz, and T. Dogu, *Microwave-assisted ammonia decomposition reaction over iron incorporated mesoporous carbon catalysts*. Applied Catalytic B: Environmental, 2017. **201**: p. 370-380.
16. Men ndez, J., et al., *Microwave heating processes involving carbon materials*. Fuel Processing Technology, 2010. **91**(1): p. 1-8.
17. Chun, S.M., et al., *CO₂ microwave plasma—catalytic reactor for efficient reforming of methane to syngas*. Catalysts, 2019. **9**(3): p. 292.
18. Bo, Z., et al., *Plasma assisted dry methane reforming using gliding arc gas discharge: effect of feed gases proportion*. International Journal of Hydrogen Energy, 2008. **33**(20): p. 5545-5553.
19. Ghorbanzadeh, A., R. Lotfalipour, and S. Rezaei, *Carbon dioxide reforming of methane at near room temperature in low energy pulsed plasma*. international journal of hydrogen energy, 2009. **34**(1): p. 293-298.
20. Li, D., et al., *CO₂ reforming of CH₄ by atmospheric pressure glow discharge plasma: a high conversion ability*. International Journal of Hydrogen Energy, 2009. **34**(1): p. 308-313.
21. Czyrkowski, D., et al., *Microwave plasma-based method of hydrogen production via combined steam reforming of methane*. Energy, 2016. **113**: p. 653-661.
22. Rutberg, P.G., et al., *Conversion of methane by CO₂ + H₂O + CH₄ plasma*. Applied Energy, 2015. **148**: p. 159-168.
23. Tao, X., et al., *CH₄–CO₂ reforming by plasma – challenges and opportunities*. Progress in Energy and Combustion Science, 2011. **37**(2): p. 113-124.

24. Dastan, A., A. Kulkarni, and B. Torok, *Environmentally benign synthesis of heterocyclic compounds by combined microwave-assisted heterogeneous catalytic approaches*[dagger]. *Green Chemistry*, 2012. **14**(1): p. 17-37.
25. Fidalgo, B., et al., *Microwave-assisted dry reforming of methane*. *International Journal of Hydrogen Energy*, 2008. **33**(16): p. 4337-4344.
26. Hamzehlouia, S., S.A. Jaffer, and J. Chaouki, *Microwave heating-assisted catalytic dry reforming of methane to syngas*. *Scientific Reports*, 2018. **8**(1): p. 8940.
27. Li, L., et al., *Methane dry reforming with microwave heating over carbon-based catalyst obtained by agriculture residues pyrolysis*. *Journal of CO2 Utilization*, 2018. **28**: p. 41-49.
28. Li, L., et al., *Methane dry and mixed reforming on the mixture of bio-char and nickel-based catalyst with microwave assistance*. *Journal of Analytical and Applied Pyrolysis*, 2017. **125**: p. 318-327.
29. Li, L., et al., *Fe-rich biomass derived char for microwave-assisted methane reforming with carbon dioxide*. *Science of The Total Environment*, 2019. **657**: p. 1357-1367.
30. Odedairo, T., et al., *Influences of doping Cr/Fe/Ta on the performance of Ni/CeO₂ catalyst under microwave irradiation in dry reforming of CH₄*. *Journal of Solid State Chemistry*, 2016. **233**(Supplement C): p. 166-177.
31. Domínguez, A., et al., *Biogas to syngas by microwave-assisted dry reforming in the presence of char*. *Energy & Fuels*, 2007. **21**(4): p. 2066-2071.
32. Fidalgo, B., A. Arenillas, and J.A. Menéndez, *Influence of porosity and surface groups on the catalytic activity of carbon materials for the microwave-assisted CO₂ reforming of CH₄*. *Fuel*, 2010. **89**(12): p. 4002-4007.
33. Bermudez, J.M., et al., *Mixtures of steel-making slag and carbons as catalyst for microwave-assisted dry reforming of CH₄*. *Chinese Journal of Catalytic*, 2012. **33**(7): p. 1115-1118.

34. Li, L., et al., *Performance of bio-char and energy analysis on CH₄ combined reforming by CO₂ and H₂O into syngas production with assistance of microwave*. Fuel, 2018. **215**: p. 655-664.
35. Menéndez, J.A., et al., *Microwave heating processes involving carbon materials*. Fuel Processing Technology, 2010. **91**(1): p. 1-8.
36. Zhang, X., et al., *Carbon dioxide reforming of methane with Pt catalysts using microwave dielectric heating*. Catalytic Letters, 2003. **88**(3): p. 129-139.
37. Gangurde, L.S., et al., *Synthesis, characterization, and application of ruthenium-doped SrTiO₃ perovskite catalysts for microwave-assisted methane dry reforming*. Chemical Engineering and Processing - Process Intensification, 2018. **127**: p. 178-190.
38. Varsano, F., et al., *Dry reforming of methane powered by magnetic induction*. International Journal of Hydrogen Energy, 2019.
39. Kim, S.-S., et al., *Magnetic, dielectric, and microwave absorbing properties of iron particles dispersed in rubber matrix in gigahertz frequencies*. Journal of Applied Physics, 2005. **97**(10): p. 10F905.
40. Kittel, C., *On the theory of ferromagnetic resonance absorption*. Physical Review, 1948. **73**(2): p. 155.
41. Lakshmi, K., et al., *Microwave absorption, reflection and EMI shielding of PU–PANI composite*. Acta Materialia, 2009. **57**(2): p. 371-375.
42. Tsyntsar, N., et al., *Structural, magnetic, and mechanical properties of electrodeposited cobalt–tungsten alloys: Intrinsic and extrinsic interdependencies*. Electrochimica Acta, 2013. **104**: p. 94-103.
43. Brondino, C.D., et al., *Structural and electron paramagnetic resonance (EPR) studies of mononuclear molybdenum enzymes from sulfate-reducing bacteria*. Accounts of chemical research, 2006. **39**(10): p. 788-796.
44. Petrov, V. and V. Gagulin, *Microwave absorbing materials*. Inorganic Materials, 2001. **37**(2): p. 93-98.
45. Pendyala, V.R.R., et al., *Fischer–Tropsch synthesis: effect of ammonia on product selectivities for a Pt promoted Co/alumina catalyst*. RSC Advances, 2017. **7**(13): p. 7793-7800.

46. Ayodele, B.V., et al., *Syngas production from CO₂ reforming of methane over neodymium sesquioxide supported cobalt catalyst*. Journal of Natural Gas Science and Engineering, 2016. **34**: p. 873-885.
47. Ayodele, B.V., et al., *Production of CO-rich hydrogen from methane dry reforming over lanthania-supported cobalt catalyst: Kinetic and mechanistic studies*. International Journal of Hydrogen Energy, 2016. **41**(8): p. 4603-4615.
48. Abd Ghani, N.A., et al., *Dry reforming of methane for hydrogen production over NiCo catalysts: Effect of NbZr promoters*. International Journal of Hydrogen Energy, 2018. **In Press**(In Press): p. 1-8.
49. Ayodele, B.V., M.R. Khan, and C.K. Cheng, *Catalytic performance of ceria-supported cobalt catalyst for CO-rich hydrogen production from dry reforming of methane*. International Journal of Hydrogen Energy, 2016. **41**(1): p. 198-207.
50. Marin-Flores, O., et al., *Nanoparticle molybdenum dioxide: A highly active catalyst for partial oxidation of aviation fuels*. Applied Catalytic B: Environmental, 2010. **98**(3-4): p. 186-192.
51. Awadallah, A.E., A.A. Aboul-Enein, and A.K. Aboul-Gheit, *Effect of progressive Co loading on commercial Co-Mo/Al₂O₃ catalyst for natural gas decomposition to CO_x-free hydrogen production and carbon nanotubes*. Energy Conversion and Management, 2014. **77**(Supplement C): p. 143-151.
52. Ewbank, J.L., et al., *Effect of preparation methods on the performance of Co/Al₂O₃ catalysts for dry reforming of methane*. Green Chemistry, 2014. **16**(2): p. 885-896.
53. Horváth, É., et al., *Dry reforming of CH₄ on Co/Al₂O₃ catalysts reduced at different temperatures*. Catalytic Today, 2017. **281**: p. 233-240.
54. Gaillard, M., M. Virginie, and A.Y. Khodakov, *New molybdenum-based catalysts for dry reforming of methane in presence of sulfur: A promising way for biogas valorization*. Catalytic Today, 2017. **289**: p. 143-150.
55. Li, M., et al., *The relation between morphology of (Co)MoS₂ phases and selective hydrodesulfurization for CoMo catalysts*. Catalytic Today, 2010. **149**(1): p. 35-39.

56. Ali, S.A., et al., *Simultaneous hydrodesulfurization of dibenzothiophene and substituted dibenzothiophenes over phosphorus modified CoMo/Al₂O₃ catalysts*. Fuel Processing Technology, 2012. **98**(Supplement C): p. 39-44.
57. Chen, W., et al., *Influence of active phase structure of CoMo/Al₂O₃ catalyst on the selectivity of hydrodesulfurization and hydrodearomatization*. Catalytic Today, 2017. **292**(Supplement C): p. 97-109.
58. Kim, H.K., et al., *Preparation of CoMo/Al₂O₃, CoMo/CeO₂, CoMo/TiO₂ catalysts using ultrasonic spray pyrolysis for the hydro-desulfurization of 4, 6-dimethyldibenzothiophene for fuel cell applications*. International Journal of Hydrogen Energy, 2016. **41**(41): p. 18846-18857.
59. Nikulshin, P.A., et al., *CoMo/Al₂O₃ catalysts prepared on the basis of Co₂Mo₁₀-heteropolyacid and cobalt citrate: Effect of Co/Mo ratio*. Fuel, 2012. **100**(Supplement C): p. 24-33.
60. Maximov, N.M., et al., *Co-Mo/Al₂O₃ and Ni-W/Al₂O₃ catalysts: Potential and prospects for use in hydrotreating of light cycle oil from catalytic cracking*. Russian Journal of Applied Chemistry, 2017. **90**(4): p. 574-581.
61. Ardakani, S.J., M. Alyani, and K.J. Smith, *Stability of a Cs-promoted Co-Mo/Al₂O₃ catalyst during synthesis gas conversion*. The Canadian Journal of Chemical Engineering, 2016. **94**(4): p. 655-661.
62. Elwell, C.E., et al., *Copper–oxygen complexes revisited: Structures, spectroscopy, and reactivity*. Chemical Reviews, 2017. **117**(3): p. 2059-2107.
63. Mirica, L.M., X. Ottenwaelde, and T.D.P. Stack, *Structure and spectroscopy of copper–dioxygen complexes*. Chemical Reviews, 2004. **104**(2): p. 1013-1046.
64. Aboelella, N.W., et al., *Snapshots of dioxygen activation by copper: The structure of a 1:1 Cu/O₂ adduct and its use in syntheses of asymmetric bis(μ -oxo) complexes*. Journal of the American Chemical Society, 2002. **124**(36): p. 10660-10661.
65. Liu, X., et al., *Earth-abundant copper-based bifunctional electrocatalyst for both catalytic hydrogen production and water oxidation*. ACS Catalytic, 2015. **5**(3): p. 1530-1538.

66. Petrov, L., K. Kumbilieva, and N. Kirkov, *Kinetic model of nitrobenzene hydrogenation to aniline over industrial copper catalyst considering the effects of mass transfer and deactivation*. *Applied catalytic*, 1990. **59**(1): p. 31-43.
67. Greeley, J.P., *Active site of an industrial catalyst*. *Science*, 2012. **336**(6083): p. 810-811.
68. Van Den Berg, R., et al., *Structure sensitivity of Cu and CuZn catalysts relevant to industrial methanol synthesis*. *Nature communications*, 2016. **7**: p. 13057.
69. Li, W., et al., *General and chemoselective copper oxide catalysts for hydrogenation reactions*. *ACS Catalytic*, 2019.
70. Zhang, J., H. Wang, and A.K. Dalai, *Development of stable bimetallic catalysts for carbon dioxide reforming of methane*. *Journal of Catalytic*, 2007. **249**(2): p. 300-310.
71. Wu, T., et al., *Cu–Ni@SiO₂ alloy nanocomposites for methane dry reforming catalytic*. *RSC Advances*, 2013. **3**(46): p. 23976-23979.
72. Lee, J.-H., et al., *Stabilization of Ni/Al₂O₃ catalyst by Cu addition for CO₂ reforming of methane*. *Applied Catalytic A: General*, 2004. **269**(1-2): p. 1-6.
73. Rahemi, N., et al., *Syngas production from reforming of greenhouse gases CH₄/CO₂ over Ni–Cu/Al₂O₃ nanocatalyst: Impregnated vs. plasma-treated catalyst*. *Energy conversion and management*, 2014. **84**: p. 50-59.
74. Pinheiro, A.L., et al., *Analysis of coke deposition and study of the structural features of MAI₂O₄ catalysts for the dry reforming of methane*. *Catalytic Communications*, 2009. **11**(1): p. 11-14.
75. Marino, F., et al., *Hydrogen production from steam reforming of bioethanol using Cu/Ni/K/γ-Al₂O₃ catalysts. Effect of Ni*. *International Journal of Hydrogen Energy*, 2001. **26**(7): p. 665-668.
76. Bernardo, C., I. Alstrup, and J. Rostrup-Nielsen, *Carbon deposition and methane steam reforming on silica-supported Ni-Cu catalysts*. *Journal of Catalytic*, 1985. **96**(2): p. 517-534.

77. Huang, T.-J. and S.-Y. Jhao, *Ni-Cu/samarium-doped ceria catalysts for steam reforming of methane in the presence of carbon dioxide*. Applied Catalytic A: General, 2006. **302**(2): p. 325-332.
78. Stankiewicz, A., et al., *Perspectives of microwaves-enhanced heterogeneous catalytic gas-phase processes in flow systems*. The Chemical Record, 2019. **19**(1): p. 40-50.
79. Shukla, A. and H. Karki, *Application of robotics in onshore oil and gas industry—A review Part I*. Robotics and Autonomous Systems, 2016. **75**: p. 490-507.
80. Chen, W., *Status and challenges of Chinese deepwater oil and gas development*. Petroleum Science, 2011. **8**(4): p. 477-484.
81. Halim, S.Z., et al., *In search of causes behind offshore incidents: Fire in offshore oil and gas facilities*. Journal of Loss Prevention in the Process Industries, 2018. **54**: p. 254-265.
82. Wood, D.A., C. Nwaoha, and B.F. Towler, *Gas-to-liquids (GTL): A review of an industry offering several routes for monetizing natural gas*. Journal of Natural Gas Science and Engineering, 2012. **9**: p. 196-208.
83. Agency, U.S.E.P. 2010; Available from: <https://www.epa.gov/ghgemissions/global-greenhouse-gas-emissions-data>
84. Kappe, C.O., *Controlled microwave heating in modern organic synthesis*. Angewandte Chemie International Edition, 2004. **43**(46): p. 6250-6284.
85. Remón, J., et al., *Analysis and optimisation of a microwave-assisted hydrothermal process for the production of value-added chemicals from glycerol*. Green Chemistry, 2018. **20**(11): p. 2624-2636.
86. Meng, H., L. Kloul, and A. Rauzy, *Production availability analysis of floating production storage and offloading (FPSO) systems*. Applied Ocean Research, 2018. **74**: p. 117-126.
87. Makogon, Y.F., *Natural gas hydrates – A promising source of energy*. Journal of Natural Gas Science and Engineering, 2010. **2**(1): p. 49-59.
88. Christian Enger, B., R. Lødeng, and A. Holmen, *A review of catalytic partial oxidation of methane to synthesis gas with emphasis on reaction*

- mechanisms over transition metal catalysts*. Applied Catalytic A: General, 2008. **346**(1): p. 1-27.
89. Barelli, L., et al., *Hydrogen production through sorption-enhanced steam methane reforming and membrane technology: A review*. Energy, 2008. **33**(4): p. 554-570.
 90. Van Der Laan, G.P. and A.A.C.M. Beenackers, *Kinetics and selectivity of the fischer–Tropsch synthesis: A literature review*. Catalytic Reviews, 1999. **41**(3-4): p. 255-318.
 91. Adris, A.M., et al., *On the reported attempts to radically improve the performance of the steam methane reforming reactor*. The Canadian Journal of Chemical Engineering, 1996. **74**(2): p. 177-186.
 92. Byrne, P.J., et al., *Recent progress in hydrogenation of petroleum*. Industrial & Engineering Chemistry, 1932. **24**(10): p. 1129-1135.
 93. Wei, Z., et al., *Bimetallic catalysts for hydrogen generation*. Chemical Society Reviews, 2012. **41**(24): p. 7994-8008.
 94. Xu, J. and G.F. Froment, *Methane steam reforming, methanation and water-gas shift: I. Intrinsic kinetics*. AIChE Journal, 1989. **35**(1): p. 88-96.
 95. Matsumura, Y. and T. Nakamori, *Steam reforming of methane over nickel catalysts at low reaction temperature*. Applied Catalytic A: General, 2004. **258**(1): p. 107-114.
 96. Dissanayake, D., et al., *Partial oxidation of methane to carbon monoxide and hydrogen over a Ni/Al₂O₃ catalyst*. Journal of Catalytic, 1991. **132**(1): p. 117-127.
 97. York, A.P., T. Xiao, and M.L. Green, *Brief overview of the partial oxidation of methane to synthesis gas*. Topics in Catalytic, 2003. **22**(3-4): p. 345-358.
 98. Amin, N.A.S. and T.C. Yaw, *Thermodynamic equilibrium analysis of combined carbon dioxide reforming with partial oxidation of methane to syngas*. International Journal of Hydrogen Energy, 2007. **32**(12): p. 1789-1798.
 99. Nematollahi, B., M. Rezaei, and M. Khajenoori, *Combined dry reforming and partial oxidation of methane to synthesis gas on noble metal catalysts*. International journal of hydrogen energy, 2011. **36**(4): p. 2969-2978.

100. Meshkani, F., M. Rezaei, and M. Andache, *Investigation of the catalytic performance of Ni/MgO catalysts in partial oxidation, dry reforming and combined reforming of methane*. Journal of Industrial and Engineering Chemistry, 2014. **20**(4): p. 1251-1260.
101. Sinev, M.Y., V. Korshak, and O.V. Krylov, *The mechanism of the partial oxidation of methane*. Russian Chemical Reviews, 1989. **58**(1): p. 22.
102. Tsang, S.C., J.B. Claridge, and M.L.H. Green, *Recent advances in the conversion of methane to synthesis gas*. Catalytic Today, 1995. **23**(1): p. 3-15.
103. Ziebart, C. and M. Beller, *Hydrogenation and related reductions of carbon dioxide with molecular catalysts*, in *Transformation and Utilization of Carbon Dioxide*, B.M. Bhanage and M. Arai, Editors. 2014, Springer Berlin Heidelberg: Berlin, Heidelberg. p. 73-102.
104. Quadrelli, E.A., et al., *Carbon dioxide recycling: Emerging large-scale technologies with industrial potential*. ChemSusChem, 2011. **4**(9): p. 1194-1215.
105. Van-Dal, É.S. and C. Bouallou, *Design and simulation of a methanol production plant from CO₂ hydrogenation*. Journal of Cleaner Production, 2013. **57**: p. 38-45.
106. Kattel, S., et al., *Active sites for CO₂ hydrogenation to methanol on Cu/ZnO catalysts*. Science, 2017. **355**(6331): p. 1296-1299.
107. Jun, K.-W., et al., *Residual sodium effect on the catalytic activity of Cu/ZnO/Al₂O₃ in methanol synthesis from CO₂ hydrogenation*. Applied Catalytic A: General, 1998. **174**(1): p. 231-238.
108. Schakel, W., et al., *Assessing the techno-environmental performance of CO₂ utilization via dry reforming of methane for the production of dimethyl ether*. Journal of CO₂ Utilization, 2016. **16**: p. 138-149.
109. Nikoo, M.K. and N.A.S. Amin, *Thermodynamic analysis of carbon dioxide reforming of methane in view of solid carbon formation*. Fuel Processing Technology, 2011. **92**(3): p. 678-691.
110. Wang, S., G.Q. Lu, and G.J. Millar, *Carbon dioxide reforming of methane to produce synthesis gas over metal-supported catalysts: State of the art*. Energy & Fuels, 1996. **10**(4): p. 896-904.

111. Aramouni, N.A.K., et al., *Catalyst design for dry reforming of methane: Analysis review*. Renewable and Sustainable Energy Reviews, 2018. **82**: p. 2570-2585.
112. Guo, J., H. Lou, and X. Zheng, *The deposition of coke from methane on a Ni/MgAl₂O₄ catalyst*. Carbon, 2007. **45**(6): p. 1314-1321.
113. Ferreira-Aparicio, P., et al., *Mechanistic aspects of the dry reforming of methane over ruthenium catalysts*. Applied Catalytic A: General, 2000. **202**(2): p. 183-196.
114. Sierra Gallego, G., et al., *Dual active-site mechanism for dry methane reforming over Ni/La₂O₃ produced from LaNiO₃ perovskite*. Industrial & Engineering Chemistry Research, 2008. **47**(23): p. 9272-9278.
115. Nagaoka, K., et al., *Activation mechanism of methane-derived coke (CH_x) by CO₂ during dry reforming of methane – comparison for Pt/Al₂O₃ and Pt/ZrO₂*. Catalytic Letters, 2000. **70**(3): p. 109-116.
116. Cui, Y., et al., *Kinetic study of the catalytic reforming of CH₄ with CO₂ to syngas over Ni/ α -Al₂O₃ catalyst: The effect of temperature on the reforming mechanism*. Applied Catalytic A: General, 2007. **318**: p. 79-88.
117. Bobin, A.S., et al., *Mechanism of CH₄ dry reforming on nanocrystalline doped ceria-zirconia with supported Pt, Ru, Ni, and Ni–Ru*. Topics in Catalytic, 2013. **56**(11): p. 958-968.
118. Shah, Y.T. and T.H. Gardner, *Dry reforming of hydrocarbon feedstocks*. Catalytic Reviews, 2014. **56**(4): p. 476-536.
119. Will, H., P. Scholz, and B. Ondruschka, *Heterogeneous gas-phase catalytic under microwave irradiation—a new multi-mode microwave applicator*. Topics in Catalytic, 2004. **29**(3): p. 175-182.
120. Hayward, D., *Apparent equilibrium shifts and hot-spot formation for catalytic reactions induced by microwave dielectric heating*. Chemical Communications, 1999(11): p. 975-976.
121. Zhang, X., et al., *Microwave assisted catalytic reduction of sulfur dioxide with methane over MoS₂ catalysts*. Applied Catalytic B: Environmental, 2001. **33**(2): p. 137-148.

122. Perry, W.L., et al., *On the possibility of a significant temperature gradient in supported metal catalysts subjected to microwave heating*. Catalytic letters, 1997. **47**(1): p. 1-4.
123. Roussy, G., et al., *C₂₊ selectivity enhancement in oxidative coupling of methane over microwave-irradiated catalysts*. Fuel processing technology, 1997. **50**(2-3): p. 261-274.
124. Fidalgo, B. and J. Menéndez, *Syngas production by CO₂ reforming of CH₄ under microwave heating—Challenges and opportunities*. 2013, Nova Science Publishers: New York. p. 121-149.
125. Jacob, J., L.H.L. Chia, and F.Y.C. Boey, *Thermal and non-thermal interaction of microwave radiation with materials*. Journal of Materials Science, 1995. **30**(21): p. 5321-5327.
126. Tang, J., et al., *Microwave discharge-assisted catalytic conversion of NO to N₂*. Chemical Communications, 2000(19): p. 1861-1862.
127. Xu, W., et al., *Microwave selective effect: a new approach towards oxygen inhibition removal for highly-effective NO decomposition by microwave catalytic over BaMn_xMg_{1-x}O₃ mixed oxides at low temperature under excess oxygen*. Chemical Communications, 2015. **51**(19): p. 4073-4076.
128. Xu, W., et al., *Development of MgCo₂O₄–BaCO₃ composites as microwave catalysts for the highly effective direct decomposition of NO under excess O₂ at a low temperature*. Catalytic Science & Technology, 2019. **9**(16): p. 4276-4285.
129. Xu, W., et al., *Microwave catalytic effect: a new exact reason for microwave-driven heterogeneous gas-phase catalytic reactions*. Catalytic Science & Technology, 2016. **6**(3): p. 698-702.
130. Horikoshi, S., H. Hidaka, and N. Serpone, *Environmental remediation by an integrated microwave/UV-illumination technique: IV. Non-thermal effects in the microwave-assisted degradation of 2, 4-dichlorophenoxyacetic acid in UV-irradiated TiO₂/H₂O dispersions*. Journal of Photochemistry and Photobiology A: Chemistry, 2003. **159**(3): p. 289-300.

131. Langa, F., et al., *Microwave irradiation: more than just a method for accelerating reactions*. Contemporary Organic Synthesis, 1997. **4**(5): p. 373-386.
132. Kuhnert, N., *Microwave-assisted reactions in organic synthesis - Are there any nonthermal microwave effects?* Angewandte Chemie - International Edition, 2002. **41**(11): p. 1863-1866.
133. Stuerger, D.A.C. and P. Gaillard, *Microwave Athermal Effects in Chemistry: A Myth's Autopsy: Part I: Historical background and fundamentals of wave-matter interaction*. Journal of Microwave Power and Electromagnetic Energy, 1996. **31**(2): p. 87-100.
134. Stuerger, D.A.C. and P. Gaillard, *Microwave athermal effects in chemistry: A myth's autopsy: Part II: Orienting effects and thermodynamic consequences of electric field*. Journal of Microwave Power and Electromagnetic Energy, 1996. **31**(2): p. 101-113.
135. Fidalgo, B., A. Arenillas, and J.A. Menéndez, *Mixtures of carbon and Ni/Al₂O₃ as catalysts for the microwave-assisted CO₂ reforming of CH₄*. Fuel Processing Technology, 2011. **92**(8): p. 1531-1536.
136. Sharifvaghefi, S., et al., *Application of microwave in hydrogen production from methane dry reforming: Comparison between the conventional and microwave-assisted catalytic reforming on improving the energy efficiency*. Catalysts, 2019. **9**(7): p. 618.
137. Argyle, M. and C. Bartholomew, *Heterogeneous catalyst deactivation and regeneration: A review*. Catalysts, 2015. **5**(1): p. 145.
138. Xu, J., et al., *Characterization and analysis of carbon deposited during the dry reforming of methane over Ni/La₂O₃/Al₂O₃ catalysts*. Chinese Journal of Catalytic, 2009. **30**(11): p. 1076-1084.
139. Swaan, H.M., et al., *Deactivation of supported nickel catalysts during the reforming of methane by carbon dioxide*. Catalytic Today, 1994. **21**(2): p. 571-578.
140. Chen, Y.-G., K. Tomishige, and K. Fujimoto, *Formation and characteristic properties of carbonaceous species on nickel-magnesia solid solution catalysts during CH₄-CO₂ reforming reaction*. Applied Catalytic A: General, 1997. **161**(1): p. L11-L17.

141. Baker, R.T.K., et al., *Nucleation and growth of carbon deposits from the nickel catalyzed decomposition of acetylene*. Journal of Catalytic, 1972. **26**(1): p. 51-62.
142. Gronchi, P., et al., *Carbon deposition in methane reforming with carbon dioxide*. Journal of thermal analysis, 1996. **47**(1): p. 227-234.
143. Baker, R.T.K., et al., *Formation of filamentous carbon from iron, cobalt and chromium catalyzed decomposition of acetylene*. Journal of Catalytic, 1973. **30**(1): p. 86-95.
144. Baghalha, M., M. Mohammadi, and A. Ghorbanpour, *Coke deposition mechanism on the pores of a commercial Pt-Re/ γ -Al₂O₃ naphtha reforming catalyst*. Fuel Processing Technology, 2010. **91**(7): p. 714-722.
145. Alstrup, I., *A new model explaining carbon filament growth on nickel, iron, and Ni-Cu alloy catalysts*. Journal of Catalytic, 1988. **109**(2): p. 241-251.
146. Rostrup-Nielsen, J. and D.L. Trimm, *Mechanisms of carbon formation on nickel-containing catalysts*. Journal of Catalytic, 1977. **48**(1): p. 155-165.
147. Pakhare, D., et al., *Characterization and activity study of the Rh-substituted pyrochlores for CO₂ (dry) reforming of CH₄*. Applied Petrochemical Research, 2013. **3**(3): p. 117-129.
148. Guo, F., et al., *Dry re-forming of methane to synthesis gas over lignite semicokes catalyst at high pressure*. Energy Reports, 2016. **2**: p. 163-170.
149. Arora, S. and R. Prasad, *An overview on dry reforming of methane: strategies to reduce carbonaceous deactivation of catalysts*. RSC Advances, 2016. **6**(110): p. 108668-108688.
150. Ginsburg, J.M., et al., *Coke formation over a nickel catalyst under methane dry reforming conditions: thermodynamic and kinetic models*. Industrial & engineering chemistry research, 2005. **44**(14): p. 4846-4854.
151. Oyama, S.T., et al., *Dry reforming of methane has no future for hydrogen production: Comparison with steam reforming at high pressure in standard and membrane reactors*. International Journal of Hydrogen Energy, 2012. **37**(13): p. 10444-10450.

152. Pan, Y.-X., C.-J. Liu, and P. Shi, *Preparation and characterization of coke resistant Ni/SiO₂ catalyst for carbon dioxide reforming of methane*. Journal of Power Sources, 2008. **176**(1): p. 46-53.
153. Zhang, J. and F. Li, *Coke-resistant Ni@ SiO₂ catalyst for dry reforming of methane*. Applied Catalytic B: Environmental, 2015. **176**: p. 513-521.
154. Corthals, S., et al., *Influence of composition of MgAl₂O₄ supported NiCeO₂ZrO₂ catalysts on coke formation and catalyst stability for dry reforming of methane*. Catalytic today, 2008. **138**(1-2): p. 28-32.
155. Koo, K.Y., et al., *CeO₂ promoted Ni/Al₂O₃ catalyst in combined steam and carbon dioxide reforming of methane for gas to liquid (GTL) process*. Catalytic letters, 2009. **130**(1-2): p. 217.
156. Li, Y., et al., *Thermodynamic analysis of autothermal steam and CO₂ reforming of methane*. International Journal of Hydrogen Energy, 2008. **33**(10): p. 2507-2514.
157. Guo, S., et al., *Microwave-absorbing characteristics of mixtures of different carbonaceous reducing agents and oxidized ilmenite*. International Journal of Mineral Processing, 2009. **93**(3-4): p. 289-293.
158. Zhao, T., et al., *Electromagnetic wave absorbing properties of amorphous carbon nanotubes*. Scientific reports, 2014. **4**: p. 5619.
159. Kim, T., J. Lee, and K.-H. Lee, *Microwave heating of carbon-based solid materials*. Carbon letters, 2014. **15**(1): p. 15-24.
160. Melvin, G.J.H., et al., *Microwave-absorbing properties of silver nanoparticle/carbon nanotube hybrid nanocomposites*. Journal of Materials Science, 2014. **49**(14): p. 5199-5207.
161. Jou, C.-J.G. and C.C. Lo, *Using a microwave-induced method to regenerate platinum catalyst*. Sustainable Environment Research, 2017. **27**(6): p. 279-282.
162. Lin, G., et al., *Process optimization of spent catalyst regeneration under microwave and ultrasonic spray-assisted*. Catalytic Today, 2018. **318**: p. 191-198.
163. Xin-hui, D., et al., *Regeneration of microwave assisted spent activated carbon: Process optimization, adsorption isotherms and kinetics*.

- Chemical Engineering and Processing: Process Intensification, 2012. **53**: p. 53-62.
164. Cherbański, R., *Regeneration of granular activated carbon loaded with toluene – Comparison of microwave and conductive heating at the same active powers*. Chemical Engineering and Processing - Process Intensification, 2018. **123**: p. 148-157.
 165. Palma, V., et al., *Catalytic DPF microwave assisted active regeneration*. Fuel, 2015. **140**: p. 50-61.
 166. Gangadharan, P., K.C. Kanchi, and H.H. Lou, *Evaluation of the economic and environmental impact of combining dry reforming with steam reforming of methane*. Chemical Engineering Research and Design, 2012. **90**(11): p. 1956-1968.
 167. Soria, M.A., et al., *Thermodynamic and experimental study of combined dry and steam reforming of methane on Ru/ ZrO₂-La₂O₃ catalyst at low temperature*. International Journal of Hydrogen Energy, 2011. **36**(23): p. 15212-15220.
 168. Ryi, S.-K., et al., *Combined steam and CO₂ reforming of methane using catalytic nickel membrane for gas to liquid (GTL) process*. Catalytic Today, 2014. **236**: p. 49-56.
 169. Siang, T.J., et al., *Combined steam and CO₂ reforming of methane for syngas production over carbon-resistant boron-promoted Ni/SBA-15 catalysts*. Microporous and Mesoporous Materials, 2018. **262**: p. 122-132.
 170. Jang, W.-J., et al., *Combined steam and carbon dioxide reforming of methane and side reactions: Thermodynamic equilibrium analysis and experimental application*. Applied Energy, 2016. **173**: p. 80-91.
 171. Luyben, W.L., *Control of parallel dry methane and steam methane reforming processes for Fischer–Tropsch syngas*. Journal of Process Control, 2016. **39**: p. 77-87.
 172. Álvarez M, A., M.Á. Centeno, and J.A. Odriozola, *Ru–Ni Catalyst in the Combined Dry-Steam Reforming of Methane: The Importance in the Metal Order Addition*. Topics in Catalytic, 2016. **59**(2): p. 303-313.
 173. Soria, M., et al., *Thermodynamic and experimental study of combined dry and steam reforming of methane on Ru/ZrO₂-La₂O₃ catalyst at low*

- temperature*. International journal of hydrogen energy, 2011. **36**(23): p. 15212-15220.
174. Al-Nakoua, M.A. and M.H. El-Naas, *Combined steam and dry reforming of methane in narrow channel reactors*. International Journal of Hydrogen Energy, 2012. **37**(9): p. 7538-7544.
175. Álvarez, A., M.Á. Centeno, and J.A. Odriozola, *Ru–Ni catalyst in the combined dry-steam reforming of methane: The importance in the metal order addition*. Topics in Catalytic, 2016. **59**(2-4): p. 303-313.
176. Abashar, M., *Coupling of steam and dry reforming of methane in catalytic fluidized bed membrane reactors*. International Journal of Hydrogen Energy, 2004. **29**(8): p. 799-808.
177. Noronha, F.B., et al., *Catalytic performance of Pt/ZrO₂ And Pt/Ce-ZrO₂ catalysts on CO₂ reforming of CH₄ coupled with steam reforming or under high pressure*. Catalytic letters, 2003. **90**(1-2): p. 13-21.
178. Shahkarami, P. and S. Fatemi, *Mathematical modeling and optimization of combined steam and dry reforming of methane process in catalytic fluidized bed membrane reactor*. Chemical Engineering Communications, 2015. **202**(6): p. 774-786.
179. Li, L., et al., *Microwave-enhanced methane combined reforming by CO₂ and H₂O into syngas production on biomass-derived char*. Fuel, 2016. **185**: p. 692-700.
180. Kokarev, N.I., et al., *Use of reformed natural gas for heating glass furnaces*. Glass and Ceramics, 1975. **32**(1): p. 14-16.
181. Wang, Y., et al., *Low-temperature catalytic CO₂ dry reforming of methane on Ni-based catalysts: A review*. Fuel Processing Technology, 2018. **169**: p. 199-206.
182. Abasaeed, A.E., et al., *Catalytic performance of CeO₂ and ZrO₂ supported Co catalysts for hydrogen production via dry reforming of methane*. International Journal of Hydrogen Energy, 2015. **40**(21): p. 6818-6826.
183. Castillo-Villalón, P., et al., *Influence of the support on the catalytic performance of Mo, CoMo, and NiMo catalysts supported on Al₂O₃ and TiO₂ during the HDS of thiophene, dibenzothiophene, or 4,6-dimethyldibenzothiophene*. Catalytic Today, 2016. **259**: p. 140-149.

184. Blanksby, S.J. and G.B. Ellison, *Bond dissociation energies of organic molecules*. Accounts Chem. Res., 2003. **36**(4): p. 255-263.
185. Blanksby, S.J. and G.B. Ellison, *Bond dissociation energies of organic molecules*. Accounts of Chemical Research, 2003. **36**(4): p. 255-263.
186. Edwards, J.H. and A.M. Maitra, *The chemistry of methane reforming with carbon dioxide and its current and potential applications*. Fuel Processing Technology, 1995. **42**(2-3): p. 269-289.
187. Kehres, J., et al., *Dynamical Properties of a Ru/MgAl₂O₄ Catalyst during Reduction and Dry Methane Reforming*. The Journal of Physical Chemistry C, 2012. **116**(40): p. 21407-21415.
188. Stagg-Williams, S.M., et al., *CO₂ reforming of CH₄ over Pt/ZrO₂ catalysts promoted with La and Ce oxides*. Journal of Catalytic, 2000. **194**(2): p. 240-249.
189. Maestri, M., et al., *Steam and dry reforming of methane on Rh: Microkinetic analysis and hierarchy of kinetic models*. Journal of Catalytic, 2008. **259**(2): p. 211-222.
190. Özkara-Aydınoğlu, Ş., E. Özensoy, and A.E. Aksoylu, *The effect of impregnation strategy on methane dry reforming activity of Ce promoted Pt/ZrO₂*. International Journal of Hydrogen Energy, 2009. **34**(24): p. 9711-9722.
191. Wang, H.Y. and E. Ruckenstein, *Carbon dioxide reforming of methane to synthesis gas over supported rhodium catalysts: the effect of support*. Applied Catalytic A: General, 2000. **204**(1): p. 143-152.
192. Ballarini, A.D., et al., *Reforming of CH₄ with CO₂ on Pt-supported catalysts: Effect of the support on the catalytic behaviour*. Catalytic Today, 2005. **107-108**: p. 481-486.
193. Djinović, P., et al., *Catalytic syngas production from greenhouse gasses: Performance comparison of Ru-Al₂O₃ and Rh-CeO₂ catalysts*. Chemical Engineering and Processing: Process Intensification, 2011. **50**(10): p. 1054-1062.
194. Jing, Q.S., et al., *Effective reforming of methane with CO₂ and O₂ to low H₂/CO ratio syngas over Ni/MgO–SiO₂ using fluidized bed reactor*. Energy Conversion and Management, 2004. **45**(20): p. 3127-3137.

195. Wolfbeisser, A., et al., *Methane dry reforming over ceria-zirconia supported Ni catalysts*. Catalytic Today, 2016. **277**: p. 234-245.
196. Safariamin, M., et al., *Dry reforming of methane in the presence of ruthenium-based catalysts*. Comptes Rendus Chimie, 2009. **12**(6): p. 748-753.
197. Yasyerli, S., et al., *Ru incorporated Ni-MCM-41 mesoporous catalysts for dry reforming of methane: Effects of Mg addition, feed composition and temperature*. International Journal of Hydrogen Energy, 2011. **36**(8): p. 4863-4874.
198. Singha, R.K., et al., *Low temperature dry reforming of methane over Pd-CeO₂ nanocatalyst*. Catalytic Communications, 2017. **92**: p. 19-22.
199. Ma, Q., et al., *Ordered mesoporous alumina-supported bimetallic Pd-Ni catalysts for methane dry reforming reaction*. Catalytic Science & Technology, 2016. **6**(17): p. 6542-6550.
200. Wisniewski, M., A. Boréave, and P. Gélin, *Catalytic CO₂ reforming of methane over Ir/Ce_{0.9}Gd_{0.1}O_{2-x}*. Catalytic Communications, 2005. **6**(9): p. 596-600.
201. Pakhare, D. and J. Spivey, *A review of dry (CO₂) reforming of methane over noble metal catalysts*. Chemical Society Reviews, 2014. **43**(22): p. 7813-7837.
202. Tsyganok, A.I., et al., *Dry reforming of methane over supported noble metals: a novel approach to preparing catalysts*. Catalytic Communications, 2003. **4**(9): p. 493-498.
203. Ferreira-Aparicio, P., et al., *A transient kinetic study of the carbon dioxide reforming of methane over supported Ru catalysts*. Journal of Catalytic, 1999. **184**(1): p. 202-212.
204. Shi, C. and P. Zhang, *Effect of a second metal (Y, K, Ca, Mn or Cu) addition on the carbon dioxide reforming of methane over nanostructured palladium catalysts*. Applied Catalytic B: Environmental, 2012. **115-116**: p. 190-200.
205. Hou, Z., et al., *Production of synthesis gas via methane reforming with CO₂ on noble metals and small amount of noble-(Rh-) promoted Ni*

- catalysts*. International Journal of Hydrogen Energy, 2006. **31**(5): p. 555-561.
206. Bitter, J.H., K. Seshan, and J.A. Lercher, *Mono and bifunctional pathways of CO₂/CH₄ reforming over Pt and Rh based catalysts*. Journal of Catalytic, 1998. **176**(1): p. 93-101.
207. Richardson, J.T., M. Garrait, and J.K. Hung, *Carbon dioxide reforming with Rh and Pt–Re catalysts dispersed on ceramic foam supports*. Applied Catalytic A: General, 2003. **255**(1): p. 69-82.
208. Matsui, N.-o., et al., *Reaction mechanisms of carbon dioxide reforming of methane with Ru-loaded lanthanum oxide catalyst*. Applied Catalytic A: General, 1999. **179**(1): p. 247-256.
209. Ocsachoque, M., F. Pompeo, and G. Gonzalez, *Rh–Ni/CeO₂–Al₂O₃ catalysts for methane dry reforming*. Catalytic Today, 2011. **172**(1): p. 226-231.
210. Wu, J.C.S. and H.-C. Chou, *Bimetallic Rh–Ni/BN catalyst for methane reforming with CO₂*. Chemical Engineering Journal, 2009. **148**(2): p. 539-545.
211. Basile, F., et al., *Rh–Ni synergy in the catalytic partial oxidation of methane: surface phenomena and catalyst stability*. Catalytic Today, 2002. **77**(3): p. 215-223.
212. García-Diéguez, M., et al., *Characterization of alumina-supported Pt, Ni and PtNi alloy catalysts for the dry reforming of methane*. Journal of Catalytic, 2010. **274**(1): p. 11-20.
213. Pompeo, F., et al., *Study of Ni and Pt catalysts supported on α -Al₂O₃ and ZrO₂ applied in methane reforming with CO₂*. Applied Catalytic A: General, 2007. **316**(2): p. 175-183.
214. García-Diéguez, M., et al., *Improved Pt-Ni nanocatalysts for dry reforming of methane*. Applied Catalytic A: General, 2010. **377**(1): p. 191-199.
215. Steinhauer, B., et al., *Development of Ni-Pd bimetallic catalysts for the utilization of carbon dioxide and methane by dry reforming*. Applied Catalytic A: General, 2009. **366**(2): p. 333-341.

216. Damyanova, S., et al., *MCM-41 supported PdNi catalysts for dry reforming of methane*. Applied Catalytic B: Environmental, 2009. **92**(3): p. 250-261.
217. Crisafulli, C., et al., *CO₂ reforming of methane over Ni–Ru and Ni–Pd bimetallic catalysts*. Catalytic Letters, 1999. **59**(1): p. 21-26.
218. García-Diéguez, M., et al., *RhNi nanocatalysts for the CO₂ and CO₂+H₂O reforming of methane*. Catalytic Today, 2011. **172**(1): p. 136-142.
219. Lucrédio, A.F., J.M. Assaf, and E.M. Assaf, *Methane conversion reactions on Ni catalysts promoted with Rh: Influence of support*. Applied Catalytic A: General, 2011. **400**(1): p. 156-165.
220. Arandiyán, H., et al., *Effects of noble metals doped on mesoporous LaAlNi mixed oxide catalyst and identification of carbon deposit for reforming CH₄ with CO₂*. Journal of Chemical Technology & Biotechnology, 2014. **89**(3): p. 372-381.
221. El Hassan, N., et al., *Low temperature dry reforming of methane on rhodium and cobalt based catalysts: Active phase stabilization by confinement in mesoporous SBA-15*. Applied Catalytic A: General, 2016. **520**: p. 114-121.
222. Djinović, P., J. Batista, and A. Pintar, *Efficient catalytic abatement of greenhouse gases: Methane reforming with CO₂ using a novel and thermally stable Rh–CeO₂ catalyst*. International Journal of Hydrogen Energy, 2012. **37**(3): p. 2699-2707.
223. Rostrupnielsen, J.R. and J.H.B. Hansen, *CO₂-Reforming of methane over transition metals*. Journal of Catalytic, 1993. **144**(1): p. 38-49.
224. Al-Sabban, B.E., *Development of coke-tolerant transition metal catalysts for dry reforming of methane*.
225. Nguyen, H.M., C.M. Phan, and T. Sen, *Degradation of sodium dodecyl sulfate by photoelectrochemical and electrochemical processes*. Chemical Engineering Journal, 2016. **287**: p. 633-639.
226. Nguyen, H.M., et al., *TOC removal from laundry wastewater by photoelectrochemical process on Fe₂O₃ nanostructure*. Desalination and Water Treatment, 2016. **57**(31): p. 14379-14385.

227. Liu, L., et al., *A new strategy to transform mono and bimetallic non-noble metal nanoparticles into highly active and chemoselective hydrogenation catalysts*. *Journal of Catalytic*, 2017. **350**: p. 218-225.
228. Smith, R.D., et al., *Water oxidation catalytic: electrocatalytic response to metal stoichiometry in amorphous metal oxide films containing iron, cobalt, and nickel*. *Journal of the American Chemical Society*, 2013. **135**(31): p. 11580-11586.
229. Ananikov, V.P., *Nickel: The "Spirited Horse" of transition metal catalytic*. *ACS Catalytic*, 2015. **5**(3): p. 1964-1971.
230. Chu, W., et al., *Cobalt species in promoted cobalt alumina-supported Fischer–Tropsch catalysts*. *Journal of Catalytic*, 2007. **252**(2): p. 215-230.
231. Jasinski, R., *A new fuel cell cathode catalyst*. *Nature*, 1964. **201**: p. 1212.
232. Gadalla, A.M. and B. Bower, *The role of catalyst support on the activity of nickel for reforming methane with CO₂*. *Chemical Engineering Science*, 1988. **43**(11): p. 3049-3062.
233. Zhang, Z. and X.E. Verykios, *A stable and active nickel-based catalyst for carbon dioxide reforming of methane to synthesis gas*. *Journal of the Chemical Society, Chemical Communications*, 1995(1): p. 71-72.
234. Rostrupnielsen, J. and J.B. Hansen, *CO₂-reforming of methane over transition metals*. *Journal of Catalytic*, 1993. **144**(1): p. 38-49.
235. Lercher, J., et al., *Design of stable catalysts for methane-carbon dioxide reforming*, in *Studies in Surface Science and Catalytic*. 1996, Elsevier. p. 463-472.
236. Liu, X., et al., *Enhanced performance of catalyst pellets for methane dry reforming by engineering pore network structure*. *Chemical Engineering Journal*, 2019.
237. Bian, Z., et al., *A review on bimetallic nickel-based catalysts for CO₂ reforming of methane*. *ChemPhysChem*, 2017. **18**(22): p. 3117-3134.
238. Wisniak, J., *The history of catalytic. From the beginning to nobel prizes*. *Educación Química*, 2010. **21**(1): p. 60-69.
239. Murray, R., *Method of preparing catalytic material*. 1933, Google Patents.

240. Johnstone, R.A., A.H. Wilby, and I.D. Entwistle, *Heterogeneous catalytic transfer hydrogenation and its relation to other methods for reduction of organic compounds*. Chemical Reviews, 1985. **85**(2): p. 129-170.
241. Wang, S. and G.Q. Lu, *Reforming of methane with carbon dioxide over Ni/Al₂O₃ catalysts: Effect of nickel precursor*. Applied Catalytic A: General, 1998. **169**(2): p. 271-280.
242. Wei, J.-M., et al., *Highly active and stable Ni/ZrO₂ catalyst for syngas production by CO₂ reforming of methane*. Applied Catalytic A: General, 2000. **196**(2): p. L167-L172.
243. Gonzalez-Delacruz, V.M., et al., *Study of nanostructured Ni/CeO₂ catalysts prepared by combustion synthesis in dry reforming of methane*. Applied Catalytic A: General, 2010. **384**(1): p. 1-9.
244. Djaidja, A., et al., *Characterization and activity in dry reforming of methane on NiMg/Al and Ni/MgO catalysts*. Catalytic Today, 2006. **113**(3): p. 194-200.
245. Liu, D., et al., *Carbon dioxide reforming of methane to synthesis gas over Ni-MCM-41 catalysts*. Applied Catalytic A: General, 2009. **358**(2): p. 110-118.
246. Zhang, S., et al., *Ceria-doped Ni/SBA-16 catalysts for dry reforming of methane*. ACS Catalytic, 2013. **3**(8): p. 1855-1864.
247. Shinde, V.M. and G. Madras, *Catalytic performance of highly dispersed Ni/TiO₂ for dry and steam reforming of methane*. RSC Advances, 2014. **4**(10): p. 4817-4826.
248. Pompeo, F., et al., *Characterization of Ni/SiO₂ and Ni/Li-SiO₂ catalysts for methane dry reforming*. Catalytic Today, 2005. **107-108**: p. 856-862.
249. Huang, J., et al., *Carbon dioxide reforming of methane over Ni/Mo/SBA-15-La₂O₃ catalyst: Its characterization and catalytic performance*. Journal of Natural Gas Chemistry, 2011. **20**(5): p. 465-470.
250. Zhu, J., et al., *Synthesis gas production from CO₂ reforming of methane over Ni-Ce/SiO₂ catalyst: The effect of calcination ambience*. International Journal of Hydrogen Energy, 2013. **38**(1): p. 117-126.
251. Liu, D., et al., *MCM-41 supported nickel-based bimetallic catalysts with superior stability during carbon dioxide reforming of methane: Effect of*

- strong metal–support interaction*. Journal of Catalytic, 2009. **266**(2): p. 380-390.
252. de Lima, S.M. and J.M. Assaf, *Ni–Fe catalysts based on perovskite-type oxides for dry reforming of methane to syngas*. Catalytic Letters, 2006. **108**(1): p. 63-70.
253. Sutthiumporn, K., et al., *CO₂ dry-reforming of methane over La_{0.8}Sr_{0.2}Ni_{0.8}M_{0.2}O₃ perovskite (M = Bi, Co, Cr, Cu, Fe): Roles of lattice oxygen on C–H activation and carbon suppression*. International Journal of Hydrogen Energy, 2012. **37**(15): p. 11195-11207.
254. San-José-Alonso, D., et al., *Ni, Co and bimetallic Ni–Co catalysts for the dry reforming of methane*. Applied Catalytic A: General, 2009. **371**(1): p. 54-59.
255. Kawi, S., et al., *Progress in synthesis of highly active and stable nickel-based catalysts for carbon dioxide reforming of methane*. ChemSusChem, 2015. **8**(21): p. 3556-3575.
256. Bartholomew, C.H., *Mechanisms of catalyst deactivation*. Applied Catalytic A: General, 2001. **212**(1): p. 17-60.
257. Roh, H.-S., et al., *Highly stable Ni catalyst supported on Ce–ZrO₂ for oxy-steam reforming of methane*. Catalytic Letters, 2001. **74**(1): p. 31-36.
258. Zhang, M., et al., *Structural characterization of highly stable Ni/SBA-15 catalyst and its catalytic performance for methane reforming with CO₂*. Chinese Journal of Catalytic, 2006. **27**(9): p. 777-781.
259. Wang, J.B., L.-E. Kuo, and T.-J. Huang, *Study of carbon dioxide reforming of methane over bimetallic Ni-Cr/yttria-doped ceria catalysts*. Applied Catalytic A: General, 2003. **249**(1): p. 93-105.
260. Choi, J.-S., et al., *Stable carbon dioxide reforming of methane over modified Ni/Al₂O₃ catalysts*. Catalytic Letters, 1998. **52**(1): p. 43-47.
261. Takanabe, K., et al., *Titania-supported cobalt and nickel bimetallic catalysts for carbon dioxide reforming of methane*. Journal of Catalytic, 2005. **232**(2): p. 268-275.
262. Frusteri, F., et al., *Potassium-enhanced stability of Ni/MgO catalysts in the dry-reforming of methane*. Catalytic Communications, 2001. **2**(2): p. 49-56.

263. Quincoces, C.E., et al., *Role of Mo in CO₂ reforming of CH₄ over Mo promoted Ni/Al₂O₃ catalysts*. Materials Letters, 2002. **56**(5): p. 698-704.
264. Seok, S.H., et al., *Mn-promoted Ni/Al₂O₃ catalysts for stable carbon dioxide reforming of methane*. Journal of Catalytic, 2002. **209**(1): p. 6-15.
265. Theofanidis, S.A., et al., *Enhanced carbon-resistant dry reforming Fe-Ni catalyst: Role of Fe*. ACS Catalytic, 2015. **5**(5): p. 3028-3039.
266. Zhu, J., et al., *The promoting effect of La, Mg, Co and Zn on the activity and stability of Ni/SiO₂ catalyst for CO₂ reforming of methane*. International Journal of Hydrogen Energy, 2011. **36**(12): p. 7094-7104.
267. Goldwasser, M.R., et al., *Perovskites as catalysts precursors: CO₂ reforming of CH₄ on Ln_{1-x}Ca_xRu_{0.8}Ni_{0.2}O₃ (Ln = La, Sm, Nd)*. Applied Catalytic A: General, 2003. **255**(1): p. 45-57.
268. Bitter, J.H., K. Seshan, and J.A. Lercher, *The state of zirconia supported platinum catalysts for CO₂/CH₄ reforming*. Journal of Catalytic, 1997. **171**(1): p. 279-286.
269. Nakamura, J., et al., *Role of support in reforming of CH₄ with CO₂ over Rh catalysts*. Catalytic Letters, 1994. **25**(3): p. 265-270.
270. Li, B., et al., *Catalytic performance of iron-promoted nickel-based ordered mesoporous alumina FeNiAl catalysts in dry reforming of methane*. Fuel Processing Technology, 2019. **193**: p. 348-360.
271. Barelli, L., et al., *Development and validation of a Ni-based catalyst for carbon dioxide dry reforming of methane process coupled to solid oxide fuel cells*. International Journal of Hydrogen Energy, 2019.
272. Kharasch, M.S. and E.K. Fields, *Factors determining the course and mechanisms of grignard reactions. IV. The effect of metallic halides on the reaction of aryl grignard reagents and organic halides1*. Journal of the American Chemical Society, 1941. **63**(9): p. 2316-2320.
273. Yamaguchi, A. and E. Iglesia, *Catalytic activation and reforming of methane on supported palladium clusters*. Journal of Catalytic, 2010. **274**(1): p. 52-63.
274. Horn, R. and R. Schlögl, *Methane activation by heterogeneous catalytic*. Catalytic Letters, 2015. **145**(1): p. 23-39.

275. Tang, P., et al., *Methane activation: the past and future*. Energy & Environmental Science, 2014. **7**(8): p. 2580-2591.
276. Arevalo, R.L., et al., *Tuning methane decomposition on stepped Ni surface: The role of subsurface atoms in catalyst design*. Scientific Reports, 2017. **7**(1): p. 13963.
277. Harris, S. and R.R. Chianelli, *Catalytic by transition metal sulfides: The relation between calculated electronic trends and HDS activity*. Journal of Catalytic, 1984. **86**(2): p. 400-412.
278. Budiman, A.W., et al., *Dry reforming of methane over cobalt catalysts: A literature review of catalyst development*. Catalytic Surveys from Asia, 2012. **16**(4): p. 183-197.
279. Moselage, M., J. Li, and L. Ackermann, *Cobalt-catalyzed C–H activation*. ACS Catalytic, 2016. **6**(2): p. 498-525.
280. Ruckenstein, E. and H.Y. Wang, *Carbon dioxide reforming of methane to synthesis gas over supported cobalt catalysts*. Applied Catalytic A: General, 2000. **204**(2): p. 257-263.
281. Ruckenstein, E. and H.Y. Wang, *Combined catalytic partial oxidation and CO₂ reforming of methane over supported cobalt catalysts*. Catalytic Letters, 2001. **73**(2): p. 99-105.
282. Xu, J., et al., *Biogas reforming for hydrogen production over nickel and cobalt bimetallic catalysts*. International Journal of Hydrogen Energy, 2009. **34**(16): p. 6646-6654.
283. Bouarab, R., et al., *Effect of MgO additive on catalytic properties of Co/SiO₂ in the dry reforming of methane*. Applied Catalytic A: General, 2004. **264**(2): p. 161-168.
284. Reuel, R.C. and C.H. Bartholomew, *The stoichiometries of H₂ and CO adsorptions on cobalt: Effects of support and preparation*. Journal of Catalytic, 1984. **85**(1): p. 63-77.
285. Song, H. and U.S. Ozkan, *Ethanol steam reforming over Co-based catalysts: Role of oxygen mobility*. Journal of Catalytic, 2009. **261**(1): p. 66-74.
286. de la Peña O'Shea, V.A., et al., *Development of robust Co-based catalysts for the selective H₂-production by ethanol steam-reforming*. The Fe-

- promoter effect*. International Journal of Hydrogen Energy, 2008. **33**(13): p. 3601-3606.
287. Llorca, J., et al., *Effect of sodium addition on the performance of Co-ZnO-based catalysts for hydrogen production from bioethanol*. Journal of Catalytic, 2004. **222**(2): p. 470-480.
288. Urasaki, K., et al., *Production of hydrogen by steam reforming of ethanol over cobalt and nickel catalysts supported on perovskite-type oxides*. Catalytic Communications, 2008. **9**(5): p. 600-604.
289. Takanabe, K., K. Nagaoka, and K.-i. Aika, *Improved resistance against coke deposition of titania supported cobalt and nickel bimetallic catalysts for carbon dioxide reforming of methane*. Catalytic Letters, 2005. **102**(3): p. 153-157.
290. Li, D., et al., *Production of renewable hydrogen by steam reforming of tar from biomass pyrolysis over supported Co catalysts*. International Journal of hydrogen energy, 2013. **38**(9): p. 3572-3581.
291. Vicente, J., et al., *Coke deactivation of Ni and Co catalysts in ethanol steam reforming at mild temperatures in a fluidized bed reactor*. International Journal of Hydrogen Energy, 2014. **39**(24): p. 12586-12596.
292. Bian, Z., et al., *A review on bimetallic nickel-based catalysts for CO₂ reforming of methane*. ChemPhysChem, 2017. **18**(22): p. 3117-3134.
293. Luisetto, I., S. Tuti, and E. Di Bartolomeo, *Co and Ni supported on CeO₂ as selective bimetallic catalyst for dry reforming of methane*. international journal of hydrogen energy, 2012. **37**(21): p. 15992-15999.
294. Xiao, T.-C., et al., *Preparation and characterisation of bimetallic cobalt and molybdenum carbides*. Journal of Catalytic, 2001. **202**(1): p. 100-109.
295. Guczi, L., G. Boskovic, and E. Kiss, *Bimetallic cobalt based catalysts*. Catalytic Reviews, 2010. **52**(2): p. 133-203.
296. Nagaoka, K., K. Takanabe, and K.I. Aika, *Modification of Co/TiO₂ for dry reforming of methane at 2 MPa by Pt, Ru or Ni*. Applied Catalytic A: General, 2004. **268**(1-2): p. 151-158.
297. Jabbour, K., et al., *Promotional effect of Ru on the activity and stability of Co/SBA-15 catalysts in dry reforming of methane*. International Journal of Hydrogen Energy, 2014. **39**(15): p. 7780-7787.

298. Xie, Z., et al., *Dry reforming of methane over CeO₂-supported Pt-Co catalysts with enhanced activity*. Applied Catalytic B: Environmental, 2018. **236**: p. 280-293.
299. Nagaoka, K., K. Takanabe, and K.I. Aika, *Influence of the reduction temperature on catalytic activity of Co/TiO₂ (anatase-type) for high pressure dry reforming of methane*. Applied Catalytic A: General, 2003. **255**(1): p. 13-21.
300. González, O., et al., *New Co-Ni catalyst systems used for methane dry reforming based on supported catalysts over an INT-MMI mesoporous material and a perovskite-like oxide precursor LaCo_{0.4}Ni_{0.6}O₃*. Catalytic Today, 2005. **107-108**: p. 436-443.
301. Chen, L., Q. Zhu, and R. Wu, *Effect of Co-Ni ratio on the activity and stability of Co-Ni bimetallic aerogel catalyst for methane Oxy-CO₂ reforming*. International Journal of Hydrogen Energy, 2011. **36**(3): p. 2128-2136.
302. Foo, S.Y., et al., *Kinetic study of methane CO₂ reforming on Co-Ni/Al₂O₃ and Ce-Co-Ni/Al₂O₃ catalysts*. Catalytic Today, 2011. **164**(1): p. 221-226.
303. Takanabe, K., K. Nagaoka, and K.I. Aika, *Improved resistance against coke deposition of titania supported cobalt and nickel bimetallic catalysts for carbon dioxide reforming of methane*. Catalytic Letters, 2005. **102**(3-4): p. 153-157.
304. Topsøe, N.-Y. and H. Topsøe, *Characterization of the structures and active sites in sulfided Co-MoAl₂O₃ and Ni-MoAl₂O₃ catalysts by NO chemisorption*. Journal of Catalytic, 1983. **84**(2): p. 386-401.
305. Du, X., et al., *Dry reforming of methane over ZrO₂-supported Co-Mo carbide catalyst*. Applied Petrochemical Research, 2014. **4**(1): p. 137-144.
306. Bridgewater, A.J., R. Burch, and P.C.H. Mitchell, *Molybdenum/carbon catalysts for reforming reactions*. Journal of the Chemical Society, Faraday Transactions 1: Physical Chemistry in Condensed Phases, 1980. **76**(0): p. 1811-1820.
307. Chen, H. and A.A. Adesina, *Kinetic modelling of methanation reaction over a Co-Mo/SiO₂ catalyst*. Journal of Chemical Technology & Biotechnology, 1994. **60**(1): p. 103-113.

308. Reddy, K.M., B. Wei, and C. Song, *Mesoporous molecular sieve MCM-41 supported Co–Mo catalyst for hydrodesulfurization of petroleum resid.* Catalytic Today, 1998. **43**(3): p. 261-272.
309. Song, C. and K. Madhusudan Reddy, *Mesoporous molecular sieve MCM-41 supported Co–Mo catalyst for hydrodesulfurization of dibenzothiophene in distillate fuels.* Applied Catalytic A: General, 1999. **176**(1): p. 1-10.
310. Wivel, C., et al., *On the catalytic significance of a Co-Mo-S phase in Co-MoAl₂O₃ hydrodesulfurization catalysts: Combined in situ Mössbauer emission spectroscopy and activity studies.* Journal of Catalytic, 1981. **68**(2): p. 453-463.
311. Wang, A., et al., *Hydrodesulfurization of dibenzothiophene over siliceous MCM-41-supported catalysts: I. Sulfided Co–Mo catalysts.* Journal of Catalytic, 2001. **199**(1): p. 19-29.
312. Okamoto, Y., et al., *Preparation of Co–Mo/Al₂O₃ model sulfide catalysts for hydrodesulfurization and their application to the study of the effects of catalyst preparation.* Journal of Catalytic, 2003. **217**(1): p. 12-22.
313. Turaga, U.T. and C. Song, *MCM-41-supported Co-Mo catalysts for deep hydrodesulfurization of light cycle oil.* Catalytic Today, 2003. **86**(1): p. 129-140.
314. Khavarian, M., S.P. Chai, and A.R. Mohamed, *Direct use of as-synthesized multi-walled carbon nanotubes for carbon dioxide reforming of methane for producing synthesis gas.* Chemical Engineering Journal, 2014. **257**: p. 200-208.
315. Khavarian, M., S.-P. Chai, and A.R. Mohamed, *The effects of process parameters on carbon dioxide reforming of methane over Co–Mo–MgO/MWCNTs nanocomposite catalysts.* Fuel, 2015. **158**: p. 129-138.
316. Kuld, S., et al., *Quantifying the promotion of Cu catalysts by ZnO for methanol synthesis.* Science, 2016. **352**(6288): p. 969-974.
317. Shi, L., et al., *An introduction of CO₂ conversion by dry reforming with methane and new route of low-temperature methanol synthesis.* Accounts of Chemical Research, 2013. **46**(8): p. 1838-1847.

318. Sá, S., et al., *Catalysts for methanol steam reforming—a review*. Applied Catalytic B: Environmental, 2010. **99**(1-2): p. 43-57.
319. Eren, B., et al., *Catalyst chemical state during CO oxidation reaction on Cu (111) studied with ambient-pressure X-ray photoelectron spectroscopy and near edge X-ray adsorption fine structure spectroscopy*. Journal of the American Chemical Society, 2015. **137**(34): p. 11186-11190.
320. Gokhale, A.A., J.A. Dumesic, and M. Mavrikakis, *On the mechanism of low-temperature water gas shift reaction on copper*. Journal of the American Chemical Society, 2008. **130**(4): p. 1402-1414.
321. Chen, L.-F., et al., *Cu/SiO₂ catalysts prepared by the ammonia-evaporation method: Texture, structure, and catalytic performance in hydrogenation of dimethyl oxalate to ethylene glycol*. Journal of Catalytic, 2008. **257**(1): p. 172-180.
322. Wang, F., et al., *Highly efficient dehydrogenation of primary aliphatic alcohols catalyzed by Cu nanoparticles dispersed on rod-shaped La₂O₂CO₃*. ACS Catalytic, 2013. **3**(5): p. 890-894.
323. Liu, X.-M., et al., *Recent advances in catalysts for methanol synthesis via hydrogenation of CO and CO₂*. Industrial & Engineering Chemistry Research, 2003. **42**(25): p. 6518-6530.
324. Wang, W., et al., *Recent advances in catalytic hydrogenation of carbon dioxide*. Chemical Society Reviews, 2011. **40**(7): p. 3703-3727.
325. Wang, Z., et al., *Exploration of the preparation of Cu/TiO₂ catalysts by deposition–precipitation with urea for selective hydrogenation of unsaturated hydrocarbons*. Journal of Catalytic, 2016. **340**: p. 95-106.
326. Wang, B., et al., *Remarkable crystal phase effect of Cu/TiO₂ catalysts on the selective hydrogenation of dimethyl oxalate*. RSC Advances, 2015. **5**(37): p. 29040-29047.
327. Shishido, T., et al., *Active Cu/ZnO and Cu/ZnO/Al₂O₃ catalysts prepared by homogeneous precipitation method in steam reforming of methanol*. Applied Catalytic A: General, 2004. **263**(2): p. 249-253.
328. Yao, C.Z., et al., *Effect of preparation method on the hydrogen production from methanol steam reforming over binary Cu/ZrO₂ catalysts*. Applied Catalytic A: General, 2006. **297**(2): p. 151-158.

329. Liu, Q., et al., *Waste-free soft reactive grinding synthesis of high-surface-area copper–manganese spinel oxide catalysts highly effective for methanol steam reforming*. *Catalytic Letters*, 2008. **121**(1): p. 144-150.
330. Águila, G., et al., *A novel method for preparing high surface area copper zirconia catalysts. Influence of the preparation variables*. *Applied Catalytic A: General*, 2009. **360**(1): p. 98-105.
331. Khani, Y., et al., *Hydrogen production from steam reforming of methanol over Cu-based catalysts: The behavior of $Zn_xLa_xAl_{1-x}O_4$ and $ZnO/La_2O_3/Al_2O_3$ lined on cordierite monolith reactors*. *International Journal of Hydrogen Energy*, 2019.
332. Lee, J.K., J.B. Ko, and D.H. Kim, *Methanol steam reforming over $Cu/ZnO/Al_2O_3$ catalyst: kinetics and effectiveness factor*. *Applied Catalytic A: General*, 2004. **278**(1): p. 25-35.
333. Jiang, C., et al., *Kinetic mechanism for the reaction between methanol and water over a $Cu-ZnO-Al_2O_3$ catalyst*. *Applied Catalytic A: General*, 1993. **97**(2): p. 145-158.
334. Purnama, H., et al., *CO formation/selectivity for steam reforming of methanol with a commercial $CuO/ZnO/Al_2O_3$ catalyst*. *Applied Catalytic A: General*, 2004. **259**(1): p. 83-94.
335. Rybakov, K., et al., *Microwave heating of conductive powder materials*. *Journal of Applied Physics*, 2006. **99**(2): p. 023506.
336. Luo, J., et al., *Excellent microwave absorption properties by tuned electromagnetic parameters in polyaniline-coated $Ba_{0.9}La_{0.1}Fe_{11.9}Ni_{0.1}O_{19}$ /reduced graphene oxide nanocomposites*. *RSC Advances*, 2017. **7**(58): p. 36433-36443.
337. Chen, C.-S., W.-H. Cheng, and S.-S. Lin, *Study of reverse water gas shift reaction by TPD, TPR and CO_2 hydrogenation over potassium-promoted Cu/SiO_2 catalyst*. *Applied Catalytic A: General*, 2003. **238**(1): p. 55-67.
338. Chen, C.-S., W.-H. Cheng, and S.-S. Lin, *Study of iron-promoted Cu/SiO_2 catalyst on high temperature reverse water gas shift reaction*. *Applied Catalytic A: General*, 2004. **257**(1): p. 97-106.

339. Barrabes, N., et al., *Hydrodechlorination of trichloroethylene on noble metal promoted Cu-hydrotalcite-derived catalysts*. Journal of catalytic, 2009. **263**(2): p. 239-246.
340. Usman, M., W.M.A. Wan Daud, and H.F. Abbas, *Dry reforming of methane: Influence of process parameters—A review*. Renewable and Sustainable Energy Reviews, 2015. **45**: p. 710-744.
341. Villacampa, J.I., et al., *Catalytic decomposition of methane over Ni-Al₂O₃ coprecipitated catalysts: Reaction and regeneration studies*. Applied Catalytic A: General, 2003. **252**(2): p. 363-383.
342. Tsyganok, A.I., et al., *Dry reforming of methane over catalysts derived from nickel-containing Mg–Al layered double hydroxides*. Journal of Catalytic, 2003. **213**(2): p. 191-203.
343. Wang, N., et al., *Manganese promoting effects on the Co–Ce–Zr–O_x nano catalysts for methane dry reforming with carbon dioxide to hydrogen and carbon monoxide*. Chemical Engineering Journal, 2011. **170**(2): p. 457-463.
344. Kambolis, A., et al., *Ni/CeO₂-ZrO₂ catalysts for the dry reforming of methane*. Applied Catalytic A: General, 2010. **377**(1): p. 16-26.
345. Albarazi, A., M.E. Gálvez, and P. Da Costa, *Synthesis strategies of ceria–zirconia doped Ni/SBA-15 catalysts for methane dry reforming*. Catalytic Communications, 2015. **59**: p. 108-112.
346. Petcharoen, K. and A. Sirivat, *Synthesis and characterization of magnetite nanoparticles via the chemical co-precipitation method*. Materials Science and Engineering: B, 2012. **177**(5): p. 421-427.
347. Echegoyen, Y., et al., *Thermo catalytic decomposition of methane over Ni–Mg and Ni–Cu–Mg catalysts: effect of catalyst preparation method*. Applied Catalytic A: General, 2007. **333**(2): p. 229-237.
348. Lázaro, M.J., et al., *Decomposition of methane over Ni-SiO₂ and Ni-Cu-SiO₂ catalysts: Effect of catalyst preparation method*. Applied Catalytic A: General, 2007. **329**: p. 22-29.
349. Chen, L., et al., *Catalytic selective reduction of NO with propylene over Cu-Al₂O₃ catalysts: influence of catalyst preparation method*. Applied Catalytic B: Environmental, 1999. **23**(4): p. 259-269.

350. Lambert, S., et al., *Synthesis of very highly dispersed platinum catalysts supported on carbon xerogels by the strong electrostatic adsorption method*. Journal of Catalytic, 2009. **261**(1): p. 23-33.
351. Munnik, P., P.E. de Jongh, and K.P. de Jong, *Recent developments in the synthesis of supported catalysts*. Chemical Reviews, 2015. **115**(14): p. 6687-6718.
352. Korah, J., W.A. Spieker, and J.R. Regalbuto, *Why ion-doped, PZC-altered silica and alumina fail to influence platinum adsorption*. Catalytic Letters, 2003. **85**(1): p. 123-127.
353. Benrabaa, R., et al., *Sol-gel synthesis and characterization of silica supported nickel ferrite catalysts for dry reforming of methane*. Catalytic Communications, 2015. **58**: p. 127-131.
354. Fukuhara, C., et al., *A novel nickel-based catalyst for methane dry reforming: A metal honeycomb-type catalyst prepared by sol-gel method and electroless plating*. Applied Catalytic A: General, 2013. **468**: p. 18-25.
355. Phan, C.M. and H.M. Nguyen, *Role of capping agent in wet synthesis of nanoparticles*. The Journal of Physical Chemistry A, 2017. **121**(17): p. 3213-3219.
356. Ward, D.A. and E.I. Ko, *Preparing catalytic materials by the sol-gel method*. Industrial & engineering chemistry research, 1995. **34**(2): p. 421-433.
357. Anderson, C. and A.J. Bard, *An improved photocatalyst of TiO₂/SiO₂ prepared by a sol-gel synthesis*. The Journal of Physical Chemistry, 1995. **99**(24): p. 9882-9885.
358. Lakshmi, B.B., C.J. Patrissi, and C.R. Martin, *Sol-gel template synthesis of semiconductor oxide micro-and nanostructures*. Chemistry of Materials, 1997. **9**(11): p. 2544-2550.
359. Wright, J.D. and N.A. Sommerdijk, *Sol-gel materials: chemistry and applications*. 2018: CRC press.
360. *Sols, gels, and organic chemistry*, in *Ceramic Materials: Science and Engineering*. 2007, Springer New York: New York, NY. p. 400-411.

361. Sajjadi, S.M., M. Haghghi, and F. Rahmani, *Dry reforming of greenhouse gases CH₄/CO₂ over MgO-promoted Ni-Co/Al₂O₃-ZrO₂ nanocatalyst: effect of MgO addition via sol-gel method on catalytic properties and hydrogen yield*. Journal of Sol-Gel Science and Technology, 2014. **70**(1): p. 111-124.
362. Hao, Z., et al., *Fluidization characteristics of aerogel Co/Al₂O₃ catalyst in a magnetic fluidized bed and its application to CH₄-CO₂ reforming*. Powder Technology, 2008. **183**(1): p. 46-52.
363. Danks, A.E., S.R. Hall, and Z. Schnepp, *The evolution of 'sol-gel' chemistry as a technique for materials synthesis*. Materials Horizons, 2016. **3**(2): p. 91-112.
364. Munoz, M., et al., *Preparation of magnetite-based catalysts and their application in heterogeneous Fenton oxidation—a review*. Applied Catalytic B: Environmental, 2015. **176**: p. 249-265.
365. Qiu, S., et al., *A simple method to prepare highly active and dispersed Ni/MCM-41 catalysts by co-impregnation*. Catalytic Communications, 2013. **42**: p. 73-78.
366. Nava, R., et al., *Influence of the preparation method on the activity of phosphate-containing CoMo/HMS catalysts in deep hydrodesulphurization*. Applied Catalytic A: General, 2007. **321**(1): p. 58-70.
367. Cao, X., et al., *Investigation of the preparation methodologies of Pd-Cu single atom alloy catalysts for selective hydrogenation of acetylene*. Frontiers of Chemical Science and Engineering, 2015. **9**(4): p. 442-449.
368. Lee, S.-J. and A. Gavriilidis, *Supported Au catalysts for low-temperature CO oxidation prepared by impregnation*. Journal of Catalytic, 2002. **206**(2): p. 305-313.
369. Grasso, G., et al., *A modified robotic system for catalyst preparation by wet or dry impregnation*. Catalytic today, 2003. **81**(3): p. 369-375.
370. Zhu, X., et al., *Charge-enhanced dry impregnation: A simple way to improve the preparation of supported metal catalysts*. ACS Catalytic, 2013. **3**(4): p. 625-630.

371. Jiang, S.P., *A review of wet impregnation—an alternative method for the fabrication of high performance and nano-structured electrodes of solid oxide fuel cells*. *Materials Science and Engineering: A*, 2006. **418**(1-2): p. 199-210.
372. Therdthianwong, S., et al., *Synthesis gas production from dry reforming of methane over Ni/Al₂O₃ stabilized by ZrO₂*. *International Journal of Hydrogen Energy*, 2008. **33**(3): p. 991-999.
373. Liu, D., et al., *Carbon dioxide reforming of methane over nickel-grafted SBA-15 and MCM-41 catalysts*. *Catalytic Today*, 2009. **148**(3): p. 243-250.
374. Wang, N., et al., *Synthesis, characterization and catalytic performance of MgO-coated Ni/SBA-15 catalysts for methane dry reforming to syngas and hydrogen*. *International Journal of Hydrogen Energy*, 2013. **38**(23): p. 9718-9731.
375. Quek, X.-Y., et al., *Nickel-grafted TUD-1 mesoporous catalysts for carbon dioxide reforming of methane*. *Applied Catalytic B: Environmental*, 2010. **95**(3): p. 374-382.
376. Paksoy, A.I., B.S. Caglayan, and A.E. Aksoylu, *A study on characterization and methane dry reforming performance of Co–Ce/ZrO₂ catalyst*. *Applied Catalytic B: Environmental*, 2015. **168-169**: p. 164-174.
377. Ay, H. and D. Üner, *Dry reforming of methane over CeO₂ supported Ni, Co and Ni–Co catalysts*. *Applied Catalytic B: Environmental*, 2015. **179**: p. 128-138.
378. Satsuma, A., et al., *Effect of preparation method of Co-promoted Pd/alumina for methane combustion*. *Catalytic Today*, 2015. **242**: p. 308-314.
379. Huang, T., et al., *Methane reforming reaction with carbon dioxide over SBA-15 supported Ni–Mo bimetallic catalysts*. *Fuel Processing Technology*, 2011. **92**(10): p. 1868-1875.
380. Miller, J.T., et al., *A fundamental study of platinum tetraammine impregnation of silica: 2. The effect of method of preparation, loading, and calcination temperature on (reduced) particle size*. *Journal of Catalytic*, 2004. **225**(1): p. 203-212.

381. Wang, H.Y. and E. Ruckenstein, *Conversions of methane to synthesis gas over Co/ γ -Al₂O₃ by CO₂ and/or O₂*. Catalytic Letters, 2001. **75**(1): p. 13-18.
382. Arnoldy, P., et al., *Temperature-programmed sulfiding and reduction of CoOAl₂O₃ catalysts*. Journal of Catalytic, 1985. **96**(1): p. 122-138.
383. Xiong, H., et al., *Fischer–Tropsch synthesis: the effect of Al₂O₃ porosity on the performance of Co/Al₂O₃ catalyst*. Catalytic Communications, 2005. **6**(8): p. 512-516.
384. Ferencz, Z., et al., *Dry reforming of CH₄ on Rh doped Co/Al₂O₃ catalysts*. Catalytic Today, 2014. **228**: p. 123-130.
385. Hou, Z. and T. Yashima, *Supported Co catalysts for methane reforming with CO₂*. Reaction Kinetics and Catalytic Letters, 2004. **81**(1): p. 153-159.
386. Iglesia, E., et al., *Bimetallic synergy in cobalt ruthenium Fischer-Tropsch synthesis catalysts*. Journal of Catalytic, 1993. **143**(2): p. 345-368.
387. Borg, Ø., et al., *Effect of calcination atmosphere and temperature on γ -Al₂O₃ supported cobalt Fischer-Tropsch catalysts*. Topics in Catalytic, 2007. **45**(1): p. 39-43.
388. Mondloch, J.E., E. Bayram, and R.G. Finke, *A review of the kinetics and mechanisms of formation of supported-nanoparticle heterogeneous catalysts*. Journal of Molecular Catalytic A: Chemical, 2012. **355**: p. 1-38.
389. Zabeti, M., W.M.A.W. Daud, and M.K. Aroua, *Activity of solid catalysts for biodiesel production: a review*. Fuel Processing Technology, 2009. **90**(6): p. 770-777.
390. Trueba, M. and S.P. Trasatti, *γ -Alumina as a support for catalysts: a review of fundamental aspects*. European journal of inorganic chemistry, 2005. **2005**(17): p. 3393-3403.
391. Schätz, A., O. Reiser, and W.J. Stark, *Nanoparticles as semi-heterogeneous catalyst supports*. Chemistry–A European Journal, 2010. **16**(30): p. 8950-8967.
392. Feng, J., et al., *Hydrogenolysis of glycerol to glycols over ruthenium catalysts: Effect of support and catalyst reduction temperature*. Catalytic Communications, 2008. **9**(6): p. 1458-1464.

393. Bradford, M.C.J. and M.A. Vannice, *CO₂ reforming of CH₄*. Catal Rev Sci Eng, 1999. **41**(1): p. 1-42.
394. Swaan, H., et al., *Deactivation of supported nickel catalysts during the reforming of methane by carbon dioxide*. Catalytic Today, 1994. **21**(2-3): p. 571-578.
395. Muraza, O. and A. Galadima, *A review on coke management during dry reforming of methane*. International Journal of Energy Research, 2015. **39**(9): p. 1196-1216.
396. Nagaoka, K., M. Okamura, and K.-i. Aika, *Titania supported ruthenium as a coking-resistant catalyst for high pressure dry reforming of methane*. Catalytic Communications, 2001. **2**(8): p. 255-260.
397. Moulijn, J.A., A.E. van Diepen, and F. Kapteijn, *Catalyst deactivation: is it predictable?: What to do?* Applied Catalytic A: General, 2001. **212**(1): p. 3-16.
398. Moulijn, J.A., A. Van Diepen, and F. Kapteijn, *Catalyst deactivation: is it predictable?: What to do?* Applied Catalytic A: General, 2001. **212**(1-2): p. 3-16.
399. Llorca, J., et al., *Efficient production of hydrogen over supported cobalt catalysts from ethanol steam reforming*. Journal of Catalytic, 2002. **209**(2): p. 306-317.
400. Zhang, Z., et al., *Reforming of methane with carbon dioxide to synthesis gas over supported rhodium catalysts: I. Effects of support and metal crystallite size on reaction activity and deactivation characteristics*. Journal of Catalytic, 1996. **158**(1): p. 51-63.
401. Song, S.-H., et al., *Effect of calcination temperature on the activity and cobalt crystallite size of Fischer–Tropsch Co–Ru–Zr/SiO₂ catalyst*. Catalytic Letters, 2009. **129**(1): p. 233-239.
402. Bian, Z. and S. Kawi, *Highly carbon-resistant Ni–Co/SiO₂ catalysts derived from phyllosilicates for dry reforming of methane*. Journal of CO₂ Utilization, 2017. **18**: p. 345-352.
403. Song, S.-H., et al., *Influence of Ru segregation on the activity of Ru–Co/γ-Al₂O₃ during FT synthesis: A comparison with that of Ru–Co/SiO₂ catalysts*. Catalytic Communications, 2008. **9**(13): p. 2282-2286.

404. Lucredio, A.F., et al., *Co catalysts supported on SiO₂ and γ -Al₂O₃ applied to ethanol steam reforming: Effect of the solvent used in the catalyst preparation method*. Fuel, 2011. **90**(4): p. 1424-1430.
405. Liu, S., et al., *CO₂ reforming of CH₄ over stabilized mesoporous Ni-CaO-ZrO₂ composites*. Fuel, 2008. **87**(12): p. 2477-2481.
406. Choudhary, V.R., K.C. Mondal, and T.V. Choudhary, *CO₂ Reforming of methane to syngas over CoO_x/MgO supported on low surface area macroporous catalyst carrier: Influence of Co loading and process conditions*. Industrial & Engineering Chemistry Research, 2006. **45**(13): p. 4597-4602.
407. Mirzaei, F., et al., *Carbon dioxide reforming of methane for syngas production over Co-MgO mixed oxide nanocatalysts*. Journal of Industrial and Engineering Chemistry, 2015. **21**: p. 662-667.
408. Roh, H.-S., H. Potdar, and K.-W. Jun, *Carbon dioxide reforming of methane over co-precipitated Ni-CeO₂, Ni-ZrO₂ and Ni-Ce-ZrO₂ catalysts*. Catalytic Today, 2004. **93**: p. 39-44.
409. Odedairo, T., J. Chen, and Z. Zhu, *Metal-support interface of a novel Ni-CeO₂ catalyst for dry reforming of methane*. Catalytic Communications, 2013. **31**(Supplement C): p. 25-31.
410. Chen, W., et al., *High carbon-resistance Ni/CeAlO₃-Al₂O₃ catalyst for CH₄/CO₂ reforming*. Applied Catalytic B: Environmental, 2013. **136-137**: p. 260-268.
411. Horváth, A., et al., *Methane dry reforming with CO₂ on CeZr-oxide supported Ni, NiRh and NiCo catalysts prepared by sol-gel technique: Relationship between activity and coke formation*. Catalytic Today, 2011. **169**(1): p. 102-111.
412. Rezaei, M., et al., *CO₂ reforming of CH₄ over nanocrystalline zirconia-supported nickel catalysts*. Applied Catalytic B: Environmental, 2008. **77**(3-4): p. 346-354.
413. Zeng, S., et al., *Co/Ce_xZr_{1-x}O₂ solid-solution catalysts with cubic fluorite structure for carbon dioxide reforming of methane*. Applied Catalytic B: Environmental, 2013. **136-137**: p. 308-316.

414. Brungs, A.J., et al., *Dry reforming of methane to synthesis gas over supported molybdenum carbide catalysts*. Catalytic Letters, 2000. **70**(3-4): p. 117-122.
415. Park, J.-H., et al., *Effect of Zn promoter on catalytic activity and stability of Co/ZrO₂ catalyst for dry reforming of CH₄*. Journal of CO₂ Utilization, 2018. **23**: p. 10-19.
416. Ozawa, M. and M. Kimura, *Effect of cerium addition on the thermal stability of gamma alumina support*. Journal of materials science letters, 1990. **9**(3): p. 291-293.
417. Chen, Y.-J. and C.-t. Yeh, *Deposition of highly dispersed gold on alumina support*. Journal of Catalytic, 2001. **200**(1): p. 59-68.
418. Trueba, M. and S.P. Trasatti, *γ-Alumina as a Support for Catalysts: A Review of Fundamental Aspects*. European Journal of Inorganic Chemistry, 2005. **2005**(17): p. 3393-3403.
419. Wilson, S.J. and M.H. Stacey, *The porosity of aluminum oxide phases derived from well-crystallized boehmite: Correlated electron microscope, adsorption, and porosimetry studies*. Journal of Colloid and Interface Science, 1981. **82**(2): p. 507-517.
420. Latella, B.A. and B.H. O'Connor, *Detection of minor crystalline phases in alumina ceramics using synchrotron radiation diffraction*. Journal of the American Ceramic Society, 1997. **80**(11): p. 2941-2944.
421. Levin, I., et al., *Cubic to monoclinic phase transformations in alumina*. Acta Materialia, 1997. **45**(9): p. 3659-3669.
422. Lee, J., E.J. Jang, and J.H. Kwak, *Acid-base properties of Al₂O₃: Effects of morphology, crystalline phase, and additives*. Journal of Catalytic, 2017. **345**: p. 135-148.
423. Shang, Z., et al., *Highly active and stable alumina supported nickel nanoparticle catalysts for dry reforming of methane*. Applied Catalytic B: Environmental, 2017. **201**: p. 302-309.
424. Park, J.-H., et al., *Enhanced stability of Co catalysts supported on phosphorus-modified Al₂O₃ for dry reforming of CH₄*. Fuel, 2018. **212**: p. 77-87.

425. Therdthianwong, S., C. Siangchin, and A. Therdthianwong, *Improvement of coke resistance of Ni/Al₂O₃ catalyst in CH₄/CO₂ reforming by ZrO₂ addition*. Fuel Processing Technology, 2008. **89**(2): p. 160-168.
426. Sarusi, I., et al., *CO₂ reforming of CH₄ on doped Rh/Al₂O₃ catalysts*. Catalytic Today, 2011. **171**(1): p. 132-139.
427. Bychkov, V.Y., et al., *Carbonization of nickel catalysts and its effect on methane dry reforming*. Applied Catalytic A: General, 2013. **453**: p. 71-79.
428. Zeng, S., et al., *Modification effect of natural mixed rare earths on Co/ γ -Al₂O₃ catalysts for CH₄/CO₂ reforming to synthesis gas*. International Journal of Hydrogen Energy, 2012. **37**(13): p. 9994-10001.
429. Pena, D.A., B.S. Uphade, and P.G. Smirniotis, *TiO₂-supported metal oxide catalysts for low-temperature selective catalytic reduction of NO with NH₃: I. Evaluation and characterization of first row transition metals*. Journal of catalytic, 2004. **221**(2): p. 421-431.
430. Bradford, M.C.J. and M.A. Vannice, *Catalytic reforming of methane with carbon dioxide over nickel catalysts I. Catalyst characterization and activity*. Applied Catalytic A: General, 1996. **142**(1): p. 73-96.
431. Seo, H.O., et al., *Carbon dioxide reforming of methane to synthesis gas over a TiO₂-Ni inverse catalyst*. Applied Catalytic A: General, 2013. **451**: p. 43-49.
432. Morales, F., et al., *Mn promotion effects in Co/TiO₂ Fischer-Tropsch catalysts as investigated by XPS and STEM-EELS*. Journal of Catalytic, 2005. **230**(2): p. 301-308.
433. Schacht, P., et al., *Hydrodesulfurization activity of CoMo catalysts supported on stabilized TiO₂*. Energy & Fuels, 2003. **17**(1): p. 81-86.
434. Takanahe, K., et al., *Titania-supported cobalt and nickel bimetallic catalysts for carbon dioxide reforming of methane*. Journal of Catalytic, 2005. **232**(2): p. 268-275.
435. Raskó, J., A. Hancz, and A. Erdőhelyi, *Surface species and gas phase products in steam reforming of ethanol on TiO₂ and Rh/TiO₂*. Applied Catalytic A: General, 2004. **269**(1): p. 13-25.

436. Nagaoka, K., K. Takanabe, and K.-i. Aika, *Influence of the phase composition of titania on catalytic behavior of Co/TiO₂ for the dry reforming of methane*. Chemical Communications, 2002(9): p. 1006-1007.
437. Wang, Q., et al., *Well-dispersed Pd-Cu bimetallics in TiO₂ nanofiber matrix with enhanced activity and selectivity for nitrate catalytic reduction*. Chemical Engineering Journal, 2017. **326**: p. 182-191.
438. Shiraishi, Y., et al., *Pt-Cu bimetallic alloy nanoparticles supported on anatase TiO₂: highly active catalysts for aerobic oxidation driven by visible light*. ACS nano, 2013. **7**(10): p. 9287-9297.
439. Kim, M.-S., et al., *Catalytic reduction of nitrate in water over Pd-Cu/TiO₂ catalyst: Effect of the strong metal-support interaction (SMSI) on the catalytic activity*. Applied Catalytic B: Environmental, 2013. **142-143**: p. 354-361.
440. Reuel, R.C. and C.H. Bartholomew, *Effects of support and dispersion on the CO hydrogenation activity/selectivity properties of cobalt*. Journal of Catalytic, 1984. **85**(1): p. 78-88.
441. Brik, Y., et al., *Titania-supported cobalt and cobalt-phosphorus catalysts: Characterization and performances in ethane oxidative dehydrogenation*. Journal of Catalytic, 2001. **202**(1): p. 118-128.
442. Voß, M., D. Borgmann, and G. Wedler, *Characterization of alumina, silica, and titania supported cobalt catalysts*. Journal of Catalytic, 2002. **212**(1): p. 10-21.
443. Jalama, K., et al., *Effect of the addition of Au on Co/TiO₂ catalyst for the Fischer-Tropsch reaction*. Topics in Catalytic, 2007. **44**(1): p. 129-136.
444. Li, J., et al., *Fischer-Tropsch synthesis: effect of water on the catalytic properties of a ruthenium promoted Co/TiO₂ catalyst*. Applied Catalytic A: General, 2002. **233**(1): p. 255-262.
445. Feltes, T.E., et al., *Selective adsorption of manganese onto cobalt for optimized Mn/Co/TiO₂ Fischer-Tropsch catalysts*. Journal of Catalytic, 2010. **270**(1): p. 95-102.
446. Li, J. and N.J. Coville, *Effect of boron on the sulfur poisoning of Co/TiO₂ Fischer-Tropsch catalysts*. Applied Catalytic A: General, 2001. **208**(1): p. 177-184.

447. Duvenhage, D.J. and N.J. Coville, *Effect of K, Mn and Cr on the Fischer–Tropsch Activity of Fe:Co/TiO₂ Catalysts*. *Catalytic Letters*, 2005. **104**(3): p. 129-133.
448. Ishihara, A., et al., *Investigation of sulfur behavior on CoMo-based HDS catalysts supported on high surface area TiO₂ by 35S radioisotope tracer method*. *Applied Catalytic A: General*, 2005. **292**: p. 50-60.
449. Wang, D., et al., *Elucidation of promotion effect of cobalt and nickel on Mo/TiO₂ catalyst using a 35S tracer method*. *Applied Catalytic A: General*, 2003. **238**(1): p. 109-117.
450. Ola, O. and M.M. Maroto-Valer, *Review of material design and reactor engineering on TiO₂ photocatalytic for CO₂ reduction*. *Journal of Photochemistry and Photobiology C: Photochemistry Reviews*, 2015. **24**: p. 16-42.
451. Zhou, M., et al., *Morphology-controlled synthesis and novel microwave absorption properties of hollow urchinlike α -MnO₂ nanostructures*. *The Journal of Physical Chemistry C*, 2011. **115**(5): p. 1398-1402.
452. Li, Z., et al., *Preparation and microwave absorption properties of Ni-Fe₃O₄ hollow spheres*. *Materials Science and Engineering: B*, 2009. **164**(2): p. 112-115.
453. Liu, J.-r., et al., *Enhanced electromagnetic wave absorption properties of Fe nanowires in gigahertz range*. *Applied Physics Letters*, 2007. **91**(9): p. 093101.
454. de la Hoz, A., A. Diaz-Ortiz, and A. Moreno, *Microwaves in organic synthesis. Thermal and non-thermal microwave effects*. *Chemical Society Reviews*, 2005. **34**(2): p. 164-178.
455. Whittaker, A. and D. Mingos, *The application of microwave heating to chemical syntheses*. *Journal of Microwave Power and Electromagnetic Energy*, 1994. **29**(4): p. 195-219.
456. Grant, E. and B.J. Halstead, *Dielectric parameters relevant to microwave dielectric heating*. *Chemical society reviews*, 1998. **27**(3): p. 213-224.
457. Lew, A., et al., *Increasing rates of reaction: microwave-assisted organic synthesis for combinatorial chemistry*. *Journal of combinatorial chemistry*, 2002. **4**(2): p. 95-105.

458. Bilecka, I. and M. Niederberger, *Microwave chemistry for inorganic nanomaterials synthesis*. *Nanoscale*, 2010. **2**(8): p. 1358-1374.
459. Rees, W.G. and P. Pellika, *Principles of remote sensing*. Remote Sensing of Glaciers. London, 2010.
460. Schiffmann, R., *Food product development for microwave processing*. Food technology (USA), 1986.
461. Williams, N.H., *Curing epoxy resin impregnates pipe at 2450 megahertz*. *Journal of Microwave Power*, 1967. **2**(4): p. 123-127.
462. Bacci, M., et al., *Microwave heating for the rapid determination of thermodynamic functions of chemical reactions*. *Journal of the Chemical Society, Faraday Transactions 1: Physical Chemistry in Condensed Phases*, 1981. **77**(7): p. 1503-1509.
463. Giguere, R.J., et al., *Application of commercial microwave ovens to organic synthesis*. *Tetrahedron Letters*, 1986. **27**(41): p. 4945-4948.
464. Gedye, R., et al., *The use of microwave ovens for rapid organic synthesis*. *Tetrahedron Letters*, 1986. **27**(3): p. 279-282.
465. Zhang, X. and D.O. Hayward, *Applications of microwave dielectric heating in environment-related heterogeneous gas-phase catalytic systems*. *Inorganica Chimica Acta*, 2006. **359**(11): p. 3421-3433.
466. Aguilar-Reynosa, A., et al., *Microwave heating processing as alternative of pretreatment in second-generation biorefinery: an overview*. *Energy conversion and management*, 2017. **136**: p. 50-65.
467. Horikoshi, S. and N. Serpone, *Role of microwaves in heterogeneous catalytic systems*. *Catalytic Science & Technology*, 2014. **4**(5): p. 1197-1210.
468. Horikoshi, S. and N. Serpone, *Microwaves in nanoparticle synthesis: Fundamentals and applications*. 2013.
469. Stuerger, D., et al., *Microwaves in organic synthesis*. 2006.
470. Xu, W., et al., *Temperature gradient control during microwave combined with hot air drying*. *Biosystems Engineering*, 2018. **169**: p. 175-187.
471. Pert, E., et al., *Temperature Measurements during Microwave Processing: The Significance of Thermocouple Effects*. *Journal of the American Ceramic Society*, 2001. **84**(9): p. 1981-1986.

472. Stefanidis Georgios, D., et al., *A helicopter view of microwave application to chemical processes: reactions, separations, and equipment concepts*, in *Reviews in Chemical Engineering*. 2014. p. 233.
473. Peng, Z., et al., *Microwave penetration depth in materials with non-zero magnetic susceptibility*. ISIJ international, 2010. **50**(11): p. 1590-1596.
474. Wei, J., J. Liu, and S. Li, *Electromagnetic and microwave absorption properties of Fe₃O₄ magnetic films plated on hollow glass spheres*. Journal of Magnetism and Magnetic Materials, 2007. **312**(2): p. 414-417.
475. Ayappa, K., et al., *Analysis of microwave heating of materials with temperature-dependent properties*. AIChE Journal, 1991. **37**(3): p. 313-322.
476. Oghbaei, M. and O. Mirzaee, *Microwave versus conventional sintering: A review of fundamentals, advantages and applications*. Journal of Alloys and Compounds, 2010. **494**(1): p. 175-189.
477. Golubov, A.A., et al., *Multiband model for penetration depth in MgB₂*. Physical Review B, 2002. **66**(5): p. 054524.
478. Hayes, B.L., *Recent advances in microwave-assisted synthesis*. Aldrichimica Acta, 2004. **37**(2): p. 66-77.
479. Horikoshi, S., et al., *Environmental remediation by an integrated microwave/UV illumination method: VII. Thermal/non-thermal effects in the microwave-assisted photocatalyzed mineralization of bisphenol-A*. Journal of Photochemistry and Photobiology A: Chemistry, 2004. **162**(1): p. 33-40.
480. Shazman, A., et al., *Examining for possible non-thermal effects during heating in a microwave oven*. Food Chemistry, 2007. **103**(2): p. 444-453.
481. Mishra, R.R. and A.K. Sharma, *Microwave-material interaction phenomena: Heating mechanisms, challenges and opportunities in material processing*. Composites Part A: Applied Science and Manufacturing, 2016. **81**: p. 78-97.
482. Baghbanzadeh, M., et al., *Microwave-assisted synthesis of colloidal inorganic nanocrystals*. Angewandte Chemie International Edition, 2011. **50**(48): p. 11312-11359.

483. Kaatze, U., *Complex permittivity of water as a function of frequency and temperature*. Journal of Chemical and Engineering Data, 1989. **34**(4): p. 371-374.
484. Saltiel, C. and A.K. Datta, *Heat and mass transfer in microwave processing*, in *Advances in Heat Transfer*. 1999. p. 1-94.
485. Zhang, H. and A.K. Datta, *Microwave power absorption in single- and multiple-item foods*. Food and Bioproducts Processing: Transactions of the Institution of Chemical Engineers, Part C, 2003. **81**(3): p. 257-265.
486. Clark, D.E., D.C. Folz, and J.K. West, *Processing materials with microwave energy*. Materials Science and Engineering A, 2000. **287**(2): p. 153-158.
487. Anwar, J., et al., *Microwave chemistry: Effect of ions on dielectric heating in microwave ovens*. Arabian Journal of Chemistry, 2015. **8**(1): p. 100-104.
488. Mello, P.A., J.S. Barin, and R.A. Guarnieri, *Chapter 2 - Microwave heating*, in *Microwave-Assisted Sample Preparation for Trace Element Analysis*, É.M.d.M. Flores, Editor. 2014, Elsevier: Amsterdam. p. 59-75.
489. Sun, G., et al., *Hierarchical dendrite-like magnetic materials of Fe_3O_4 , γ - Fe_2O_3 , and Fe with high performance of microwave absorption*. Chemistry of Materials, 2011. **23**(6): p. 1587-1593.
490. Kim, S.-S., et al., *Magnetic and microwave absorbing properties of Co-Fe thin films plated on hollow ceramic microspheres of low density*. Journal of Magnetism and Magnetic Materials, 2004. **271**(1): p. 39-45.
491. Schramm, W., D. Yang, and D. Haemmerich. *Contribution of direct heating, thermal conduction and perfusion during radiofrequency and microwave ablation*. in *2006 International Conference of the IEEE Engineering in Medicine and Biology Society*. 2006.
492. Cheng, J., R. Roy, and D. Agrawal, *Radically different effects on materials by separated microwave electric and magnetic fields*. Material Research Innovations, 2002. **5**(3): p. 170-177.
493. Ziping, C., et al., *Microwave heating origination and rapid crystallization of PZT thin films in separated H field*. Journal of Physics D: Applied Physics, 2008. **41**(9): p. 092003.

494. Nguyen, P.P., et al., *Microwave hysteretic losses in $YBa_2Cu_3O_{7-x}$ and NbN thin films*. Physical Review B, 1995. **51**(10): p. 6686-6695.
495. Ghasemi, A., et al., *Electromagnetic properties and microwave absorbing characteristics of doped barium hexaferrite*. Journal of Magnetism and Magnetic Materials, 2006. **302**(2): p. 429-435.
496. Horikoshi, S., T. Sumi, and N. Serpone, *Unusual effect of the magnetic field component of the microwave radiation on aqueous electrolyte solutions*. Journal of Microwave Power and Electromagnetic Energy, 2012. **46**(4): p. 215-228.
497. Pardavi-Horvath, M., *Microwave applications of soft ferrites*. Journal of Magnetism and Magnetic Materials, 2000. **215**: p. 171-183.
498. Lee, W.C., K.S. Liu, and I.N. Lin, *Microwave sintering $Pb(Zr_{0.52}Ti_{0.48})O_3$ piezoelectric ceramics*. Ferroelectrics, 2001. **262**(1): p. 293-298.
499. Zhao, C., et al., *Hybrid sintering with a tubular susceptor in a cylindrical single-mode microwave furnace*. Acta Materialia, 2000. **48**(14): p. 3795-3801.
500. Bhattacharya, M. and T. Basak, *A review on the susceptor assisted microwave processing of materials*. Energy, 2016. **97**: p. 306-338.
501. Zhang, Y., et al., *Microwave power absorption mechanism of metallic powders*. IEEE Transactions on Microwave Theory and Techniques, 2018. **66**(5): p. 2107-2115.
502. Wan, J.K.S., G. Bamwenda, and M.C. Depew, *Microwave induced catalytic reactions of carbon dioxide and water: mimicry of photosynthesis*. Research on Chemical Intermediates, 1991. **16**(3): p. 241-255.
503. Wan, J. and T. Koch, *Application of microwave radiation for the synthesis of hydrogen cyanide*. Research on Chemical Intermediates, 1994. **20**(1): p. 29-37.
504. Wan, J.K.S., *Microwaves and chemistry: The catalytic of an exciting marriage*. Research on Chemical Intermediates, 1993. **19**(2): p. 147.
505. Ioffe, M.S., S.D. Pollington, and J.K.S. Wan, *High-power pulsed radio-frequency and microwave catalytic processes: Selective production of*

- acetylene from the reaction of methane over carbon*. Journal of Catalytic, 1995. **151**(2): p. 349-355.
506. Wan, J.K., *Microwave production of C₂ hydrocarbons, using a carbon catalyst*. 1995, Google Patents.
507. Horikoshi, S., et al., *Microwave heating*, in *Microwave chemical and materials processing: A tutorial*. 2018, Springer Singapore: Singapore. p. 47-85.
508. Pollington, S.D., et al., *A high-power X-band pulsed microwave induced catalytic decomposition of methane with integral acoustic measurements*. Research on Chemical Intermediates, 1995. **21**(1): p. 59-68.
509. Tse, M.Y., M.C. Depew, and J.K.S. Wan, *Applications of high power micro wave catalytic in chemistry*. Research on Chemical Intermediates, 1990. **13**(3): p. 221-236.
510. Wan, J., et al., *High – power pulsed micro – wave catalytic processes: Decomposition of methane*. Journal of Microwave Power and Electromagnetic Energy, 1990. **25**(1): p. 32-38.
511. Cooney, D.O. and Z. Xi, *Production of hydrogen from methane and methane/steam in a microwave irradiated char-loaded reactor*. Fuel Science and Technology International, 1996. **14**(8): p. 1111-1141.
512. Bi, X.-j., et al., *Microwave effect on partial oxidation of methane to syngas*. Reaction Kinetics and Catalytic Letters, 1999. **66**(2): p. 381-386.
513. Tanashev, Y.Y., et al., *Methane processing under microwave radiation: Recent findings and problems*. Catalytic Today, 1998. **42**(3): p. 333-336.
514. Chen, C., et al., *Microwave effects on the oxidative coupling of methane over proton conductive catalysts*. Journal of the Chemical Society, Faraday Transactions, 1995. **91**(7): p. 1179-1180.
515. Chen, C.-l., et al., *Microwave effects on the oxidative coupling of methane over Bi₂O₃-WO₃ oxygen ion conductive oxides*. Reaction Kinetics and Catalytic Letters, 1997. **61**(1): p. 175-180.
516. Roussy, G., et al., *Controlled oxidation of methane doped catalysts irradiated by microwaves*. Catalytic Today, 1994. **21**(2): p. 349-355.

517. Domínguez, A., et al., *Microwave-assisted catalytic decomposition of methane over activated carbon for CO₂-free hydrogen production*. International Journal of Hydrogen Energy, 2007. **32**(18): p. 4792-4799.
518. Roussy, G., et al., *C₂₊ selectivity enhancement in oxidative coupling of methane over microwave-irradiated catalysts*. Fuel Processing Technology, 1997. **50**(2): p. 261-274.
519. Zhang, X., et al., *Oxidative coupling of methane using microwave dielectric heating*. Applied Catalytic A: General, 2003. **249**(1): p. 151-164.
520. Marún, C., L.D. Conde, and S.L. Suib, *Catalytic oligomerization of methane via microwave heating*. The Journal of Physical Chemistry A, 1999. **103**(22): p. 4332-4340.
521. Conde, L.D., et al., *Frequency effects in the catalytic oligomerization of methane via microwave heating*. Journal of Catalytic, 2001. **204**(2): p. 324-332.
522. Koch, T.A., K.R. Krause, and M. Mehdizadeh, *Improved safety through distributed manufacturing of hazardous chemicals*. Process Safety Progress, 1997. **16**(1): p. 23-24.
523. Zhang, X., D. O. Hayward, and D. Michael P. Mingos, *Apparent equilibrium shifts and hot-spot formation for catalytic reactions induced by microwave dielectric heating*. Chemical Communications, 1999(11): p. 975-976.
524. Cha, C.-Y., *Microwave induced reactions of SO₂ and NO_x decomposition in the char-bed*. Research on Chemical Intermediates, 1994. **20**(1): p. 13-28.
525. Chang, Y.-f., et al., *Microwave-assisted NO reduction by methane over Co-ZSM-5 zeolites*. Catalytic Letters, 1999. **57**(4): p. 187-191.
526. Kong, Y. and C.Y. Cha, *NO_x abatement with carbon adsorbents and microwave energy*. Energy & Fuels, 1995. **9**(6): p. 971-975.
527. Perry, W.L., et al., *Kinetics of the microwave-heated CO oxidation reaction over alumina-supported Pd and Pt catalysts*. Journal of Catalytic, 1997. **171**(2): p. 431-438.

528. Silverwood, I., G. McDougall, and G. Whittaker, *Comparison of conventional versus microwave heating of the platinum catalysed oxidation of carbon monoxide over EUROPT-1 in a novel infrared microreactor cell*. Journal of Molecular Catalytic A: Chemical, 2007. **269**(1): p. 1-4.
529. Silverwood, I.P., G.S. McDougall, and A. Gavin Whittaker, *A microwave-heated infrared reaction cell for the in situ study of heterogeneous catalysts*. Physical Chemistry Chemical Physics, 2006. **8**(46): p. 5412-5416.
530. Will, H., et al., *Multimode microwave reactor for heterogeneous gas-phase catalytic*. Chemical Engineering & Technology, 2003. **26**(11): p. 1146-1149.
531. Beckers, J., L.M. van der Zande, and G. Rothenberg, *Clean diesel power via microwave susceptible oxidation catalysts*. ChemPhysChem, 2006. **7**(3): p. 747-755.
532. Cooney, D.O. and Z. Xi, *Production of ethylene and propylene from ethane, propane, and N-butane mixed steam in a microwave-irradiated silicon-carbide loaded reactor*. Fuel Science and Technology International, 1996. **14**(10): p. 1315-1336.
533. Sinev, I., et al., *Interaction of vanadium containing catalysts with microwaves and their activation in oxidative dehydrogenation of ethane*. Catalytic Today, 2009. **141**(3): p. 300-305.
534. Liu, Y., et al., *The effects of microwaves on the catalyst preparation and the oxidation of o-xylene over a V₂O₅/SiO₂ system*. Catalytic Today, 1999. **51**(1): p. 147-151.
535. Seyfried, L., et al., *Microwave electromagnetic-field effects on reforming catalysts .: 1. Higher selectivity in 2-Methylpentane isomerization on alumina-supported Pt catalysts*. Journal of Catalytic, 1994. **148**(1): p. 281-287.
536. Thiebaut, J.-M., et al., *Durable changes of the catalytic properties of alumina-supported platinum induced by microwave irradiation*. Catalytic Letters, 1993. **21**(1): p. 133-138.

537. Zhang, X.-R., et al., *A unique microwave effect on the microstructural modification of Cu/ZnO/Al₂O₃ catalysts for steam reforming of methanol*. Chemical Communications, 2005(32): p. 4104-4106.
538. Perry, W.L., et al., *Microwave heating of endothermic catalytic reactions: Reforming of methanol*. AIChE Journal, 2002. **48**(4): p. 820-831.
539. Bond, G., et al., *The effect of microwave heating on the reaction of propan-2-ol over alkalised carbon catalysts*. Topics in Catalytic, 1994. **1**(1): p. 177-182.
540. Zhang, X., D.O. Hayward, and D.M.P. Mingos, *Effects of microwave dielectric heating on heterogeneous catalytic*. Catalytic Letters, 2003. **88**(1-2): p. 33-38.
541. Bond, G., et al., *Measurement of temperature during microwave heating (chemical reactions enhancement)*. Measurement Science and Technology, 1991. **2**(6): p. 571-572.
542. Durka, T., et al., *On the accuracy and reproducibility of fiber optic (FO) and infrared (IR) temperature measurements of solid materials in microwave applications*. Measurement Science and Technology, 2010. **21**(4): p. 045108.
543. Zhang, X., D.O. Hayward, and D.M.P. Mingos, *Microwave dielectric heating behavior of supported MoS₂ and Pt catalysts*. Industrial & Engineering Chemistry Research, 2001. **40**(13): p. 2810-2817.
544. Bogdal, D., et al., *Microwave-assisted oxidation of alcohols using Magtrieve™*. Tetrahedron, 2003. **59**(5): p. 649-653.
545. Durka, T., et al., *Microwave-activated methanol steam reforming for hydrogen production*. International Journal of Hydrogen Energy, 2011. **36**(20): p. 12843-12852.
546. Ramirez, A., et al., *In situ temperature measurements in microwave-heated gas-solid catalytic systems. Detection of hot spots and solid-fluid temperature gradients in the ethylene epoxidation reaction*. Chemical Engineering Journal, 2017. **316**: p. 50-60.
547. Ramírez, A., et al., *Ethylene epoxidation in microwave heated structured reactors*. Catalytic Today, 2016. **273**: p. 99-105.

548. Kyuma, K., et al., *Fiber-optic instrument for temperature measurement*. IEEE Transactions on Microwave Theory and Techniques, 1982. **30**(4): p. 522-525.
549. Nüchter, M., et al., *Microwave assisted synthesis—a critical technology overview*. Green chemistry, 2004. **6**(3): p. 128-141.
550. Robinson, J., et al., *Understanding microwave heating effects in single mode type cavities—theory and experiment*. Physical Chemistry Chemical Physics, 2010. **12**(18): p. 4750-4758.
551. Goudere, D., M. Giroux, and R. Bosisi, *Dynamic high temperature microwave complex permittivity measurements on samples heated via microwave absorption*. Journal of Microwave Power, 1973. **8**(1): p. 69-82.
552. Gangurde, L.S., et al., *Complexity and challenges in noncontact high temperature measurements in microwave-assisted catalytic reactors*. Industrial & Engineering Chemistry Research, 2017. **56**(45): p. 13379-13391.
553. Kappe, C.O., *How to measure reaction temperature in microwave-heated transformations*. Chemical Society Reviews, 2013. **42**(12): p. 4977-4990.
554. Obermayer, D. and C.O. Kappe, *On the importance of simultaneous infrared/fiber-optic temperature monitoring in the microwave-assisted synthesis of ionic liquids*. Organic & Biomolecular Chemistry, 2010. **8**(1): p. 114-121.
555. Stephan, P., E. Wagner, and R. Nasarek, *Liquid crystal technique for measuring temperature*, in *Encyclopedia of Microfluidics and Nanofluidics*, D. Li, Editor. 2008, Springer US: Boston, MA. p. 1012-1022.
556. Geitenbeek, R.G., et al., *In situ luminescence thermometry to locally measure temperature gradients during catalytic reactions*. ACS Catalytic, 2018. **8**(3): p. 2397-2401.
557. Ramirez, A., et al., *Escaping undesired gas-phase chemistry: Microwave-driven selectivity enhancement in heterogeneous catalytic reactors*. Science advances, 2019. **5**(3): p. eaau9000.
558. Caddick, S., *Microwave assisted organic reactions*. Tetrahedron, 1995. **51**(38): p. 10403-10432.

559. Moseley, J.D. and C.O. Kappe, *A critical assessment of the greenness and energy efficiency of microwave-assisted organic synthesis*. Green Chemistry, 2011. **13**(4): p. 794-806.
560. Wathey, B., et al., *The impact of microwave-assisted organic chemistry on drug discovery*. Drug discovery today, 2002. **7**(6): p. 373-380.
561. Jie, W. and Y. Jiankang, *Behaviour of coal pyrolysis desulfurization with microwave energy*. Fuel, 1994. **73**(2): p. 155-159.
562. Marland, S., A. Merchant, and N. Rowson, *Dielectric properties of coal*. Fuel, 2001. **80**(13): p. 1839-1849.
563. Fang, Z., et al., *The electromagnetic characteristics of carbon foams*. Carbon, 2007. **45**(15): p. 2873-2879.
564. Wu, K.H., et al., *Synthesis and microwave electromagnetic characteristics of bamboo charcoal/polyaniline composites in 2-40 GHz*. Synthetic Metals, 2008. **158**(17-18): p. 688-694.
565. Challa, S., W.E. Little, and C.Y. Cha, *Measurement of the dielectric properties of char at 2.45 GHz*. Journal of Microwave Power and Electromagnetic Energy, 1994. **29**(3): p. 131-137.
566. Atwater, J.E. and R.R. Wheeler Jr, *Temperature dependent complex permittivities of graphitized carbon blacks at microwave frequencies between 0.2 and 26 GHz*. Journal of Materials Science, 2004. **39**(1): p. 151-157.
567. Ma, J., et al., *Microwave-assisted catalytic combustion of diesel soot*. Applied Catalytic A: General, 1997. **159**(1-2): p. 211-228.
568. Atwater, J.E. and R.R. Wheeler Jr, *Complex permittivities and dielectric relaxation of granular activated carbons at microwave frequencies between 0.2 and 26 GHz*. Carbon, 2003. **41**(9): p. 1801-1807.
569. Atwater, J.E. and R.R. Wheeler Jr, *Microwave permittivity and dielectric relaxation of a high surface area activated carbon*. Applied Physics A: Materials Science and Processing, 2004. **79**(1): p. 125-129.
570. Dawson, E.A., et al., *The generation of microwave-induced plasma in granular active carbons under fluidised bed conditions*. Carbon, 2008. **46**(2): p. 220-228.

571. Lin, H., et al., *Microwave-absorbing properties of Co-filled carbon nanotubes*. Materials Research Bulletin, 2008. **43**(10): p. 2697-2702.
572. Zhang, L. and H. Zhu, *Dielectric, magnetic, and microwave absorbing properties of multi-walled carbon nanotubes filled with Sm₂O₃ nanoparticles*. Materials Letters, 2009. **63**(2): p. 272-274.
573. Yao, Y., A. Jänis, and U. Klement, *Characterization and dielectric properties of β -SiC nanofibres*. Journal of Materials Science, 2008. **43**(3): p. 1094-1101.
574. Domínguez, A., et al., *Conventional and microwave induced pyrolysis of coffee hulls for the production of a hydrogen rich fuel gas*. Journal of Analytical and Applied Pyrolysis, 2007. **79**(1): p. 128-135.
575. Kustov, L.M., et al., *Nickel–alumina catalysts in the reaction of carbon dioxide re-forming of methane under thermal and microwave heating*. Industrial & Engineering Chemistry Research, 2017. **56**(45): p. 13034-13039.
576. Hunt, J., et al., *Microwave-specific enhancement of the carbon–carbon dioxide (Boudouard) reaction*. The Journal of Physical Chemistry C, 2013. **117**(51): p. 26871-26880.
577. Nguyen, H.M., et al., *Dry reforming of methane over Co–Mo/Al₂O₃ catalyst under low microwave power irradiation*. Catalytic Science & Technology, 2018. **8**(20): p. 5315-5324.
578. Egawa, C., *Methane dry reforming reaction on Ru(0 0 1) surfaces*. Journal of Catalytic, 2018. **358**: p. 35-42.
579. Abdel Karim Aramouni, N., et al., *Thermodynamic analysis of methane dry reforming: Effect of the catalyst particle size on carbon formation*. Energy Conversion and Management, 2017. **150**: p. 614-622.
580. Zagaynov, I.V., et al., *Ni(Co)–Gd_{0.1}Ti_{0.1}Zr_{0.1}Ce_{0.7}O₂ mesoporous materials in partial oxidation and dry reforming of methane into synthesis gas*. Chemical Engineering Journal, 2016. **290**: p. 193-200.
581. Li, W., J. Liu, and D. Zhao, *Mesoporous materials for energy conversion and storage devices*. Nature Reviews Materials, 2016. **1**: p. 16023.
582. He, F., et al., *Solvothermal synthesis of mesoporous TiO₂: The effect of morphology, size and calcination progress on photocatalytic activity in the*

- degradation of gaseous benzene*. Chemical Engineering Journal, 2014. **237**: p. 312-321.
583. Cao, Z., et al., *Pore structure characterization of Chang-7 tight sandstone using MICP combined with N₂GA techniques and its geological control factors*. Scientific Reports, 2016. **6**: p. 36919.
584. Ferencz, Z., et al., *Effects of support and Rh additive on Co-based catalysts in the ethanol steam reforming reaction*. ACS Catalytic, 2014. **4**(4): p. 1205-1218.
585. Ji, J., et al., *Towards an efficient CoMo/ γ -Al₂O₃ catalyst using metal amine metallate as an active phase precursor: Enhanced hydrogen production by ammonia decomposition*. International Journal of Hydrogen Energy, 2014. **39**(24): p. 12490-12498.
586. Wang, B., et al., *Effect of different catalyst supports on the (n,m) selective growth of single-walled carbon nanotube from Co–Mo catalyst*. Journal of Materials Science, 2009. **44**(12): p. 3285-3295.
587. Gaytan, S.M., et al., *Comparison of microstructures and mechanical properties for solid and mesh Cobalt-base alloy prototypes fabricated by electron beam melting*. Metallurgical and Materials Transactions A, 2010. **41**(12): p. 3216-3227.
588. Khani, Y., Z. Shariatinia, and F. Bahadoran, *High catalytic activity and stability of ZnLaAlO₄ supported Ni, Pt and Ru nanocatalysts applied in the dry, steam and combined dry-steam reforming of methane*. Chemical Engineering Journal, 2016. **299**: p. 353-366.
589. Das, S., et al., *Microwave absorption properties of double-layer composites using CoZn/NiZn/MnZn-ferrite and titanium dioxide*. Journal of Magnetism and Magnetic Materials, 2015. **377**(Supplement C): p. 111-116.
590. Li, X., et al., *One-pot synthesis of CoFe₂O₄/graphene oxide hybrids and their conversion into FeCo/graphene hybrids for lightweight and highly efficient microwave absorber*. Journal of Materials Chemistry A, 2015. **3**(10): p. 5535-5546.
591. Maqsood, A. and K. Khan, *Structural and microwave absorption properties of Ni_(1-x)Co_(x)Fe₂O₄ (0.0 ≤ x ≤ 0.5) nanoferrites synthesized via*

- co-precipitation route*. Journal of Alloys and Compounds, 2011. **509**(7): p. 3393-3397.
592. Kustov, L.M. and I.M. Sinev, *Microwave activation of catalysts and catalytic processes*. Russian Journal of Physical Chemistry A, 2010. **84**(10): p. 1676-1694.
593. Clark, D.E., D.C. Folz, and J.K. West, *Processing materials with microwave energy*. Materials Science and Engineering: A, 2000. **287**(2): p. 153-158.
594. Nagaoka, K., K. Takanabe, and K.-i. Aika, *Influence of the reduction temperature on catalytic activity of Co/TiO₂ (anatase-type) for high pressure dry reforming of methane*. Applied Catalytic A: General, 2003. **255**(1): p. 13-21.
595. Sadanandam, G., et al., *Cobalt doped TiO₂: A stable and efficient photocatalyst for continuous hydrogen production from glycerol: Water mixtures under solar light irradiation*. International Journal of Hydrogen Energy, 2013. **38**(23): p. 9655-9664.
596. Rossetti, I., et al., *TiO₂-supported catalysts for the steam reforming of ethanol*. Applied Catalytic A: General, 2014. **477**: p. 42-53.
597. Thomas, A.G., et al., *Comparison of the electronic structure of anatase and rutile TiO₂ single-crystal surfaces using resonant photoemission and X-ray absorption spectroscopy*. Physical Review B, 2007. **75**(3): p. 035105.
598. Shao, X., et al., *Enhanced photocatalytic activity of TiO₂-C hybrid aerogels for methylene blue degradation*. Scientific Reports, 2013. **3**: p. 3018.
599. Wrana, D., et al., *Tuning the surface structure and conductivity of niobium-doped rutile TiO₂ single crystals via thermal reduction*. Physical Chemistry Chemical Physics, 2017. **19**(45): p. 30339-30350.
600. Alexeev, O.S., et al., *Effects of reduction temperature and metal–support interactions on the catalytic activity of Pt/γ-Al₂O₃ and Pt/TiO₂ for the oxidation of CO in the presence and absence of H₂*. The Journal of Physical Chemistry B, 2005. **109**(49): p. 23430-23443.

601. Panagiotopoulou, P., et al., *Particle size effects on the reducibility of titanium dioxide and its relation to the water–gas shift activity of Pt/TiO₂ catalysts*. Journal of Catalytic, 2006. **240**(2): p. 114-125.
602. Reucroft, P.J. and J.W. Park, *Reducibility and surface area of coprecipitated supported nickel methanation catalysts*. Journal of Materials for Energy Systems, 1980. **2**(1): p. 28.
603. Morales, F., et al., *In situ X-ray absorption of Co/Mn/TiO₂ catalysts for Fischer–Tropsch synthesis*. The Journal of Physical Chemistry B, 2004. **108**(41): p. 16201-16207.
604. Liu, H. and Y. Xu, *H₂-TPR study on Mo/HZSM-5 catalyst for CH₄ dehydroaromatization*. Chinese Journal of Catalytic, 2006. **27**(4): p. 319-323.
605. Kong, I., et al., *Magnetic and microwave absorbing properties of magnetite–thermoplastic natural rubber nanocomposites*. Journal of Magnetism and Magnetic Materials, 2010. **322**(21): p. 3401-3409.
606. Yang, R.-B., et al., *Synthesis and characterization of Fe₃O₄/polypyrrole/carbon nanotube composites with tunable microwave absorption properties: Role of carbon nanotube and polypyrrole content*. Chemical Engineering Journal, 2016. **285**: p. 497-507.
607. Wang, Z., et al., *Magnetite nanocrystals on multiwalled carbon nanotubes as a synergistic microwave absorber*. The Journal of Physical Chemistry C, 2013. **117**(10): p. 5446-5452.
608. Zhang, R.-j., et al., *Effect of support on the performance of Ni-based catalyst in methane dry reforming*. Journal of Fuel Chemistry and Technology, 2015. **43**(11): p. 1359-1365.
609. Xia, T., et al., *Strong microwave absorption of hydrogenated wide bandgap semiconductor nanoparticles*. ACS Applied Materials & Interfaces, 2015. **7**(19): p. 10407-10413.
610. Dadfar, M.R., S.A.S. ebrahimi, and M. Dadfar, *Microwave absorption properties of 50% SrFe₁₂O₁₉–50% TiO₂ nanocomposites with porosity*. Journal of Magnetism and Magnetic Materials, 2012. **324**(24): p. 4204-4208.

611. Zeng, Y.X., et al., *Low temperature reforming of biogas over K-, Mg- and Ce-promoted Ni/Al₂O₃ catalysts for the production of hydrogen rich syngas: Understanding the plasma-catalytic synergy*. Applied Catalytic B: Environmental, 2018. **224**: p. 469-478.
612. Nguyen, H.M., et al., *Dry reforming of methane over Co-Mo/Al₂O₃ catalyst at low microwave power irradiation*. Catalytic Science & Technology, 2018.
613. Kim, S.-J., et al., *Effect of pressure on high-temperature water gas shift reaction in microporous zeolite membrane reactor*. Industrial & Engineering Chemistry Research, 2012. **51**(3): p. 1364-1375.
614. Challiwala, M.S., et al., *A combined thermo-kinetic analysis of various methane reforming technologies: Comparison with dry reforming*. Journal of CO₂ Utilization, 2017. **17**: p. 99-111.
615. Pashchenko, D., *Thermodynamic equilibrium analysis of combined dry and steam reforming of propane for thermochemical waste-heat recuperation*. International Journal of Hydrogen Energy, 2017. **42**(22): p. 14926-14935.
616. Serrano-Lotina, A. and L. Daza, *Influence of the operating parameters over dry reforming of methane to syngas*. International Journal of Hydrogen Energy, 2014. **39**(8): p. 4089-4094.
617. Leadbeater, N.E., *Microwave heating as a tool for sustainable chemistry*. 1 ed. 2010.
618. Dicks, A.L., K.D. Pointon, and A. Siddle, *Intrinsic reaction kinetics of methane steam reforming on a nickel/zirconia anode*. Journal of Power Sources, 2000. **86**(1): p. 523-530.
619. Gallucci, F., et al., *Experimental study of the methane steam reforming reaction in a dense Pd/Ag membrane reactor*. Industrial & Engineering Chemistry Research, 2004. **43**(4): p. 928-933.
620. Hou, K. and R. Hughes, *The kinetics of methane steam reforming over a Ni/ α -Al₂O₃ catalyst*. Chemical Engineering Journal, 2001. **82**(1-3): p. 311-328.

621. Kechagiopoulos, P., S. Angeli, and A. Lemonidou, *Low temperature steam reforming of methane: A combined isotopic and microkinetic study*. Applied Catalytic B: Environmental, 2017. **205**: p. 238-253.
622. Che, F., et al., *Reducing reaction temperature, steam requirements, and coke formation during methane steam reforming using electric fields: A microkinetic modeling and experimental study*. ACS Catalytic, 2017. **7**(10): p. 6957-6968.
623. Yang, E.-h., et al., *Combined steam and CO₂ reforming of methane over La_{1-x}Sr_xNiO₃ perovskite oxides*. Catalytic Today, 2017.
624. Chen, W.-H., J.-G. Jheng, and A.B. Yu, *Hydrogen generation from a catalytic water gas shift reaction under microwave irradiation*. International Journal of Hydrogen Energy, 2008. **33**(18): p. 4789-4797.
625. Ferrari, A., et al., *Microwave-specific effects on the equilibrium constants and thermodynamics of the steam-carbon and related reactions*. The Journal of Physical Chemistry C, 2014. **118**(18): p. 9346-9356.
626. Özkara-Aydınoğlu, Ş., *Thermodynamic equilibrium analysis of combined carbon dioxide reforming with steam reforming of methane to synthesis gas*. International Journal of Hydrogen Energy, 2010. **35**(23): p. 12821-12828.
627. Demidov, D.V., I.V. Mishin, and M.N. Mikhailov, *Gibbs free energy minimization as a way to optimize the combined steam and carbon dioxide reforming of methane*. International Journal of Hydrogen Energy, 2011. **36**(10): p. 5941-5950.
628. Ojeda-Niño, O.H., F. Gracia, and C. Daza, *Role of Pr on Ni-Mg-Al mixed oxides synthesized by microwave-assisted self-combustion for dry reforming of methane*. Industrial & Engineering Chemistry Research, 2019.
629. Li, L., et al., *Toluene microwave-assisted reforming with CO₂ or a mixed agent of CO₂-H₂O on Fe-doped activated biochar*. Energy, 2019.
630. Sang, X., et al., *Ionic liquid accelerates the crystallization of Zr-based metal-organic frameworks*. Nature Communications, 2017. **8**(1): p. 175.

631. Bagheri, S., N. Muhd Julkapli, and S. Bee Abd Hamid, *Titanium dioxide as a catalyst support in heterogeneous catalytic*. ScientificWorldJournal, 2014. **2014**: p. 727496.
632. Fang, J., et al., *The support effect on the size and catalytic activity of thiolated Au 25 nanoclusters as precatalysts*. Nanoscale, 2015. **7**(14): p. 6325-6333.
633. Min, B.K., W.T. Wallace, and D.W. Goodman, *Synthesis of a sinter-resistant, mixed-oxide support for Au nanoclusters*. The Journal of Physical Chemistry B, 2004. **108**(38): p. 14609-14615.
634. Vinogradov, A., A. Agafonov, and V. Vinogradov, *Low-temperature sol-gel synthesis photochromic Cu/TiO₂ films*. Journal of Alloys and Compounds, 2012. **515**: p. 1-3.
635. Xing, J., et al., *Cu-Cu₂O-TiO₂ nanojunction systems with an unusual electron-hole transportation pathway and enhanced photocatalytic properties*. Chemistry—An Asian Journal, 2013. **8**(6): p. 1265-1270.
636. Ma, J., et al., *Direct synthesis of MOF-derived nanoporous CuO/carbon composites for high impedance matching and advanced microwave absorption*. Journal of Materials Chemistry C, 2016. **4**(48): p. 11419-11426.
637. Bhattacharya, P., et al., *Graphene decorated with hexagonal shaped M-type ferrite and polyaniline wrapper: a potential candidate for electromagnetic wave absorbing and energy storage device applications*. RSC Advances, 2014. **4**(33): p. 17039-17053.
638. Zhang, K., et al., *Porous MoO₂-Cu/C/Graphene nano-octahedrons quadruple nanocomposites as an advanced anode for lithium ion batteries with enhanced rate capability*. Journal of Alloys and Compounds, 2018. **731**: p. 646-654.
639. Zhang, Y., et al., *MoO₂@ Cu@ C composites prepared by using polyoxometalates@ metal-organic frameworks as template for all-solid-state flexible supercapacitor*. Electrochimica Acta, 2016. **188**: p. 490-498.
640. Bini, S., et al., *Molybdenum sputtering film characterization for high gradient accelerating structures*. Chinese Physics C, 2013. **37**(9): p. 097005.

641. Zhang, P., et al., *Facile fabrication of faceted copper nanocrystals with high catalytic activity for p-nitrophenol reduction*. Journal of Materials Chemistry A, 2013. **1**(5): p. 1632-1638.
642. Lee, B.-H., et al., *Reversible and cooperative photoactivation of single-atom Cu/TiO₂ photocatalysts*. Nature Materials, 2019.
643. Park, S.-M., et al., *Hybrid Cu_xO–TiO₂ heterostructured composites for photocatalytic CO₂ reduction into methane using solar irradiation: Sunlight into fuel*. ACS Omega, 2016. **1**(5): p. 868-875.
644. Gotou, M., et al., *Copper-molybdenum source ratio and complexing agent for high molybdenum content in electrodeposited cu-mo*. Journal of The Electrochemical Society, 2014. **161**(12): p. D628-D631.
645. Li, Z., et al., *A novel Cu-Mo/ZSM-5 catalyst for NO_x catalytic reduction with ammonia*. Journal of Natural Gas Chemistry, 2005. **14**(2): p. 115.
646. Wang, Y., et al., *Electronic structures of Cu₂O, Cu₄O₃, and CuO: A joint experimental and theoretical study*. Physical Review B, 2016. **94**(24): p. 245418.
647. Chen, L., et al., *Electrochemical deposition of copper oxide nanowires for photoelectrochemical applications*. Journal of Materials Chemistry, 2010. **20**(33): p. 6962-6967.

Every reasonable effort has been made to acknowledge the owners of copyright material. I would be pleased to hear from any copyright owner who has been omitted or incorrectly acknowledged.

APENDIX

Attribution statement

Published paper

1. "Dry reforming of methane over Co-Mo/Al₂O₃ catalyst under low microwave power irradiation. Catalysis Science & Technology, 2018, 8, 5315-5324".

Authors	Conception and design	Acquisition of data and method	Data conditioning and manipulation	Analysis & statistical method	Interpretation & discussion	Final Approval
Prof. Shaomin Liu	X				X	X
I acknowledge that these represent my contribution to the above research output						
Singed.						
Dr. Gia Hung Pham	X				X	X
I acknowledge that these represent my contribution to the above research output						
Singed.						
Dr. Ran Ran	X					
I acknowledge that these represent my contribution to the above research output						
Singed.						
Mr. Robert Vagoni	X					
I acknowledge that these represent my contribution to the above research output						
Singed.						
Prof. Vishnu Pareek	X					
I acknowledge that these represent my contribution to the above research output						
Singed.						

Patent logging

1. Hoang M. Nguyen, Gia Hung Pham, Shaomin Liu, *Catalysts for reforming of methane reactions.*

Originator/Contributor	Percentage Share	Signature
Gia Hung Pham	33.3 %	
Shaomin Liu	33.3 %	

Planned papers

1. Hoang M. Nguyen, Gia Hung Pham^{*}, Robert Vagnoni, Shaomin Liu^{*}, *Role of TiO₂ support in the enhancement of catalytic activity of CoMo catalyst for dry and steam combined dry reforming of methane under microwave heating.*

Authors	Conception and design	Acquisition of data and method	Data conditioning and manipulation	Analysis & statistical method	Interpretation & discussion	Final Approval
Prof. Shaomin Liu	X				X	X
I acknowledge that these represent my contribution to the above research output Singed.						
Dr. Gia Hung Pham	X				X	X
I acknowledge that these represent my contribution to the above research output Singed.						
Mr. Robert Vagoni	X					
I acknowledge that these represent my contribution to the above research output Singed.						

2. Hoang M. Nguyen, Gia Hung Pham, Shaomin Liu^{*}, *Catalysts for MW assisted reforming of methane: a review.*

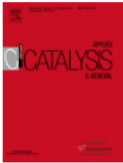
Authors	Conception and design	Acquisition of data and method	Data conditioning and manipulation	Analysis & statistical method	Interpretation & discussion	Final Approval
Prof. Shaomin Liu	X				X	X
I acknowledge that these represent my contribution to the above research output Singed.						
Dr. Gia Hung Pham	X					
I acknowledge that these represent my contribution to the above research output Singed.						

3. Hoang M. Nguyen, Gia Hung Pham*, Robert Vagnoni, Shaomin Liu*, *Syngas production via steam combined CO₂ reforming of methane over CuMo/TiO₂ catalyst under MW heating.*

Authors	Conception and design	Acquisition of data and method	Data conditioning and manipulation	Analysis & statistical method	Interpretation & discussion	Final Approval
Prof. Shaomin Liu	X				X	X
I acknowledge that these represent my contribution to the above research output Singed.						
Dr. Gia Hung Pham	X				X	X
I acknowledge that these represent my contribution to the above research output Singed.						
Mr. Robert Vagoni	X					
I acknowledge that these represent my contribution to the above research output Singed.						

Copyright permission statements.

Home Account Info Help 



Title: Formation and characteristic properties of carbonaceous species on nickel-magnesia solid solution catalysts during CH₄ CO₂ reforming reaction

Author: Yang-Guang Chen, Keiichi Tomishige, Kaoru Fujimoto

Publication: Applied Catalysis A: General

Publisher: Elsevier

Date: 4 November 1997
Copyright © 1997 Published by Elsevier B.V.

Logged in as:
Hoang Nguyen
Curtin University
Account #: 3001349848
[Logout](#)

Order Completed
Thank you for your order.

This Agreement between Curtin University -- Hoang Nguyen ("You") and Elsevier ("Elsevier") consists of your license details and the terms and conditions provided by Elsevier and Copyright Clearance Center.

Your confirmation email will contain your order number for future reference.

[printable details](#)

License Number	4501730765899
License date	Jan 04, 2019
Licensed Content Publisher	Elsevier
Licensed Content Publication	Applied Catalysis A: General
Licensed Content Title	Formation and characteristic properties of carbonaceous species on nickel-magnesia solid solution catalysts during CH ₄ CO ₂ reforming reaction
Licensed Content Author	Yang-Guang Chen, Keiichi Tomishige, Kaoru Fujimoto
Licensed Content Date	Nov 4, 1997
Licensed Content Volume	161
Licensed Content Issue	1-2
Licensed Content Pages	7
Type of Use	reuse in a thesis/dissertation
Portion	figures/tables/illustrations
Number of figures/tables/illustrations	3
Format	print
Are you the author of this Elsevier article?	No
Will you be translating?	No
Title of your thesis/dissertation	Microwave assisted dry reforming of methane
Expected completion date	Mar 2019
Estimated size (number of pages)	200
Requestor Location	Curtin University 183b manning Road Bentley, WA 6102 Australia Attn: Hoang Nguyen
Publisher Tax ID	GB 494 6272 12
Total	0.00 USD

[ORDER MORE](#) [CLOSE WINDOW](#)

Copyright © 2019 [Copyright Clearance Center, Inc.](#) All Rights Reserved. [Privacy statement](#) [Terms and Conditions](#)
Comments? We would like to hear from you. E-mail us at customerscare@copyright.com

Copyright permission from Elsevier for **Figure 2-6**.



Title: CO2 dry-reforming of methane over La0.8Sr0.2Ni0.8M0.2O3 perovskite (M = Bi, Co, Cr, Cu, Fe): Roles of lattice oxygen on C-H activation and carbon suppression

Author: K. Sutthiumporn, T. Maneerung, Y. Kathiraser, S. Kawi

Publication: International Journal of Hydrogen Energy

Publisher: Elsevier

Date: August 2012
Copyright © 2012 Hydrogen Energy Publications, LLC. Published by Elsevier Ltd. All rights reserved.

Logged in as:
Hoang Nguyen
Curtin University

LOGOUT

Order Completed

Thank you for your order.

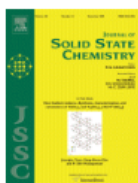
This Agreement between Curtin University -- Hoang Nguyen ("You") and Elsevier ("Elsevier") consists of your license details and the terms and conditions provided by Elsevier and Copyright Clearance Center.

Your confirmation email will contain your order number for future reference.

[printable details](#)

License Number	4447520385729
License date	Oct 14, 2018
Licensed Content Publisher	Elsevier
Licensed Content Publication	International Journal of Hydrogen Energy
Licensed Content Title	CO2 dry-reforming of methane over La0.8Sr0.2Ni0.8M0.2O3 perovskite (M = Bi, Co, Cr, Cu, Fe): Roles of lattice oxygen on C-H activation and carbon suppression
Licensed Content Author	K. Sutthiumporn, T. Maneerung, Y. Kathiraser, S. Kawi
Licensed Content Date	Aug 1, 2012
Licensed Content Volume	37
Licensed Content Issue	15
Licensed Content Pages	13
Type of Use	reuse in a thesis/dissertation
Portion	figures/tables/illustrations
Number of figures/tables/illustrations	12
Format	both print and electronic
Are you the author of this Elsevier article?	No
Will you be translating?	No
Original figure numbers	12
Title of your thesis/dissertation	Microwave assisted dry reforming of methane
Expected completion date	Mar 2019
Estimated size (number of pages)	200
Requestor Location	Curtin University 183b manning Road Bentley, WA 6102 Australia Attn: Hoang Nguyen
Publisher Tax ID	GB 494 6272 12
Total	0.00 AUD

Copyright permission from Elsevier for **Figure 2-8**.



Title: Influences of doping Cr/Fe/Ta on the performance of Ni/CeO₂ catalyst under microwave irradiation in dry reforming of CH₄
Author: Taiwo Odedairo, Jun Ma, Jiuling Chen, Shaobin Wang, Zhonghua Zhu
Publication: Journal of Solid State Chemistry
Publisher: Elsevier
Date: January 2016
 Copyright © 2015 Elsevier Inc. All rights reserved.

Logged in as:
 Hoang Nguyen
 Curtin University
 Account #: 3001349848
 LOGOUT

Order Completed

Thank you for your order.

This Agreement between Curtin University -- Hoang Nguyen ("You") and Elsevier ("Elsevier") consists of your license details and the terms and conditions provided by Elsevier and Copyright Clearance Center.

Your confirmation email will contain your order number for future reference.

[printable details](#)

License Number	4616341327961
License date	Jun 26, 2019
Licensed Content Publisher	Elsevier
Licensed Content Publication	Journal of Solid State Chemistry
Licensed Content Title	Influences of doping Cr/Fe/Ta on the performance of Ni/CeO ₂ catalyst under microwave irradiation in dry reforming of CH ₄
Licensed Content Author	Taiwo Odedairo, Jun Ma, Jiuling Chen, Shaobin Wang, Zhonghua Zhu
Licensed Content Date	Jan 1, 2016
Licensed Content Volume	233
Licensed Content Issue	n/a
Licensed Content Pages	12
Type of Use	reuse in a thesis/dissertation
Portion	figures/tables/illustrations
Number of figures/tables/illustrations	2
Format	both print and electronic
Are you the author of this Elsevier article?	No
Will you be translating?	No
Original figure numbers	Fig.5 and Fig.6
Title of your thesis/dissertation	Microwave assisted dry reforming of methane
Expected completion date	Mar 2019
Estimated size (number of pages)	200
Requestor Location	Curtin University 1830 manning Road Bentley, WA 6102 Australia Attn: Hoang Nguyen
Publisher Tax ID	GB 494 6272 12
Total	0.00 USD

ORDER MORE CLOSE WINDOW

Copyright permission from Elsevier for **Figure 2-18**.

Permissions for re-using our published paper in this thesis.

Journal/Book Title: **Dry reforming of methane over Co–Mo/Al₂O₃ catalyst under low microwave power irradiation**

Editor/Author(s) : Hoang M. Nguyen, Gia Hung Pham*, Ran Ran, Robert Vagnoni, Vishnu Pareek and Shaomin Liu *

Volume Number : 8

Year of Publication : 2018

Description of Material :

Page(s) : 5315-5324

Publisher : RSC

Minh Hoang Nguyen

From: CONTRACTS-COPYRIGHT (shared) <Contracts-Copyright@rsc.org>
Sent: Thursday, 27 June 2019 12:01 AM
To: Minh Hoang Nguyen
Subject: RE: Permission Request Form: Hoang M. Nguyen

Many thanks for sending the permissions request below. The Royal Society of Chemistry (RSC) hereby grants permission for the use of your paper(s) specified below in the printed and microfilm version of your thesis. You may also make available the PDF version of your paper(s) that the RSC sent to the corresponding author(s) of your paper(s) upon publication of the paper(s) in the following ways: in your thesis via any website that your university may have for the deposition of theses, via your university's Intranet or via your own personal website. We are however unable to grant you permission to include the PDF version of the paper(s) on its own in your institutional repository. The Royal Society of Chemistry is a signatory to the STM Guidelines on Permissions (available on request).

Please note that if the material specified below or any part of it appears with credit or acknowledgement to a third party then you must also secure permission from that third party before reproducing that material.

Please ensure that the thesis states the following:

Reproduced by permission of The Royal Society of Chemistry

and include a link to the paper on the Royal Society of Chemistry's website.

Please ensure that your co-authors are aware that you are including the paper in your thesis.

Best wishes,

Chloe Szebrat
Contracts and Copyright Executive
Royal Society of Chemistry
Thomas Graham House
Science Park, Milton Road
Cambridge, CB4 0WF, UK
Tel: +44 (0) 1223 438329
www.rsc.org

Author reused his published works in this thesis following the agreement of the Royal Society of Chemistry. Full Link of this statement:
<https://www.rsc.org/journals-books-databases/journal-authors-reviewers/licences-copyright-permissions/#deposition-sharing>

Author reusing their own work published by the Royal Society of Chemistry

You do not need to request permission to reuse your own figures, diagrams, etc, that were originally published in a Royal Society of Chemistry publication. However, permission should be requested for use of the whole article or chapter except if reusing it in a thesis. If you are including an article or book chapter published by us in your thesis please ensure that your co-authors are aware of this.

Reuse of material that was published originally by the Royal Society of Chemistry must be accompanied by the appropriate acknowledgement of the publication. The form of the acknowledgement is dependent on the journal in which it was published originally, as detailed in 'Acknowledgements'.